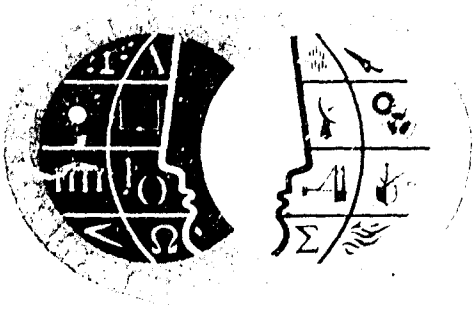

R. B. MacAnally
C. Yeh

ACOUSTIC IMAGING BY HOLOGRAPHY

August 1969
Report No. 69-48

Report No. 69-48
August 1969

ACOUSTIC IMAGING BY HOLOGRAPHY*

Richard B. MacAnally
C. Yeh

Technical Report

Sponsored by

The Office of Naval Research
Grant No. N00014-67-A-0111-0014

Electrical Engineering Department
University of California
Los Angeles, California

*This report is based on a thesis submitted by one of the authors (R. B. MacAnally) in partial fulfillment of the requirements for the degree of Doctor of Philosophy in Electrical Engineering at the University of Southern California, Los Angeles.

ABSTRACT

A method for visualizing objects immersed in water is formulated analytically and demonstrated experimentally. The technique, called "acoustic holography," is an adaptation of Gabor's two-step imaging process known as wavefront reconstruction or holography. The hologram is first formed from coherent acoustic radiation and then the image is reconstructed optically using coherent light source. Acoustic holography has advantage over other schemes for imaging in optically opaque media in that lenses or other focusing devices are not required, and a complete amplitude and phase reconstruction of the scattered field may be obtained. Since instantaneous amplitude is an acoustic observable, the reference field may be simulated electronically. Moreover, by resorting to heterodyne or phase detection the cross product term between object and reference signals may be generated without the undesired extraneous terms which occur in conventional holography. A scanning technique for generating acoustic holograms of underwater objects in the laboratory is described in detail. Using this system, acoustic holograms have been recorded which show angular resolution of 3.6 milliradians, approximately 1.5 times the Rayleigh limit. A variable contrast television display was used to view the acoustic holograms. To limit the attenuation of acoustic wave in sea water to a tolerable value, only acoustic signal with frequencies below 1 MHz should be used. We used 1 MHz signal for our experiment. Consequently, the quality of any acoustic image is degraded by poor resolution and specular reflection. It is suggested that diffuse or incoherent illumination be used to overcome the defect that acoustic images often appear as diffracted highlights rather than as extended forms. Thus, it appears that acoustic holography is not necessarily optimum for all acoustic imaging situations.

ACKNOWLEDGMENTS

We wish to express our deepest appreciation and gratitude to Dr. A.G. Diloreto and John Mays of the Naval Undersea Research and Development Center, Pasadena Laboratory for unflagging assistance and for providing the major acoustic facilities and electronics requirement indispensible to the experiments, to Professor N. George of the California Institute of Technology for his invaluable critical comments and stimulating discussions of various aspects of the work, to L.G. Ebeling of Vero Inc. for his generous contribution of expert micro-photography services and to W. Kolb and R. Weebe of the Hughes Aircraft Company for providing access to laser and photographic laboratory facilities.

We sincerely thank Mrs. Tina Spagon for her patience and expertise in preparing major portions of the typescript.

The financial support from the Office of Naval Research as well as the laboratory facilities and funds made available by the Naval Undersea Research and Development Center, Pasadena Laboratory are gratefully acknowledged. One of us (R.B.M.) also wishes to thank the U.S. Steel Foundation and the Hoffman Electronics Corporation for their financial support through their fellowship programs.

TABLE OF CONTENTS

TABLE OF CONTENTS (CONT.)

TABLE OF CONTENTS (CONT.)

CHAPTER I

INTRODUCTION

Historically, optics has referred primarily to the study of light; imaging, to the specific class of optical phenomena in which material bodies (objects) are represented by geometrically similar patterns of light (images). However, this is unduly restrictive since imaging is merely a consequence of the wave-like properties of electromagnetic radiation. More properly, imaging concepts should be extended to include mathematically related phenomena in which the object is "illuminated" with wave fields other than light and invisible "image" patterns are formed from the scattered radiation. The scope of optics is thereby enlarged to encompass a broad group of physically distinct but mathematically similar wave phenomena.

Here we are concerned with acoustic imaging, a process belonging in this more general category. In acoustic imaging the object scene is "illuminated" with acoustic radiation rather than light, and acoustic "image" patterns are formed from the scattered acoustic fields by various means. The acoustic images may then be visualized - rendered visible - through application of some sort of acousto-optic interaction. Since by definition all wave fields obey mathematically similar equations of motion we are guaranteed that, at least to first order, visualized acoustic images will bear some recognizable resemblance to the original scene. Imaging of this type may be extremely useful whenever the object is imbedded in media opaque to light.

Acoustic imaging differs from and should not be confused with the conventional echo ranging techniques commonly known by the generic term sonar in that imaging provides displays of the object scene lying in planes transverse to, as well as along, the direction of propagation whereas sonar provides primarily range profiles along the direction of propagation; i.e., longitudinal "images."

The reasons for the study of acoustic imaging should be clear. The quantity of information transmitted via wave fields and displayed as images is enormous. Indeed, under ideal conditions (infinitely large appertures and unlimited detector resolution) the maximum information density in an optical display is limited only by the information carrier, here scalar wave fields of wavelength λ from which the image is formed. Gabor[1] and others have shown that wave fields cannot transmit information about boundary details with characteristic spacings much smaller than λ because such information is carried by evanescent waves which decay so rapidly that at distances beyond a few wavelengths from the boundary the field amplitude associated with these details will always be less than the ambient noise amplitude. For example, conventional images formed with light may contain information densities exceeding 10^9 bits/cm^2 of retrievable information; information densities as high as 10^8 bits/cm^2 have been recorded by photographic means.*

---

* This figure is representative of the Kodak series 649 emulsions which are known to resolve in excess of 2000 lines/mm. The average black and white snapshot film, such as Kodak Panatomic-X can record image detail to 100 lines/mm or 10^6 bits/cm^2. (See Reference 2.) For comparison, high density integrated circuit superconducting computer memories are presently capable of storing approximately 2000 bits/cm^2. (See Reference 3.)

Information densities of this magnitude are typical of microscopic scenes. Resolution of molecular or atomic detail requires illumination at wavelengths much shorter than that of visible light, say at x-ray or electron wavelengths.

Information transmitting capacity of such magnitude is of inestimable value in scientific investigation and exploration. However, the information contained in wave fields is often vastly greater than the capacity of the eye or other device to receive directly. For example, natural virtual images* of the cosmic, microscopic and atomic regions of the universe, always of great interest to the scientist, contain information densities far exceeding that which the eye can detect and adequately resolve without auxiliary apparatus. Such regions are usually regarded as "invisible."

Quite apart from resolution and field of view restrictions imposed by any realizable receiving or display process, the information which can be transmitted from the object into an optical display is often severely limited by the medium interposing object and receiver. Information loss occurs by scattering and absorption of the wave field as it propagates through the medium. For example, light propagating through even pure water is both absorbed and scattered by the water molecules to such great extent that vision, in the ordinary sense, is limited to distances less than 50 to 100 meters[4,5]. In other cases,

---

* Normal, unaided vision always involves viewing virtual images.

although intrinsic absorption by the medium may be small, random turbulence induces scattering which limits the detail which can be resolved through such media. For example, observation of stellar bodies from the Earth's surface is severely hampered by uncontrollable fluctuations of the terrestrial atmosphere[6].

Hence, from the time of Galileo (the telescope) and Leeuwenhoek (the microscope) one of the great challenges of experimental science has been to render visible those regions beyond the ability of the eye to perceive; more technically, to extend visual perception into regions outside the space bandwidth product of the eye.* The quest for greater visibility has led to imaging with fields to which the eye does not directly respond; to wit, x-rays (crystallography), electrons (electron and field emission microscopy), acoustic radiation (acoustic holography), etc. The emphasis here is directed toward <u>acoustic imaging</u> by which is meant the visualization through acoustic means of objects imbedded in solid or liquid media usually opaque to light.

Interest in acoustic imaging has arisen in response to rapidly expanding activity in two relatively new but quite unrelated fields, biomedical engineering and oceanography. The use of x-rays in medical diagnosis has always been somewhat problematical. Not only does x-ray imaging subject the patient to extremely hazardous radiation, but the resulting images often do not fully satisfy the requirements of the examiner. For example, the technique does not readily distinguish different types of tissue. Further, because it is difficult to focus

---

* This concept is discussed in Chapter II.

x-rays, the display is actually an x-ray shadow rather than a truly three dimensional focused image of internal body structure. Acoustic imaging need not possess either of these drawbacks.

Acoustic imaging may also play a role in an entirely different endeavor, the development of underwater resources. Lack of visibility is becoming an impediment to more rapid progress in undersea exploration, mining, and transportation. Even in absolutely pure water, light will not propagate much further than perhaps 100 meters. Worse, one is usually most interested in operating along the ocean floor where the water has likely been churned into murky clouds of mud stirred up from the bottom. The range of x-rays in underwater situations is limited to the order of a few centimeters. On the other hand, acoustic fields can propagate through water for hundreds to thousands of meters, depending upon frequency, without excessive attenuation. Thus, for oceanographic applications acoustic imaging assumes importance as a means of extending visibility beyond the range of electromagnetic radiation.

Acoustic imaging is an infant science, at a stage of development which may be likened to that of conventional optics when Galileo first observed the moons of Jupiter. A multitude of challenges must be overcome in order to make acoustic imaging viable with other investigative techniques. The goal is an acoustic system which provides in real time* visualization with approximately the quality of inexpensive camera

---

* Standard broadcast television frame rates (30/sec) will satisfy the real time requirement. However, this is probably restrictive and 8mm movie frame rates (16/sec) or lower (8-10/sec) will be sufficient.

snapshots or standard television displays. The sophisticated refinements of light optics are not required.

If acoustic imaging is to proceed along conventional lines then an acoustic lens or other focusing device will be needed. However, such devices present formidable development and fabrication problems. Consider a typical camera apperture; a comparable apperture for 1 MHz acoustic radiation would be a thousand times larger, measuring perhaps 100 meters or more in diameter. Such a device could hardly be considered portable. Further, the scale of the object scene will be the same whether the illumination is acoustic or visible. Hence the F number (focal length to diameter ratio) of ideal acoustic lenses must be quite small and the images will then be subject to the severe abberations and distortions inherent in nonparaxial imaging. Therefore, for practical reasons acoustic lenses will very likely be appreciably smaller than ideal and the resulting displays will be comparable to those obtained by pinhole imaging with light.

Recently, an entirely new and different method of imaging <u>which does not require lenses</u>, the two step process invented by Dennis Gabor[7,8,9,10,11,12] and known as holography, has become the subject of intense research activity in visible optics. Because Gabor's technique does not require lenses, crude experiments in acoustic imaging can actually be performed more easily by adopting the methods of holography rather than conventional methods employing auxiliary focusing apparatus. Ironically, this is just the reverse of the situation in visible optics where good lenses are easily fabricated but holograms require carefully controlled laboratory setups. Of course, the reason is clear.

Holography requires coherent radiation. Coherent acoustic radiation is easily generated by crystal controlled oscillators. Conversely, coherent light usually requires a laser source and special precautions to ensure that the illumination is sufficiently coherent to produce high quality holograms. We shall present a study of acoustic imaging by holography; i.e., acoustic holography.

In order to include holography in optical discussions, the term "image" must be replaced with the broader concept of optical representation. By an optical representation of any object we include not only those referred to conventionally as "images" which bear some geometrical similarity to the object, but, more generally, any field configuration which may result from an illuminated or luminous boundary or volume. For example, a snapshot is a conventional image but a hologram is an optical representation in the more general sense; holograms usually bear no resemblance to the objects from which they are formed although they actually contain more information about those objects than do conventional photographs.* The entire process of forming optical representations of any type shall be referred to loosely as imaging.

The plan for the discussion of acoustic imaging to follow is

---

* There has been some confusion surrounding this point. It is often concluded that the reconstruction from a hologram contains more information than the image from a lens. This is not correct; the lens image is also three dimensional. However, the three dimensional nature of the lens image cannot be recorded on a two dimensional medium without resorting to special methods such as holography or stereoscopy. (See Reference 13.)

simple. In Chapter II the elements of scalar imaging are presented as they apply to simple acoustic imaging systems; the basic imaging problem is to determine the causal relation between contrast of object boundary field spatial structure and contrast of corresponding image field structure. In general, image contrast is a decreasing function of spatial frequency; object structure for which the corresponding image contrast vanishes is not resolved. In acoustic imaging it is especially important to maximize the resolution obtainable from a given aperture because of the relatively long wavelength of acoustic radiation. No doubt image resolution and contrast is one of the major criteria by which acoustic imaging systems must be evaluated.

The properties of the detector and the statistical behavior of the scalar image field significantly constrain the contrast transfer characteristics, hence resolution, of imaging systems. In this sense acoustic imaging systems are more interesting than optical imaging systems. To wit, imaging with light is restricted to detectors whose output is some long time average of the electromagnetic field energy. Conversely, the piezoelectric and ferroelectric compounds form an important class of acoustic radiation detectors for which the output is proportional to instantaneous acoustic pressure ampltidue[14]. This allows latitude in the design of acoustic imaging systems which is not possible for optical imaging systems.

The significance of the flexibility inherent in acoustic imaging with arrays of piezoelectric elements becomes apparent when the statistical time evolution of the field is taken into account. For detector outputs which are long time averages of the field energy,

spatially incoherent imaging tends to provide greater ultimate resolution but less contrast than coherent imaging. In addition, incoherent images do not suffer from edge ringing and other interference effects. By electronically synthesizing higher order moments, say the fourth order, it should be possible to further improve the resolution of incoherent acoustic imaging systems. Moreover, by employing scanning systems such as the Covington-Drane antenna rather than lens systems the contrast of the incoherent acoustic system can be made to approach that of the coherent system but with twice the resolution.

Heretofore, acoustic imaging has been confined to spatially coherent point source acoustic illumination and using holographic techniques. It seems clear that a new class of experiments in acoustic imaging is called for, namely using spatially incoherent, extended acoustic sources, lenses or other focusing devices, and a variety of electronically synthesized detection characteristics. Such experiments have scientific merit without regard to practical applications since similar experiments cannot be performed optically. For example, by varying the averaging time of the detector output, easily accomplished electronically, the effective degree of coherence of an acoustic imaging system can be varied continuously from completely incoherent to completely coherent.

The other major factor to be considered in judging the viability of acoustic imaging systems is the adaptability of the imaging process to real time imaging. Holography is basically a two-step process therefore is not readily adaptable to real time imaging with piezo-

electric detectors.* In this regard it should also be noted that since incoherent imaging requires finite detector averaging times the frame rate at which acoustic images are formed may be less than one might desire.

The variety of acoustic imaging systems which can be devised is certainly more extensive than the list presented in Chapter II. In this context acoustic holography must then be regarded simply as one of many possible acoustic imaging schemes and it seems rather premature to assess the viability of acoustic holography until other imaging methods have been investigated experimentally.

Difficulties of unique importance in acoustic imaging are posed in Chapter III. Specular reflection and attenuation will significantly degrade the quality of images obtained by long range acoustic imaging of objects in the sea. Specular reflection is the most severe problem; it renders most objects mere highlights of extended objects. The problem of specular reflection can be eliminated by using diffuse, extended sources of acoustic illumination. Here again incoherent accustic sources, either natural or man made, may prove superior to coherent sources.

In Chapter IV a theory of holography is formulated in terms of an eigenvalue equation. This type of equation represents mathematically the phenomena of wave front reconstruction. It is interesting to note

---

* In order to provide real time acoustic imaging by holographic means and employing piezoelectric detectors it will be necessary to form the hologram on some photosensitive material such as the heat developing film manufactured by The Minnesota Mining and Manufacturing Company which can be dry-developed essentially instantaneously.

that equations of this type play a central role in many scientific disiplines. Following an outline of the eigenvalue formalism, the holographic process is described in terms of a diffraction theory based upon expanding the fields in plane wave spectra rather than the more usual treatment employing a double application of the Rayleigh-Sommerfeld-Green or Fresnel-Kirchoff diffraction integrals. Plane wave expansions are used because the situations encountered in acoustic imaging are often non-paraxial. Special properties of the detector which do not arise in the theory of optical holography but which must be considered in acoustic holography are included in the theory. If certain simplifying assumptions are made then the eigenvalue equation possesses a continuum of solutions. In the more genral non-paraxial case it is not known if there are any solutions: i.e., if perfect reconstruction is possible.

Finally, in Chapter V the results of experiments are presented which demonstrate that images of underwater objects may indeed be obtained by acoustic means employing the techniques of holography. These experiments involve a scanning procedure which proved expedient for the purpose of demonstrating the feasibility of acoustic holography but which does not bear practical merit. Special effort was expended to make the experiments representative of the type of situations that would be encountered in practical undersea acoustic imaging problems. For example, the frequency was low enough (1 MHz, λ = 1.5 mm) to provide a range of perhaps 50 - 100 m in clear sea water, the aperture was a realistic size (approximately 1.5 m square), objects were imaged in reflection rather than backlighting, and the ranges were 1.5 - 3 m.

Included is a demonstration of the severity of the highlight problem and special techniques for viewing acoustic images.

CHAPTER II

ELEMENTS OF SCALAR IMAGING

1. IMAGING, A GENERAL PROBLEM IN SCALAR WAVE PROPAGATION

Optics, in the broad sense to be taken here, refers to the study of any propagating disturbance (not necessarily electromagnetic) describable by a real scalar function $\Psi(\underline{r},t)$ of position $\underline{r}$ and time t, hereafter called the optical or wave field, which satisfies the homogeneous scalar wave equation

$$\nabla^2\Psi(\underline{r},t) - \frac{1}{[c(\underline{r})]^2}\frac{\partial^2\Psi(\underline{r},t)}{\partial t^2} = 0 \qquad \text{(II.1)}$$

subject to Cauchy boundary conditions on open space-time boundaries[15]. The disturbance propagates through a medium M with velocity $c(\underline{r})$, the position dependence of c denoting an inhomogeneous material. More generally, the material will also be anisotropic and dispersive and wave propagation therein more complex than that implied in Equation (II.1). Nevertheless, the extensive and important class of optical phenomena known as scalar imaging is contained in Equation (II.1).

Many quantities of diverse physical origin obey the scalar wave equation, at least approximately, hence qualify as optical fields. Among others we may list small amplitude acoustic pressure, velocity, and displacement fields in non-viscous fluids, and the components of any electromagnetic field. Indeed, under certain conditions, electromagnetic radiation in the visible spectrum (light) is fully represented by a single scalar field $V(\underline{r},t)$ referred to as the light amplitude[16].

Imaging, the process of forming optical representations, is an important and venerable branch of optics which, historically, has been associated almost entirely with light. In this chapter the more important aspects of scalar imaging theory will be extended to encompass related acoustic phenomena as well.

A general imaging situation is depicted schematically in Figure II.1 . A simply or multiply connected region O, the object space, is "illuminated" by a wave field $\Psi_L(\underline{r},t)$ radiating from luminous source region L. The object scatters a field $\Psi_O(\underline{r},t)$ which, in general, will propagate in all directions. After passing through the intervening medium $M(\underline{r},t)$ a portion of Ψ_O may happen to fall upon some arrangement of material $F(\underline{r})$, the imaging or focusing device. The imaging device transforms the field Ψ_O in the space O into a new field Ψ_I in the space I, the image space, immediately adjacent to F. In the image space Ψ_I forms various spatial patterns $H(\underline{r},t)$ which are optical representations for the object O. These patterns may be recorded for use at a later time.

For any given object, the exact configuration of H has considerable latitude. It may be geometrically similar to the object in which case it is known as an image and is recorded as a photograph. However, in one important situation, holography, H is an interference pattern bearing little or no resemblance to the object; a record of this interference pattern is called a hologram. The emphasis in the remaining chapters is upon holography. However, before taking up this study, certain elementary properties characteristic of any imaging system

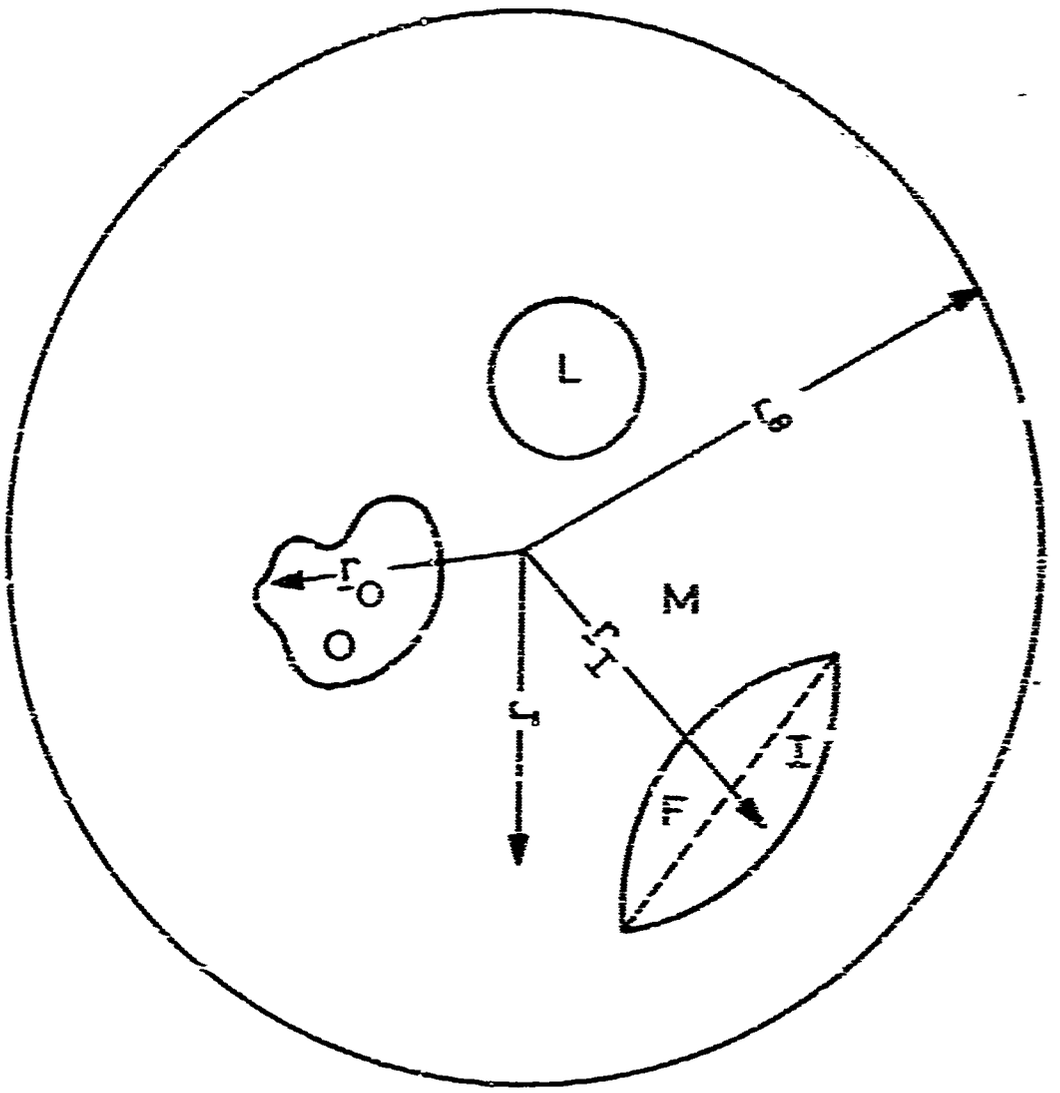

Figure II.1. A General Arrangement for Scalar Imaging

O	Object space
I	Image space
M	Intervening medium
L	Illumination source
F	Imaging device
$\underline{r}$	General position coordinate
$\underline{r}_O$	General position in an object plane
$\underline{r}_I$	General position in an image plane
r_∞	Sphere at ∞

must be provided; in particular, basic relations governing resolution will be formulated.

2. THE OBSERVABLES OF ACOUSTIC IMAGING

We begin by defining the observables of any imaging system. The general propagation problem is to determine $\Psi(\underline{r},t)$ satisfying Equation (II.1) and specified boundary conditions in space-time. The imaging problem requires two additional constraints: (1) only certain functionals $D(\underline{r},t)$ of optical fields are observable; i.e., can be measured, and (2) $\Psi(\underline{r},t)$ is a stochastic function; i.e., a function which represents a physical quantity exhibiting random fluctuations in space-time.

Condition (1) merely reflects the properties of the apparatus used to detect optical fields, namely that the output of the detection elements may not respond directly to the field amplitude, rather to various physical quantities D called image observables which are functionals of the field amplitude. Condition (2) is a statement that any physical process giving rise to optical fields is inherently statistical in nature. The manner in which the field statistics will influence imaging depends upon the characteristics of the detection process, the study of which we now take up.

A general class of image observables may be written as

$$D(\underline{r},t) = \int_{-\infty}^{t} f[\Psi(\underline{r},t')]w(t-t')dt' \qquad \text{(II.2)}$$

where f represents some function of the field and $w(t-t')$ is a temporal weighting factor. For example, the only detectors known to be

sensitive to light respond to incident field energy flux rather than to field amplitude. Moreover, the response time of any known light sensitive detector (photographic emulsion, bolometer, photocell, retina, etc.) is much longer than the period of oscillation of light, hence the detector output D cannot follow the instantaneous oscillations of the light. Accordingly, Skinner[17] has shown that only the time averaged intensity of light can be measured and the appropriate image observable is

$$D(\underline{r}) \propto \left\langle [\Psi(\underline{r},t]^2 \right\rangle = \left\langle \psi(\underline{r},t)\psi^*(\underline{r},t) \right\rangle \qquad \text{(II.3)}$$

where angular brackets $\langle \quad \rangle$ indicate an infinite time average

$$= \lim_{T\to\infty} \frac{1}{2T} \int_{-T}^{T} (\ )\, dt \qquad \text{(II.4)}$$

and superscript * denotes complex conjugation.

Here we have adopted the convention that the complex valued mathematical fields ψ are to be taken as the analytic signal representations of the real valued physical fields Ψ[18]. It is understood that at the end of a calculation the physical quantity is regained as the real part of the analytic signal, thus $\Psi = \mathrm{Re}\psi$. The infinite time average is a mathematical convenience. It should be interpreted as meaning an average over times long compared to the period of oscillation of the radiation and the mean time between statistical fluctuations of field amplitude and/or phase. Devices obeying response (II.3) are known as energy or square law detectors. Because all phase information is lost

in the time averaging process, they belong to the general class of incoherent detectors.

Since the observable is intensity I not field ψ it is desirable to formulate imaging directly in terms of the former rather than the latter. However, this is not possible because the intensity in any region is not uniquely related to the intensity on the boundaries surrounding that region. It is possible to introduce a new function called the mutual coherence function[19,20] $\Gamma(\underline{r}_1, \underline{r}_2, t_1, t_2)$,

$$\Gamma(\underline{r}_1, \underline{r}_2, t_1, t_2) \equiv \left\langle \psi(\underline{r}_1, t_1+t)\psi^*(\underline{r}_2, t_2+t) \right\rangle \quad , \tag{II.5}$$

which contracts to the intensity

$$\Gamma(\underline{r}_1, \underline{r}_2, t_1, t_2) \to I(\underline{r}, t) \tag{II.6a}$$

as

$$\begin{aligned} \underline{r}_1 &\to \underline{r}_2 \to \underline{r} \\ t_1 &\to t_2 \end{aligned} \tag{II.6b}$$

and for which the propagation problem is unique. Moreover, because Γ is in the form of a correlation, the statistics of the field are conveniently included in this function. If the temporal dependence of Γ is only through the time difference $\tau = t_2 - t_1$, Γ is stationary in time and we may then write

$$\Gamma(\underline{r}_1, \underline{r}_2, t_1, t_2) \to \Gamma(\underline{r}_1, \underline{r}_2, \tau) \equiv \Gamma_{12}(\tau) \quad . \tag{II.7}$$

The equations of motion for $\Gamma_{12}(\tau)$ are well known[19], we merely repeat them here

$$\nabla_1^2\Gamma_{12}(\tau) - \frac{1}{c^2}\frac{\partial^2\Gamma_{12}(\tau)}{\partial\tau^2} = 0$$
$$\nabla_2^2\Gamma_{12}(\tau) - \frac{1}{c^2}\frac{\partial^2\Gamma_{12}(\tau)}{\partial\tau^2} = 0 \quad . \tag{II.8}$$

Solutions for Γ_{12} may be found by the standard techniques.

Because acoustic fields are a mechanical phenomena, electromechanical processes are required for their detection, and acoustic observables may have properties quite different from the intensity observable of light. The most common acoustic detectors operate through the phenomena of piezoelectricity (quartz or any other crystal lacking a center of symmetry) or ferroelectricity (barium titanate, etc.). We shall not enter into a detailed discussion of these mechanisms here but merely point out that with either phenomena is associated the generation of an electric potential linearly related to the incident acoustic stress or strain[21]. Provided the detector is suitably terminated, the frequency of acoustic oscillations is so low that the potential across the crystal will follow the instantaneous acoustic field. Accordingly, for acoustic fields the fundamental observable is

$$D(\underline{r},t) \propto \Psi(\underline{r},t) \quad . \tag{II.9}$$

Response law (II.9) belongs to the class of <u>coherent</u> detectors and is especially important because many other response laws can be

electronically synthesized from it. Among others we distinguish the square law detector, Equation (II.3), and the correlation detector

$$D(\underline{r},t) \propto \Psi(\underline{r},t) \bigstar_t S(\underline{r},t) \qquad \text{(II.10)}$$

where $\bigstar_t$ denotes time correlation according to the prescription given in Appendix B, $S(\underline{r},t)$ is a "reference" against which the signal is compared, and $\Psi(\underline{r},t)$ is assumed to be of finite duration. A special case of (II.10) is the time-matched filter[22] for which

$$D(\underline{r},t) \propto \Psi(\underline{r},t) \bigstar_t \Psi(\underline{r},t) \quad . \qquad \text{(II.11)}$$

Finally higher order detection processes, for example

$$D(\underline{r}) \propto \left\langle [\Psi(\underline{r},y)]^4 \right\rangle \quad , \qquad \text{(II.12)}$$

are possible.

3. TEMPORAL STRUCTURE OF WAVE FIELDS

Mathematically, imaging is simply finding solutions of the propagation problem, Section (1), for the image observables, Section (2). Since instantaneous amplitude is observable in acoustic imaging, a formal analysis directly in terms of field rather than mutual coherence is valid. In view of the linearity of Equation (II.1), the imaging process can be formulated as a superposition using appropriate Green's functions. To see how the superposition should be accomplished we must consider the temporal structure of the fields.

Wave fields are either polychromatic or quasi-monochromatic; purely monochromatic fields are impossible. For quasi-monochromatic radiation the temporal spectrum $\tilde{\psi}(\underline{r},\nu)$ is confined to a narrow frequency range $\Delta\nu$ about a central line $\bar{\nu}$ such that $\Delta\nu<<\bar{\nu}$, and may be written

$$\tilde{\psi}(\underline{r},\nu) = \tilde{\xi}(\underline{r},\nu)*_t\delta(\nu-\bar{\nu}) \qquad \text{(II.13)}$$

where

$$\tilde{\xi}(\underline{r},\nu) = 0 \text{ for } |\nu-\bar{\nu}| \geq \Delta\nu/2 \quad , \qquad \text{(II.14)}$$

δ is the Dirac delta function[23], and $*_t$ denotes time correlation according to the prescription given in Appendix B. Acoustic fields with sufficient spectral purity to satisfy the quasi-monochromatic approximation are easily generated; indeed, spectral purities exceeding 1 part in 10^6 are common. Unless otherwise noted, the quasi-monochromatic approximation is hereafter assumed valid.

Applying relation (B.7) for the inverse Fourier Transform of a convolution yields

$$\psi(\underline{r},t) = \xi(\underline{r},t)e^{-2\pi i\bar{\nu}t} \quad , \qquad \text{(II.15)}$$

the analytic signal representation for quasi-monochromatic fields. It is a simple matter to show that $\xi(\underline{r},t)$, a function varying slowly with time, obeys the relation

$$\nabla^2\xi(\underline{r},t) + \bar{k}^2\xi(\underline{r},t) = 0 \qquad \text{(II.16)}$$

where $\bar{k}^2 = \frac{(2\pi\bar{\nu})^2}{c^2}$. It is then clear that quasi-monochromatic fields can be treated as purely monochromatic if the temporal variation of ξ is small during some time interval τ characteristic of the specific problem to which (II.16) is applied. The time dependence of ξ can then be omitted in Equation (II.16) and the result recognized as the Helmholtz equation

$$\nabla^2\xi(\underline{r}) + \bar{k}^2\xi(\underline{r}) = 0 \quad , \tag{II.17}$$

long familiar as the equation of propagation for purely monochromatic radiation.

Now the only time spans of significance in imaging are those required for an optical disturbance to propagate over the possible optical paths from object to image. Calling the maximum optical path length L, the characteristic time interval for imaging problems is no greater than

$$\tau = \frac{L}{c} \quad . \tag{II.18}$$

We then require that the time τ' for ξ to undergo significant change be restricted so that

$$\tau' >> \frac{L}{c} \quad . \tag{II.19}$$

An approximate value for τ' can be obtained by considering Ψ as consisting of wave trains of duration τ'. Then

$$\xi = \text{Const} \qquad |t| < \tau/2$$
$$= 0 \qquad |t| > \tau/2 \quad . \tag{II.20}$$

Taking the Fourier Transform of (II.20) gives

$$\tilde{\xi}(\underline{r},\nu) \propto \frac{\sin \pi\nu\tau}{\pi\nu\tau} \tag{II.21}$$

so that

$$\tau' \cong \frac{1}{\Delta\nu} \quad . \tag{II.22}$$

Therefore, in order to treat the fields as purely monochromatic we demand

$$\Delta\nu << \frac{c}{L} \quad \text{or} \quad L << \frac{c}{\Delta\nu} \quad . \tag{II.23}$$

For example, if the radiation is a 1 MHz acoustic signal with spectral purity of 1 part in 10^6 then L is approximately 1500 meters in water.

The foregoing has been concerned only with determining the proper wave equation. To complete the discussion requires additional comment on the statistical behavior of the field, in particular on the comparative time evolution of the field at two arbitrary points $\underline{r}_1$, and $\underline{r}_2$ in space. The parameter which measures this is the two point temporal cross correlation or mutual coherence function $\Gamma_{12}(\tau)$ previously defined, or a related quantity, the <u>complex degree of coherence</u> $\gamma_{12}(\tau)$ which is normalized so that

$$0 \leq |\gamma_{12}(\tau)| \leq 1 \quad . \tag{II.24}$$

By definition

$$\gamma_{12}(\tau) = \frac{\Gamma_{12}(\tau)}{[\Gamma_{11}(0)\Gamma_{22}(0)]^{1/2}} \quad . \tag{II.25}$$

If the two points $\underline{r}_1$ and $\underline{r}_2$ are allowed to contract to a single point in space $\gamma_{12}(\tau)$ becomes the normalized <u>autocorrelation</u> $\gamma_{11}(\tau)$ of the field at that point; autocorrelation is a measure of the <u>temporal coherence</u> properties of the field. If the time evolution of the phase of the field is perfectly linear and deterministic then the time structure of the field is correlated for all time differences τ and

$$|\gamma_{11}(\tau)| = 1 \quad . \tag{II.26}$$

We then speak of a temporally coherent field. This condition can exist only if the field is purely monochromatic. For quasi-monochromatic fields the autocorrelation vanishes beyond some interval τ_c called the <u>coherence time</u>; for quasi-monochromatic fields

$$\begin{aligned} |\gamma_{11}(\tau)| &= 1 \qquad \tau << \tau_c \\ &= 0 \qquad \tau > \tau_c \quad ; \end{aligned} \tag{II.27}$$

we identify τ' with τ_c.

Temporal coherence plays an important role in <u>interference</u> phenomena, particularly those involving the self-interference of

optical beams. For example, the speckled images characteristic of coherently illuminated objects occur when the scattered illumination interfers with the incident illumination. This can happen as long as the optical path length difference ΔL satisfies

$$\Delta L << \frac{c}{\Delta\nu} \quad . \tag{II.28}$$

Since path length differences rather than absolute path lengths are involved in (II.28) the latter is less restrictive than the condition for validity of the Helmholtz equation. Thus, we usually assume that quasi-monochromatic radiation is temporally coherent.

The other limiting form for the complex degree of coherence is of more importance in imaging. If the time difference τ is allowed to vanish, $\gamma_{12}(\tau)$ becomes the normalized mutual intensity $\gamma_{12}(0)$; mutual intensity is a measure of the spatial coherence properties of the field. If the time evolutions of the phase of the field at two points in space are in unison then the time structure of the field at the two points is correlated and

$$|\gamma_{12}(0)| = 1, \text{ all } \underline{r}_1 \text{ and } \underline{r}_2 \quad . \tag{II.29}$$

We then speak of spatially coherent fields. If the two time evolutions are independent then the time structure of the field at the two points is uncorrelated and

$$|\gamma_{12}(0)| = 0, \ \underline{r}_1 \neq \underline{r}_2 \quad . \tag{II.30}$$

We then speak of spatially incoherent fields.

It is physically impossible to obtain a field which is either entirely coherent or entirely incoherent. The former obtains only for purely monochromatic fields. For quasi-monochromatic radiation Skinner[17] has demonstrated that an arbitrarily narrow power spectrum does not guarantee spatial coherence anywhere, a somewhat surprising result in view of the van Cittert-Zernike Theorem[24]. Conversely, Beran and Parrent[25] have shown that any field for which $\gamma_{12}(0) = 0$ everywhere does not propagate, hence cannot exist except possibly as rapidly decaying evanescent waves. Hence, for all quasi-monochromatic fields there will be some region over which spatial coherence will obtain. Thus, in general

$$\begin{aligned} |\gamma_{12}(0)| &= 1 \qquad |\underline{r}_2 - \underline{r}_1| \ll \alpha\lambda \\ &= 0 \qquad |\underline{r}_2 - \underline{r}_1| > \alpha\lambda \end{aligned} \tag{II.31}$$

where the condition $\alpha > 1$ is necessary in order that the field radiate. If the field is spatially coherent $\alpha \gg 1$; if spatially incoherent, $\alpha \cong 1$.

4. WAVE THEORY OF IMAGING

Although neither completely coherent nor completely incoherent fields are physically realizable, there are many situations of practical importance in which the fields are approximately coherent or approximately incoherent over the spatial region of interest. We now study the influence of the field statistics upon imaging processes for these

limiting cases. The motivation for this investigation arises from a need to maximize acoustic image quality.

Acoustic imaging is beset with a multitude of limitations of practical origin, most being attributed to the relatively long wavelength of acoustic radiation. The result is acoustic images of inferior quality, often barely discernable. However, since the fundamental acoustic observable is instantaneous field amplitude rather than field intensity, acoustic imaging is not limited to energy detection processes as is light imaging. Other processes may be synthesized electronically. We wish to determine if image quality may be improved over that which can be obtained with energy detection.

On the basis of Equation (II.17) the formation of an image with quasi-monochromatic radiation can be given as a spatial superposition of fields. To wit, see Figure II.2

$$\xi_I(\underline{r}_I,t) = \int_0 \xi_0(\underline{r}_0,t)G(\underline{r}_I,\underline{r}_0)d^2r_0 \qquad (II.32)$$

where $\xi_I(\underline{r}_I,t)$ is the image field amplitude, $\xi_0(\underline{r}_0,t)$ is the object field amplitude, and $G(\underline{r}_I,\underline{r}_0)$ is the Green's function for the imaging process; i.e., the field amplitude at image coordinate $\underline{r}_I$ in image plane I resulting from a point source at object coordinate $\underline{r}_0$ in object plane 0. For simplicity assume that the image formation process is stationary in spatial coordinates; i.e.,

$$G(\underline{r}_I,\underline{r}_0) = G(\underline{r}_I-\underline{r}_0) \quad . \qquad (II.33)$$

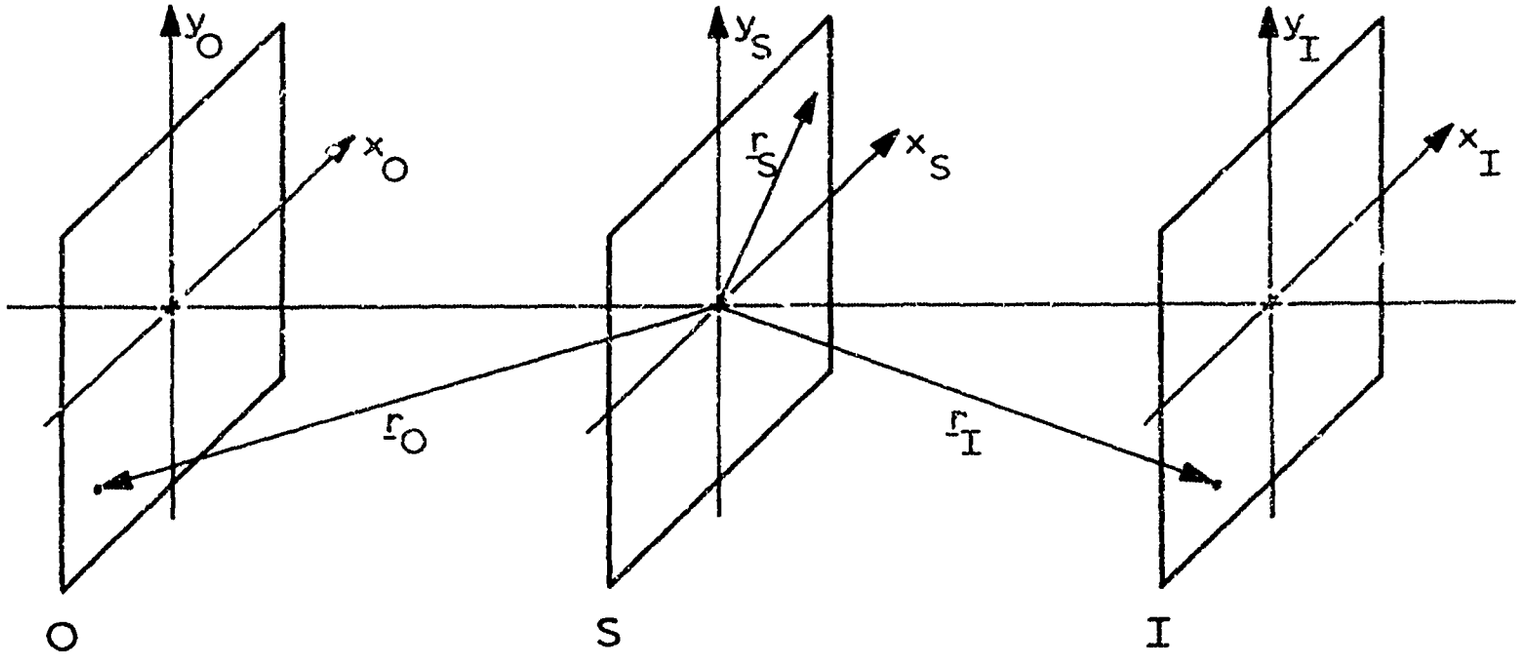

Figure II.2. A Typical Arrangement for Scalar Imaging

O	Object plane
I	Image plane
S	Exit plane of image device or hologram plane
$\underline{r}_O$	General position in an object plane
$\underline{r}_I$	General position in an image plane
$\underline{r}_S$	General position in the exit plane or hologram plane

The relative scale of the coordinate systems is taken so that the overall magnification is unity.

Then

$$\xi_I(\underline{r}_I,t) = \int_0 \xi_0(\underline{r}_0,t)G(\underline{r}_I-\underline{r}_0)d^2r_o \qquad \text{(II.34)}$$

which is valid for <u>isoplanatic</u> image formation.

To proceed further requires that the process be stated in terms of image observables. For light the observable is

$$D(\underline{r}) = \left\langle \xi(\underline{r},t)\xi^*(\underline{r},t) \right\rangle = I(\underline{r}) \quad . \qquad \text{(II.35)}$$

Substituting from (II.34) and commuting the spatial integration with the time average yields

$$I_I(\underline{r}_I) = \int_0 \int G(\underline{r}_I-\underline{r}_0)G^*(\underline{r}_I-\underline{r}_0') \left\langle \xi_0(\underline{r}_0,t)\xi_0^*(\underline{r}_0',t) \right\rangle d^2r_0 d^2r_0' \quad . \qquad \text{(II.36)}$$

At this point the statistical nature of the optical field must be introduced. We distinguish two cases. If the light is spatially incoherent the time evolutions of the fields $\xi_0(\underline{r}_0,t)$ and $\xi_0(\underline{r}_0',t)$ are statistically independent and

$$\left\langle \xi_0(\underline{r}_0,t)\xi_0^*(\underline{r}_0',t) \right\rangle = \delta(\underline{r}_0-\underline{r}_0') \left\langle \xi_0(\underline{r}_0,t)\xi_0^*(\underline{r}_0,t) \right\rangle \quad . \qquad \text{(II.37)}$$

Then

$$I_I(\underline{r}_I) = \left\langle \xi_I(\underline{r}_I,t)\,\xi_I^*(\underline{r}_I,t)\right\rangle =$$

$$\iint_0 G(\underline{r}_I-\underline{r}_0)G^*(\underline{r}_I-\underline{r}_0')\,\delta(\underline{r}_0-\underline{r}_0')\left\langle \xi_0(\underline{r}_0,t)\,\xi_0^*(\underline{r}_0,t)\right\rangle d^2r_0 d^2r_0'$$

$$= \int_0 |G(\underline{r}_I-\underline{r}_0)|^2 \left\langle \xi_0(\underline{r}_0,t)\,\xi_0^*(\underline{r}_0,t)\right\rangle d^2r_0 \quad . \qquad \text{(II.38)}$$

Equation (II.38) may be written in the compact form

$$I_I(\underline{r}) = I_0(\underline{r}) * |G(\underline{r})|^2 \quad , \qquad \text{(II.39)}$$

the isoplanatic imaging law for incoherent optical fields when the image observable in the output of a square law detector. Clearly, in this case the image formation process is linear in intensity. By employing suitable electronics, acoustic imaging systems may be devised which also obey Equation (II.39).

If the field is spatially coherent, the time evolutions of $\xi_0(\underline{r}_0,t)$ and $\xi_0(\underline{r}_0',t)$ are identical except possibly for a uniform translation $\tau(\underline{r})$ in time. To describe this synchronization it is convenient to reference all fields to some standard $\xi_S(t)$ which represents the characteristic structure of the time evolution and which is normalized so that

$$\left\langle \xi_S(t)\xi_S^*(t)\right\rangle = 1 \quad . \qquad \text{(II.40)}$$

Then

$$\xi_0(\underline{r}_0,t) = \xi_0(\underline{r}_0)\xi_S[t+\tau(\underline{r}_0)] \tag{II.41}$$

$$\xi_0(\underline{r}'_0,t) = \xi_0(\underline{r}'_0)\xi_S[t+\tau(\underline{r}'_0)] \quad , \tag{II.42}$$

where $\xi_0(\underline{r}_0)$ and $\xi_0(\underline{r}'_0)$ are real constants representing the "magnitudes" of the fields. To find the $\xi_0(\underline{r})$ multiply the appropriate defining equation by its complex conjugate, time average the resulting product, and recognize that infinite time averages are invariant under time translations, thereby obtaining

$$\xi_0(\underline{r}_0) = \sqrt{\left\langle \xi_0(\underline{r}_0,t)\xi_0^*(\underline{r}_0,t)\right\rangle} \tag{II.43}$$

$$\xi_0(\underline{r}'_0) = \sqrt{\left\langle \xi_0(\underline{r}'_0,t)\xi_0^*(\underline{r}'_0,t)\right\rangle} \quad . \tag{II.44}$$

The correlation between fields then becomes

$$\xi_0(\underline{r}_0,t)\xi_0^*(\underline{r}'_0,t) = \sqrt{\left\langle \xi_0(\underline{r}_0,t)\xi_0^*(\underline{r}_0,t)\right\rangle}\sqrt{\left\langle \xi_0(\underline{r}'_0,t)\xi_0^*(\underline{r}'_0,t)\right\rangle} \cdot \cdot \left\langle \xi_S[t+\tau(\underline{r}_0)]\xi_S^*[t+\tau(\underline{r}'_0)]\right\rangle \quad . \tag{II.45}$$

By suitable change of variables we obtain

$$\left\langle \xi_S[t+\tau(\underline{r}_0)]\xi_S^*[t+\tau(\underline{r}'_0)]\right\rangle = \left\langle \xi_S(\eta)\xi_S^*[\eta+\tau(\underline{r}'_0)-\tau(\underline{r}_0)]\right\rangle \tag{II.46}$$

Edwards and Parrent[26] have shown that the normalized autocorrelation of a coherent quasi-monochromatic function may be written

$$\left\langle \xi(\underline{r},t)\xi^{*}(\underline{r},t+\tau)\right\rangle = e^{i2\pi\nu\tau} \quad . \tag{II.47}$$

Thus

$$\xi_0(\underline{r}_0,t)\xi_0^{*}(\underline{r}_0',t) = \sqrt{\left\langle \xi_0(\underline{r}_0,t)\xi_0^{*}(\underline{r}_0,t)\right\rangle}\sqrt{\left\langle \xi_0(\underline{r}_0',t)\xi_0^{*}(\underline{r}_0',t)\right\rangle}\cdot$$
$$\cdot e^{i2\pi[\tau(\underline{r}_0')-\tau(\underline{r}_0)]} \quad . \tag{II.48}$$

Substituting (II.48) into (II.35) we obtain for coherent imaging

$$I_I(\underline{r}_I) = \left[\int_0 G(\underline{r}_I-\underline{r}_0)\sqrt{\left\langle \xi_0(\underline{r}_0,t)\xi_0^{*}(\underline{r}_0,t)\right\rangle}\; e^{-2\pi i\tau(\underline{r}_0)}\, d^2r_0\right]\cdot$$
$$\cdot\left[\int_0 G^{*}(\underline{r}_I-\underline{r}_0')\sqrt{\left\langle \xi_0(\underline{r}_0',t)\xi_0^{*}(\underline{r}_0',t)\right\rangle}\; e^{2\pi i\tau(\underline{r}_0')}\, d^2r_0'\right] . \tag{II.49}$$

Note that $I_I(\underline{r}_I)$ has been separated into independent $\underline{r}_0$ and $\underline{r}_0'$ integrations. Thus

$$I_I(\underline{r}_I) = \left|\int_0 G(\underline{r}_I-\underline{r}_0)\sqrt{\left\langle |\xi_0(\underline{r}_0,t)|^2\right\rangle}\; e^{-2\pi i\tau(\underline{r}_0)}\, d^2r_0\right|^2 . \tag{II.50}$$

Defining an equivalent time independent complex field amplitude as

$$U(\underline{r}) = \sqrt{\left\langle |\xi(\underline{r},t)|^2\right\rangle}\, e^{-2\pi i\tau(\underline{r})} \quad . \tag{II.51}$$

Equation (II.50) may be written in the compact form

$$I_I(\underline{r}) = |U_0(\underline{r})*G(\underline{r})|^2 \quad , \tag{II.52}$$

the isoplanatic imaging law for coherent optical fields when the image observable is the output of a square law detector. Clearly, in this case the image formation process is nonlinear in intensity; in fact, image intensity is not even directly related to object intensity, rather to a complicated functional of the complex valued amplitude. By employing suitable electronics, acoustic imaging systems may be devised which also obey Equation (II.52).

5. RESOLUTION AND FIELD STATISTICS

We now compare the characteristics of coherent (II.52) and incoherent (II.39) imaging. When the radiation is light there are many ways to make the comparison, depending upon the application, and it is not possible to formulate a general statement classifying one type of illumination as always "better" than the other. However, when the radiation is acoustic there is no doubt concerning the choice of criteria by which image quality is to be judged. Restricted apperture size, long wavelengths, and coarse detector resolution severely limit the resolution of acoustic imaging systems. Clearly then, the problem of maximizing the degree to which details of the object structure are resolved as distinct and similar details in the image structure must be considered of prime importance in acoustic imaging. Thus, it is appropriate to examine here the relation between resolution and field statistics.

To compare the resolution of coherent and incoherent imaging systems begin by taking the Spatial Fourier transforms of Equations (II.39) and (II.52) (see Appendix A). From the former

$$\tilde{I}_I(\underline{s}) = \tilde{I}_0(\underline{s})[\tilde{G}(\underline{s}) \star \tilde{G}^*(\underline{s})] \qquad \text{(II.53)}$$

and from the latter

$$\tilde{I}_I(\underline{s}) = [\tilde{U}_0(\underline{s})\tilde{G}(\underline{s})] \star [\tilde{U}_0^*(\underline{s})\tilde{G}^*(\underline{s})] \quad . \qquad \text{(II.54)}$$

The physical interpretation of Equation (II.53) is clear. If the radiation is incoherent, each spectral component $\tilde{I}_0(\underline{s})$ of the object boundary intensity has a corresponding spectral counterpart $\tilde{I}_I(\underline{s})$ in the image intensity except for multiplication by the complex factor $\tilde{G}(\underline{s}) \star \tilde{G}^*(\underline{s}) \equiv \tilde{H}(\underline{s})$; $\tilde{H}(\underline{s})$ is called the <u>spatial frequency transfer function</u>.

The zero-frequency spectral component $\tilde{I}_I(0)$ represents an intensity uniformly distributed in space, and requires special consideration. Since $I_I(\underline{r})$ is non-negative, $\tilde{I}_I(0) > 0$ unless $I_I(\underline{r}) = 0$ everywhere, a trivial case. Thus, there will always be a background intensity $\tilde{I}_I(0)$ distributed uniformly over any image formed with incoherent radiation. It is convenient to normalize each spectral component of the image intensity to this background. Defining

$$\frac{\tilde{I}_I(\underline{s})}{\tilde{I}_I(0)} = \hat{I}_I(\underline{s}), \quad \frac{\tilde{I}_0(\underline{s})}{\tilde{I}_0(0)} = \hat{I}_0(\underline{s}), \quad \frac{\tilde{G}(\underline{s})}{\tilde{G}(0)} = \hat{G}(\underline{s}), \quad \frac{\tilde{H}(\underline{s})}{\tilde{H}(0)} = \hat{H}(\underline{s}) \qquad \text{(II.55)}$$

we obtain the normalized form of (II.53)

$$\hat{I}_I(\underline{s}) = \hat{I}_0(\underline{s})[\hat{G}(\underline{s}) \star \hat{G}^*(\underline{s})] = \hat{I}_0(\underline{s})\hat{H}(\underline{s}) \quad . \qquad \text{(II.56)}$$

The normalized component $\hat{I}_I(\underline{s})$ is the ratio of intensity component $\tilde{I}_I(\underline{s})$ to the uniform background intensity $\tilde{I}_I(0)$; accordingly, $\hat{H}(\underline{s})$ is called the contrast transfer function.

Equation (II.56) can be used to determine the resolution limit for incoherent images. Clearly, unlimited resolution demands

$$\left.\begin{array}{l}\hat{H}(\underline{s}) > 0 \\ \\ \hat{G}(\underline{s}) > 0\end{array}\right\} \quad \text{for all } \underline{s} \quad . \tag{II.57}$$

If, in addition, the image is to be aberration-free the constraint

$$\hat{G}(\underline{s}) = \text{constant} \tag{II.58}$$

is also required. Of course, no system with these characteristics has ever been derised. The first condition can never be realized because object details separated by less than a wavelength do not excite propagating waves. It is unlikely that the second condition will hold over more than a small angle about the axis of the imaging system (paraxial approximation) because of path length differences. More realistically, we assume that for reasonably good imaging

$$\hat{G}(\underline{s}) = \Pi\left(\frac{\underline{s}}{\underline{s}_m}\right) = \Pi\left(\frac{s_x}{s_{mx}}\right)\Pi\left(\frac{s_y}{s_{my}}\right) \tag{II.59}$$

where

$$\begin{array}{lll}\Pi(x) = 1 & & |x| < 1 \\ \\ \quad = 0 & & |x| > 1 \quad .\end{array} \tag{II.60}$$

Then

$$\hat{H}(\underline{s}) = \Lambda\left(\frac{\underline{s}}{2\underline{s}_m}\right) = \Lambda\left(\frac{s_x}{2s_{mx}}\right)\Lambda\left(\frac{s_y}{2s_{my}}\right) \quad , \tag{II.61}$$

where

$$\begin{aligned} \Lambda(x) &= 1 - |x| \qquad |x| < 1 \\ &= 0 \qquad\quad |x| > 1 \quad . \end{aligned} \tag{II.62}$$

These idealized forms for $\hat{G}(\underline{s})$ and $\hat{H}(\underline{s})$ are shown for positive spatial frequencies in Figure II.3. We see that all spatial frequency components of the object boundary intensity lying below $s = 2s_m$ are resolved in the image although the contrast near the limit $2s_m$ will be very poor and the image barely discernible against the uniform background.

The physical interpretations of Equation (II.54) is not as simple as the interpretation of Equation (II.53). Whereas incoherent imaging is linear in intensity, coherent imaging is nonlinear in intensity. Consider an object boundary field U_0 containing spatial frequency components up to $s = s_0$. The spatial frequency spectrum $\tilde{U}_0(\underline{s})$ may then be written

$$\tilde{U}_0(\underline{s}) = \tilde{U}_0'(s)\,\Pi\left(\frac{\underline{s}}{\underline{s}_0}\right) \tag{II.63}$$

where $\tilde{U}_0'$ represents the "strength" of each component. Since the zero frequency spectral component $\tilde{U}_0(0)$ may vanish, Equation (II.54) cannot be normalized in a meaningful way. Assuming again the ideal form

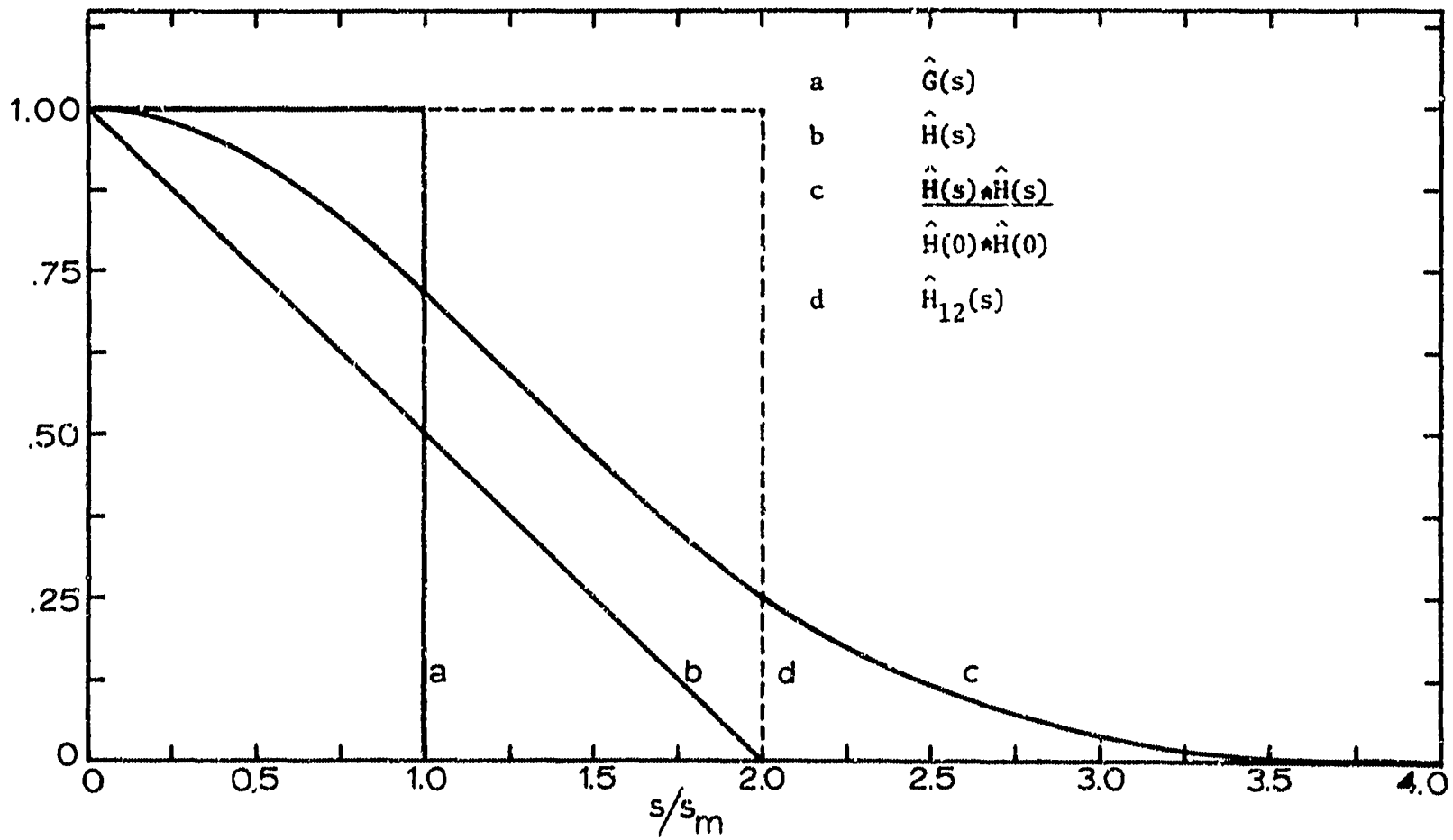

Figure II.3. Transfer of Spatial Frequencies from Object to Image

$$\tilde{G}(\underline{s}) = \tilde{G}(0)\Pi\left(\frac{\underline{s}}{\underline{s}_m}\right) \quad , \tag{II.64}$$

Equation (II.54) may be rewritten as

$$\tilde{I}_I(\underline{s}) = \left[\tilde{U}_0'(\underline{s})\Pi\left(\frac{\underline{s}}{\underline{s}_0}\right)\right] * \left[\tilde{U}_0'^{*}(\underline{s})\Pi\left(\frac{\underline{s}}{\underline{s}_0}\right)\right]|\tilde{G}(0)|^2 \qquad s_m > s_0$$

$$= \left[\tilde{U}_0'(s)\Pi\left(\frac{\underline{s}}{\underline{s}_m}\right)\right] * \left[\tilde{U}_0'^{*}(\underline{s})\Pi\left(\frac{\underline{s}}{\underline{s}_m}\right)\right]|\tilde{G}(0)|^2 \qquad s_m < s_0 \quad . \tag{II.65}$$

Relations (II.65) indicate that for spatially coherent fields the image intensity may contain spatial frequency components up to $2s_0$ when $s_m > s_0$ and up to $2s_m$ when $s_m < s_0$. However, those image components in the range $s > s_0$ in the first case and $s > s_m$ in the second case do not arise from object components lying within corresponding ranges of the object spectrum, hence do not represent resolution of object spectra above s_0 in the first case, above s_m in the second case. The spurious image spectra is simply a manifestation of the interference which occurs as the coherent field propagates from object to image. Thus, the coherent imaging law (II.54) is interpreted to mean that all spatial frequency components of the object boundary field lying below $s = s_m$ are resolved in the image.

Comparing the form of $\hat{G}(\underline{s})$ with the form of $\hat{H}(\underline{s})$ it is evident that the contrast of coherent images is greater than that of incoherent images. However, because of the interference phenomena alluded to above coherent images suffer from edge ringing, edge displacement, speckling[17], etc., effects which are not present in incoherent images.

On the basis of the preceding analysis it is sometimes claimed that the resolution of object detail through a well-corrected imaging system operating with incoherent radiation is twice the resolution of object detail through the same system operating with coherent radiation. However, this statement requires qualification. More properly, if an optical system operating with coherent radiation resolves spatial frequency components of the object boundary field less than $\underline{s} = \underline{s}_m$ then the same system operating with incoherent radiation will resolve frequency components of the object boundary intensity less than $\underline{s} = 2\underline{s}_m$. Therefore, in order that resolution be determined in a meaningful way we must distinguish between fine structure of the object boundary surface $O(\underline{r})$, fine structure of the corresponding object boundary field $U_0(\underline{r})$, and fine structure of the corresponding object boundary intensity $|U_0(\underline{r})|^2$. In most practical situations the three may be considered essentially identical. However, when operating under diffraction limited conditions the distinction is important.

Assume, for simplicity, a planar test object (lying in the xy plane) constructed such that some physical property $P(x,y)$ of the object material, for example the blackening of a photographic emulsion, varies over the object surface in a one-dimensional cosinusoidal pattern. Thus,

$$P(x,y) = P(x) = \cos 2\pi s_x x + B \qquad (11.66)$$

where s_x is the spatial frequency of the cosinusoidal variation and B is the unperturbed (quiscent) state of P. Assume further that with P may be associated some optical characteristic of the material such that

when the object is uniformly illuminated, the resulting boundary field $U_0(x,y)$ at the object surface will be proportional to P. Typically, for small variations of P about the nominal, the boundary field will assume one of the following characteristic forms. Either

$$U_0(x,y) = 2 + \cos 2\pi s_x x \tag{II.67}$$

or

$$U_0(x,y) = |\cos 2\pi s_x x| \tag{II.68}$$

or

$$U_0(x,y) = \cos 2\pi s_x x \quad . \tag{II.69}$$

Forms (II.67) and (II.68) represent objects which do not introduce phase variations into the field (non-phase objects), for example when the object is a photographic transparency or a thin metal plate. Form (II.69) represents objects which do introduce phase variations into the field (phase objects), for example a suitably designed phase grating. In many instances the object will be of type (II.67). Certainly, this is true of the acoustic targets used in the experiments detailed in Chapter V.

If the boundary field is given by (II.67) then the boundary intensity $I_0(x)$ is

$$I_0(x) = [|U_0(x)|]^2 = (2+\cos 2\pi s_x x)^2 = \tag{II.70}$$

$$\frac{9}{2} + 4 \cos 2\pi s_x x + \frac{1}{2} \cos 4\pi s_x x \quad .$$

Thus, if the physical boundary has a spatial frequency component s_x, the intensity at the boundary will have an additional component $2s_x$. However, this spatial harmonic will be only 1/8 the amplitude of the fundamental component, hence can be neglected in determining resolution. Therefore, for non-phase objects of the type (II.67) the spectral compositions of object, object field, and object intensity are substantially the same and to resolve one is to resolve the others.

If the boundary field is given by either (II.68) or (II.69) then the boundary intensity is

$$I_0(x) = \frac{1}{2} (1+ \cos 4\pi s_x x) \quad . \tag{II.71}$$

Again for non-phase objects the spectral composition of intensity and field are the same. In contrast, for phase objects the <u>intensity</u> contains the first spatial harmonic $2s_x$ plus the usual uniform background, whereas the <u>field</u> contains only the fundamental spatial frequency s_x. Thus the resolution of phase objects is different from the resolution of non-phase objects, and any statement comparing coherent and incoherent resolution must include this fact.

In acoustic imaging we shall have occasion to consider orders of the field higher than n = 2. In particular, consider U_0^4. If the boundary field is given by (II.67) then

$$[U_0(x)]^4 = \frac{227}{8} + 38 \cos 2\pi s_x x + \frac{25}{2} \cos 4\pi s_x x + 2 \cos 6\pi s_x x + \frac{1}{8} \cos 8\pi s_x x \quad . \tag{II.72}$$

If the boundary field is given by either (II.68) or (II.69) then

$$[U_0(x)]^4 = \frac{3}{8} + \frac{1}{2} \cos 4\pi s_x x + \frac{1}{4} \cos 8\pi s_x x \quad . \tag{II.73}$$

Again, phase objects are characterized by a predominance of higher order harmonics in the spatial frequency spectrum of U_0^4 whereas for non-phase objects the fundamental is still predominate. These results are compiled in Table II.1.

We can now compare coherent and incoherent resolution directly in terms of the object boundary itself. If the phase of the field does not vary across the object boundary surface (non-phase object) then, as we have shown, the spectral compositions of object, object field, and object intensity are substantially the same and incoherent resolution is indeed twice that of coherent resolution. Conversly, if the phase of the field is not constant across the object boundary surface, (phase object) then the predominate spectral component of the object intensity occurs at twice the spatial frequency of the object field. In this case incoherent resolution of object detail is no greater than that of coherent resolution of object detail. These results are compiled in Table II.2. Note however, that resolution with coherent radiation is never greater than s_m whereas resolution with incoherent radiation is never less than s_m. For this reason incoherent radiation may be of considerable utility in acoustic imaging.

TABLE II.1
Predominate Spatial Frequency Component

	Object	U_0	$U_0U_0^*$	$(U_0U_0^*)^2$
$\cos 2\pi s_x$	s_x	s_x	$2s_x$	$2s_x$
$\lvert\cos 2\pi s_x\rvert$	$2s_x$	$2s_x$	$2s_x$	$2s_x$
$2 + \cos 2\pi s_x$	s_x	s_x	s_x	s_x

TABLE II.2
Maximum Resolvable Object Spatial Frequency Component

	n=2		n=4	
	Coherent	Incoherent	Coherent	Incoherent
$\cos 2\pi s_x$	s_m	s_m	s_m	$2s_m$
$\lvert\cos 2\pi s_x\rvert$	$s_m/2$	s_m	$s_m/2$	$2s_m$
$2 + \cos 2\pi s_x$	s_m	$2s_m$	s_m	$4s_m$

6. ACOUSTIC IMAGING WITH FOURTH ORDER DETECTORS

As we have stated, the fundamental observable for acoustic radiation is instantaneous field amplitude; other observables may be synthesized electronically. An analysis of acoustic imaging based upon field intensity as the synthesized observable has just been completed. We now consider another observable

$$D(\underline{r}) = \left\langle [\Psi(\underline{r},t)]^4 \right\rangle \quad . \tag{II.74}$$

Interest in 4th order detection for imaging follows from the analysis of the preceding section wherein it was demonstrated that

resolution with spatially incoherent radiation is often greater than with spatially coherent radiation. Mathematically, improved resolution arises from the convolution $\hat{G}(\underline{s}) * \hat{G}^*(\underline{s})$ occurring in the spatial frequency transfer function. The convolution occurs because the field is spatially incoherent and because the image observable is intensity. Thus, one is naturally led to consider imaging with higher orders of the field, say the 4th order. We now inquire into the optical properties, particularly resolution of an imaging system when the observable is $\left\langle [\Psi(\underline{r},t)]^4 \right\rangle$ rather than $\left\langle [\Psi(\underline{r},t)]^2 \right\rangle$.

First, the time average of the 4th power of the field must be calculated. To do this recall that for quasi-monochromatic radiation

$$\Psi(\underline{r},t) = \mathrm{Re}\,[\xi(\underline{r},t)e^{2\pi i\bar{\nu}t}] \quad . \tag{II.75}$$

Thus

$$\Psi(\underline{r},t) = \frac{\xi(\underline{r},t)e^{2\pi i\bar{\nu}t} + \xi^*(\underline{r},t)e^{-2\pi i\bar{\nu}t}}{2} \quad . \tag{II.76}$$

Substituting (II.76) into $\left\langle [\Psi(\underline{r},t)]^4 \right\rangle$, expanding, and supressing the $\underline{r}$ and t dependence of $\xi(\underline{r},t)$ yields

$$\begin{aligned}\left\langle [\Psi(\underline{r},t)]^4 \right\rangle = &\left\langle \frac{\xi^4 e^{i8\pi\bar{\nu}t}}{16} \right\rangle + \left\langle \frac{\xi^{*4} e^{-i8\pi\bar{\nu}t}}{16} \right\rangle \\ &+ \left\langle \frac{1}{4}\xi^3\xi^* e^{i4\pi\bar{\nu}t} \right\rangle + \left\langle \frac{1}{4}\xi\xi^{*3} e^{-i4\pi\bar{\nu}t} \right\rangle \\ &+ \left\langle \frac{3}{8}\xi^2\xi^{*2} \right\rangle \quad .\end{aligned} \tag{II.77}$$

Now consider the first term (II.77). Expressing the time dependence of ξ in terms of temporal Fourier transforms and commuting time and frequency integrations we obtain

$$\left\langle \frac{\xi^4 e^{i8\pi\bar{\nu}t}}{16} \right\rangle = \lim_{T\to\infty} \left\{ \int\int\int\int_{-\infty}^{\infty} \tilde{\xi}(\nu_1)\tilde{\xi}(\nu_2)\tilde{\xi}(\nu_3)\tilde{\xi}(\nu_4) \left[\frac{1}{2T} \int_{-T}^{T} e^{2\pi i(\nu_1+\nu_2+\nu_3+\nu_4+4\underline{\nu})t} dt \right] d\nu_1 d\nu_2 d\nu_3 d\nu_4 \right\} . \tag{II.78}$$

Carrying out the time integration gives

$$\left\langle \frac{\xi^4 e^{i8\pi\bar{\nu}t}}{16} \right\rangle = \lim_{T\to\infty} \left\{ \int\int\int\int_{-\infty}^{\infty} \tilde{\xi}(\nu_1)\tilde{\xi}(\nu_2)\tilde{\xi}(\nu_3)\tilde{\xi}(\nu_4) \frac{\sin 2\pi(\nu_1+\nu_2+\nu_3+\nu_4+4\underline{\nu})T}{2\pi(\nu_1+\nu_2+\nu_3+\nu_4+4\underline{\nu})T} d\nu_1 d\nu_2 d\nu_3 d\nu_4 \right\} . \tag{II.79}$$

For quasi-monochromatic radiation (II.79) is readily evaluated. As T becomes large $\frac{\sin 2\pi(\nu_1+\nu_2+\nu_3+\nu_4+4\underline{\nu})T}{2\pi(\nu_1+\nu_2+\nu_3+\nu_4+4\underline{\nu})T}$ becomes an increasingly narrow spike centered at $\nu_1+\nu_2+\nu_3+\nu_4+4\underline{\nu} = 0$. Further, recall that for quasi-monochromatic radiation

$$\begin{aligned} \tilde{\xi}(\nu) &> 0 \qquad |\nu| < \Delta\nu \\ &= 0 \qquad |\nu| > \Delta\nu \end{aligned} \tag{II.80}$$

and $\frac{\Delta\nu}{\bar{\nu}} << 1$.

Hence, in the limit of time averages over durations 2T long compared with the mean period $1/\underline{\nu}$ of the radiation, no combination of the ν_i exists for which both the $\sin x/x$ term and all $\xi(\nu_i)$ are simultaneously non-zero. Therefore,

$$\left\langle \frac{\xi^4 e^{i8\pi\bar{\nu}t}}{16} \right\rangle = 0 \quad . \tag{II.81}$$

Similar results obtain for the second, third, and fourth terms in (II.77) leaving as the final expression for the fourth order acoustic image observable

$$\left\langle [\Psi(\underline{r},t)]^4 \right\rangle = \frac{3}{8} \left\langle [\xi(\underline{r},t)]^2 [\xi^*(\underline{r},t)]^2 \right\rangle = D(\underline{r}) \quad . \tag{II.82}$$

In passing note that by applying similar techniques we may show

$$\left\langle [\Psi(\underline{r},t)]^2 \right\rangle = \frac{1}{2} \left\langle \xi(\underline{r},t)\xi^*(\underline{r},t) \right\rangle \quad , \tag{II.83}$$

long familiar as the expression for the intensity of purely monochromatic radiation, and

$$\left\langle [\Psi(\underline{r},t)]^{2n+1} \right\rangle = 0 \quad , \tag{II.84}$$

demonstrating that time-averaged odd order acoustic image observables are not possible.

Substituting (II.82) into (II.34) and, as before, invoking commutability of time and space integrations obtain

$$D_I(\underline{r}_I) = \int\int_0\int\int G(\underline{r}_I-\underline{r}_1)G^*(\underline{r}_I-\underline{r}_2)G(\underline{r}_I-\underline{r}_3)G^*(\underline{r}_I-\underline{r}_4)$$

$$\left\langle \xi_0(\underline{r}_1,t)\xi_0^*(\underline{r}_2,t)\xi_0(\underline{r}_3,t)\xi_0^*(\underline{r}_4,t)\right\rangle d^2r_1 d^2r_2 d^2r_3 d^2r_4 \quad . \tag{II.85}$$

To proceed further the statistical properties of the optical field must be introduced. The situation for 4th order detection is more complex than for 2nd order detection because of the need in the former to consider 4th order as well as 2nd order time averages. In general, the two will not be related; i.e., $\left\langle \xi_0(\underline{r}_1,t)\xi_0^*(\underline{r}_2,t)\xi_0(\underline{r}_3,t)\xi_0^*(\underline{r}_4,t)\right\rangle$ is not related to $\left\langle \xi_0(\underline{r}_1,t)\xi_0^*(\underline{r}_2,t)\right\rangle$, and images formed according to (II.85) will provide additional information about the object region, hopefully in the form of greater resolution of object detail.

If the field is spatially incoherent then when the $\underline{r}_i$ are widely separated the time evolutions of the corresponding $\xi(\underline{r}_i,t)$ are statistically independent and the fourth order time average may be decomposed into products of second order time averages thus

$$\left\langle \xi_0(\underline{r}_i,t)\xi_0^*(\underline{r}_j,t)\xi_0(\underline{r}_k,t)\xi_0^*(\underline{r}_l,t)\right\rangle = \left\langle \xi_0(\underline{r}_i,t)\xi_0^*(\underline{r}_j,t)\right\rangle \left\langle \xi_0(\underline{r}_k,t)\xi_0^*(\underline{r}_l,t)\right\rangle , \tag{II.86}$$

or any permutation of (II.86). Beran and Parrent[25] have shown that for any radiating field

$$\left\langle \xi_0(\underline{r}_i,t)\xi_0^*(\underline{r}_j,t)\right\rangle > 0 \qquad |\underline{r}_i-\underline{r}_j| < a\lambda$$

$$= 0 \qquad |\underline{r}_i-\underline{r}_j| > a\lambda \quad , \tag{II.87}$$

meaning that as the separation between two field points becomes less than $\alpha\lambda(\alpha>1)$ the corresponding time evolutions for radiating fields must become correlated. The time average $\left\langle \xi(\underline{r}_i,t)\xi^*(\underline{r}_j,t)\right\rangle$ may be written in many different forms. For convenience we assume

$$\left\langle \xi_0(\underline{r}_i,t)\xi_0^*(\underline{r}_j,t)\right\rangle = \left\langle |\xi_0(\underline{r}_i,t)|^2\right\rangle \Pi\left(\frac{|\underline{r}_i-\underline{r}_j|}{\alpha\lambda}\right) \quad . \qquad \text{(II.88)}$$

Equations (II.86) and (II.88) are suitable expressions for the 4th order time average only when at least one of the $\underline{r}_i$ is widely separated from the other three. When <u>all</u> the $\underline{r}_i$ lie within some small distance $\beta\lambda$ of each other ($\beta\neq\alpha,\beta>1,\alpha>1$) it must then be assumed that the decomposition (II.86) is no longer valid. In this case we take

$$\left\langle \xi_0(\underline{r}_1,t)\xi_0^*(\underline{r}_2,t)\xi_0(\underline{r}_3,t)\xi_0^*(\underline{r}_4,t)\right\rangle = \qquad \text{(II.89)}$$

$$\left\langle |\xi_0(\underline{r}_1,t)|^4\right\rangle \Pi\left(\frac{|\underline{r}_2-\underline{r}_1|}{\beta\lambda}\right)\Pi\left(\frac{|\underline{r}_3-\underline{r}_1|}{\beta\lambda}\right)\Pi\left(\frac{|\underline{r}_4-\underline{r}_1|}{\beta\lambda}\right) \quad .$$

Thus, it is necessary to write the 4th order time average in different forms depending upon whether the field points are separated or clustered together.

Using Equations (II.86), (II.88), and (II.89), Equation (II.85) becomes

$$D_I(\underline{r}_I) = 2 \iiiint_0 G(\underline{r}_I-\underline{r}_1)\left[G^*(\underline{r}_I-\underline{r}_2)\Pi\left(\frac{|\underline{r}_2-\underline{r}_1|}{\alpha\lambda}\right)\right]\left\langle|\xi(\underline{r}_1,t)|^2\right\rangle \cdot$$

$$\cdot\ G(\underline{r}_I-\underline{r}_3)\left[G^*(\underline{r}_I-\underline{r}_4)\Pi\left(\frac{|\underline{r}_4-\underline{r}_3|}{\alpha\lambda}\right)\right]\left\langle|\xi_0(\underline{r}_3,t)|^2\right\rangle \cdot$$

$$\cdot\ \left[1-\Pi\left(\frac{|\underline{r}_3-\underline{r}_1|}{\beta\lambda}\right)\right]\ d^2r_1d^2r_2d^2r_3d^2r_4\ +$$

$$\iiiint_0 G(\underline{r}_I-\underline{r}_1)\left[G(\underline{r}_I-\underline{r}_3)\Pi\left(\frac{|\underline{r}_3-\underline{r}_1|}{\alpha\lambda}\right)\right]\left\langle[\xi_0(\underline{r}_1,t)]^2\right\rangle \cdot$$

$$\cdot\ G^*(\underline{r}_I-\underline{r}_2)\left[G^*(\underline{r}_I-\underline{r}_4)\Pi\left(\frac{|\underline{r}_4-\underline{r}_2|}{\alpha\lambda}\right)\right]\left\langle[\xi_0^*(\underline{r}_2,t)]^2\right\rangle \cdot \quad \text{(II.90)}$$

$$\cdot\ \left[1-\Pi\left(\frac{|\underline{r}_2-\underline{r}_1|}{\beta\lambda}\right)\right]\ d^2r_1d^2r_2d^2r_3d^2r_4\ +$$

$$\iiiint_0 G(\underline{r}_I-\underline{r}_1)\left[G^*(\underline{r}_I-\underline{r}_2)\Pi\left(\frac{|\underline{r}_2-\underline{r}_1|}{\beta\lambda}\right)\right]\ \cdot$$

$$\cdot\ \left[G(\underline{r}_I-\underline{r}_3)\Pi\left(\frac{|\underline{r}_3-\underline{r}_1|}{\beta\lambda}\right)\right]\ \cdot$$

$$\cdot\ \left[G^*(\underline{r}_I-\underline{r}_4)\Pi\left(\frac{|\underline{r}_4-\underline{r}_1|}{\beta\lambda}\right)\right]\ B_0(\underline{r}_1)\ d^2r_1d^2r_2d^2r_3d^2r_4\ .$$

Usually G varies slowly over distances $\alpha\lambda$ or $\beta\lambda$ in the object plane. Then

$$D_I(\underline{r}_I) = 2\pi^2\alpha^4\lambda^4\left[\int_O |G(\underline{r}_I-\underline{r}_O)|^2 I_O(\underline{r}_O)d^2r_O\right]^2 +$$

$$\pi^2\alpha^4\lambda^4\left|\int_O [G(\underline{r}_I-\underline{r}_O)]^2 \left\langle[\xi_O(\underline{r}_O,t)]^2\right\rangle d^2r_O\right|^2 + \qquad \text{(II.91)}$$

$$\pi^3\beta^6\lambda^6\int_O |G(\underline{r}_I-\underline{r}_O)|^4 D_O(\underline{r}_O)d^2r_O \quad .$$

Written more compactly

$$D_I(\underline{r}) = 2\left[\pi\alpha^2\lambda^2|G(\underline{r})|^2 * I_O(\underline{r})\right]^2 +$$

$$\left|\pi\alpha^2\lambda^2[G(\underline{r})]^2 * \left\langle[\xi_O(\underline{r},t)]^2\right\rangle\right|^2 + \qquad \text{(II.92)}$$

$$\pi^3\beta^6\lambda^6|G(\underline{r})|^4 * D_O(\underline{r}) \quad ,$$

the isoplanatic imaging law for spatially incoherent acoustic fields when the image observable is the output of a 4th law detector. If $D_O(\underline{r}_O)$ is statistically independent of $I_O(\underline{r}_O)$ then an image formed according to (II.92) may exhibit better resolution of object boundary detail than one formed according to (II.39).

In order to satisfy simultaneously conditions (II.88) and (II.89) it is necessary that the modulus as well as the phase of the field amplitude be random functions of time. To see this write

$$\xi(\underline{r},t) = |\xi(\underline{r},t)|e^{i\phi(\underline{r},t)} \tag{II.93}$$

where, in general, the modulus $|\xi(\underline{r},t)|$ and phase $\phi(\underline{r},t)$ are statistically independent random functions of time. Then

$$\left\langle \xi(\underline{r}_i,t)\xi^*(\underline{r}_j,t) \right\rangle = \left\langle |\xi(\underline{r}_i,t)|^2 \right\rangle \left\langle e^{i[\phi(\underline{r}_i,t)-\phi(\underline{r}_j,t)]} \right\rangle \tag{II.94}$$

and it is clear that a spatially incoherent field in the sense (II.88) can be synthesized simply by ensuring

$$\left\langle e^{i[\phi(\underline{r}_i,t)-\phi(\underline{r}_j,t)]} \right\rangle = 0 \tag{II.95}$$

which is possible if $\phi(\underline{r},t)$ is a suitably random function of time. However, if $|\xi(\underline{r},t)|$ is deterministic then D_0 and I_0 are not independent which violates condition (II.89). Therefore, in order that 4th order detection provide additional information we demand that the modules and phase of the field be statistically independent random functions of time.

Fields of this type are called <u>fluctuating</u> fields. Fluctuating fields may be synthesized by employing large arrays suitably driven or they may occur naturally as a result of turbulence and scattering in the medium interposing object and image, a common occurrence in the sea.

To test the contention that increased resolution of object boundary detail is obtained with 4th order detection take the Spatial Fourier Transform of (II.92) obtaining

$$\tilde{D}_I(\underline{s}) = 2\pi^2\alpha^4\lambda^4 \left\{\widetilde{[|G(\underline{r})|^2]}\tilde{I}_0(\underline{s})\right\} * \left\{\widetilde{[|G(\underline{r})|^2]}\tilde{I}_0(\underline{s})\right\} +$$

$$\pi^2\alpha^4\lambda^4 \left\{\widetilde{[G(\underline{r})]^2}\widetilde{\langle[\xi_0(\underline{r},t)]^2\rangle}\right\} * \left\{\widetilde{[G(\underline{r})]^2}\widetilde{\langle[\xi_0(\underline{r},t)]^2\rangle}\right\} \tag{II.96}$$

$$+ \pi^3\beta^6\lambda^6\widetilde{[|G(\underline{r})|^4]}\tilde{D}_0(\underline{s}) \quad .$$

As before the higher spatial frequency components of the first and second terms in (II.96) do not represent increased resolution of the object. However, the third term presents interesting posibilities.

With no loss of generality assume $\tilde{G}(\underline{s}) = \tilde{G}(-\underline{s})$. Then

$$\widetilde{|G(\underline{r})|^4} = \tilde{G}(\underline{s}) * \tilde{G}(\underline{s}) * \tilde{G}(\underline{s}) * \tilde{G}(\underline{s}) \quad . \tag{II.97}$$

Computation of the four-fold convolution yields

$$\widetilde{|\hat{G}(\underline{r})|^4} = \left(\frac{16}{3}s_{mx}^3 \pm \frac{s_x^3}{2} - 2s_{mx}s_x^2\right) \cdot \left(\frac{16}{3}s_{my}^3 \pm \frac{s_y^3}{2} - 2s_{my}s_y^2\right) \qquad -2s_m < s_x, s_y < 2s_m$$

$$= \left(\frac{32}{3}s_{mx}^3 \mp \frac{s_x^3}{6} + 2s_{mx}s_x^2 \mp 8s_{mx}^2 s_x\right) \cdot \left(\frac{32}{3}s_{my}^3 \mp \frac{s_y^3}{6} + 2s_{my}s_y^2 \mp 8s_{my}^2 s_y\right) \qquad 2s_m < |s_x|, |s_y| < 4s_m \tag{II.98}$$

which is plotted normalized in Figure II.3. Note that the spatial spectrum of $\widetilde{|G(\underline{r})|^4}$ extends over a range four times broader than that of $\tilde{G}(\underline{s})$.

Referring to Table II.1 it is apparent that for non-phase objects, spatial frequency $\underline{s}_0$, the predominant spatial frequency component in $U_0^4(\underline{r})$ is also $\underline{s}_0$, although spatial harmonics through the third order will be present as well. Maximization of object resolution does not require the total spatial spectrum of U_0^4 be imaged, only the spectrum of the object boundary itself. Therefore, if the object boundary component $\underline{s}_0$ in U_0^4 is transferred to the image and is not lost in the background noise then the corresponding object boundary detail will be resolved. Thus, in principle the resolution of any optical system operating with 4th law detectors and spatially incoherent fluctuating fields may be greater than the same system operating with coherent radiation.

Since only the $\widetilde{|G(\underline{r})|^4}$ term in Equation (II.92) provides useful imaging it is desirable to eliminate the other two. In principle this may be accomplished simply by subtraction. Even so, the $\widetilde{|G(\underline{r})|^4}$ term cannot be too small or else it will be buried in the noise. An approximate worst case evaluation of the relative size of the terms can be found by comparing contributions to the uniform background. Straightforward calculation gives the ratio of contributions to the uniform background from the first and third terms of (II.98) as approximately

$$\frac{2\pi^2\alpha^4\lambda^4 \left\{ \left[\widetilde{|G(\underline{r})|^2}\, \tilde{I}_0(\underline{s}) \right] * \left[\widetilde{|G(\underline{r})|^2}\, \tilde{I}_0(\underline{s}) \right] \right\}\Big|_{\underline{s}=0}}{\pi^3\beta^6\lambda^6 \left\{ \widetilde{|G(\underline{r})|^4}\, D_0^4 \right\}\Big|_{s=0}} = \frac{\pi\beta^6}{18\gamma^2\alpha^4} \qquad \text{(II.99)}$$

where $s_{mx} = s_{my} = 1/\gamma\lambda$, $\gamma > 1$. It should be possible to arrange the field statistics (α and β) so that (II.99) is of the order 10^{-1} to 1 for typical γ's. It may be that the desired effect will be too small to be readily applicable to real time imaging systems. However, 4th order detection could be useful for seismic investigations, such as fault location, where real time imaging is of little value.

In order to understand physically why resolution of object boundary detail should depend upon field statistics we must distinguish between resolution and total quantity of information transferred from object space to image space. The two are not necessarily the same[27]. The general imaging process involves information transfer from an object to some optical representation of that object via a field which is not completely deterministic. The information is transmitted as spatial variations of the modulus and phase of the optical field amplitude; and is received, in the case of real time visible imaging, by some device which senses only time averages of various functions of the optical field. Because of the time averaging characteristic of the receiver the phase information will be lost, except for those situations outlined in the following paragraph, and complete reconstruction of the object scene is impossible. However, resolution of a boundary detail in the detected optical image requires merely that some intensity pattern in the image can be isolated and uniquely associated with a corresponding boundary detail of the object. In principle, the phase of the field is of no consequence except to enhance contrast, in the case of spatially coherent fields. Thus, resolution does not require the entire information carried by the optical field.

For convenience we have classified optical fields into two rather broad categories based upon idealized statistical properties; spatially coherent and spatially incoherent fields, clearly special cases of the more general partially coherent field. These categories are useful because of their markedly different behavior under time averaging. Either class of field contains phase and amplitude information. However, because of the long response time of the detection process all phase information will be averaged out unless interference situations (such as holography) can be arranged. Interference with coherent radiation is easily arranged; interference with incoherent radiation entails considerable difficulty[28,29]. Nevertheless, since resolution does not require phase information we cannot conclude that the resolution of incoherent systems should be less than of coherent systems.

The question remains, why can incoherent resolution be <u>greater</u> than coherent resolution? The answer is that whereas the phase and amplitude relation between object points coherently illuminated is independent of time, the phase and amplitude relation between points incoherently illuminated is a random function of time and position. Thus, for incoherent radiation the detector output is a composite or ensemble over many of the possible illuminated configurations of the object and we may expect that time averaging will provide additional information, possibly in the form of enhanced spatial resolution of object detail. For coherent radiation spatial coherence severely restricts the number of illuminated configurations contained in any time average; hence no new information is obtained. Clearly, the

averaging time must be long compared with the mean time between random fluctuations of the field parameters or else the detected incoherent field will appear as if it were a coherent field. We expect that there is a relation between resolution and averaging time for any specified statistical behavior of the field. This relation could be of use in acoustic imaging.

7. TWO POINT RESOLUTION

The resolution comparisons given in Sections 5 and 6 are mathematical concepts based upon transformation of an object spatial frequency spectrum into an image spatial frequency spectrum. Resolution was compared strictly in terms of the cutoff frequency of the transfer function without regard for its shape. Although in principle the eye should be able to resolve to the limit of the transfer function, because of noise and because of the physiological processes involved in vision there is no guarantee that this will ever be possible. Thus a more appropriate test of an optical system is based upon the ability of the eye to resolve object detail in the image. It is obvious that contrast, hence the shape of the transfer function, must play an important role in determining visual perception of an image. However, since visual perception is a subjective concept it is not amenable to precise calculation. The best we can do is construct mathematical models which approximate the process by which the eye recognizes object detail as being distinct.

One such criteria is the Sparrow two point resolution condition[30]. Consider two idealized point sources symmetrically disposed about the

origin along the x' axis and separated by distance 2a. By the Sparrow criterion, the images of two such points will be considered distinct (resolved) when the separation 2a between object points is such that

$$\left.\frac{\partial^2 I_I(x)}{\partial x^2}\right|_{x=0} = 0 \quad . \tag{II.100}$$

We first apply (II.100) to square law detection of incoherent radiation. For simplicity consider line sources parallel to the y' axis rather than point sources. Then we have

$$\begin{aligned} I_I(x) &= |G(x)|^2 * I_0(x) \\ I_0(x') &= \delta(x'-a) + \delta(x'+a) \end{aligned} \tag{II.101}$$

and desire that separation for which

$$\begin{aligned} \left.\frac{\partial^2 I_I}{\partial x^2}\right|_{x=0} &= \left\{\frac{\partial^2}{\partial x^2}\int_0 |G(x-x')|^2 I_0(x')dx'\right\}\Bigg|_{x=0} \\ &= \int_0 \left.\frac{\partial^2 |G(x-x')|^2}{\partial^2(x-x')} I_0(x')dx'\right|_{x=0} = 0 \quad . \end{aligned} \tag{II.102}$$

Calculation of (II.115) is facilitated by using the identity

$$f(x) = \tilde{\underbrace{f(s)}} \tag{II.103}$$

whence after some manipulation

$$\left.\frac{\partial^2 I_I}{\partial x^2}\right|_{x=0} = \left\{\tilde{I}_0(s)\,\widetilde{\frac{\partial^2 |G(x)|^2}{\partial^2 x}}\right\}\Big|_{x=0} = \tag{II.104}$$

$$\tilde{H}(0)\int_{-\infty}^{\infty}(e^{2\pi isa}+e^{-2\pi isa})\,(2\pi is)^2\,\hat{H}(s)\,ds = 0 \quad .$$

Substituting

$$\hat{H}(s) = \left(1+\frac{s}{s_m}\right)\Pi\left(1+\frac{s}{s_m}\right) + \left(1-\frac{s}{s_m}\right)\Pi\left(1-\frac{s}{s_m}\right) \tag{II.105}$$

into (II.104) yields the following condition upon the spacing of incoherent line sources if they are to be resolved by square law detectors according to the Sparrow criterion;

$$(3-8\pi^2a^2s_m^2)\cos 4\pi as_m + 8\pi as_m \sin 4\pi as_m = 3 \quad . \tag{II.106}$$

It is relatively simple to find a numerical solution to (II.106). We obtain the minimum spacing for Sparrow resolution as

$$2a = \frac{.415}{s_m} = \frac{.83}{2s_m} = \frac{2.61}{\pi(2s_m)} \quad . \tag{II.107}$$

If the radiation is coherent then

$$I_I(x) = |U_0(x) * G(x)|^2 \quad ,$$

$$U_0(x') = \delta(x'-a) + \delta(x'+a) \quad . \tag{II.108}$$

Employing methods similar to those used to obtain (II.104) gives

$$\left.\frac{\partial^2 I}{\partial x^2}\right|_{x=0} = 2\mathrm{Re}\left[\left(U_0^* \frac{\partial^2 G}{\partial x^2}\right)\left(U_0^* * G^*\right)\right]_{x=0} +$$

$$2\left|U_0^* \frac{\partial^2 G}{\partial x^2}\right|^2_{x=0} =$$

$$2\mathrm{Re}\left\{\int\int_{-\infty}^{\infty} (e^{2\pi i a s'} + e^{-2\pi i a s'})(2\pi i s')^2 \tilde{G}(s') \cdot \right.$$

$$\left. \cdot\, [e^{2\pi i a(s-s')} + e^{-2\pi i a(s-s')}]\tilde{G}^*(s-s')\,ds\,ds'\right\} - \qquad \text{(II.109)}$$

$$2\left\{\int\int_{-\infty}^{\infty} (e^{2\pi i a s'} + e^{-2\pi i a s'})(2\pi i s')\tilde{G}(s') \cdot \right.$$

$$\left. \cdot\, [e^{2\pi i a(s-s')} + e^{-2\pi i a(s-s')}]2\pi i(s-s')\tilde{G}^*(s-s')\,ds\,ds'\right\} = 0$$

assuming $\tilde{G}(s) = \tilde{G}(-s)$. Substituting

$$G(s) = \Pi\left(\frac{s}{s_m}\right) \qquad \text{(II.110)}$$

into (II.109) yields the following condition upon the spacing of coherent line sources if they are to be resolved by square law detectors according to the Sparrow criterion;

$$4\pi s_m a \cos 2\pi s_m a + [(2\pi s_m a)^2 - 2] \sin 2\pi s_m a = 0 \quad . \qquad \text{(II.111)}$$

The minimum spacing for Sparrow resolution is then

$$2a = \frac{.65}{s_m} = \frac{4.16}{\pi(2s_m)} \quad . \tag{II.112}$$

For 4th order detection of fluctuating incoherent radiation

$$D_I(x) = D_0(x) * |G(x)|^4$$

$$D_0(x') = \delta(x'-a) + \delta(x'+a) \tag{II.113}$$

and the Sparrow resolution condition then becomes

$$\left.\frac{\partial^2 D_I}{\partial x^2}\right|_{x=0} = \left\{\tilde{D}_0(s)\ \widetilde{\frac{\partial^2 |G(x)|^4}{\partial x^2}}\right\}_{x=0} = 0 \quad . \tag{II.114}$$

Substituting

$$\widetilde{|G(x)|^4} = \frac{1}{t^2}\left(\frac{4}{3}t^3 + \frac{s^3}{6} + ts^2 - 2t^2 s\right) \qquad \begin{matrix} -2t < s < t \\ t < s < 2t \end{matrix}$$

$$= \frac{1}{t^2}\left(\frac{2t^3}{3} + \frac{s^3}{2} - ts^2\right) \qquad \begin{matrix} -t < s < 0 \\ 0 < s < t \end{matrix} \tag{II.115}$$

where $t = 2s_m$ into (II.114) yields the following condition upon the spacing of incoherent, fluctuating line sources if they are to be resolved by 4th order detectors according to the Sparrow criterion;

$$\cos 4\pi a\,[2(2\pi a)^2-10] + \cos 2\pi a\,[40-2(2\pi a)^2]$$

$$+ \sin 4\pi a\,[8(2\pi a)^5 - 8(2\pi a) - 4(2\pi a)^2] + \qquad \text{(II.116)}$$

$$\sin 2\pi a\,[-(2\pi a)^5 + (2\pi a)^4 + 16(2\pi a)] = 40 \quad .$$

The minimum spacing for Sparrow resolution is then

$$2a = \frac{.22}{s_m} = \frac{1.38}{\pi(2s_m)} \quad . \qquad \text{(II.117)}$$

We summarize the results of this and the preceding sections for non-phase objects in Table II.3.

TABLE II.3

	rms for cutoff	Sparrow res.
coherent, 2nd order	s_m	$0.66/s_m$
incoherent, 2nd order	$2s_m$	$0.41/s_m$
incoherent, 4th order	$4s_m$	$0.23/s_m$

These results agree with intuitive concepts of the relation between shape of the transfer function and corresponding Sparrow resolution. For a given cutoff frequency the Sparrow resolution is improved by making the transfer function uniform across the spatial frequency spectrum.

8. REALIZABILITY

a. Averaging Time

A few comments of practical import are in order. A fluctuating field will exhibit properties characteristic of spatial incoherence only if the detector averages over times 2T much longer than the mean time $\Delta\tau$ between fluctuations of the field. For a signal of bandwidth $\Delta\nu$

$$2T >> \Delta\tau \approx \frac{1}{\Delta\nu} \quad . \tag{II.118}$$

Conversely, real time imaging demands that a certain minimum number N of frames be formed per unit time. Thus

$$2T \leq \frac{1}{N} \qquad \text{or} \qquad \Delta\nu >> N \quad . \tag{II.119}$$

For acoustic imaging at the standard television frame rate (N = 30 frames/sec) the required bandwidth is $\Delta\nu >> 30$ Hz, probably $\Delta\nu = 300$ Hz is sufficient. However, for this bandwidth the monochromatic length is reduced (5 meters for $\bar{\nu} = 1$ MHz) hence the validity of the monochromatic assumption must be reexamined for imaging over long ranges.

b. Space Bandwidth Theorem

In the preceeding analysis image quality was presumed limited only by the Green's function for transformation of wave fields from object space into image space. Resolution and size of the detector was assumed not to affect image quality. Such systems are termed diffraction limited. We now consider the constraints which must

be imposed upon the detector in order that the system may properly be considered as diffraction limited. This is of particular importance in acoustic imaging because the wavelength/aperture ratio is large.

The constraint is known as the space bandwidth theorem, a statement of the conservation of the space bandwidth product (SBP). The SBP of any optical field or functional of the field is simply the product of its maximum spatial extent and maximum spatial frequency in any plane of interest. Clearly, the SBP characteristic of any detector must be related to the SBP of the optical fields which are to be detected.

The conservation of SBP between detected field and detector is simply a consequence of the scaling properties of Fourier Transform pairs; i.e., if

$$A(x) = \tilde{A}(s) \tag{II.120}$$

then

$$A(ax) = \frac{1}{a}\tilde{A}\left(\frac{s}{a}\right) \quad . \tag{II.121}$$

If A extends only over a spatial range $|x| < x_m$ and $\tilde{A}$ only over a spatial frequency range $|s| < s_m$ then the SBP of A(x) is $x_m s_m$. If the detector extends over a spatial range $|x| < x_d$ and can resolve over spatial frequency range $|s| < s_d$ then, in principle, if $x_d s_d \geq x_m s_m$ the field can be accommodated to the detector by use of an ideal magnifier.

Heretofore, it was assumed that the optical system was space-invariant. However, in order to calculate the field of view of any instrument, it is obvious that a space-invariant formulation is not useful since such assumptions imply unrestricted field of view. Thus we must reformulate certain parts of the preceding theory to account for the finite field of view of the instrument. In general for a space-variant optical system

$$\xi_I(\underline{r}_I) = \int_0 G(\underline{r}_I,\underline{r}_0)\xi_0(\underline{r}_0)d^2r_0. \tag{II.122}$$

For each position $\underline{r}_0$, $G(\underline{r}_I,\underline{r}_0)$ may be written as a function or $\underline{r}_I-\underline{r}_0$, see Figure II.4 , but this functional dependence will vary with $\underline{r}_0$. We denote this condition be written

$$G(\underline{r}_I,\underline{r}_0) = G(\underline{r}_I-\underline{r}_0;\underline{r}_0) \tag{II.123}$$

as the Green's function for a space-variant optical system.

In all practical situations, especially in acoustic imaging, the Green's function will vary continuously across the object, becoming less symmetrical in $\underline{r}_I-\underline{r}_0$ near the extremes of the field of view. Restricting attention to those systems which have been stepped down so that the Green's function does not vary across the field of view then

$$G(\underline{r}_I-\underline{r}_0;\underline{r}_0) = G(\underline{r}_I-\underline{r}_0)\Pi\left(\frac{\underline{r}_0}{\underline{r}_f}\right) \tag{II.124}$$

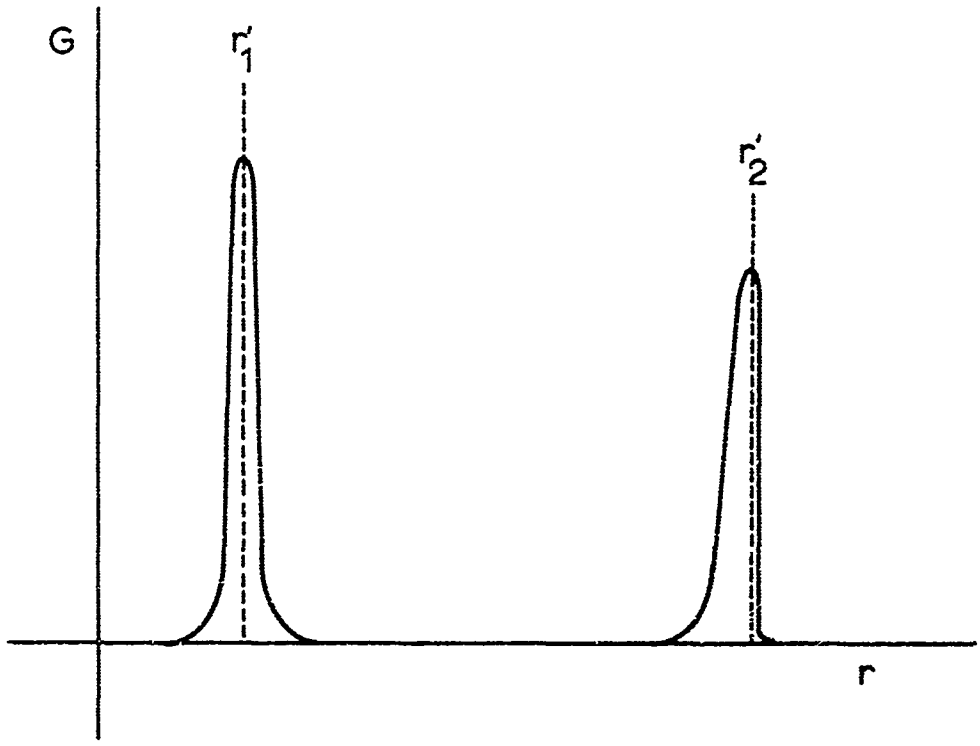

Figure II.4 G(r';r-r') Versus (r-r')

r_1' Object point in center of field

r_2' Object point near edge of field

where $\underline{r}_f$ denotes the edge of the field of view. Substituting (II.124) into (II.122) gives for the image

$$\xi_I(\underline{r}_I) = \int_0 G(\underline{r}_I - \underline{r}_0)\left[\Pi\left(\frac{\underline{r}_0}{\underline{r}_f}\right)\xi_0(\underline{r}_0)\right]d^2r_0 \qquad \text{(II.125)}$$

which is in the same form as the unlimited field of view case except that the original object field $\xi_0(\underline{r}_0)$ must be replaced with an equivalent space limited object field $\left[\Pi\left(\frac{\underline{r}_0}{\underline{r}_f}\right)\xi_0(\underline{r}_0)\right]$.

The relations for incoherent imaging then become

$$I_I(\underline{r}) = |G(\underline{r})|^2 * \left[\Pi\left(\frac{\underline{r}}{\underline{r}_f}\right) I_0(\underline{r})\right] \qquad \text{(II.126)}$$

and

$$\hat{I}_I(\underline{s}) = \hat{H}(\underline{s})\left[\hat{I}_0(\underline{s}) * \left(\frac{\sin 2\pi s_x r_{fx}}{2\pi s_x}\right)\left(\frac{\sin 2\pi s_y r_{fy}}{2\pi s_y}\right)\right] . \qquad \text{(II.127)}$$

For coherent imaging

$$I_I(\underline{r}) = \left| G(\underline{r}) * \left[\Pi\left(\frac{\underline{r}}{\underline{r}_f}\right) U_0(\underline{r})\right]\right|^2 \qquad \text{(II.128)}$$

and

$$\tilde{I}_I(\underline{s}) = \left\{\tilde{G}(\underline{s})\left[\tilde{U}_0(\underline{s}) * \left(\frac{\sin 2\pi s_x r_{fx}}{2\pi s_x}\right)\left(\frac{\sin 2\pi s_y r_{fy}}{2\pi s_y}\right)\right]\right\} * \left\{\tilde{G}^*(\underline{s})\left[\tilde{U}_0^*(\underline{s}) * \left(\frac{\sin 2\pi s_x r_{fx}}{2\pi s_x}\right)\left(\frac{\sin 2\pi s_y r_{fy}}{2\pi s_y}\right)\right]\right\} . \qquad \text{(II.129)}$$

Consider first incoherent imaging. The Green's function is such that

$$G(\underline{r}_I - \underline{r}_0) > 0 \qquad |\underline{r}_I - \underline{r}_0| < r_g$$
$$= 0 \qquad \text{otherwise} \qquad . \qquad \text{(II.130)}$$

For conventional lenses r_g is the spot size. From (II.126) it is then clear that the image intensity extends over an area $(r_{gx}+r_{fx})(r_{gy}+r_{fy})$ in the image plane. From (II.127) it follows that the maximum spatial frequency component in the image intensity is $2s_m$ since

$$\hat{H}(\underline{s}) = \Lambda\left(\frac{\underline{s}}{2\underline{s}_m}\right) \quad . \qquad \text{(II.131)}$$

Thus, the space bandwidth product of the image intensity is

$$SBP = 4s_{mx}s_{my}(r_{gx}+r_{fx})(r_{gy}+r_{fy}) \qquad \text{(II.132)}$$

and in order that the image be diffraction limited the detector area XY and resolution S_x and S_y must be such that

$$XYS_xS_y \geq 4s_{mx}s_{my}(r_{gx}+r_{fx})(r_{gy}+r_{fy}) \quad . \qquad \text{(II.133)}$$

For coherent imaging similar considerations lead to

$$XYS_xS_y \geq 2s_{mx}s_{my}(r_{gx}+r_{fx})(r_{gy}+r_{fy}) \qquad \text{(II.134)}$$

as the condition upon the detector in order that the imaging be diffraction limited.

To reduce that space bandwidth expressions further requires that the type of imaging system be known. For example, for a well

corrected lens of large aperture $r_g << r_f$ and to good approximation (II.134) reduces to

$$XYS_xS_y \geq 2s_{mx}s_{my}r_{fx}r_{fy} \quad . \tag{II.135}$$

On the other hand, this assumption may not be valid for holographic systems, particularly acoustic systems, hence the full expression (II.134) must be retained. In Chapter IV the space bandwidth theorem appropriate for acoustic holograms is discussed.

3. IMAGING WITH NONLINEAR ANTENNAS

In the preceeding we have considered imaging systems in which the field scattered from an object scene is imaged by passing through a suitable focusing aperture. An alternative scheme is to collect the field scattered from the object scene by a highly directional antenna, scanning the object scene with this antenna to map out the object scene. Various configurations have been devised for producing a narrow antenna receiving pattern. Of special interest in this connection are the nonlinear antennas, in particular the Covington-Drane antenna[20,53]. Because instantaneous pressure amplitude can be an acoustic observable the Covington-Drane antenna is readily adapted to acoustic imaging.

Consider two receiving antennas, not necessarily identical, which respond to instantaneous field amptlitude. The complex instantaneous voltage output E for the two antennas may be written

$$E_{1,2}(\underline{r}_I,t) = \int_0 \xi(\underline{r}_O,t)G_{1,2}(\underline{r}_I,\underline{r}_O)d^2r_O \tag{II.136}$$

under the same assumptions of temporal behavior as before. The antenna patterns $G_{1,2}$ are measured with respect to a common coordinate system and ξ_0 is the object boundary field distribution.

If the instantaneous outputs of the two antennas are multiplied and a long time average is taken of the resulting instantaneous product we obtain, assuming spatial stationarity,

$$\left\langle E_1(\underline{r}_I,t)E_2^*(\underline{r}_I,t)\right\rangle = \int_0\int\left\langle \xi_0(\underline{r}_0,t)\xi_0^*(\underline{r}_0',t)\right\rangle \cdot \tag{II.137}$$

$$\cdot G_1(\underline{r}_I-\underline{r}_0)G_2^*(\underline{r}_I-\underline{r}_0')d^2r_0 d^2r_0' \quad .$$

As we have already shown if the fields are illuminated with spatially incoherent radiation then

$$\left\langle \xi_0(\underline{r}_0,t)\xi_0^*(\underline{r}_0',t)\right\rangle = \delta(\underline{r}_0-\underline{r}_0')I_0(\underline{r}_0) \tag{II.138}$$

and we may write for the combined antenna outputs

$$\left\langle E_1(\underline{r}_I,t)E_2^*(\underline{r}_I,t)\right\rangle = \int_0 I_0(\underline{r}_0)G_1(\underline{r}_I-\underline{r}_0)G_2^*(\underline{r}_I-\underline{r}_0)d^2r_0 \quad . \tag{II.139}$$

Taking the Spatial Fourier Transform of (II.139) we obtain

$$\widetilde{\left\langle E_1(\underline{r}_I,t)E_2^*(\underline{r}_I,t)\right\rangle} = \tilde{I}_0(\underline{s})\left[\tilde{G}_1(\underline{s})*\tilde{G}_2^*(\underline{s})\right] \quad . \tag{II.140}$$

For convenience degine an equivalent spatial frequency transfer function $\tilde{H}_{12}(\underline{s})$ for the composite system as

$$\tilde{H}_{12}(\underline{s}) = \tilde{G}_1(\underline{s}) * \tilde{G}_2^*(\underline{s}) \quad . \tag{II.141}$$

Then it is clear that (II.140) is of the same form as (II.53), the corresponding relation for conventional incoherent imaging with square law detectors, except that whereas $\tilde{H}(\underline{s})$ is an autoconvolution $\tilde{H}_{12}(\underline{s})$ is a crossconvolution. This is an important distinction because one has considerably more latitude in the choice of forms for crossconvolutions than for auto convolutions. For example, the Covington-Drane antenna consists of a two element interferometer and a uniform array of equal length placed end to end. If a uniform array as large as the combination has a response

$$\tilde{G}(\underline{s}) = \Pi(s/s_m) \tag{II.142}$$

then the response of the Covington-Drane system can be shown to be

$$\hat{H}_{12}(s) = \tilde{H}_{12}(s)/\tilde{H}_{12}(0) = \Pi(s/2s_m) \tag{II.143}$$

which is plotted in Figure (II.3).

Many other responses can be synthesized by proper choice of G_1 and G_2. The important point here is to note that since amplitude is an acoustic observable, the use of incoherent acoustic radiation allows one to cascade responses in a way which provides considerable flexibility in the composite system response. The cascading is somewhat different than usually found in linear or optical systems because

it is in parallel rather than series. It may prove fruitful to apply this concept to imaging with more conventional devices such as lenses.

10. SUMMARY

The most serious barrier to useful acoustic imaging is the need for physically enormous apertures. It is difficult to secure acoustic detectors and focusing elements in the large sizes required for these apertures. Moreover, the ideal acoustic detector should be in a form analogous to photographic film. Such detectors have not yet been developed. Thus, maximizing image quality and resolution for a given aperture size is of primary importance in the design of acoustic imaging systems.

In this chapter we have considered the effect of field statistics and detector characteristics upon image resolution and contrast. Considerations of this type are particularly important because the choice of field statistics and concomitant detection process is the first step in the design of an imaging system. (Until the advent of the laser there was usually no choice for optical systems.) We have shown that for acoustic imaging there may be advantage to spatially incoherent fields over coherent fields if diffraction limited performance for acoustic lenses and mirrors can be achieved.* Until experimental investigation of incoherent acoustic imaging systems is carried out it

---

* It remains to be determined whether achieving diffraction limited performance is primarily a design or primarly a fabrication problem.

is premature to conclude that holography is the "best" technique for acoustic imaging. It may be that hybrid systems combining conventional focusing devices such as lenses with holographic techniques (for example the stereoscopic method of McCrickerd and George[13]) are optimum.

CHAPTER III

CHARACTERISTICS OF ACOUSTIC IMAGING

1. INTRODUCTION

In the preceding chapter certain basic properties of a general scalar imaging system were formulated; acoustic imaging was classified as involving acoustic rather than visible "illumination" of the object scene. Before investigating how a practical acoustic imaging system might be devised, certain peculiarities of acoustic wave propagation which significantly effect the quality of acoustic images should be considered. In Chapters IV and V details of a particular acoustic imaging scheme will be presented.

2. THE "HIGH-LIGHT" PROBLEM

Mathematically, assuming that scalar wave theory provides valid representation of the fields, and for the moment neglecting attenuation, the only difference between acoustic and visible electromagnetic radiation is the wavelength $\lambda = c/f$ where f is the frequency and c is the velocity of wave propagation. Typically, acoustic propagation velocities range between 200 m/sec (chlorine gas at standard temperature and pressure) and 6000 m/sec (quartz), acoustic frequencies between 20 Hz and 10 GHz[31]. Thus, acoustic wavelengths approach those of light at the extreme upper range of the acoustic spectrum. However, because of absorption due to viscous damping and other intermolecular effects, long range acoustic imaging of undersea objects is restricted to radiation at frequencies less than 1 MHz, (see Section 8), hence to

wavelengths greater than 1.5 mm; i.e., approximately 3×10^3 longer than visible wavelengths.

The significance of the restriction to relatively long wavelengths for acoustic imaging is that, in many situations of practical importance, the wavelength cannot be assumed small with respect to characteristic dimensions (such as the standard deviation of surface irregularities) of the object surface texture. Thus, most objects must be considered acoustically "smooth" even though they are visually "rough." This relation is the cause of an effect known to illumination engineers and commercial photographers as "high-lighting" and has profound influence upon the quality of acoustic images. When viewed by acoustic imaging most objects will appear as diffracted highlights rather than extended figures.

All object surfaces may be classified according to the following characteristic forms:

1. smooth (curved or planar)
2. multifaceted
3. rough.

Description of the surface texture as either rough or smooth is a convenient categorization of the texture microstructure relative to the wavelength of illumination under which the surface is viewed. However, when referring specifically to the concomitant reflecting properties of a given surface texture it is more customary to speak of either "diffuse" or "specular" reflection, the former to be associated somehow with rough surfaces, the latter with smooth surfaces.

3. THE CURVED, SMOOTH SURFACE

The degree to which an object will be highlighted depends on the reflecting properties of the object surface, and the spatial and temporal structure of the illumination. A simple example will serve to demonstrate the severity of highlighting in acoustic imaging. Consider the problem of viewing through a small aperture (width 2a centered at the origin y, z = 0) a specularly reflecting cylindrical surface (radius r centered at y = 0, z = d) illuminated by a monochromatic plane wave traveling in the z direction. An elementary analysis assuming geometrical optics will show that the extremal rays which pass through the aperture emanate from a very small patch (highlight) on the object.

Referring to Figure III.1, one finds the following relation for the extremal rays.

$$-r = -a \sin\phi - d\cos\phi + \cos\phi\sqrt{a^2+d^2+r^2-2ar\sin\phi-2dr\cos\phi}\quad , \tag{III.1}$$

which is valid providing $r \gg \lambda$. Assuming the paraxial approximations

$$\sin\phi \cong \phi,\ \cos\phi \cong 1,\ d \gg a \tag{III.2}$$

we obtain

$$\phi = \frac{1}{2}\ \frac{a}{d}\quad , \tag{III.3}$$

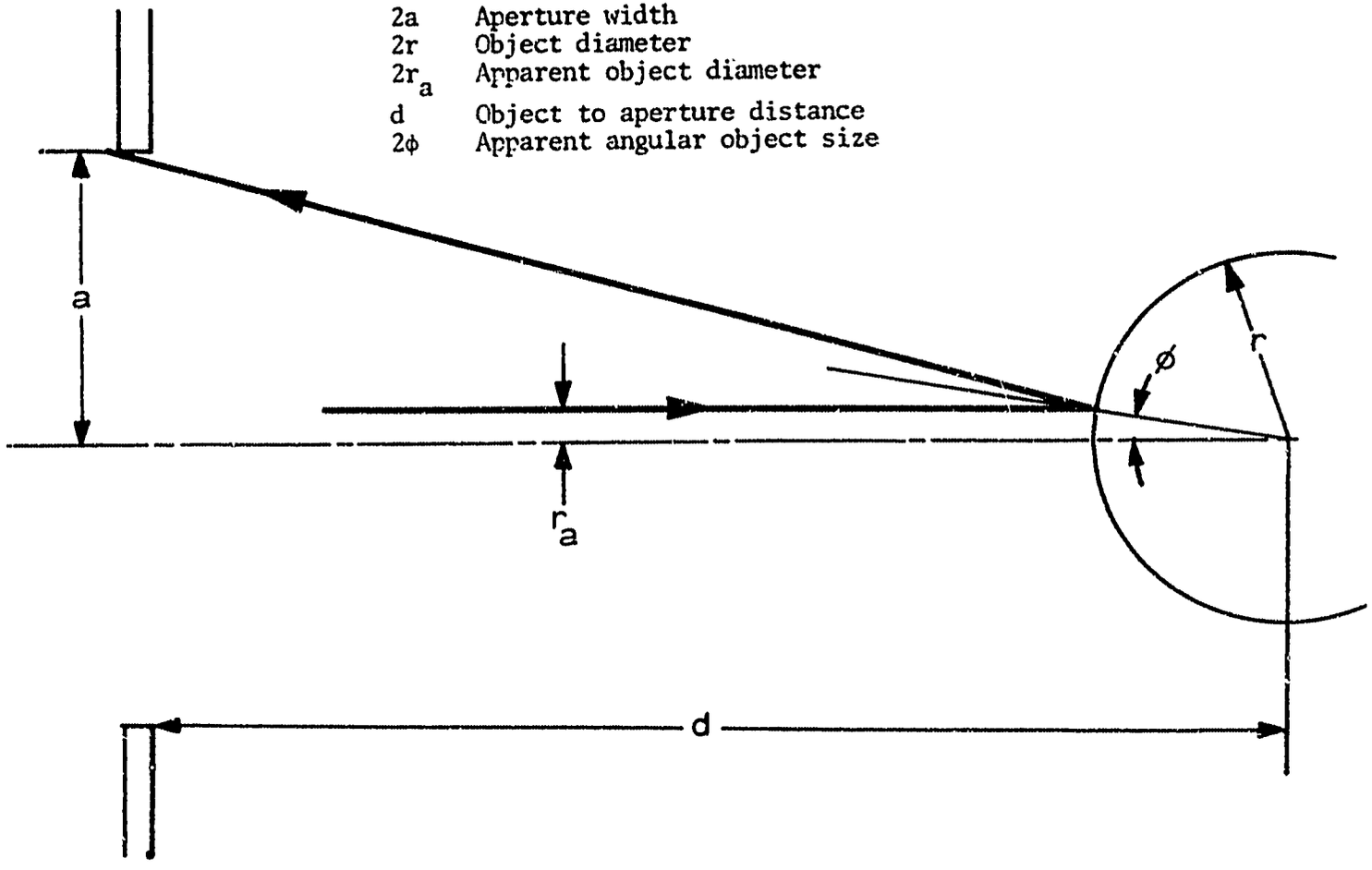

Figure III.1. Highlight of a Curved Surface

which is also the ratio of apparent diameter $2r_a$ to actual diameter 2r. Note that the highlight ratio is independent of object curvature, simply a consequence of the geometry. Equation (III.3) is accurate to within - 20% even when $d \cong a$. It is also a simple matter to show that the power density P received from a highlight is

$$P \propto \frac{r^2}{d^2} \qquad \text{(III.4)}$$

as expected.

It is apparent from (III.3) that the highlight ratio will be very small unless the aperture is enormous. In Chapter V we present the results of an experiment which dramatically illustrates the severity of highlighting in acoustic imaging and verifies Equation (III.3).

The problem imposed by highlighting may be considered from a different point of view. In principle, even though objects appear as highlights, object size can nevertheless be determined approximately from highlight size provided range d is known; range can be determined by range gating or by using the focusing characteristics of holograms or lenses. For example, such techniques might be useful for measuring size distributions of a species of fish. However, the range over which such techniques are effective is severely reduced due to highlighting.

According to the Rayleigh theory the angular resolution of an apperture of width 2a is

$$\phi_r = \frac{.61\lambda}{a} \quad . \qquad \text{(III.5)}$$

Thus, beyond a distance d',

$$d' = a\sqrt{\frac{r}{.61\lambda}} \quad , \tag{III.6}$$

it will not be possible to determine object diameters less than r by spatial measurements and it will be necessary to resort to intensity measurements (Equation III.4). Conversely, if the entire object disk were visible the corresponding maximum distance of resolution would be

$$d = \frac{2ra}{.61\lambda} \quad , \tag{III.7}$$

and

$$\frac{d'}{d} = \frac{1}{2}\sqrt{\frac{.61\lambda}{r}} \quad . \tag{III.8}$$

From (III.8) it is clear that the effective spatial resolution of highlighted objects is much less than the Rayleigh limit.

4. THE PLANAR, SMOOTH SURFACE

From the preceding discussion it is clear that satisfactory acoustic imaging of curved surfaces is difficult to obtain. As we shall now show planar objects present somewhat different although equally difficult imaging problems. Whereas at least to first order, the hignlighting of a curved surface is independent of its transverse position relative to the axis of aperture, the transverse position of a planar object is critical. Consider the situation depicted in Figure III.2 showing a planar object (width 2b) parallel to but offset f from an aperture

2a Aperture width
2b Object width
f Transverse offset of object
d Object to aperture distance

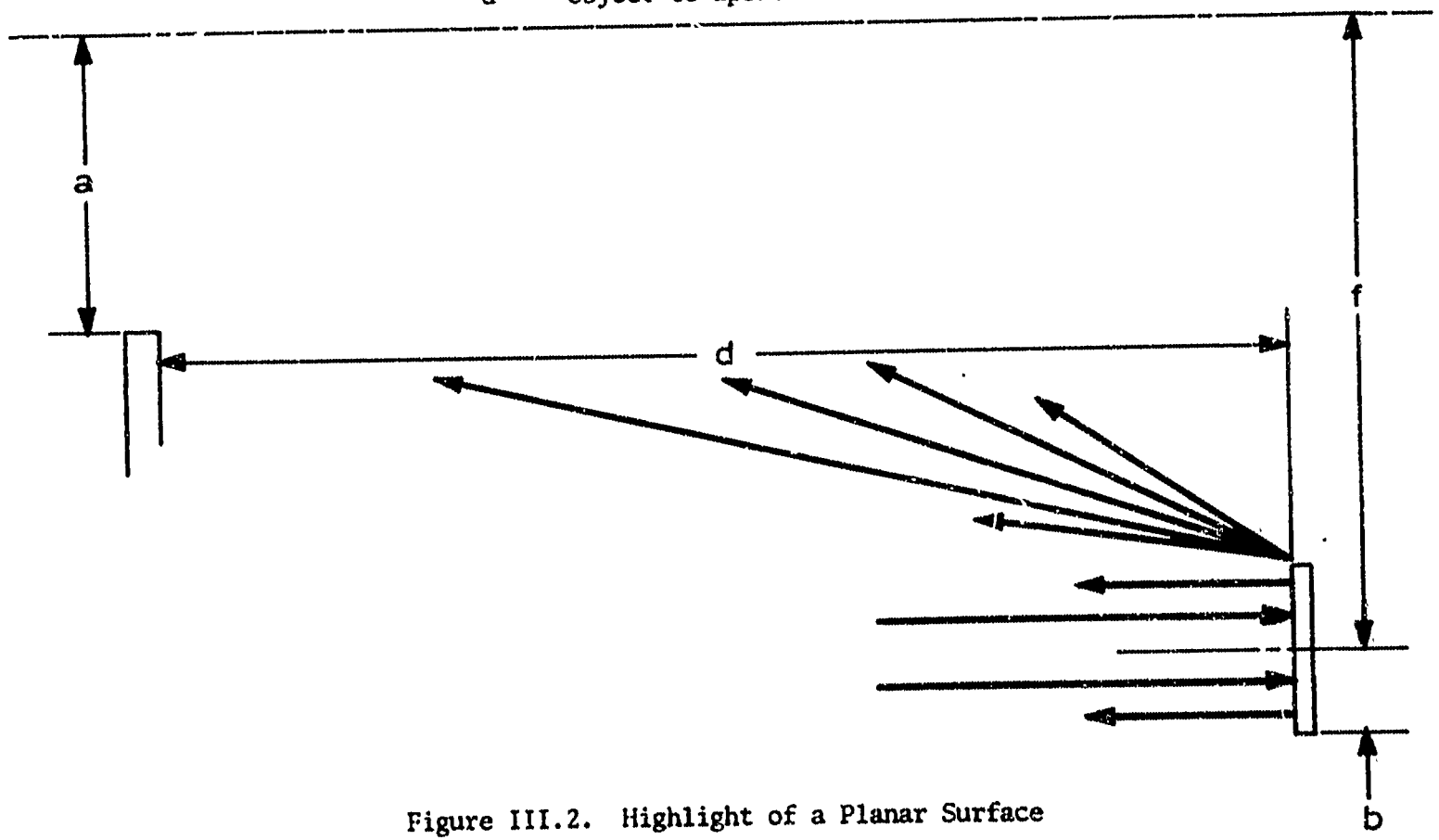

Figure III.2. Highlight of a Planar Surface

(width 2a) and illuminated with a monochromatic plane wave traveling in the z direction. If f + b < a then the entire extended object will be imaged. If f - b > a then only the field diffracted by the object edges will intercept the aperture, hence the object will appear as an outline rather than a solid; i.e., the image looks like the gradient of the object.

This can be seen analytically. From Appendix C the field reflected by the object in the plane of the imaging aperture can be written

$$\xi_a(y_a) = \int_{-\infty}^{\infty} \frac{\tilde{\xi}_0\left(\frac{\kappa}{2\pi}\right)}{2\pi} e^{i\kappa y_a} e^{ik_z(\kappa)d} d\kappa \qquad \text{(III.9)}$$

where

$$k_z^2 = k^2 - \kappa^2 \qquad \text{(III.10)}$$

and $\tilde{\xi}_0$ is the Fourier Transform of the field in the object plane. If $b \gg \lambda$ then it is permissible to take

$$k_z = k - \frac{1}{2} \frac{\kappa^2}{k} \qquad \text{(III.11)}$$

and (III.9) becomes

$$\xi_a(y_a) = e^{ikd} \int_{-\infty}^{\infty} \frac{\tilde{\xi}_0\left(\frac{\kappa}{2\pi}\right)}{2\pi} e^{i\kappa y_a} e^{-\frac{i}{2}\frac{\kappa^2}{k}d} d\kappa \quad . \qquad \text{(III.12)}$$

Expanding the exponential yields

$$\xi_a(y_a) = e^{ikd}\left[\xi_0(y_a) + C\frac{d^2\xi_0}{dy_a^2}(y_a) + \cdots\cdots\right] \qquad \text{(III.13)}$$

where C is a constant. Thus, the only contributions to the image of an offset planar object come from the space varying parts of the object; i.e., the edges.

5. MULTIFACETED AND ROUGH SURFACES

The multifaceted surface is a random distribution of curved facets disposed about some smooth median surface. For example, the barnacle encrusted hull of a ship might appear to be multifaceted for long acoustic wavelengths. An acoustic image of such a surface will be a collection of highlights, one for each facet. As one recedes from a multifaceted surface the highlights will tend to merge into a solid form. As

$$l \to \frac{ar}{2d}$$

$$r \to \frac{.61\lambda d}{2a} \quad , \qquad \text{(III.14)}$$

where l is the average spacing between facets, the multifaceted surface becomes a rough surface.

6. ILLUMINATION

Of course highlighting would present considerably less problem if diffuse acoustic illumination sources were available. Unfortunately, typical acoustic transducers tend to be point or collimated sources rather than diffuse sources. In visible optics such common sources of

illumination as light bulbs tend to be point sources. However, there is usually enough background diffused illumination to avoid serious highlight problems.

One is thus led to ask whether there is sufficient acoustic background in the sea to render a similar function for undersea acoustic imaging. Figure III.3 shows measurements of average acoustic background noise in the sea as a function of frequency[32]. The two non-biological curves represent upper and lower bounds for noise due to mechanical sources such as wave motion, rain, thermal agitation, etc. Noise due to biological or man-made sources is considerably stronger and is typically found in the range indicated near the top of the figure.

The dashed line dividing the figure is the threshold level for piezoelectric detection of acoustic radiation; this threshold is of significance because piezoelectric arrays will probably play an important part in any future undersea acoustic imaging work[14]. Piezoelectric detectors are attractive because of the very low threshold and because these devices can withstand the large hydrostatic pressures which exist even at moderate depths.

It appears from these preliminary data that noise due to mechanical sources will not be useful but that the noise due to biological sources warrants further investigation. For example, the acoustic noise above shrimp beds is quite large and animals such as the dolphin are known to be the source of considerable sonic activity. Simple man-made acoustic sources might include patterns of small explosive charges or perhaps streams of resonant air bubbles.

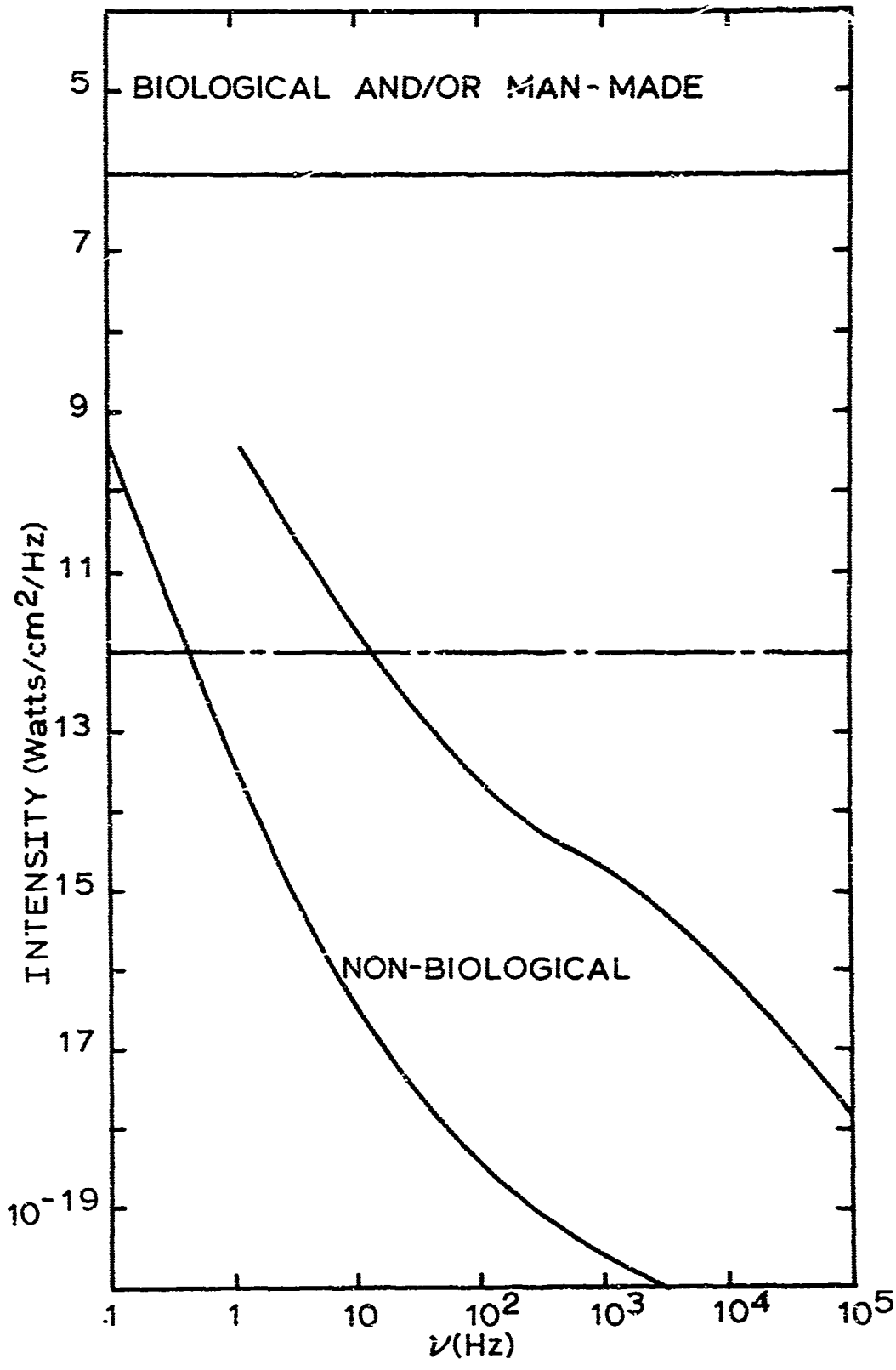

Figure III.3. Average Background Acoustic Noise in the Sea

In general, the problem of securing sufficiently diffuse illumination appears most tractable if incoherent rather than coherent acoustic radiation is used for illumination. First, although it is possible to obtain diffuse illumination from coherent sources, the design and fabrication of the necessary diffusers and extended coherent sources for acoustic radiation present considerable difficulty. On the other hand, as explained above it may be relatively simple to obtain extended, incoherent sources from which diffuse acoustic illumination can be generated. Second, of necessity incoherent radiation must diffuse as it propagates[17].

7. ACOUSTIC ATTENUATION IN WATER

Neglecting boundary effects due to the ocean bottom and surface, the primary source of acoustic attenuation in water is viscous losses and inhomogeneities such as sediment and air bubbles. For pure sea water the relation between loss and frequency is shown in Figure III.4 for various levels of salinity[53]. On the basis of this data it is concluded that long rage acoustic imaging of underwater objects will be restricted to frequencies no greater than 1 MHz; i.e., to attenuation less than .5 db/m in pure sea water.

In addition to the intrinsic absorption of water one must also consider the effect of dispersion of foreign material in the water. Such dispersions can significantly alter the attenuation and spatial frequency transfer function of the water medium. For example, resonant air bubbles may have an effective scattering cross section several orders of magnitude larger than geometrical diameter. Thus, even a relatively tenuous dispersion of microbubbles, such as might exist in

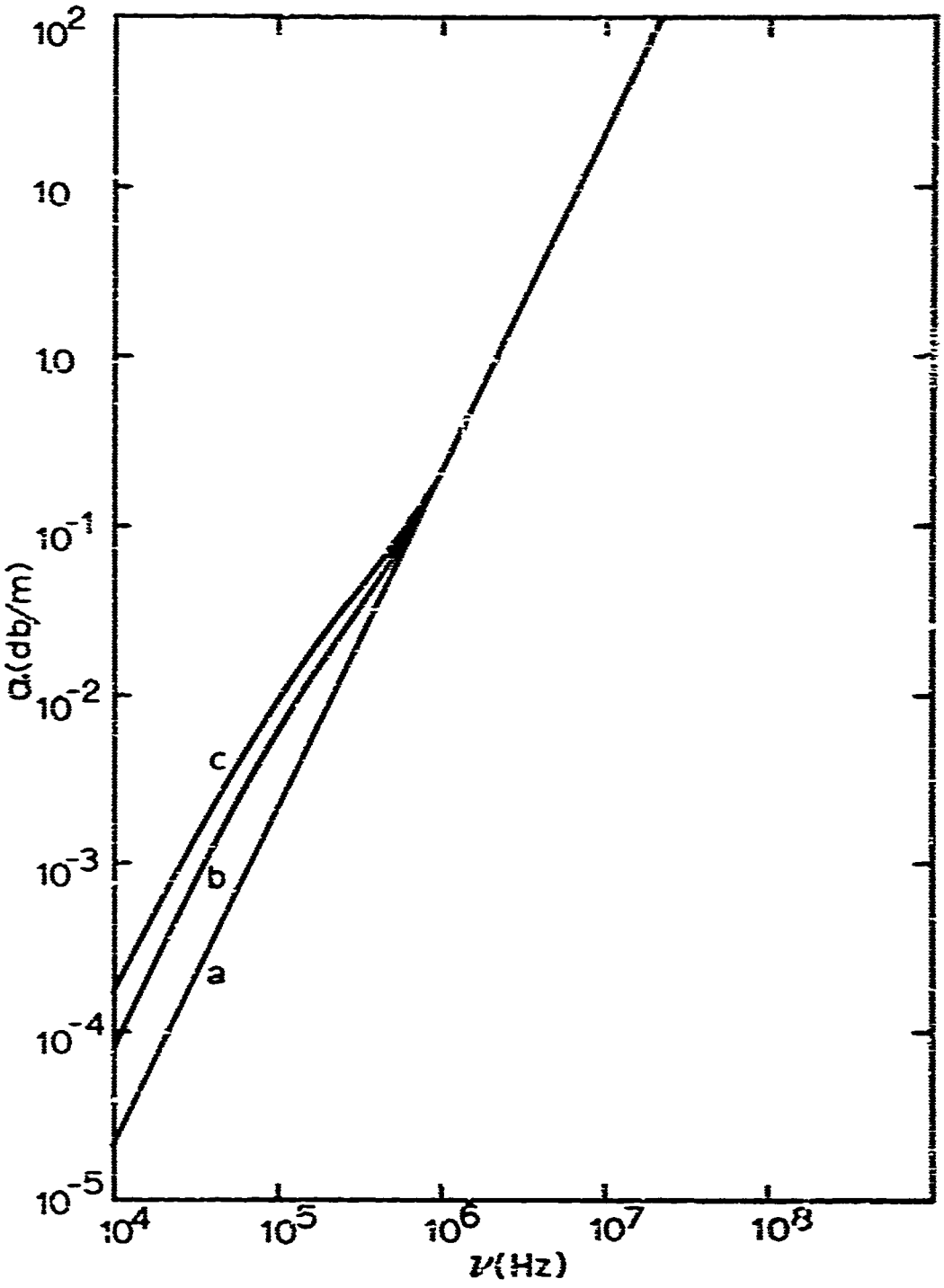

Figure III. 4. Acoustic Plane Wave Amplitude Attenuation α in Water

(a) Pure water
(b) Salinity of 35 parts/thousand
(c) Salinity of 70 parts/thousand
Temperature 20°C and pressures less than 100 atm (depths < 1000 m)

the wake of a ship many hours after passage, could significantly degrade the quality of acoustic images.

8. SUMMARY

We have shown that highlighting will be a difficult, perhaps impossible problem to overcome in undersea acoustic imaging. It appears that approaches to the problem in terms of incoherent acoustic illumination are the most promising. On the basis of attenuation undersea acoustic imaging will probably be limited to frequencies less than 1 MHz, hence to resolutions exceeding 1.5 mm.

CHAPTER IV

HOLOGRAPHY

1. INTRODUCTION

In Chapter II we presented a general formulation of scalar imaging emphasizing acoustic applications. In Chapter III we presented certain of the special problems which arise when acoustic fields are used to image objects immersed in a liquid medium such as the sea. In this chapter we turn to a specific imaging technique applicable to acoustic imaging, a two step process invented by Dennis Gabor and called wave front reconstruction, the hologram* process or, more usually, holography. We will concentrate on a formulation of the wavefront reconstruction process valid for large diffraction angles and including features peculiar to the acoustic case.

It is not intended that this be an exhaustive account of holography; only those features of immediate application to acoustic imaging are considered. For compact presentations of the entire range of holographic research the reader is referred especially to an article by Leith and Upatnieks[28] and a book by DeVelis and Reynolds[34]. Additional reference to the current research will be cited in the text as appropriate.

Holographic imaging is basically a simple process and the rudiments are, by now, familiar to most. An arrangement typical of those for recording holograms with light is shown in Figure IV.1.

---

* Hologram was coined by Professor Gabor from the Greek work HOLOS meaning whole or entire. It is appropriate since a hologram records both amplitude and phase of wave fields.

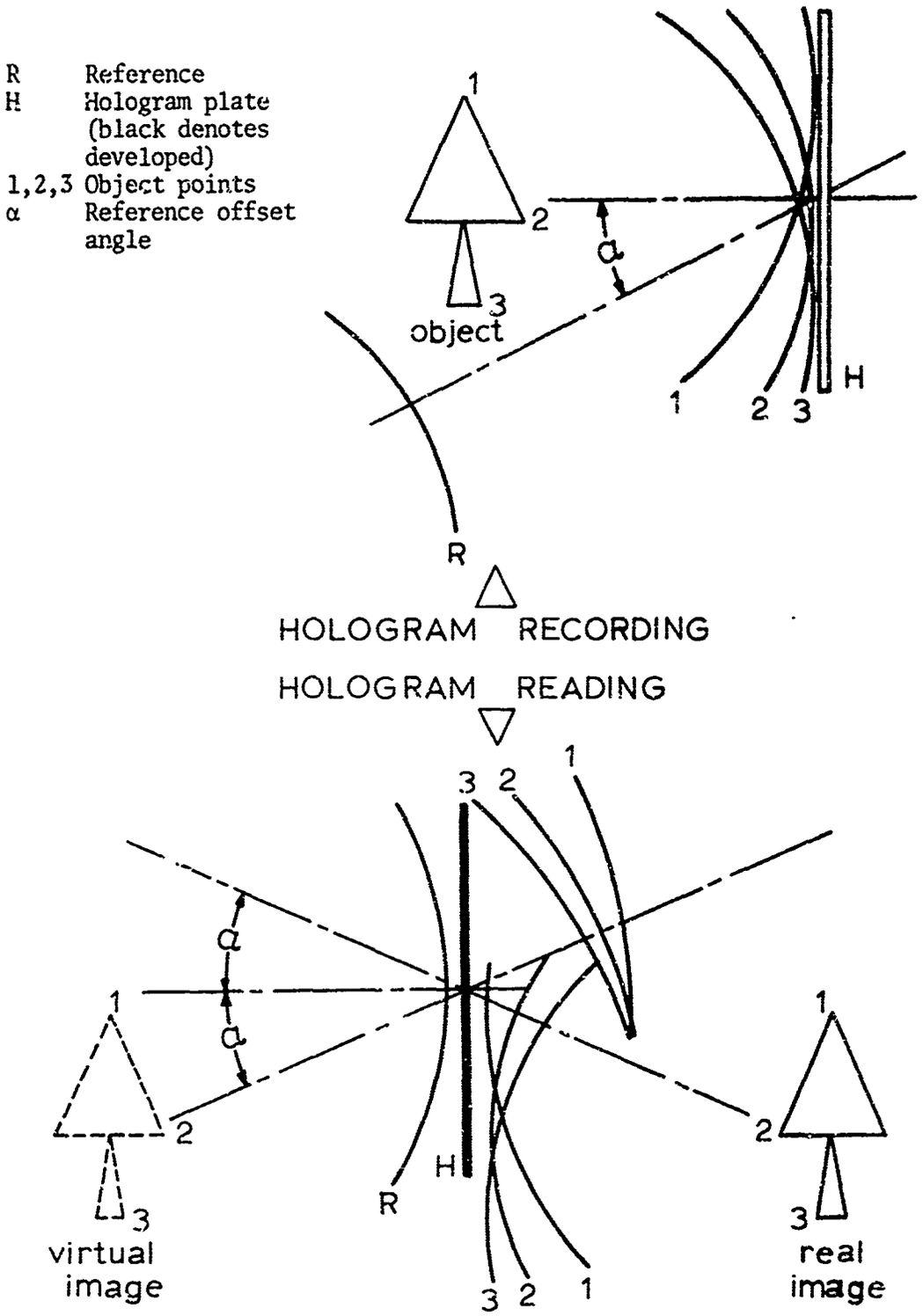

Figure IV.1. Typical Arrangement for Wavefront Reconstruction

Briefly, a hologram is recorded by adding the field scattered from a coherently illuminated three dimensional object scene to another coherent field (the reference) and allowing their sum, a complicated standing wave or interference pattern, to expose a photographic emulsion. Lenses are not required. A single spatially coherent source provides both reference and object illumination so that the two will interfere. Usually, the reference is planar or spherical, but there are situations in which it is diffuse or may even be part of the object scene. The transparency (called the hologram) which appears upon development of the exposed emulsion contains a mapping of the object-reference interference pattern. A complete record of the object field amplitude and phase is stored in this pattern.

Three dimensional images which are faithful replicas of the original object scene are obtained from the hologram by illuminating it with a duplicate of the reference. Usually two images of the object scene will be formed; one real, the other virtual. The virtual image corresponds to exact replication of the original object field, hence the term wavefront reconstruction, and is viewed by looking through the hologram as if it were a window. The real image may be observed as an object suspended in mid-space between observer and hologram or it can be projected directly onto a viewing screen.

Although light was assumed for purposes of illustration, the procedures outlined above are applicable to non-visible optical fields as well, for example, to acoustic or microwave fields. Strict preservation of the analogy would demand that acoustic holograms reconstruct acoustic fields, microwave holograms reconstruct microwave fields,

etc.[35]. However, holograms of invisible fields which reconstruct geometrically similar visible fields are more useful, therefore discussion is restricted to holograms of this type. For example, by acoustic holography we shall mean visualization of acoustic fields by converting object-reference acoustic interference patterns into geometrically similar photographic transparencies which, in turn, serve as holograms to reconstruct visible fields geometrically similar to the original acoustic fields. In this way we "see" acoustically by holography.

The motivation for holography in acoustics is not the same as in visible optics. In visible optics the need is to record information of a three-dimensional nature on a two-dimensional photographic emulsion in a form suitable for easy recovery whenever desired. In this application holography is not a real time imaging process; lenses, photoelectric devices, and the eye adequately serve that purpose.

Conversely, in acoustics the need is for real time imaging using acoustic fields as the "illumination" but with the resulting acoustic images somehow rendered visible so that we may "see" in otherwise opaque media. Simple imaging devices such as lenses of adequate quality are not readily available. More serious, as yet there are no practical acoustic sensitive materials which are analogous to the retina. Holography attains viability in acoustics as an imaging technique which does not require lenses, hence at least eliminates the first stumbling block. Moreover, in certain limited applications real time acoustic imaging by holography has been demonstrated[65].

2. THE HOLOGRAM EIGENVALUE EQUATION

The remarkable effects attributed to holography are well known, probably the most dramatic being the generation of virtual images of diffusely reflecting or diffusely illuminated three dimensional scenes from two dimensional photographic transparencies. Upon viewing these images with the unaided eye one observes what appear to be the original scenes in total three dimensional detail including foreshortening, parallax, and depth of focus as well as the stereoscopic sense of depth. Holographically generated scenes are thus indistinguishable from original scenes.

This phenomena is explained in the following manner. The holographic scene cannot be distinguished from the original scene because the hologram, when properly illuminated, diffracts an exact duplicate, both in amplitude and phase, of the complex wave field scattered from the original scene. We may say that the hologram process (recording, developing, reconstruction, etc.) operates on a field in such a way as to recreate this field at another time and place.

This relation admits of a simple mathematical representation which, because of its elegance, has appeal. Denoting the field originally diffracted from the scene by $\psi_0(\underline{r},t)$ and the process wherein the hologram $P(\underline{r})$ is recorded by an operator $H_1(\underline{r},t)$ which operates upon ψ_0, holographic recording of a field may then be represented as

$$H_1(\underline{r},t)\psi_0(\underline{r},t) = P(\underline{r}) \quad , \tag{IV.1}$$

the first step in holographic imaging.

H_1 represents some general time averaging process of the form (II.2) by which the holographic record is formed. We shall assume it reduces to a time average of the form (II.3).

Similarly, denoting the reconstruction process, whatever it may entail, by an operator $H_2(\underline{r},t_2)$ acting on the hologram $P(\underline{r})$ we may write for the second step in holographic imaging

$$H_2(\underline{r},t_2)P(\underline{r}) = \psi_I(\underline{r},t_2) \tag{IV.2}$$

where $\psi_I(\underline{r},t_2)$ is the field diffracted by the hologram.

Combining H_1 and H_2 and defining the hologram operator $H(\underline{r},t_1,t_2)$ as

$$H(\underline{r},t_1,t_2) \equiv H_1(\underline{r},t_1)H_2(\underline{r},t_2) \tag{IV.3}$$

we obtain for the entire holographic imaging process

$$H(\underline{r},t_1,t_2)\psi_0(\underline{r},t_1) = \psi_I(\underline{r},t_2) \quad . \tag{IV.4}$$

For perfect reconstruction

$$\psi_I(\underline{r},t_2) = h\psi_0(\underline{r},t_2) \tag{IV.5}$$

where h is a complex constant. Thus for perfect reconstruction (IV.4) becomes

$$H\psi = h\psi \quad . \tag{IV.6}$$

Note that the coordinate system is fixed with respect to the hologram because reconstruction should not depend on translations of the hologram after recording.

Condition (IV.5) is, in a certain sense, unduly restrictive since the field ψ is usually not directly observable. When only functionals D of the field are observable then as long as the original and reconstructed observables are identical the reconstruction will appear to be perfect. In this case (IV.5) may be replaced with the less stringent condition

$$D_I(\underline{r},t_2) = h'D_O(\underline{r},t_1) \quad . \tag{IV.7}$$

Equation (IV.6) is immediately recognized as a form occurring frequently in mathematical representations of physical processes, for example, in quantum mechanics[36]. For a given operator $H(\underline{r},t_1,t_2)$ only certain functions $\psi_{nd}(\underline{r},t)$, the eigenfunctions, will satisfy this equation and only for special corresponding values h_n of h, the eigenvalues. In general, to each eigenvalue correspond several eigenfunctions, the number being the degeneracy d_n of the eigenvalue h_n. The eigenvalues may be descrete, continuous over a range, or a combination of the two.

Equations (IV.6) and (IV.7) may be regarded as describing a general two step process in which information is permanently recorded at time t_1, not necessarily in recognizable form, to be recovered later at time t_2 in original form. Unless $H(\underline{r},t_1,t_2)$ has special properties, an arbitrary field will not be perfectly reconstructed. Indeed, even the best choice of $H(\underline{r},t_1,t_2)$ will probably not guarantee perfect

reconstruction for all possible object fields, but only some (hopefully large) class of them.

At this point, the description of holography as embodied in Equations (IV.6) and (IV.7) is purely phenomenological; it describes, approximately at least, the central feature of holography but it does not necessarily contain any essential physics of the process. Before concluding that (IV.6) or (IV.7) has any deeper significance or utility, the processes operating in holography must be studied in detail in order to obtain explicit expressions for the hologram operator. Then the implications of the eigenvalue formalism and the degree to which this formalism is valid and useful can be assessed in greater depth.

3. UNIQUENESS OF HOLOGRAPHIC RECORDINGS

Consider the general image recording situation depicted in Figure II.1 where the image space I is composed of two parts, the recording or detecting medium P (photosensitive emulsions, alkali halide crystals, etc. for visible radiation) and the image forming device F (lenses, prisms, the eye, etc.). The simplest imaginable situation would then be when I is composed entirely of recording material with no auxiliary processing apparatus. Holography is coherent imaging with precisely such elementary configurations of the imaging region.

Assume object region O is illuminated with monochromatic, spatially coherent radiation $\psi(\underline{r},t) = \xi(\underline{r})e^{2\pi i\nu t}$ emanating from luminous source region L, $\xi(\underline{r})$ then obeying the Helmholtz Equation (II.17).

Elliptic equations, such as the Helmholtz equation, have unique and stable solutions for either Dirichlet or Neumann boundary conditions over closed boundaries[37,38]. That is, when the modulus and argument of $\xi(\underline{r})$ or $\frac{\partial}{\partial n}\xi(\underline{r})$ is specified at all points on some boundary enclosing a source-free region, the solution $\xi(\underline{r})$ to the elliptic equation everywhere inside that boundary is unique. Referring to Figure IV.2, consider the region $M_>$ bounded by some portion S of the surface of P, the plane q extending from the extremities of S to the sphere at infinity, and the half sphere $R_>$ at infinity. $M_>$ shall be known as the exterior region and the field ξ_0 inside this region as the exterior field $\xi_{0>}$. Accordingly, if S is of size sufficient to intercept all of the field ξ_0 scattered from the object ($\xi_0 = 0$ on q), and taking $\xi_0(\underline{r}) \underset{r \to R}{\to} 0$, then the boundary fields $\xi_0(\underline{r}_S)$ or $\frac{\partial}{\partial n}\xi(\underline{r}_S)$ will bear unique relation to $\xi_{0>}$.

A similar relation does not hold for the interior field $\xi_{0<}$ inside the interior region $M_<$ bounded by the surface S, the plane q, and the half sphere $R_<$ at infinity beca use the source-free assumption is violated. Physically, the lack of uniqueness for $\xi_{0<}$ is clear. In general, there will be evanescent as well as propagating fields associated with $\xi_{0<}$; the former cannot be uniquely determined from $\xi_0(\underline{r}_S)$. Second, only those regions of $M_<$ which radiate toward q will contribute to $\xi_0(\underline{r}_S)$.

Thus, regardless of the size of P it is necessary to partition the scattered field ξ_0 into an interior portion $\xi_{0<}$ and an exterior portion $\xi_{0>}$ according to the prescription

$$\xi_0(\underline{r}) = \xi_{0<}(\underline{r})[1 - u(\underline{r} - \underline{r}_S)] + \xi_{0>}(\underline{r})u(\underline{r} - \underline{r}_S) \qquad \text{(IV.8)}$$

where

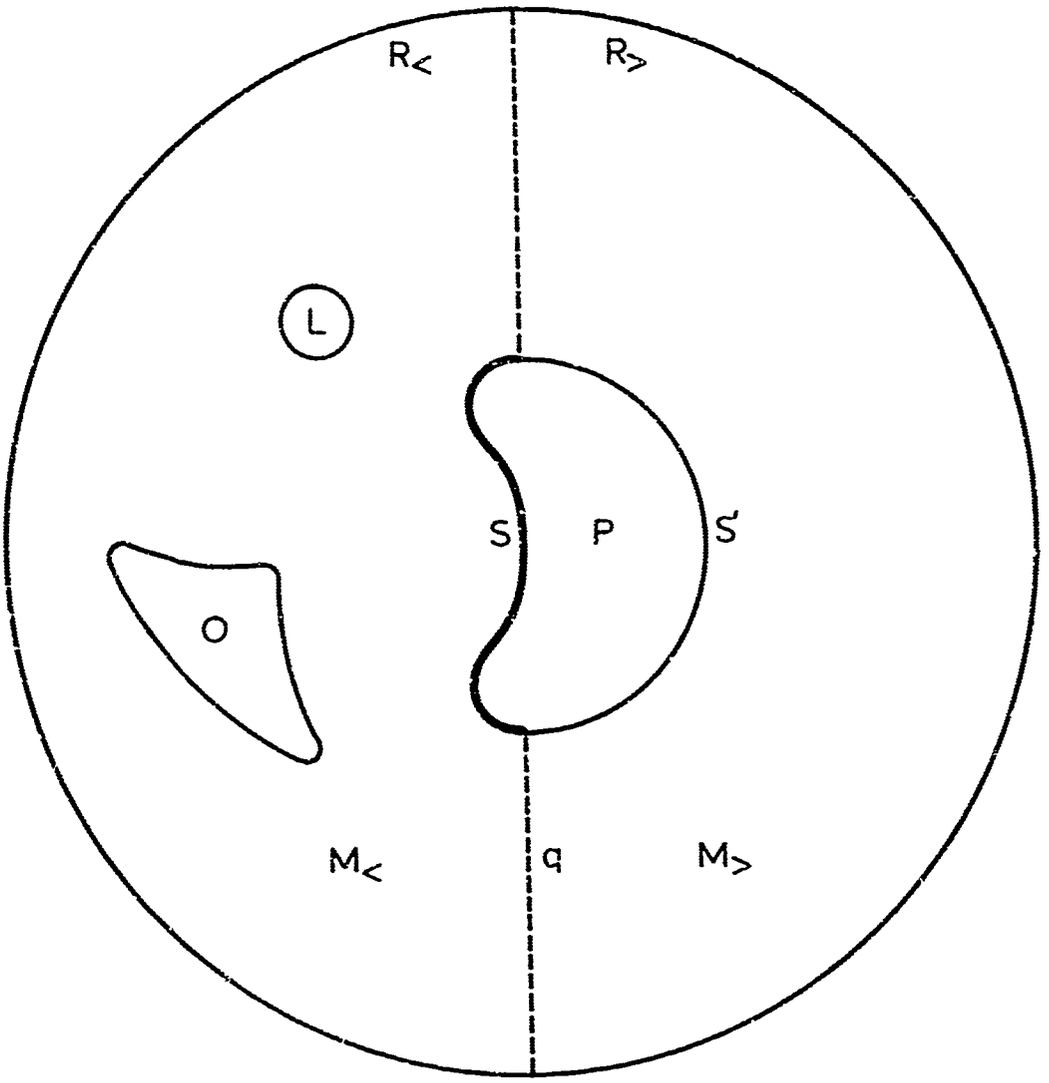

Figure IV.2. A General Boundary Configuration for Holographic Imaging, Recording

O	Object region
P	Recording region
$M_<$	Interior space
$M_>$	Exterior space
L	Illumination source
S,S'	Coterminal recording surfaces
q	Partitioning plane
$R_<, R_>$	Half spheres at infinity

$$u(\underline{r} - \underline{r}_S) = 0 \qquad \underline{r} \leq \underline{r}_S$$
$$= 1 \qquad \underline{r} > \underline{r}_S \quad . \tag{IV.9}$$

Next, suppose that exposure to radiation ξ_0 induces irreversible alteration of some physical property of the recording material inside I, thereby imbedding in the material a permanent record of the field. From the arguments presented in the preceeding paragraph, if this record retains both the amplitude and phase of $\xi_0(\underline{r}_S)$ or $\frac{\partial}{\partial n}\xi(\underline{r}_S)$, then it will be a unique and complete representation of $\xi_{0>}$, but only a partial representation of $\xi_{0<}$.

The uniqueness properties given above for recorded optical information can be summarized as a statement concerning the resolution of optical instruments. To wit, resolution is simply a consequence of the uniqueness properties of elliptic equations. If the boundary S is not large enough to intercept all of the field ξ_0 scattered from the object scene then, by the uniqueness theorem, $\xi_0(\underline{r}_S)$ is no longer uniquely related to $\xi_0(\underline{r})$. Further, as the boundary S decreases in size the number of possible configurations of $\xi_0(\underline{r})$ which coincide with a given $\xi_0(\underline{r}_S)$ or $\frac{\partial}{\partial n}\xi(\underline{r}_S)$ increases. Hence, as boundary size decreases, uncertainty in the relation between object and image increases; i.e., resolution is reduced. This agrees with intuitive notions and quantitative theories governing optical resolution.

As object fine structure becomes more intricate ξ_0 will be scattered through correspondingly greater angles thereby requiring a larger surface for complete interception of the scattered field and total resolution of the object. However, when the object structure contains spatial frequency components exceeding $1/\lambda$even a very large

aperture may not provide complete resolution because the fields scattered in response to these very high spatial frequencies will be evanescent rather than propagating. Thus, there will be irreversible attenuation of the high spatial frequency information transmitted from object to recording surface. Depending upon the sensitivity of this surface the information may be completely lost or, at the very least, severely attenuated. Because of the relatively long wavelengths associated with acoustic radiation this effect is of considerable importance in acoustic imaging. Other investigators have discussed the problem of recovering high frequency details in microwave imaging, and the partition of scattered fields into interior and exterior portions[39]. Even if evanescent propagation is absent the recording medium will not respond equally to high and low spatial frequencies, nor to large and small field amplitude, nor to all directions of propagation. These problems are also of importance in acoustic holography.

A general observation on the nature of the reconstruction process will facilitate proper formulation of the eigenvalue equation. Consider the reconstruction, Figure IV.3, from the recording, Figure IV.2. The hologram P, illuminated by coherent source C, will invariably be one of two possible types; either predominantly reflecting or predominantly transmitting. For reflection holograms the reconstructed fields will lie in the interior region $M'_<$, for transmission holograms the reconstructed fields will lie in the exterior region $M'_>$. Thus both fields $\xi_{0<}$ and $\xi_{0>}$ will be reconstructed in the same half space with respect to the hologram P, even though they were originally in opposite half spaces.

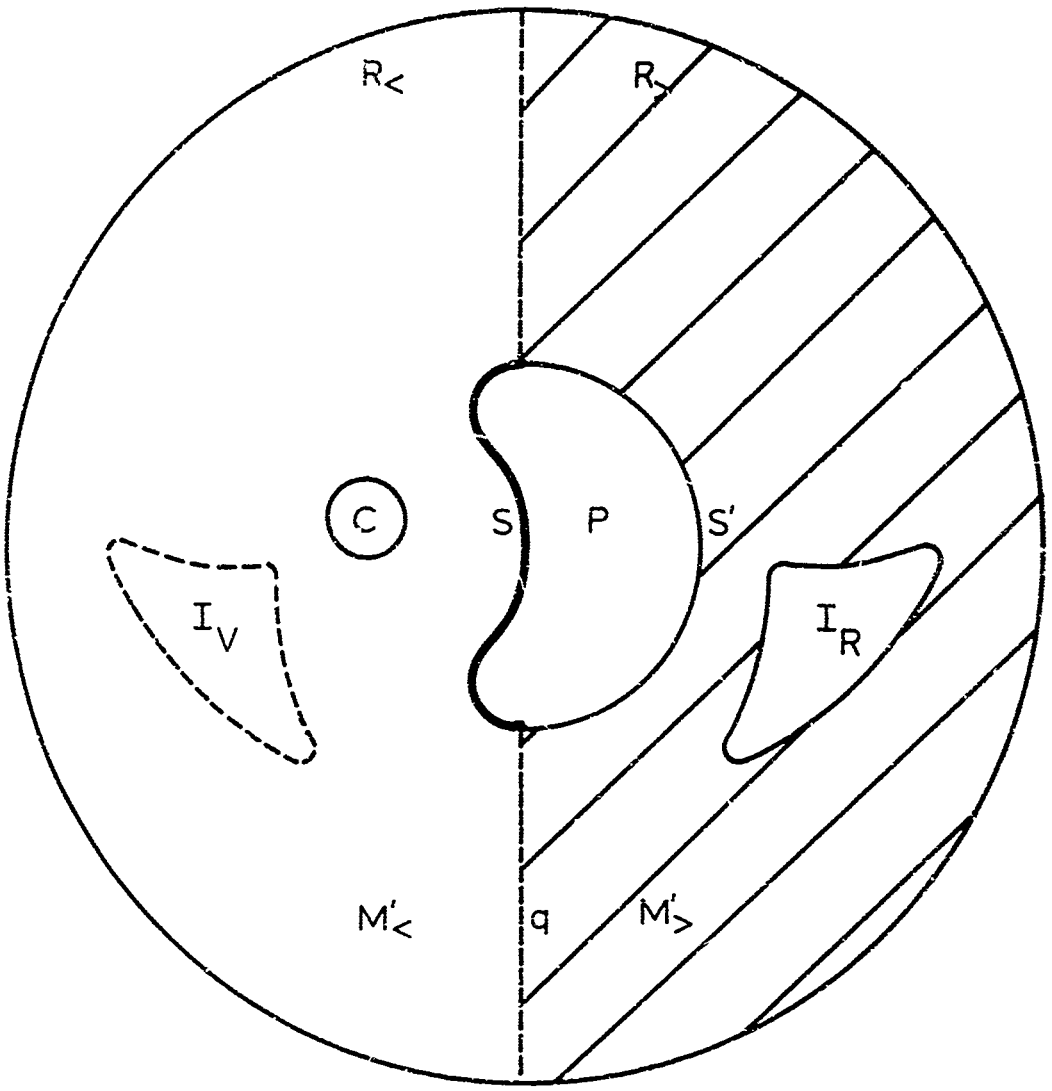

Figure IV.3. A General Boundary Configuration for Holographic Imaging, Reconstruction from Transmission Holograms

P	Recorded hologram
S,S'	Coterminal hologram surfaces
I_V	Virtual image
I_R	Real image
C	Illumination source
$M'_<$	Interior space
$M'_>$	Exterior space (<u>all</u> fields reconstructed in this space)
q	Partitioning plane
$R_<, R_>$	Half spheres at infinity

Thus, a peculiar feature of holographic imaging becomes evident and the necessity for partitioning the scattered object field ξ_0 according to Equation (IV.8) is clear. Since $\xi_{0<}$ and $\xi_{0>}$ originally propagated in opposite half spaces with respect to the hologram but are reconstructed in the same half space, obviously the holographic process operates on interior fields differently from exterior fields. For example, referring to Figure IV.3 , consider that ξ_0 is everywhere diverging; i.e., $\xi_{0<}$ and $\xi_{0>}$ are both diverging, hence represent virtual images of object O. Exact reproduction of $\xi_{0<}$ everywhere requires that over some surface O', geometrically similar to object O (can be scaled in size or rotated in orientation), an exact duplicate of the object boundary field $\xi_{0<}(\underline{r}_0)$ be formed. Since propagation of the reconstructed field is clearly from left to right this formation represents a real rather than a virtual image. Similar reasoning applied to $\xi_{0>}$ shows that it reconstructs as a virtual image.

There are other unusual effects associated with reconstruction of the interior field. The most obvious is pseudoscopic inversion[40] of the real image when it is viewed directly rather than projected on a screen. However, this is not a fundamental distortion of the image. More serious is the absence of very high spatial frequency details in the reconstructed object caused by evanescent propagation of these details from object O to hologram during recording and from hologram to image O' during reconstruction. High spatial frequency details are missing from the exterior fields so their absence in the reconstructed exterior fields is not significant. Of course, many other situations may occur but the foregoing example is representative of the

fundamental differences which may exist between holographic imaging of internal and external fields, and serves to illustrate that the normal mode formalism may only be valid for reconstruction of the exterior field. Therefore, anticipating that, at the very least, interior fields will require different mathematics than exterior fields, the two are separated in the formalism.

One further comment deserves consideration. Clearly, if the above statements are true for the surface S, they are also true for the coterminal surface S' or any other coterminal surface lying wholly within the material P. Thus, a volume recording medium provides redundancy in the recording of optical information. It has been demonstrated that this redundancy can be used to increase image brightness. For example, thick emulsion (multilayer) holograms have a theoretical efficiency of 100% whereas conventional thin emulsion (diffraction grating) holograms have a maximum efficiency of only 25%.* A concomitant use for the redundance is to relax the constraints on the reconstruction illumination ξ_C, in effect making the decoding process for thick emulsion holograms even simpler than Gabor's original method[41].

4. GENERAL FORM OF THE HOLOGRAM OPERATOR, I

In Section 2 a hologram was defined as a generalized optical record which, when properly interrogated, reconstructs a visible

---

* The classification of holograms as being multilayers, diffraction gratings, or Fresnel zone plates is due to Professor Nicholas George of Caltech.

replica of the original optical field, hopefully at all points in space (Equation IV.6). Geometrical scaling and reorientation of the reconstructed field relative to the original field is acceptable and because the final result is to be a visible field, the quality of the reconstruction can be judged only in terms of field intensity (Equation IV.7).

The most convenient method of interrogating any optical record is by reillumination of the record with visible radiation $\xi_C(\underline{r})e^{2\pi i\bar{\nu}t}$. For example, the information contained in a photograph is conveyed quite simply to the observer by visual inspection of the developed emulsion, which requires only that the photograph be well lighted. In this situation incoherent, diffuse sources are superior to all others. Gabor[7,8,9] recognized that reillumination could also be applied to holograms, in a process he called reconstruction, and stated conditions on the illumination required for this purpose. In contrast to conventional photography the illumination must be coherent and the phase contours must be carefully controlled. However the reconstruction is three-dimensional.

If we demand that the interrogation process be one or reillumination then in view of the discussion presented in Section 3 we can state that any optical record $P(\underline{r})$ of the holographic type must be such that upon illumination with $\xi_C(\underline{r})$ a replica of the original boundary field $\xi_0(\underline{r}_S)$ is produced on the surface S of the hologram. It seems quite likely that if

$$P(\underline{r}_S) \propto \xi_0(\underline{r}_S) \qquad \text{(IV.10)}$$

the required replication will be accomplished. More generally, the hologram will be a weighted record, the simplest form being

$$P(\underline{r}_S) \propto \xi_O(\underline{r}_S)\xi_R^*(\underline{r}_S) \tag{IV.11}$$

where ξ_R^* is the weighting factor. If the hologram is thick then (IV.11) will hold throughout the volume of the developed hologram; if the hologram is thin (IV.11) holds in the plane of the hologram. In the latter case the operator H_1 will be of the form

$$H_1(\underline{r}_S) \equiv \int_M (\ )\xi_R^*(\underline{r})\delta^3(\underline{r}-\underline{r}_S)d^3r \tag{IV.12}$$

where the empty parenthesis inside the integral indicates that the operator has meaning only when it operates on some field ξ_O which is placed in the parenthesis, and δ^3 is the three dimensional delta function.

The hologram may be considered thin whenever its thickness is much less than the minimum fringe spacing to be recorded[42]. Although the validity of this approximation must be carefully weighed when dealing with visible holograms[43], it is almost certainly true for acoustic holograms for two reasons. First, acoustic sensors used to generate acoustic holograms are usually no more than one acoustic wavelength thick. Second, the emulsion of an acoustic hologram transparency is usually much thinner than the minimum fringe spacing recorded thereon. Thus (IV.12) applies to the recording of acoustic holograms.

Exact calculation of the field $\xi_I(\underline{r})$ diffracted by a developed thick hologram transparency $P(\underline{r})$ illuminated by a field $\xi_C(\underline{r})$ is a formidable task involving the scattering of electromagnetic radiation from three-dimensional, semi-transparent volumes. Rigorous solution requires a multiple order scattering theory including Bragg reflection phenomena[44]. However, for thin planar holograms, particularly those with binary format* $\xi_I(\underline{r}_I)$ may be written

$$\xi_I(\underline{r}_I) = \int_S P(\underline{r}_S)\xi_C(\underline{r}_S)G(\underline{r}_I,\underline{r}_S)d^2r_S \qquad \text{(IV.13)}$$

where according to the Rayleigh-Sommerfeld theory

$$G(\underline{r}_I,\underline{r}_S) = -\frac{1}{2\pi}\frac{\partial}{\partial n}\left[\frac{e^{ik|\underline{r}_I-\underline{r}_S|}}{|\underline{r}_I-\underline{r}_S|}\right] = \qquad \text{(IV.14)}$$

$$-\frac{1}{2\pi}\frac{e^{ik|\underline{r}_I-\underline{r}_S|}}{|\underline{r}_I-\underline{r}_S|}\left(ik-\frac{1}{|\underline{r}_I-\underline{r}_S|}\right)\left[\frac{(\underline{r}_I-\underline{r}_S)\cdot\hat{n}}{|\underline{r}_I-\underline{r}_S|}\right],$$

and $\hat{n}$ is the unit vector normal to S pointing into the half space containing $\underline{r}_I$[45]; or according to the plane wave expansion theory (see Appendix C)

$$G(\underline{r}_I,\underline{r}_S) = \int_{-\infty}^{\infty} e^{ik_z(z_I-z_S)}e^{i\underline{\kappa}\cdot(\underline{r}_I-\underline{r}_S)}d^2\kappa \qquad \text{(IV.15)}$$

and k_z and $\underline{\kappa}$ are the longitudinal and transverse wave vectors respectively.

---

* Binary formats are either completely transmitting or completely opaque; there is no gray scale. Acoustic holograms tend to be of this type although such holograms may not provide optimum image fidelity.

The hologram reconstruction operator H_2 may then be defined as

$$H_2(\underline{r}_I) = \int_S (\ )\xi_C(\underline{r}_S)G(\underline{r}_I,\underline{r}_S)d^2r_S \qquad \text{(IV.16)}$$

and the hologram operator $H = H_1H_2$ becomes

$$H(\underline{r}_I) = \int_M \int_S (\ )\xi_R^*(\underline{r}_0)\xi_C(\underline{r}_S)G(\underline{r}_I,\underline{r}_S)\delta^3(\underline{r}_0-\underline{r}_S)d^3r_0d^2r_S \qquad \text{(IV.17)}$$

so that perfect wavefront reconstruction may be written as

$$\xi_I(\underline{r}_I) = \xi_0(\underline{r}_I) = h\int_M \int_S \xi_0(\underline{r}_0)\xi_R^*(\underline{r}_0)\xi_C(\underline{r}_S)G(\underline{r}_I,\underline{r}_S)\delta^3(\underline{r}_0-\underline{r}_S) \cdot \qquad \text{(IV.18)}$$

$$\cdot\, d^3r_0d^2r_S \quad .$$

It is important to determine over what region (IV.18) is valid. Consider a single point source test object located at $\underline{r}_0$. Then

$$\xi_0(\underline{r}_S) = \frac{e^{ik|\underline{r}_S-\underline{r}_0|}}{2\pi|\underline{r}_S-\underline{r}_0|} \quad . \qquad \text{(IV.19)}$$

If a hologram of this test object is illuminated by a field with $e^{-i\bar{\nu}t}$ time dependence then in the hologram plane the field will be proportional to $\frac{e^{-i\bar{\nu}t}e^{ik|\underline{r}_S-\underline{r}_0|}}{2\pi|\underline{r}_S-\underline{r}_0|}$ which is in the same form as a spherical wave diverging from the hologram plane into the exterior region $M_>$. Thus, (IV.18) can only describe reconstruction of the exterior field $\xi_{0>}$. Since by definition

$$\xi_0(\underline{r}_S) = \xi_{0<}(\underline{r}_S) = \xi_{0>}(\underline{r}_S) \quad . \tag{IV.20}$$

Equation (IV.18) is more properly written

$$\xi_{0>}(\underline{r}_I) = h \int_M \int_S \xi_{0>}(\underline{r}_0)\xi_C(\underline{r}_S)G(\underline{r}_I,\underline{r}_S)\delta^3(\underline{r}_0-\underline{r}_S)\cdot d^3r_0 d^2r_S \quad . \tag{IV.21}$$

If the factor $\xi_0\xi_R^*$ is replaced with its complex conjugate $\xi_0^*\xi_R$ then upon reconstruction the field in the hologram plane will be proportional to $\frac{e^{-i\bar{\nu}t}e^{ik|\underline{r}_S-\underline{r}_0|}}{2\pi|\underline{r}_S-\underline{r}_0|}$ which is in the same form as a spherical wave converging from the hologram plane to a point in the exterior region. In this case (IV.18) describes reconstruction of the interior field $\xi_{0<}$ except that whereas the former converges to the point, the latter diverges from the point. Equation (IV.18) should then be written

$$\xi_{0<}^*(\underline{r}_I) = h \int_M \int_S \xi_{0<}(\underline{r}_0)\xi_R^*(\underline{r}')\xi_C(\underline{r}_S)G(\underline{r}_I,\underline{r}_S)\delta^3(\underline{r}_0-\underline{r}_S)d^3r_0 d^2r_S \quad . \tag{IV.22}$$

For any particular transverse plane $\underline{r}_I$ Equations (IV.21) and (IV.22) are of the form

$$\xi(\underline{r}_I) = \lambda \int_S \xi(\underline{r}_S)K(\underline{r}_I,\underline{r}_S)d^2r_S \quad . \tag{IV.23}$$

Now in general $\xi(\underline{r}_I) \neq \xi(\underline{r}_S)$ so that (IV.23) is a Fredholm equation of the first kind with kernel $K(\underline{r}_I,\underline{r}_S)$[46]. In general K will depend on z_I

and z_S so (IV.24) represents a family of equations, one for each image plane. Thus, (IV.23) does not appear to be a tractable formulation of holography.

Moreover (IV.23) is incomplete. Unique reconstruction of $\xi_0(\underline{r})$ in M requires not only knowledge of the boundary field $\xi_0(\underline{r}_S)$ but the equation of motion; i.e., k, as well, This is particularly important in acoustic holography wherein the k for recording is much smaller than the k for reconstruction; only the k for reconstruction is contained in (IV.23).

Nevertheless, in an important number of applications the two wave numbers are the same and it is then apparent from (IV.23) that we must have

$$\xi_R^*(\underline{r}_S)\xi_C(\underline{r}_S) = \text{const} \quad . \tag{IV.24}$$

It is important to investigate the significance of the relation (IV.24) between reference and reconstruction illumination. Expressing the fields in terms of modulus $|\xi|$ and arguement ϕ (IV.24) becomes

$$|\xi_R(\underline{r}_S)|e^{-i\phi_R(\underline{r}_S)}|\xi_C(\underline{r}_S)|e^{i\phi_C(\underline{r}_S)} = \text{const} \quad . \tag{IV.25}$$

Clearly, if

$$|\xi_R(\underline{r}_S)| = \text{const} \tag{IV.26}$$

then by choosing $\xi_C = \xi_R$ condition (IV.24) is satisfied identically. The most obvious of the forms (IV.26) is a single plane wave propagating

in any direction. Another is uniform diffuse illumination characterized by random variation of the phase; again we must take $\xi_C = \xi_R$.

The foregoing are special but important situations frequently encountered in holography. We now consider more general reference and reconstruction illumination including the so-called "ghost imaging" of Collier, et al[47]. By writing the reference and reconstruction in terms of general plane wave expansions one obtains

$$\xi_R^*(\underline{r}_S)\xi_C(\underline{r}_S) = \int\int_{-\infty}^{\infty} W_R^*(\underline{\kappa}')W_C(\underline{\kappa})e^{i(\underline{\kappa}-\underline{\kappa}')\cdot\underline{r}_S} \cdot e^{i[k_z(\underline{\kappa})-k_z(\underline{\kappa}')]z_S} d^2\kappa d^2\kappa' \tag{IV.27}$$

where $W_R(\underline{\kappa})$ and $W_C(\underline{\kappa})$ are the complex amplitudes of the $\underline{\kappa}$th directed plane wave components of ξ_R and ξ_C respectively. Without loss of generality we may take $\xi_C = 0$. Changing variables according to the prescription

$$\begin{aligned} \underline{\kappa}' &= \underline{\kappa} + \underline{\beta} \\ d^2\kappa' &= d^2\beta \end{aligned} \tag{IV.28}$$

then gives

$$\xi_R^*(\underline{r}_S)\xi_C(\underline{r}_S) = \int_{-\infty}^{\infty}\left[\int_{-\infty}^{\infty} W_C(\underline{\kappa})W_R^*(\underline{\kappa}+\underline{\beta})d^2\kappa\right] e^{i\underline{\beta}\cdot\underline{r}_S} d^2\beta \tag{IV.29}$$

Taking $\underline{\beta} = 2\pi\underline{s}$ we see that (IV.29) is in the form of an inverse Spatial Fourier Transform so $M_C \bigstar M_R^*$ is related to the Spatial Fourier Transform of $\xi_R * \xi_C$. Condition (IV.24) then becomes

$$\int_{-\infty}^{\infty} M_C(\underline{\kappa}) M_R^*(\underline{\kappa}+\underline{\beta}) d^2\kappa = \begin{cases} 0 & |\underline{\beta}| > \varepsilon \\ 0 & |\underline{\beta}| < \varepsilon \end{cases} \qquad \text{(IV.30)}$$

where $\varepsilon << 1/a$ and $2a$ is the hologram size. If M_C and M_R are uncorrelated spectral distributions; i.e., ξ_C and ξ_R are sufficiently diffuse, then (IV.30) will vanish for all $\underline{\beta}$. In order that the correlation not vanish everywhere we must take $M_C = M_R$. Thus, if a diffuse reference is used the identical reference must be used for the illumination during reconstruction.

Note that in general a discrete sum of plane waves as reference cannot be made to satisfy (IV.30). The cross product terms will not vanish and there will be a background noise in the reconstruction. When the reference is spherical there will be aberations of the image[48,49,50].

5. GENERAL FORM OF THE HOLOGRAM OPERATOR, II

It is now clear that any formulation of holography along the lines of Equation (IV.6) must be in terms of an integral equation. Most of the known theory of integral equations pertains to Fredholm equations of the second kind[46]. In order to represent holography in terms of equations of this type it is necessary to include the propagation of the field from object plane $\underline{r}_0$ to hologram plane $\underline{r}_S$ during

recording. As mentioned in the preceding section by so doing we uniquely specify the reconstruction problem.

To avoid confusion the following convention will be adopted subsequently. Acoustic fields will be denoted A, electronic signals will be denoted E and visible fields (light) will be denoted V. Also we shall adopt the plane wave expansion formalism (IV.15) for a variety of reasons. For example, the analysis of acoustic holography must depart from the usual small angle theory of visible optics for two reasons. First, there are likely to be "near field" or "wide angle" situations for which the paraxial approximations of conventional Fresnel and Fraunhoffer diffraction theory are invalid, the experimental situations covered in Chapter V probably falling in this category. However, conventional paraxial theories will remain useful for calculating focal lengths since the concept of focus is meaningful only in first order theory.

Second, in visible optics no account is taken of the directional sensitivity of the molecules making up the grains of the photosensitive emulsion since this effect is integrated over many molecules and grains randomly oriented. However, for the bulk of acoustic work (including the experiments presented in Chapter V) a different situation exists because acoustic fields are detected by piezoelectric transducers. A correct analysis of this case must include the directional characteristics of the transducer and the sampling properties of the scanning procedure. The directional nature of the receiver is determined by measuring its response to an acoustic plane wave as a function of the angle of incidence. Obviously, any factor which depends upon wave

number is most easily incorporated if the plane wave expansion formalism is employed.

Finally, the most elementary holograms (holographic diffraction gratings) are those made by the interference of two plane waves. These elementary holograms are the basic building blocks from which more complex holograms are constructed. Experimental study of the properties of such holograms provides the basic data for holographic research[51]. Thus, it seems natural to formulate the theory of holography in a way which emphasizes this fact and which is related to the most basic holographic measurements.

The acoustic field scattered into the hologram plane $\underline{r}_S$ from the object plane $\underline{r}_O$ is

$$A_O(\underline{r}_S) = \frac{1}{(2\pi)^2} \int\int_{-\infty}^{\infty} A_O(\underline{r}_O) e^{i\underline{\kappa}_A \cdot (\underline{r}_S - \underline{r}_O)} e^{ik_{zA}(z_S - z_O)} d^2\kappa_A d^2 r_O \quad . \tag{IV.31}$$

In the S plane a hologram is formed by causing $A_O(\underline{r}_S)$ to interfere either acoustically or electronically (see Section V.4) to form an interference pattern which is imperfectly converted into an electronic signal by a piezoelectric detector with plane wave response $D(\underline{\kappa}_A)$. The desired interference signal looks like

$$E_O(\underline{r}_S)E_R^*(\underline{r}_S) = K_E \frac{A_R^*(\underline{r}_S)}{(2\pi)^2} \int\int_{-\infty}^{\infty} A_O(\underline{r}_O) D(\underline{\kappa}_A) \text{III}\left(\frac{\underline{r}_S \cdot \hat{x}}{d}\right) \text{III}\left(\frac{\underline{r}_S \cdot \hat{y}}{d}\right) \cdot e^{i\underline{\kappa}_A (\underline{r}_S - \underline{r}_O)} e^{ik_{zA}(z_S - z_O)} d^2\kappa_A d^2 r_O \tag{IV.32}$$

where III(x) denotes the infinite array of evenly spaced one dimensional delta functions

$$III(x) = \sum_{-\infty}^{\infty} \delta(x-n) \quad , \tag{IV.33}$$

and K_E is a conversion constant.

To produce a hologram, the field over the entire hologram aperture must be detected and recorded, either by covering the aperture with sensors or else by mechanically scanning one or several over the aperture. An array involves two dimensional sampling, linear scanning only one simensional sampling. The delta function arrays account for the sampling procedure. Vertical scanning ($\hat{y}$ directed lines evenly spaced d apart) was adopted for the experiments presented in Chapter V.

The interference signal (IV.32) is next converted imperfectly into a visible transparency (the acoustic hologram) according to

$$P(\underline{r}_S) = K_P \int_S S(\underline{r}_S,\underline{r}'_S) E_O(m\underline{r}'_S) E_R^*(m\underline{r}'_S) d^2r'_S \tag{IV.34}$$

where $S(\underline{r}_S,\underline{r}'_S)$ represents the point spread function (spot size) for the optical display and K_P is a conversion constant. For an ideal system $S(\underline{r}_S,\underline{r}'_S) = \delta(\underline{r}_S-\underline{r}'_S)$ but this is never realized in practice. For example, in the experiments presented in Chapter V the acoustic interference pattern in the hologram plane was displayed on a cathode ray tube (CRT) which had a minimum spot size of 0.2 mm diameter.

The factor m accounts for a linear reduction of transverse acoustic field dimensions by m to those of the hologram transparency. A linear reduction is required so that the resulting hologram will focus

inside the coherence volume of the light used for reconstruction and within a finite sized laboratory.

The acoustic hologram (IV.34) is then illuminated with coherent light in order to obtain a somewhat imperfect visible replica (reconstruction) of the acoustic field A_0. The reconstructed replica field $V_I(\underline{r}_I)$ in plane $\underline{r}_I$ is given by

$$V_I(\underline{r}_I) = \frac{1}{(2\pi)^2} \int\int_{-\infty}^{\infty} P(\underline{r}_S) e^{i\underline{\kappa}_V \cdot (\underline{r}_I - \underline{r}_S)} e^{ik_{zV}(z_I - z_S)} d^2\kappa_V d^2 r_S \quad . \tag{IV.35}$$

Substituting (IV.34) and (IV.32) yields

$$\begin{aligned} V_I(\underline{r}_I) = \frac{K_E K_P}{(2\pi)^4} \int\int\int\int_{-\infty}^{\infty}\int\int & A_0(\underline{r}_0) E_R^*(m\underline{r}_S') V_C(\underline{r}_S) D(\underline{\kappa}_A) \cdot \\ & \cdot \mathrm{III}\left(\frac{m\underline{r}_S' \cdot \hat{x}}{d}\right) \mathrm{III}\left(\frac{m\underline{r}_S' \cdot \hat{y}}{d}\right) S(\underline{r}_S, \underline{r}_S') \cdot \\ & \cdot e^{i\underline{\kappa}_A \cdot (m\underline{r}_S' - \underline{r}_0)} e^{ik_{zA}(z_S - z_0)} e^{i\underline{\kappa}_V \cdot (\underline{r}_I - \underline{r}_S)} e^{ik_{zV}(z_I - z_S)} \\ & d^2 r_0 d^2\kappa_A d^2 r_S' d^2\kappa_V d^2 r_S \quad . \end{aligned} \tag{IV.36}$$

Defining

$$K_{m\mu}(\underline{r}_I,\underline{r}_0) \equiv \frac{K_E K_P}{(2\pi)^4} \int\int_{-\infty}^{\infty}\int\int E_R^*(m\underline{r}_S') \text{III}\left(\frac{m\underline{r}_S'\cdot\hat{x}}{d}\right) \text{III}\left(\frac{m\underline{r}_S'\cdot\hat{y}}{d}\right) \cdot$$

$$\cdot S(\underline{r}_S,\underline{r}_S')V_L(\underline{r}_S)D(\underline{\kappa}_A)e^{i\underline{\kappa}_A\cdot(m\underline{r}_S'-\underline{r}_0)}e^{ik_{zA}(z_S-z_0)} \cdot$$

$$\cdot e^{i\underline{\kappa}_V\cdot(\underline{r}_I-\underline{r}_S)}e^{ik_{zV}(z_I-z_S)}d^2\kappa_A d^2r_S' d^2\kappa_V d^2r_S \qquad \text{(IV.37)}$$

Equation (IV.36) may be rewritten as

$$V_I(\underline{r}_I) = \int_{-\infty}^{\infty} K_{m\mu}(\underline{r}_I,\underline{r}_0)A_0(\underline{r}_0)d^2r_0 \quad . \qquad \text{(IV.38)}$$

Now holography will only be useful if it is possible to select pairs of object planes such that in these planes the positional dependence of V_I and A_0 is geometrically similar. That is we desire

$$hV_I(\underline{r}) = A_0(r) \quad . \qquad \text{(IV.39)}$$

Then (IV.38) becomes

$$A_0(\underline{r}_I) = h\int_{-\infty}^{\infty} K_{m\mu}(\underline{r}_I,\underline{r}_0)A_0(\underline{r}_0)d^2r_0 \quad . \qquad \text{(IV.40)}$$

Now (IV.38) can be reduced to (IV.40) only by selecting special combinations of z_I and z_0; i.e.,

$$z_I = f(z_0) \qquad \text{(IV.41)}$$

where f represents a functional dependence yet to be determined. The relation (IV.41) is known as a <u>focusing condition</u>. When (IV.41) is satisfied $K_{m\mu}$ reduces to a form satisfying (IV.40). However, even when the focusing condition is satisfied (IV.40) may not be valid for any field configuration A_0, only certain special ones A_{0n}. Hence (IV.40) is more properly written

$$A_{0n}(\underline{r}_I) = h_n \int_{-\infty}^{\infty} K_{m\mu}(\underline{r}_I,\underline{r}_0)A_{0n}(\underline{r}_0)d^2r_0 \qquad \text{(IV.42)}$$

where h_n represents the relative "strength" of the corresponding configuration A_{0n} in the reconstruction.

Equation (IV.42) is immediately recognized as a homogeneous Fredholm equation of the second kind with kernel $K_{m\mu}(\underline{r}_I,\underline{r}_0)$, eigenfunctions $A_{0n}(\underline{r}_0)$ and eigenvalues h_n.

Over a period of years numerous authors have contributed to the theory of Fredholm equations. Certain of the properties of Fredholm equations of special significance to holography are stated below without proof[52].

1. Corresponding to the homogeneous Fredholm equation

$$\xi(\underline{r}) = \lambda \int_I K(\underline{r},\underline{r}')\xi(\underline{r}')d^2r' \qquad \text{(IV.43)}$$

construct the inhomogeneous Fredholm equation

$$\xi(\underline{r}) = \varsigma(\underline{r}) - \int_I K(\underline{r},\underline{r}')\xi(\underline{r}')d^2r' \qquad \text{(IV.44)}$$

where $g(\underline{r})$ is arbitrary. Then either the inhomogeneous Equation (IV.44) has a unique solution for any $g(\underline{r})$, or the homogeneous Equation (IV.43) has at least one nOn-trivial solution $\xi_\lambda(\underline{r})$ with eigenvalue λ.

2. Any function $A(\underline{r})$ which can be represented as a "source" distribution in which $K(\underline{r},\underline{r}')$ plays the role of a Green's function; i.e.,

$$A(\underline{r}) = \int_I K(\underline{r},\underline{r}')B(\underline{r}')d^2r' \qquad \text{(IV.45)}$$

where $B(\underline{r}')$ is arbitrary, can be expanded in terms of the eigenfunctions $\xi_n(\underline{r})$ of $K(\underline{r},\underline{r}')$.

Although it is not known if solutions to (IV.42) (perfectly reconstructed field configurations) exist in the general case, property 1 suggests that such solutions should exist. The second property of Fredholm equations indicates the possible use of such configurations as expansion functions.

6. APPROXIMATE SOLUTIONS TO THE EIGENVALUE EQUATION

In order to reduce the eigenvalue equation to a form which is readily solved we must determine the focusing condition (IV.41). This is most easily accomplished when the fields are paraxial. Then the k_z may be expanded in a power series and only the lower order terms retained. Although the recording of an acoustic hologram is not generally a paraxial problem a simple arguement will show that the reconstruction from an acoustic hologram is always a paraxial situation.

Consider an acoustic plane wave travelling in the θ_A direction

(wave number k_A, transverse wave number κ_A where $\sin\theta_A = \kappa_A/k_A$) generated from a grating of spatial frequency $\kappa_A/2\pi$. If the grating is reduced in size by m and then illuminated with light at normal incidence (wave number $k_V = \mu k_A$) then the grating will diffract a plane wave in a new direction θ_V given by

$$\sin\theta_V = \frac{\kappa_V}{k_V} = \frac{m\kappa_A}{\mu k_A} = \frac{m}{\mu}\sin\theta_A \quad . \tag{IV.46}$$

Typical numbers for acoustic holograms (at 1 MHz in water) are $m = 30$, $\mu \simeq 3\times10^3$, $m/\mu = 10^{-2}$. Thus, even though recording an acoustic hologram is likely to involve large angles θ_A, the corresponding reconstructed angles θ_V will always be small, hence paraxial.

In the paraxial approximation

$$k_z = (k^2 - \kappa^2)^{1/2} \simeq k - \frac{1}{2}\frac{\kappa^2}{k} \quad . \tag{IV.47}$$

For simplicity and without loss of generality take the origin of coordinates to lie in the hologram plane so that $z_S = 0$. Then the κ_A integration in Equation (IV.37) becomes

$$\int_{-\infty}^{\infty} D(\underline{\kappa}_A)\, e^{i\underline{\kappa}_A\cdot(m\underline{r}'_S - \underline{r}_O)}\, e^{-ik_{zA}z_O}\, d^2\kappa_A = -i\left(\frac{k_A}{2\pi z_O}\right)(2\pi)^2 e^{-ik_A z_O} \cdot$$

$$\cdot\left[e^{i\pi(k_A/2\pi z_O)|m\underline{r}'_S - \underline{r}_O|^2}\right] * D[m\underline{r}'_S - \underline{r}_O)/2\pi] \tag{IV.48}$$

where we have used the relation

$$\underbrace{e^{\pm i\pi B|\underline{s}|^2}}_{\sim} = \frac{-}{+}\frac{i}{B}\, e^{\pm i\frac{\pi}{B}|\underline{r}|^2} \quad . \tag{IV.49}$$

In the more general case the paraxial assumptions are invalid for describing the recording of an acoustic hologram and instead of (IV.48) we must write

$$\int_{-\infty}^{\infty} D(\underline{\kappa}_A)\, e^{i\underline{\kappa}_A\cdot(m\underline{r}'_S - \underline{r}_O)}\, e^{-ik_{zA}z_O}\, d^2\kappa_A =$$

$$G(m\underline{r}'_S - \underline{r}_O) * \underset{\sim}{D}[(m\underline{r}'_S - \underline{r}_O)/2\pi] \tag{IV.50}$$

where

$$G(\underline{r}) = \underbrace{e^{ik_{zA}z_O}}_{\sim} \quad . \tag{IV.51}$$

Applying the paraxial procedure to the κ_V integration, assuming that the exponential factors in K_{mu} vary slowly in $\underline{r}'_S$ compared to the display spread function $S(\underline{r}_S,\underline{r}'_S)$, and assuming display spot size and shape is independent of position (not true for electrostatic CRT displays unless restricted to the center portion) finally yields

$$K_{mu}(\underline{r}_I,\underline{r}_O) = \frac{K_E K_P k_V k_A (2\pi)^2}{z_O z_I}\, e^{i(k_V z_I - k_A z_O)}\, e^{i\pi(k_V/2\pi z_I)r_I^2} \cdot$$

$$\cdot \int_{-\infty}^{\infty} \Pi(x_S/X)\Pi(y_S/Y) s_d(\underline{r}_S) E_R^*(m\underline{r}_S) V_C(\underline{r}_S) \cdot \tag{IV.52}$$

$$\cdot \left[e^{i\pi(k_A/2\pi z_O)|m\underline{r}_S - \underline{r}_O|^2} \right] * \underset{\sim}{D}[(m\underline{r}_S - \underline{r}_O)/2\pi] \cdot$$

$$\cdot e^{-i\pi(k_V/2\pi z_I)r_S^2}\, e^{2\pi i\underline{r}_S\cdot(k_V\underline{r}_I/2\pi z_I)}\, d^2 r_S$$

where the finite size 2X, 2Y of the hologram aperture is included in the function $\Pi(x_S/X)\Pi(y_S/Y)$, and where

$$R_d(\underline{r}_S) = S(\underline{r}_S) * [III(x_S/d)III(y_S/d)] \tag{IV.53}$$

is the raster function representing the composite effect of sampling and finite display spot size.

To evaluate (IV.52) we must choose E_R and V_C. Usually, sources of acoustic radiation tend to be point rather than planar sources. Moreover, it will prove advantageous to use spherically converging wavefronts during reconstruction. Accordingly, we consider the special but important case wherein

$$E_R(\underline{r}_S) = E_R\, e^{ik_A z_R}\, e^{i(k_A/2z_R)|\underline{r}_S - \underline{r}_R|^2}, \tag{IV.53}$$

$$V_C(\underline{r}_S) = V_C\, e^{ik_V z_C}\, e^{i(k_V/2z_C)|\underline{r}_S - \underline{r}_C|^2}; \tag{IV.54}$$

V_C is a spherical wave with focus located at $\underline{r}_C, z_C$; E_R appears to be a spherical wave with focus located at $\underline{r}_R, z_R$. E_R may originate from an actual acoustic source or it may be an electronic simulation of an acoustic source. (Electronic simulation is usually confined to planar references.) With respect to the hologram plane, Focal points $z < 0$ represent diverging waves, focal points $z > 0$ represent converging waves.

Substituting (IV.53) and (IV.54) into (IV.52) yields upon commuting the convolution with the r_S integration

$$K_{mi}(\underline{r}_I,\underline{r}_O) = \frac{K_E K_P k_V k_C E_R^* V_C (2\pi)^2}{z_O z_I} e^{ik_V(z_I + z_C)} e^{-ik_A(z_O + z_R)} \cdot$$

$$\cdot e^{i(k_V/2z_C)r_C^2} e^{-i(k_V/2z_I)r_I^2} e^{i(k_A/2z_O)r_O^2} e^{-i(k_A/2z_R)r_R^2} \cdot$$

$$\cdot \int_{-\infty}^{\infty} D(\underline{v}) e^{i(k_A/2z_O)v^2} e^{+2\pi i \underline{v}\cdot(k_A\underline{r}_O/2\pi z_O)} d^2v \cdot \qquad \text{(IV.55)}$$

$$\cdot \int_{-\infty}^{\infty} \Pi(x_S/X)\Pi(y_S/Y)\tilde{n}_d(\underline{r}_S) e^{2\pi i \underline{r}_S\cdot[(k_V\underline{r}_I/2\pi z_I) - (k_V\underline{r}_C/2\pi z_C)]} \cdot$$

$$\cdot e^{2\pi i \underline{r}_S\cdot[(mk_A\underline{r}_R/2\pi z_R) - (mk_A\underline{r}_O/2\pi z_O) - (k_A\underline{v}/2\pi z_O)]} \cdot$$

$$\cdot e^{i\pi[(k_V/2\pi z_C) - (k_V/2\pi z_I) + (m^2k_A/2\pi z_O) - (m^2k_A/2\pi z_R)]r_S^2} \cdot$$

$$\cdot d^2r_S$$

where $\underline{v}$ is a dummy variable required for the convolution operation.

The quadratic phase term appearing in (IV.55) may be eliminated by taking the image plane $z = z_I$ to be located at

$$z_I = \frac{mz_O}{m^2(1 - z_O/z_R) + mz_O/z_C} \qquad \text{(IV.56)}$$

Equation (IV.56) is the form which the focusing condition (IV_41) takes for the approximate calculation we are considering here. This condition is quite useful because the concept of focus is really only a first order phenomena anyway.

With elimination of the quadratic phase factor in the r_S integration K_{mu} becomes

$$K_{mu}(\underline{r}_I,\underline{r}_0) = \text{const}\, e^{i(k_A/2z_0)r_0^2} \cdot$$

$$\cdot \int_{-\infty}^{\infty} \underline{D}(\underline{v}) e^{i(k_A/2z_0)v^2} e^{2\pi i \underline{v}\cdot(k_A\underline{r}_0/2\pi z_0)} \cdot \qquad \text{(IV.57)}$$

$$\cdot \{\text{sinc}[2\pi X(v_x' - k_A v_x/2\pi z_0)] * \tilde{E}_d(v_x' - k_A v_x/2\pi z_0)\} \cdot$$

$$\cdot \{\text{sinc}[2\pi Y(v_y' - k_A v_y/2\pi z_0)] * \tilde{E}_d(v_y' - k_A v_y/2\pi z_0)\}\, d^2v$$

where

$$\underline{v}' = k_V\underline{r}_I/2\pi z_I - k_V\underline{r}_C/2\pi z_C - mk_A\underline{r}_0/2\pi z_0 + mk_A\underline{r}_R/2\pi z_R$$

$$\text{sinc}\, x = \frac{\sin x}{x}$$

$$\text{const} = \frac{4k_E k_P k_V k_C E_R^* V_C XY(2\pi)^2}{z_0 z_I} e^{ik_V(z_I + z_C)} e^{-ik_A(z_0 + z_R)} \cdot$$

$$\cdot e^{i(k_V/2z_C)r_C^2} e^{-i(k_V/2z_I)r_I^2} e^{-i(k_A/2z_R)r_R^2} \cdot \qquad \text{(IV.58)}$$

As X and Y become large the sinc functions become increasingly peaked around

$$k_V \underline{r}_I/z_I - k_V \underline{r}_C/z_C - mk_A \underline{r}_O/z_O + mk_A \underline{r}_R/z_R - k_A \underline{v}/z_O = 0. \qquad \text{(IV.59)}$$

Further, if the angular response $D(\underline{\kappa}_A)$ of the detector elements is sufficiently broad, $\underline{D}(\underline{v})$ will be nonzero only in a narrow range about $\underline{v} = 0$.* Thus for sufficiently large holograms and for sufficiently broad detector response $K_{m\mu}$ behaves approximately like a two-dimensional delta function and the r_O integration (IV.36) can be carried out to give

$$V_I(\underline{r}_I) = hA_O(\underline{r}_O M + \underline{o})\, e^{i(k_A/2z_O)|\underline{r}_O M + \underline{o}|^2} \qquad \text{(IV.60)}$$

where

$$M = \frac{1}{m(1 - z_O/z_R) + (\mu/m)(z_O/z_C)} \quad ,$$

$$\underline{o} = \frac{\underline{r}_C(\mu/m)(z_O/z_C) - \underline{r}_R z_O/z_R}{m(1 - z_O/z_R) + (\mu/m)(z_O/z_C)} \quad , \qquad \text{(IV.61)}$$

$$h = \frac{4K_E K_P k_V k_C E_R^* V_C XY(2\pi)^2}{z_O z_I}\, e^{ik_V(z_I + z_C)}\, e^{-ik_A(z_O + z_R)} \cdot$$

$$\cdot e^{i(k_V/2z_C)r_C^2}\, e^{-i(k_V/2z_I)r_I^2}\, e^{-i(k_A/2z_R)r_R^2} \quad .$$

Thus, from Equations (IV.56), (IV.60), and (IV.61) we see that to first order, and provided that the assumptions stated above are valid,

---

* In order that the ideal detector response $D(\underline{v}) = \delta^2(v)$ be obtained the detector would have to respond equally to propagating and to evanescent waves.

the reconstructed image is a visible replica of the object boundary acoustic field but magnified laterally by M, displaced laterally by $\underline{o}$, and magnified longitudinally by μM^2. Similar expressions are obtained if $A_O^* E_R$ is substituted for $A_O E_R^*$. The relations are

$$z_I = \frac{\mu z_O}{m^2(z_O/z_R - 1) + \mu z_O/z_C} \quad ,$$

$$M = \frac{-1}{m(1 - z_O/z_R) - (\mu/m)(z_O/z_C)} \quad , \qquad \text{(IV.62)}$$

$$\underline{o} = \frac{\underline{r}_R(z_O/z_R) - \underline{r}_C(\mu/m)(z_O/z_C)}{m(1 - z_O/z_R) - (\mu/m)(z_O/z_C)} \quad .$$

Relations (IV.56), (IV.61), and (IV.62) have been obtained through different techniques by Meier[54,55,56]. To put these equations in his form substitute 1/m for m, $1/\mu$ for μ.

We now consider a special case which is of particular importance in acoustic holography because of the ability to simulate planar references electronically. If

$$z_R \to \infty \; , \; z_C \to \infty \qquad \text{(IV.63)}$$

such that

$$\frac{r_R}{z_R} \to \text{const} = \tan\theta_R \; , \; \frac{r_C}{z_C} \to \text{const} = \tan\theta_C \; , \qquad \text{(IV.64)}$$

where θ_R and θ_C are the angles which the wave vectors of the reference

and reconstruction plane waves make with the normal to the hologram plane, then the preceeding relations reduce to

$$z_i = \pm\frac{\mu z_0}{m^2} \ ,$$

$$M = \pm\frac{1}{m} \ , \qquad \text{(IV.65)}$$

$$\underline{o} = \frac{(\hat{r}_R \tan\theta_R - \hat{r}_C \mu/m \tan\theta_C) z_0}{m} \ .$$

The + sign indicates a real image, the - sign indicates a virtual image. The last of relations (IV.65) is valid only for paraxial reference and reconstruction plane waves. In the more general case substitute sin for tan.

From (IV.65) it is clear that in this important case lateral magnification does not depend upon the wavelength ratio, and we see the desirability of minimizing the reduction m of the hologram between recording and reconstruction. We also note that there is distortion of the reconstructed object scene because the longitudinal magnification is considerably different from the lateral magnification. For example, spherical objects will appear as oblate objects in reconstruction. Depending upon the parameters this effect can be extreme.

7. EFFECT OF DETECTOR DIRECTIVITY

The directional characteristics of acoustic detecting elements

restrict

1. resolution
2. field of view.

From condition (IV.59) the effect of the form of $D(\underline{\kappa}_A)$ upon resolution is clearly evident. As the angular spectrum $D(\underline{\kappa}_A)$ becomes restricted, $\underset{\sim}{D}(\underline{v})$ becomes less sharply peaked about $\underline{v} = 0$. This, in turn, requires that $\underline{v}$ assume various non-zero values in (IV.59) thereby leading to a reconstruction which is a superposition of various images, each at a slightly different lateral position. Thus, the reconstruction appears to be blurred.

In extreme cases this effect can lead to the appearance of double images. For example, in the one-dimensional case if $\underset{\sim}{D}(v)$ were a double-humped pattern, idealized as say

$$\underset{\sim}{D}(v) = \Pi(v/a) + \Pi[(v - b)/a] \tag{IV.66}$$

where a is the width and b the separation of narrow rectangular peaks, then a double image would be formed. The corresponding angular spectrum for the detector is of the form

$$D(\kappa_A) = a\,\mathrm{sinc}(\kappa_A a)\left(1 + e^{i\kappa_A b}\right) \quad , \tag{IV.67}$$

a multi-phased response. Thus, one must give due regard to the phase characteristics of the detector. In the case of piezoelectric detectors this means desinging the structure to minimize internal reflections.

The dependence of field of view upon detector pattern is obvious although it cannot be obtained from the paraxial equations. Clearly,

objects lying at angles outside the pattern of the detection elements will not be imaged. This effect is probably more pronounced in holography than in conventional imaging because in the latter each image point is formed by rays converging to the point from all angles inside the solid angle subtended by the lens aperture at the point (provided the incoming radiation is diffuse). Thus, if a low f number lens is used surely some portion of the acoustic radiation at each image point will lie within the detector angular response pattern. It would be interesting to consider to what extent holographic techniques can be used to compensate for the detector angular response.

8. SPACE-BANDWIDTH PRODUCT FOR ACOUSTIC HOLOGRAMS

Space bandwidth products have been calculated for visible holography[34]. The technique is to assume that the hologram size 2X, 2Y is always so large that the number of Fresnel zones recorded is limited by the film resolution rather than the film size. Thus, the limit to resolution in visible holography is essentially the film, not the aperture size. In this sense holography provides very great resolution simply because of the extremely fine-grained emulsions which are available. For film limited holograms DeVelis and Reynolds have calculated that the one-dimensional space bandwidth product for coplanar reference holograms should be approximately

$$SBP \approx 1.64 s_m X \qquad \text{(IV.68)}$$

where s_m is the maximum spatial frequency which can be recorded by the film and X is the film size.

In acoustic holography a different situation will often be

encountered. Here it is quite likely that the resolution of the "film" or sampling procedure will be more than adequate and that the limit to resolution will be simply the finite number of Fresnel zones which can be accomodated in a relatively small aperture. For aperture limited holograms the Rayleigh criterion gives an approximate value for the resolution. Thus, for acoustic holograms

$$SBP \simeq \frac{X^2}{1.22\lambda z_0} \tag{IV.69}$$

where z_0 is the distance between hologram and object planes. Equation (IV.69) is also valid for acoustic holograms in which the reference is introduced externally and the interference occurs electronically in the display rather than acoustically in the propagating medium. Of course, if the resolution of the display device is a limiting factor then (IV.68) applies but with s_m replaced with s_{md}/m where s_{md} is the resolution limit of the display and m is the demagnification ratio.

Certain assumptions relative to establishing the contrast level which constitutes a "resolved" fringe are implicit in Equations (IV.68) and (IV.69). Clearly, spatial coherence and film or display MTF are important in this connection. Here it has been assumed that the fields exhibit complete spatial coherence and that the MTF is uniform up to the cutoff s_m so that fringe contrast is either one(resolved) or zero (unresolved).

It is interesting to determine the aperture size X_t for which the resolution becomes detector or film limited. Equation (IV.68) to (IV.69) we obtain

$$X_t = 2s_m \lambda z_0 \quad . \tag{IV.70}$$

Taking $s_m = 1/NA$,

$$X_t = \frac{2z_0}{N} \tag{IV.71}$$

which is independent of wavelength. Typically $1 < N < 2$ for acoustic holograms so for any reasonable range the aperture required for detector limited performance will be enormous, prohibitively large. For visible holograms $1 < N < 10$ so film limited performance is indeed possible.

9. SUMMARY

We have presented a formulation of holographic imaging in terms of an eigenvalue equation taking the form of a homogeneous Fredholm equation of the second kind. We give the explicit form which the equation assumes for acoustic holograms, including such factors as detector directivity, and present an analysis of the acoustic equation under paraxial assumptions. Even in this case there is longitudinal distortion due to unequal magnification of transverse coordinates relative to longitudinal coordinates. If the paraxial assumption is invalid then the problem becomes even more complicated and in general all images will suffer distortion and aberration. It remains to be seen if the general eigenvalue equation can be solved in the sense of finding a set of object field configurations, the eigenfunctions, which are perfectly imaged; or even to prove the existence of such configurations.

CHAPTER V

EXPERIMENTS IN ACOUSTIC IMAGING BY HOLOGRAPHY

1 INTRODUCTION

We have presented theories of scalar imaging and holography emphasizing acoustic applications. The ultimate goal of acoustic imaging is to obtain, in real time, visible images of objects imbedded in media opaque to all but acoustic fields. We now present experiments demonstrating attainment of visible images of underwater objects by acoustic means using the techniques of holography. This method is known as acoustic holography.

Because of the nature of the experiments and difficulties in performing them, it has not been possible to illustrate each aspect of the theory with an appropriate experiment. Moreover, this research was not intended to yield an immediately practical implimentation of holography into acoustic imaging. Rather, we hope for the more limited goals of showing that visible images of underwater objects can indeed be obtained by acoustic holography, even with simple equipment, and of studying various properties of acoustic holograms.

Before proceeding to a detailed description of the experiments, we must provide a motive for acoustic holography. Acoustic imaging is a relatively new field, the first significant contributions, due to Sokolov, coming only in 1936[57]. Until recently, activity in acoustic imaging has been restricted to an occasional effort along conventional lines; i.e., using acoustic lenses or mirrors, or most often merely an acoustic shadow[58,59,60,61]. The results have been only moderately

successful and, in any case, the ranges were much shorter than required for undersea applications.

Rapid progress in acoustic imaging has been impeded by two problems: (1) lack of suitable acoustic detectors, and (2) difficulty with design and fabrication of abberation free acoustic lenses and mirrors with low acoustic loss and large aperture. Holography provides a way around the second problem simply by eliminating the need for a lens. Conventional imaging is obtained by introducing a carefully controlled angular dispersion into the wave field by causing it to pass through a precisely contoured refractive lens material. In holography, the dispersion process, which presents material and fabrication problems, is replaced by comparison with an accurately known phase reference. In acoustic holography, as will be demonstrated, this reference can easily be generated electronically.

Other useful properties may be attributed to acoustic holography. A hologram contains information about all cross sections of the object scene at right angles to the direction of wave propagation, even if the hologram recording surface is two dimensional. All of this information is retained in a single hologram. Conversely, a lens requires refocusing of the system for each object plane outside of the depth of field, and only one depth of field at a time may be permanently recorded. Echo ranging or sonar techniques require very short duration acoustic pulses in order to accurately determine object positions along the direction of propagation whereas holograms may be made using continuous as well as pulsed illumination.

Unfortunately, holography does not solve the more serious detector problem, and may even aggravate it. The ideal detector should be similar to a photographic emulsion except sensitive to acoustic fields; i.e., it must be an extended surface, preferably of continuous material. The sensitivity should be at least 10^{-8} watts/cm^2, preferably greater. In a conventional imaging system the lens can always be designed so that the image is much smaller than the resolution limiting aperture which is usually the lens. On the other hand, in a holographic imaging system the hologram itself is the resolution determining aperture. Hence, for a specified resolution holographic systems require a much larger detection surface than conventional systems. Possibly a hybrid system could be arranged wherein an imperfect acoustic lens is used to reduce the detection surface to reasonable size without loss of resolution, and holographic detection is used to compensate for the lens induced distortion [62].

Although methods to produce holograms from incoherently illuminated objects are the subject of current research[63], for all practicality, holography must still be regarded as a coherent imaging process. Conversely, a lens will image with incoherent as well as coherent fields. Holography, thus, has all the disadvantages of any coherent imaging system; i.e., loss of resolution over the corresponding incoherent system, edge ringing and displacement, and speckling, phenomena which are discussed in Chapter II and elsewhere[17]. Although the other defects of coherent imaging may be significantly reduced by using diffuse rather than point source illumination [28], the loss of resolution is not thereby recovered. This shortcoming of holography may be

particularly troublesome because there is not likely to be resolution to spare due to the long wavelengths involved with acoustic imaging.

Real time acoustic imaging along conventional lines using the Sokolov device has had some success in ultrasonic flaw detection and other short range applications[64], but this device does not appear to have sufficient resolution or aperture for use as the detecting surface in holographic imaging. Other efforts at real time acoustic holography have been made, but, for the most part, acoustic holography must still be considered a two step procedure in which the hologram is a permanent record to be suitably processed for reconstruction at a later time.

The great need in acoustics, which has yet to be satisfied, is not for sophistication but simply for any practical scheme which enables us to "see" acoustically. Whether acoustic holography will ultimately prove superior to conventional or other techniques for this purpose will not be known for some time.

2. PHYSICAL ARRANGEMENT OF THE EXPERIMENT

The experiment, the physical arrangement of which is shown schematically in Figure V.1 and pictorially in Figures V.2 through V.5, is performed underwater inside an anechoic tank. The object to be visualized is "illuminated" by a 5-cm-diam barium titanate disk driven at 1 MHz (wavelength λ = 1.5 mm in water) (see Appendix D). This frequency was chosen because of its suitability for long range underwater acoustic imaging. It appears, upon examining Figure III.4, that 1 MHz is the highest frequency, hence smallest hologram aperture, for which the attenuation in water is below 200 db/km. Higher frequencies, where

Figure V.1. Arrangement for Making Underwater Acoustic Holograms

C	Carriage
H	Hologram plane
HC	Hydraulic cylinder (152 cm stroke)
L	Acoustic illumination source
LB	Lathe bed
O	Object
P	Probe (457 cm long × 2.54 cm dia)
R	Receiver
S	Tubular supports
T	Anechoic tank (3 m × 3 m × 7 m deep)
WL	Water level (usually 5.5 m deep)

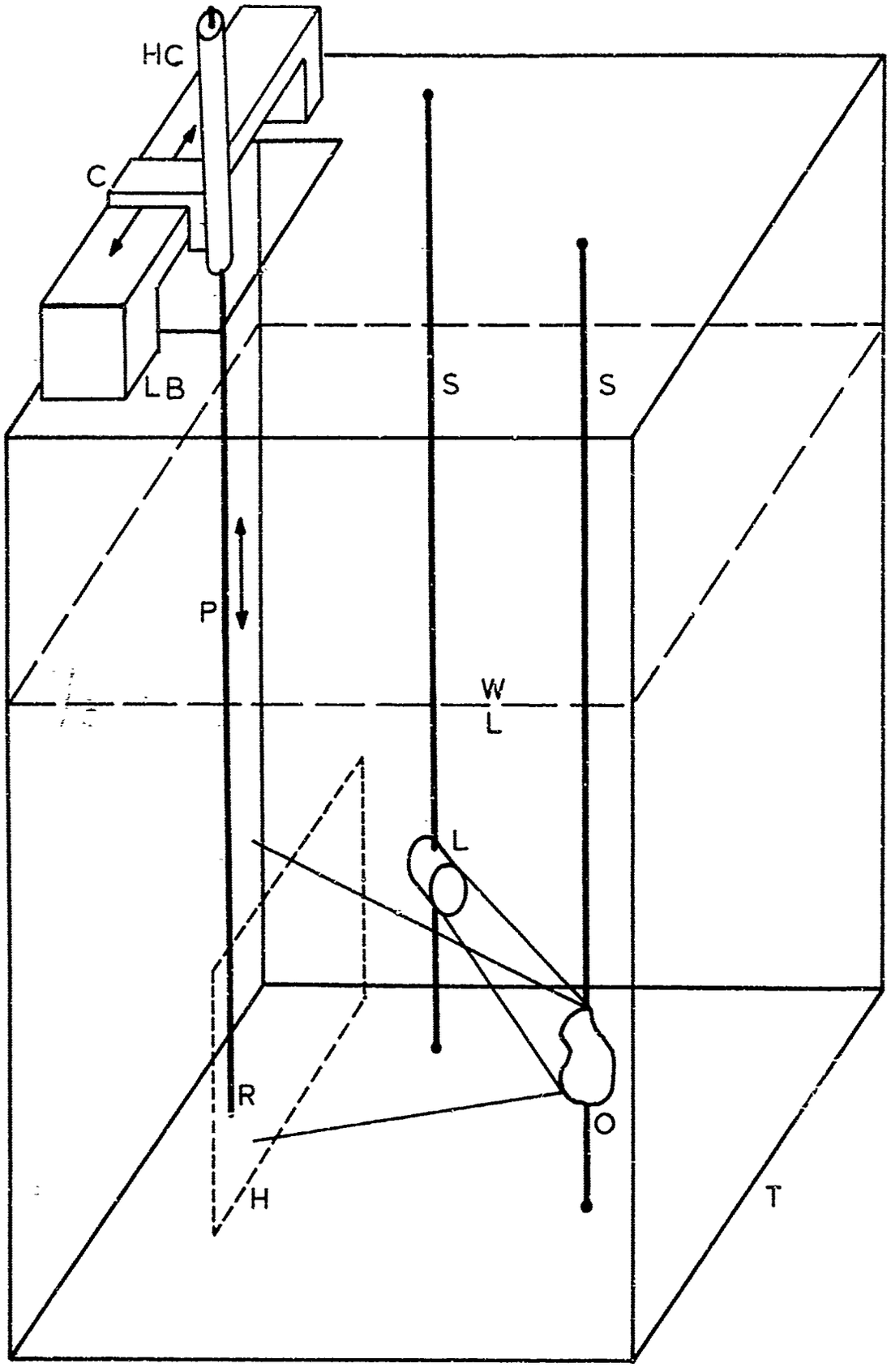
HC
C
LB
S
S
P
W
L
L
R
O
H
T

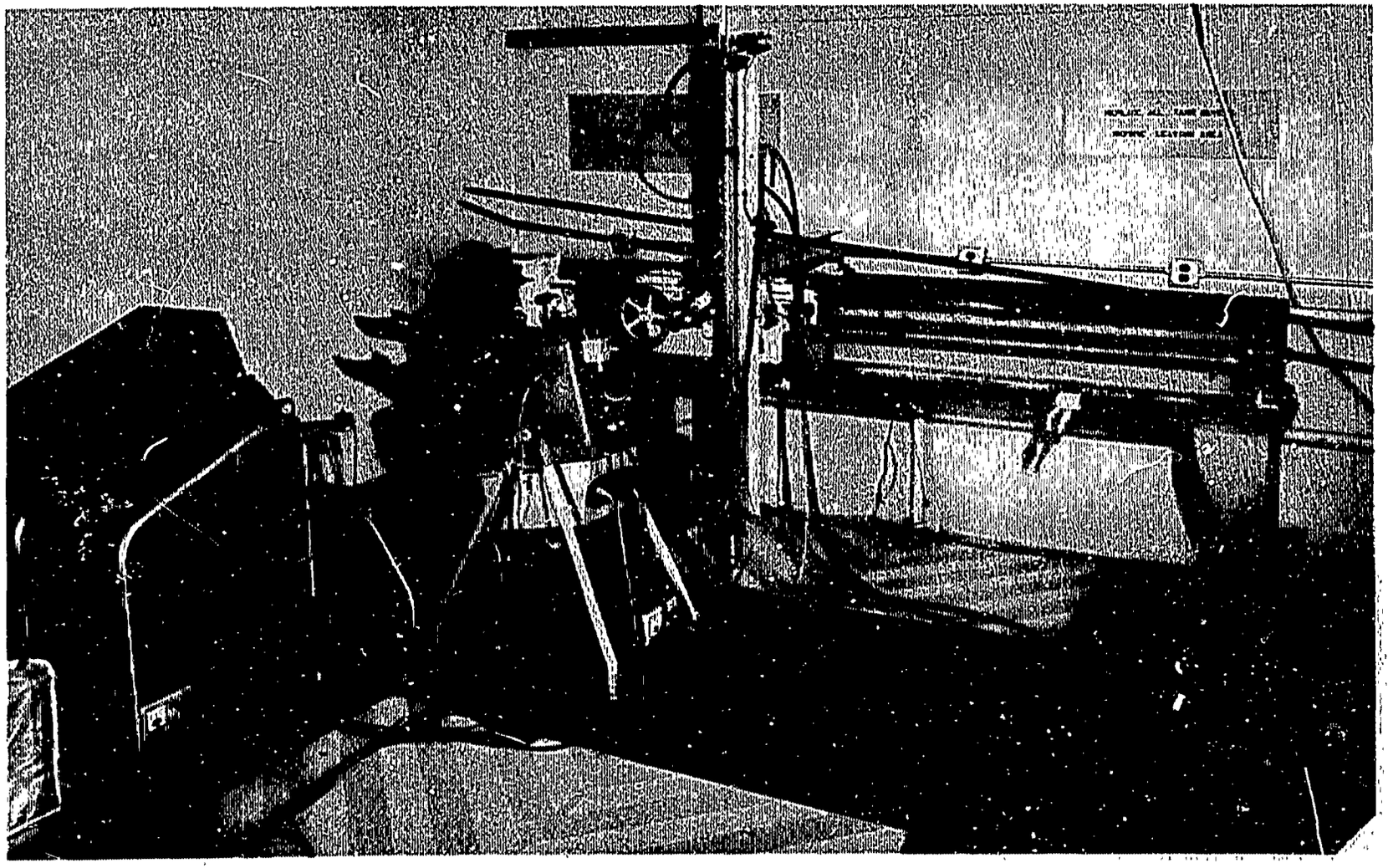

Figure V.2. View of Top of Acoustic Tank.Looking Toward Lathe Bed and Hydraulic Cylinder

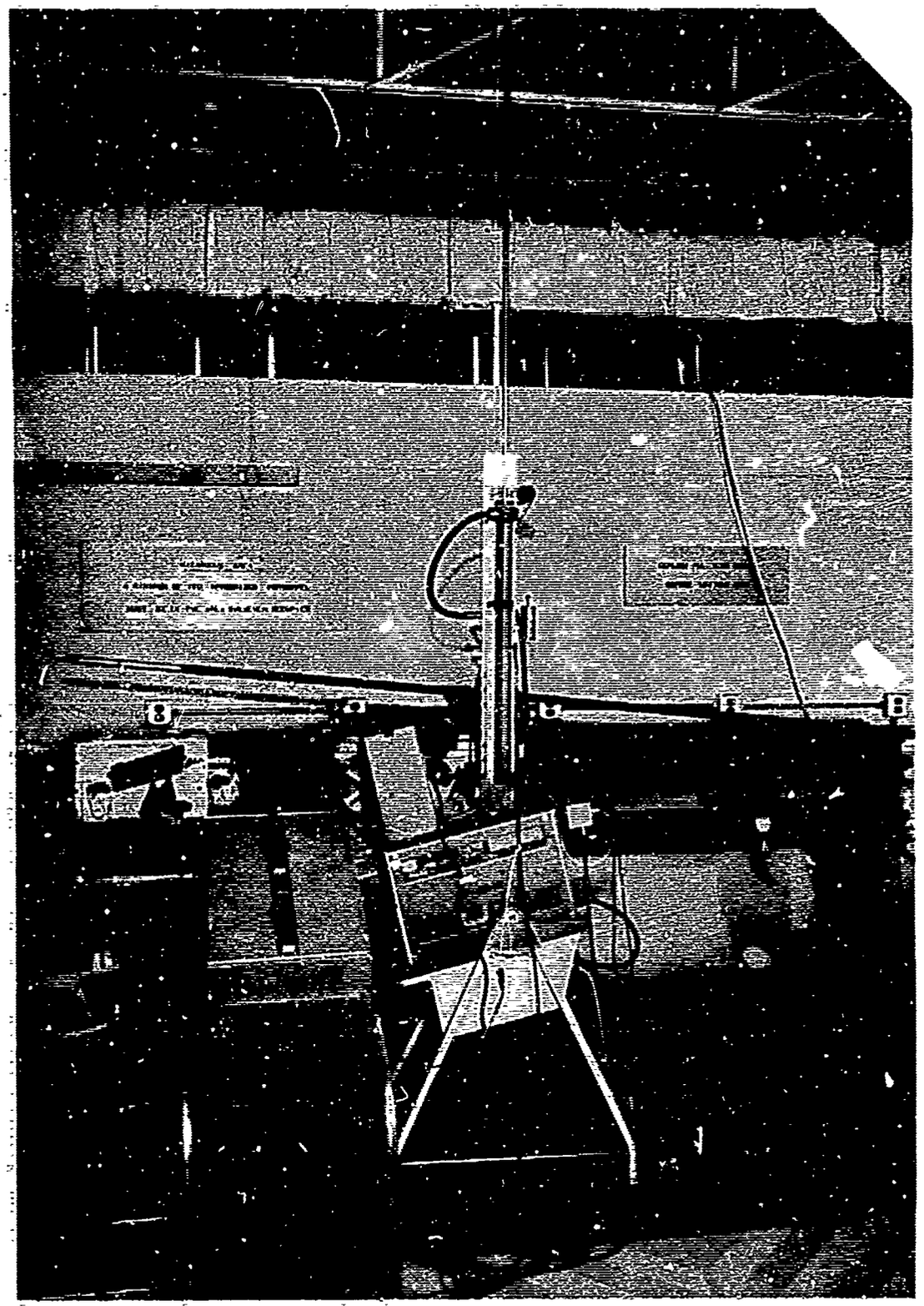

Figure V.3. View of Top of Acoustic Tank
Plane of hologram coincides with opening in tank cover.

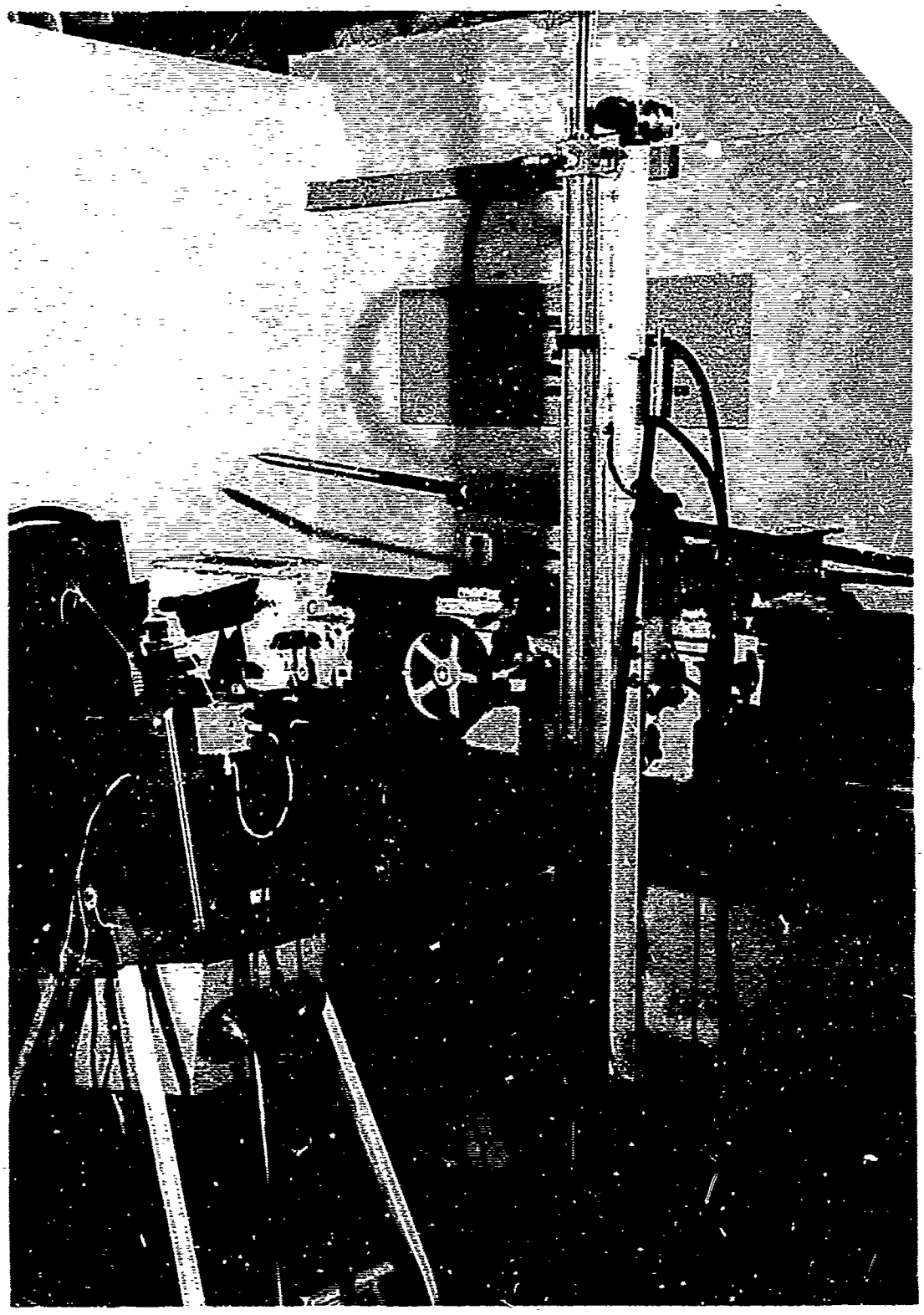

Figure V.4. Close-up of Scanning Mechanism
Probe can be seen in background, display CRO at left.

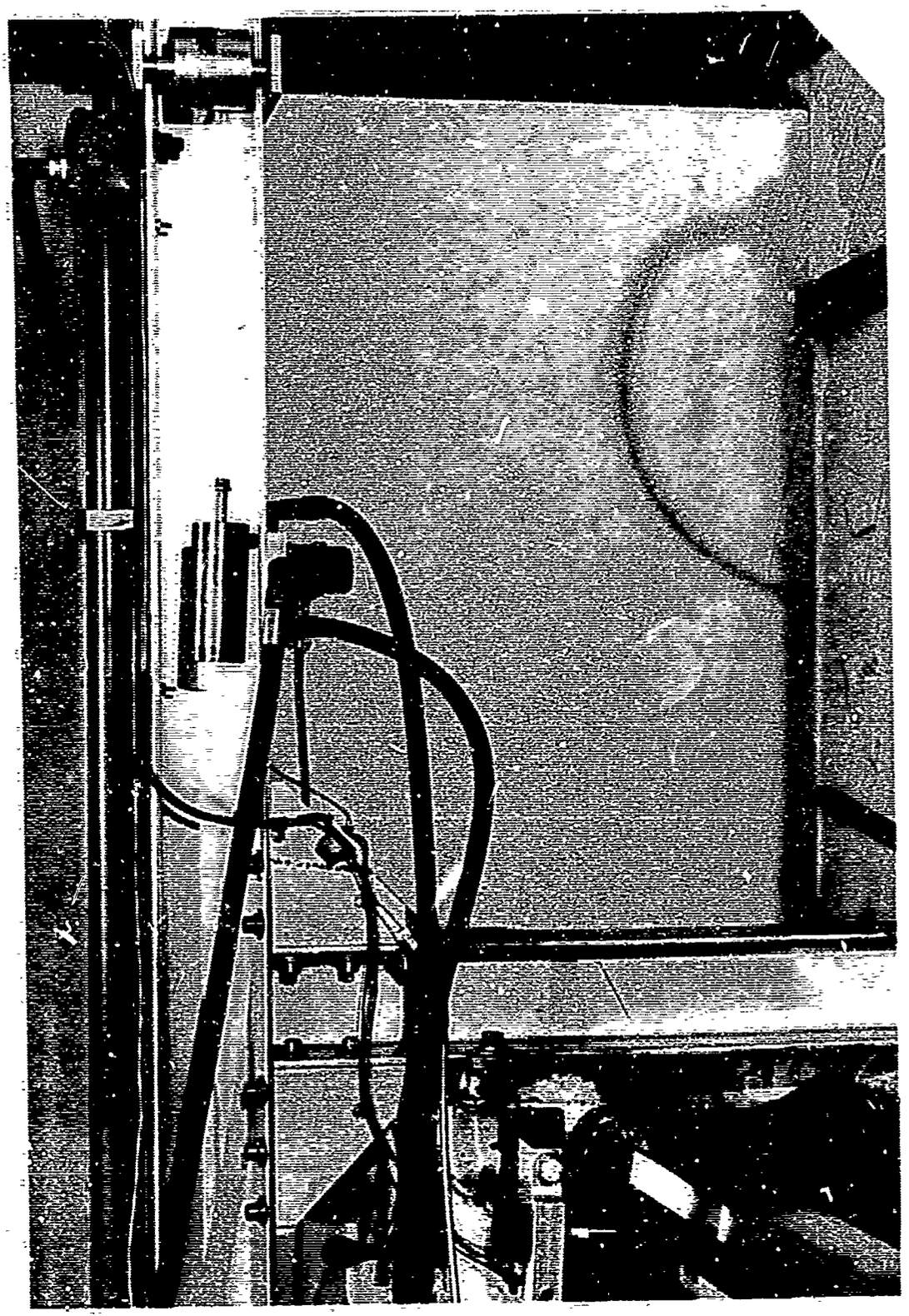

Figure V.5. Detail of Scanning Mechanism

Position sensing potentiometers are at upper left and lower middle.

the attenuation is much greater, would be more suitable for biomedical and flaw detection applications.

The scattered acoustic field is detected by a 3-mm-diam barium titanate disk mounted in a slender probe which may be scanned over a 130 cm × 150 cm vertical plane located near the bottom of the tank. (See Appendix D). The hologram plane was placed at the bottom in order to minimize possible reflections from the air-water interface at the top of the tank. The scanning mechanism consists of a hydraulic cylinder, controlled by a linear two-way servovalve, for the vertical motion, mounted on a lathe carriage and bed assembly for the horizontal motion. With this arrangement any hologram size and spacing of the raster lines may be obtained. To minimize probe vibrations and water disturbance, the raster lines were always scanned in the vertical direction from bottom to top.

The amplified output of the receiving transducer is combined with an electric reference by suitable processing (discussed in the following sections) and then applied directly to the cathode of a Tektronix type 561 oscilloscope thereby modulating the spot intensity of the CRT display. Precision potentiometers connected to the hydraulic cylinder ram and the lathe carriage provide voltages which are proportional to receiver position. These voltages are used to position the spot of the CRT display, the modulated spot thereby tracking the receiving transducer position at reduced scale. The resulting intensity modulated raster is time photographed and then photoreduced approximately 5 to 1 onto high resolution glass plates. Visible reconstructions of the

acoustically "illuminated" objects are then obtained from the reduced hologram transparencies in the usual manner by passing converging or collimated, coherent light from a laser source through them.

The time to record one hologram varied between four and nine hours because a very slow scanning rate (5 cm/sec) was required in order to minimize vibrations of the slender probe (2.5 cm diameter by 500 cm long). In retrospect, the recording process could have been speeded considerably by placing the hologram apperture near the surface, thereby shortening the probe, and electrically gating the signal to avoid interference from surface induced acoustic reflections. However, this author regards mechanical scanning as no more than a simple and inexpensive expedient for gaining information directly applicable to the design of holographic systems using arrays of transducers, possibly a more practical approach, but certainly a much greater undertaking involving costly apparatus. Therefore, the lengthy recording time was not thought to be other than a nuisance.

3. ACOUSTIC HOLOGRAPHY WITH ELECTRONIC REFERENCE

Imaging by holography was analyzed in Chapter IV. An acoustic hologram is formed by interference of two wave fields; one, $A_O(\underline{r})$, originates from the illuminated object, the other, $A_R(\underline{r})$, is the reference.

No restrictions are placed upon the object illumination other than adequate spatial coherence (Section II.3) and that the object be well illuminated (Section III.6). However, stringent requirements are placed on the reference; in addition to spatial coherence, the phase

and amplitude variation of the reference wave across the hologram plane must be carefully controlled because quality reconstructions are obtained only by illuminating the recorded and developed hologram with an accurate replica of the reference (Section IV.4). Simple wave fronts, such as aberration-free spherical or planar waves, are most easily duplicated. However, within the limits imposed in Section IV.4, the reference wave may be as complex as desired, but this complexity must then be exactly duplicated in the reconstruction illumination[47]. In visible optics good image fidelity is obtained for either case.

In acoustic holography although in principle it is easy to "illuminate" the object, it is difficult to generate true spherical or planar acoustic wavefronts of reference quality; i.e., without severe aberrations and mode effects which are difficult to reproduce optically and visual reconstructions from such holograms may be severely distorted[65]. However, perfect reference wavefronts may be simulated electronically by adding the amplified output $E_0(\underline{r})$ of the receiving transducer to an electronic reference signal $E_R(\underline{r})$ which is obtained from the same 1 MHz RF source which drives the illuminating transducer. That is, the reference is derived electronically from a local oscillator rather than acoustically in the tank. Electronic simulation of the reference is possible because piezoelectric acoustic detectors are sensitive to instantaneous amplitude rather than energy (Section II.2).

If the simulation is accomplished simply by adding the local oscillator signal directly to the scattered signal without intervening operations; i.e.,

$$E_R(\underline{r}) = \bar{E}_R = \text{constant}, \qquad (V.1)$$

the coplanar reference is obtained. This is a simple technique which has been employed by others[66,67,68]. In Figure V.6 we show a block diagram of the apparatus used to generate coplanar reference holograms.

To simulate the inclined planar reference requires only a slight complication[69]; the reference amplitude remains constant, as for the coplanar case, but the reference phase varies linearly across the hologram plane. The phase of a planar reference wave, propagating with vector wave number $\underline{k}$ lying in the xz plane and making angle θ with $\hat{z}$, varies across the hologram plane as $xk \sin\theta$. To simulate this wave electronically the phase of the reference signal, derived from the local oscillator, must vary similarly as the position of the receiver changes. However, since large reference angles θ are desired in Leith-Upatnieks holograms so that the real and virtual images are completely separated[10], the phase variation may be accomplished in a particularly simple way, as follows.

In order to uniquely define the direction of the reference, the field over the hologram plane must be sampled at intervals Δx at least as close as

$$\Delta x k \sin\theta = \pi/2 \quad . \qquad (V.2)$$

However, to avoid spurious resolution effects the raster lines must be separated by at least one receiver effective diameter a. Hence, the maximum reference inclination θ_m consistent with both criteria is

$$\theta_m = \arcsin \frac{\pi}{2ak} \quad . \tag{V.3}$$

Maximum reference inclination for scanned holograms is plotted in Figure V.8 against effective receiver diameter expressed in wavelengths.

In our experiments the receiver was approximately two acoustic wavelengths in diameter. Thus, only reference inclination angles less than about 8° could be simulated unambiguously. However, this provided adequate separation of real and virtual images. In general a larger angle, perhaps 30°, is desirable; but the sampling resolution must then be less than an acoustic wavelength, clearly illustrating the increased detector resolution required by holography compared with conventional imaging techniques.

To produce scanned acoustic holograms with reference inclined at θ_m merely advance or retard the phase of the local oscillator signal added to the scattered signal by $\pi/2$, relative to the preceding line, for each new line of the raster. In Figure V.7 we show the block diagram of the apparatus used to generate inclined reference holograms by this technique. The required phase variation was easily accomplished with a switch, a length of delay line, and the polarity inversion feature of an oscilloscope.

4. GENERATION OF THE INFORMATION STORAGE TERM

The key element in acoustic holography is formation of a photographic transparency of hologram $P(\underline{r})$ patterned after the acoustic standing wave field

$$P(\underline{r}) = Z\mathrm{Re}\{A_0(\underline{r})A_R^*(\underline{r})\} \tag{V.4}$$

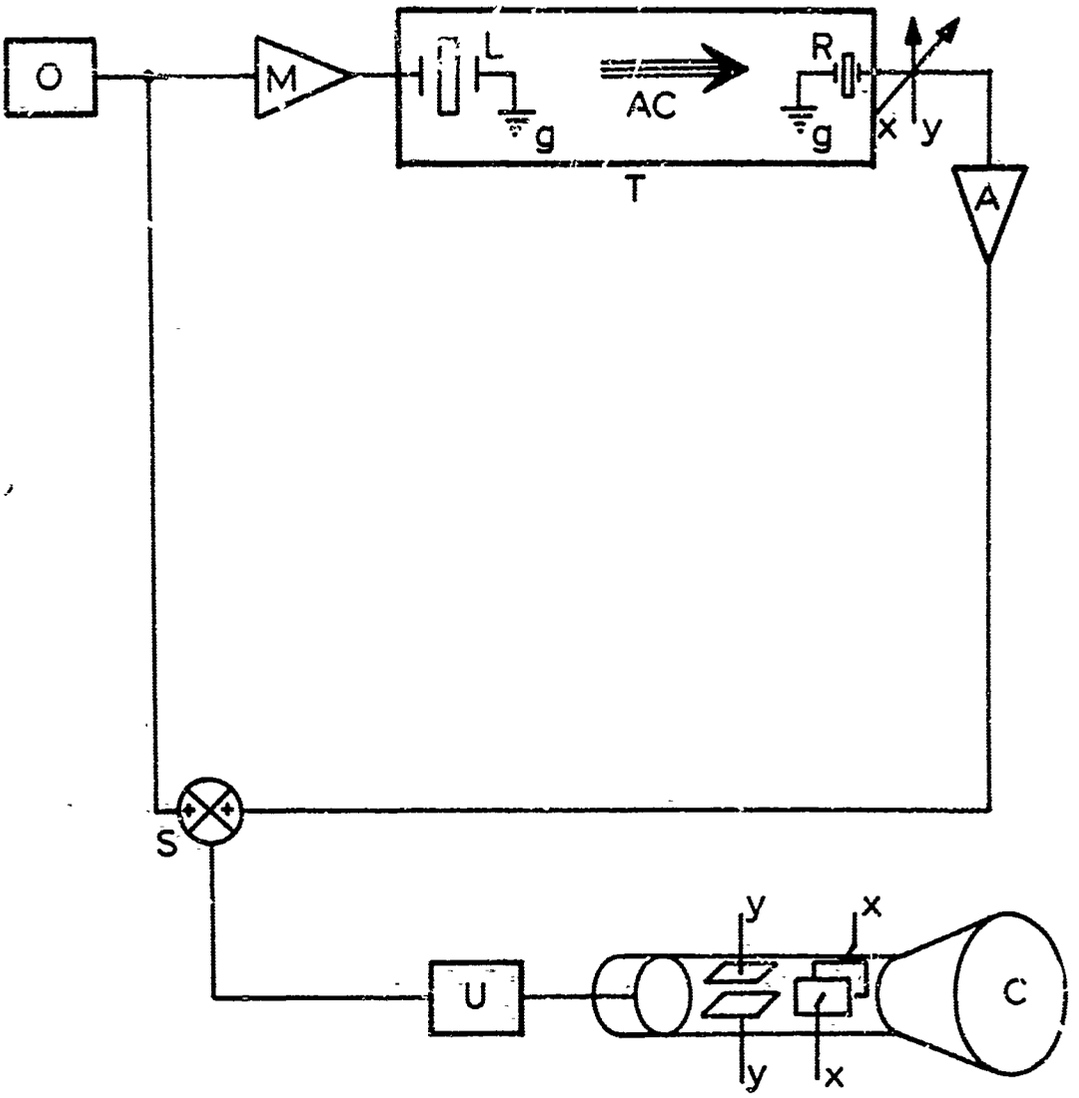

Figure V.6. Schematic of Coplanar Reference Simulation

O	1 MHz local oscillator
M	Modulator and power amplifier (50 W RF into L)
L	Acoustic illumination transducer
AC	Acoustic coupling via propagation through water
R	Acoustic receiving transducer
A	Amplifier
S	Summing network
U	Electronic processing
C	Cathode ray tube display
T	Anechoic water tank
g	Ground through water

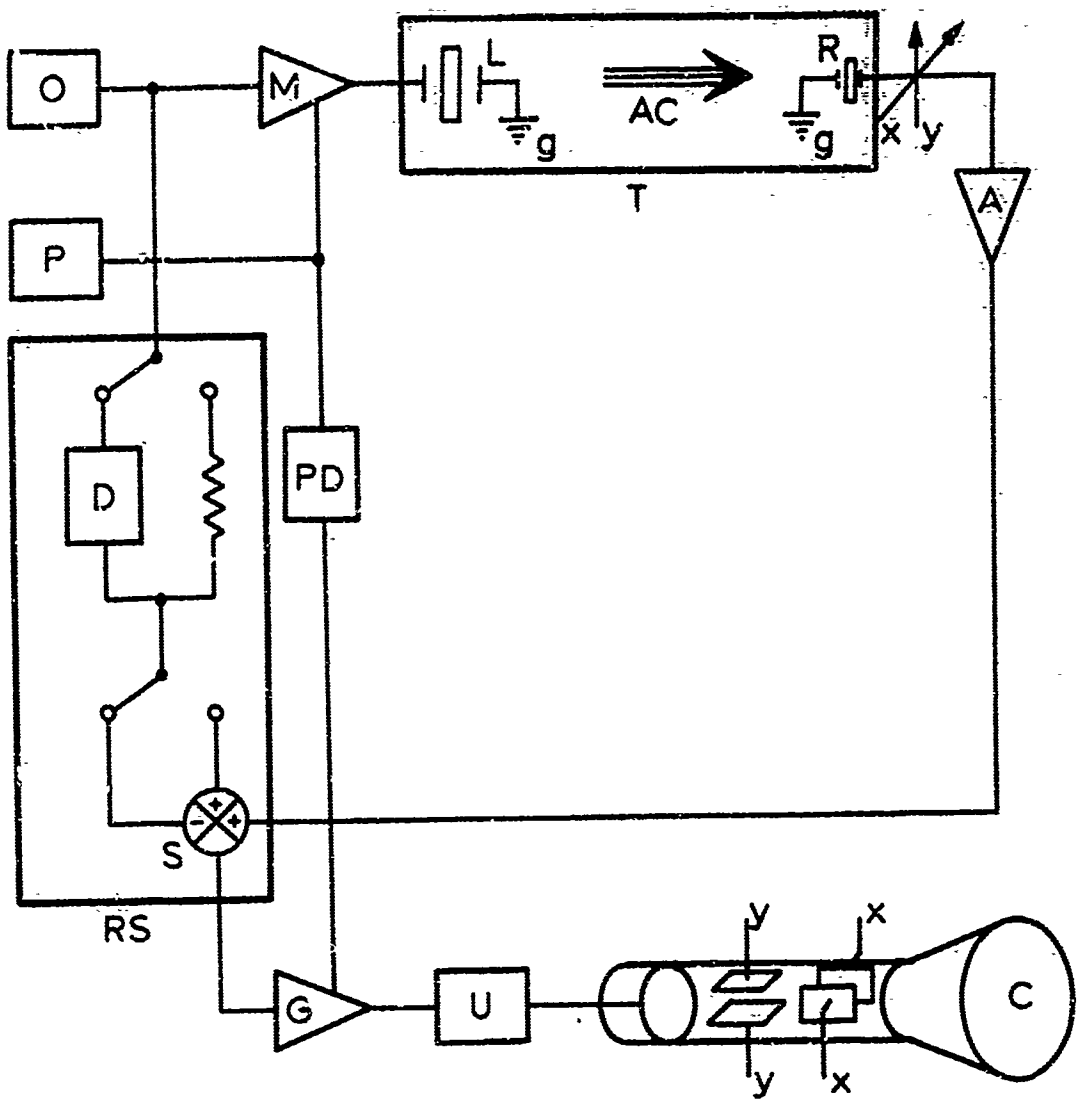

Figure V.7. Schematic of Inclined Reference Simulation

P	Pulse generator (0.8 msec pulse at 300 Hz rr typical)
PD	Pulse delay (1.5 msec typical)
G	Gated amplifier
RS	Inclined reference simulation network
D	Delay line (0.25 μsec)

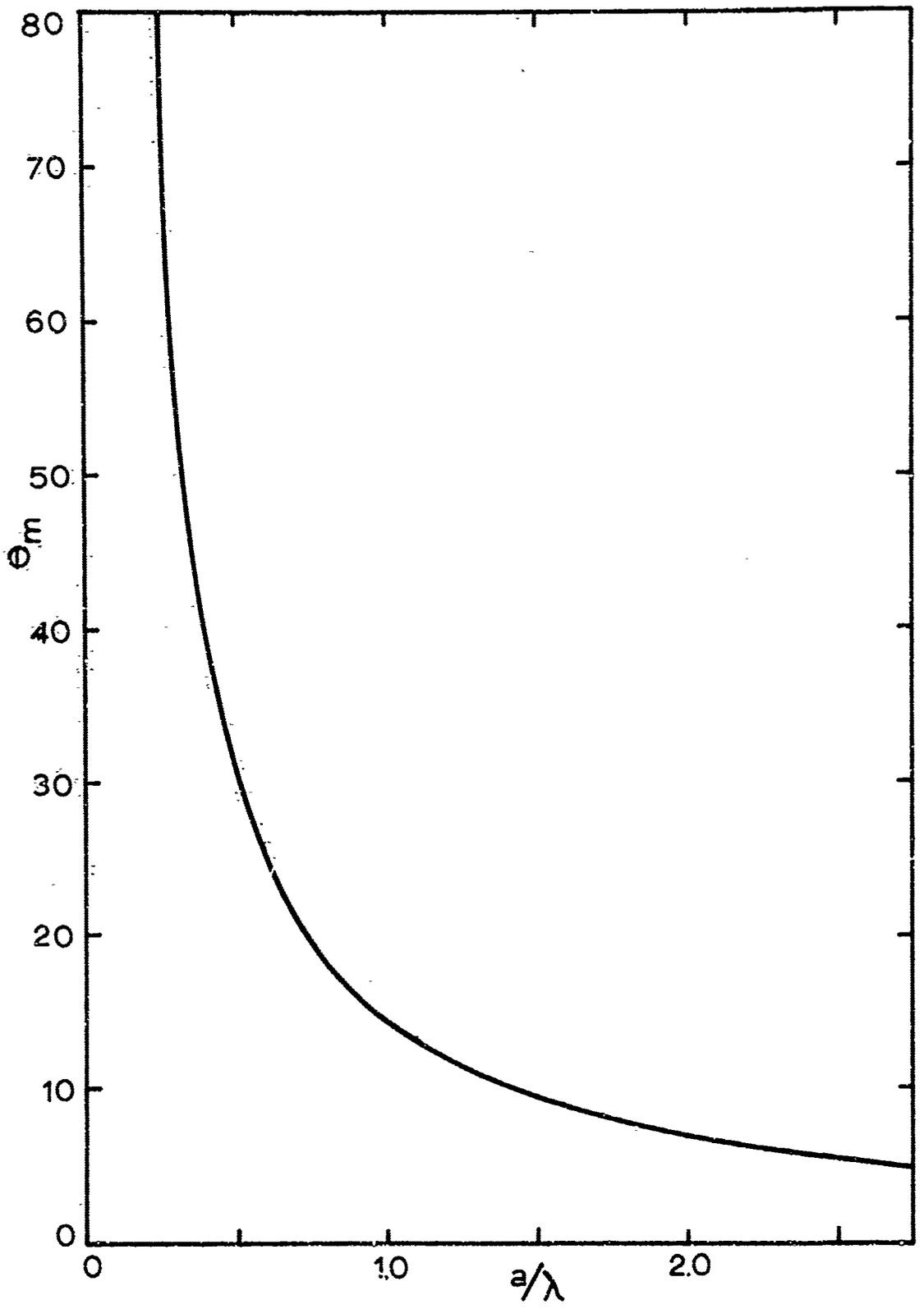

Figure V.8. Maximum Reference Inclination for Scanned Acoustic Holograms

where $A_0(\underline{r})$ is the complex propagating acoustic field scattered by some coherently illuminated object O and $A_R(\underline{r})$ is a suitable acoustic reference field. When such a transparency is reilluminated with the reference $A_R(\underline{r})$, a field is diffracted by $P(\underline{r})$ which duplicates $A_0(\underline{r})$ in some region, hence $A_0(\underline{r})$ is "reconstructed."

The procedure by which the informating containing term is obtained depends upon the type of detector used to form the hologram. For example, when the detector is sensitive to field intensity rather than amplitude

$$P(\underline{r}) \propto A(\underline{r})A^*(\underline{r}) \quad , \tag{V.5}$$

and interferometric techniques are required to produce holograms. To wit, the reference and object fields are coherently added (hence the strict coherence requirements) and then applied to the detector. The output of the detector is

$$P(\underline{r}) \propto \left[A_0^2(\underline{r})+A_R^2(\underline{r})+2\mathrm{Re}A_0(\underline{r})A_R^*(\underline{r})\right] \quad . \tag{V.6}$$

Ideally, the film processing is controlled to provide perfect square law response. Then, if either the reference is large

$$A_R^2(\underline{r}) >> A_0^2(\underline{r}) \tag{V.7}$$

or the object is diffusely illuminated

$$A_0^2(\underline{r}) = \text{constant} \tag{V.8}$$

Equation (V.6) becomes

$$P(\underline{r}) \propto \text{constant} + 2\mathrm{Re}A_0(\underline{r})A_R^*(\underline{r}) \quad , \tag{V.9}$$

the desired result.

If the fields are acoustic, amplitude detection is possible and generation of the information containing term is not restricted to interferometric techniques. As described in the preceding section, the acoustic fields $A_0(\underline{r})$ and $A_R(\underline{r})$ are first converted by a linear process into equivalent electronic signals $E_0(\underline{r})$ and $E_R(\underline{r})$ which are then combined to form the hologram. If they are added and their sum converted by electro-optical means into a photographic transparency according to a square law or at least power law transformation, the holograms thus formed are equivalent to those formed from visible radiation. This technique was introduced in the preceding section.

There is an alternative technique which offers certain advantages over the interferometric method. Instead of adding the object and reference signal amplitudes they may be applied to a modulator which multiplies them. This technique shall be called <u>heterodyne detection</u>.

Consider the situation presented in Figure V.9 in which the object and reference signals are multiplied in some sort of modulator M. If the signals are monochromatic (radial frequency ω) the real output $E_M(\underline{r},t)$ of the modulator is

$$E_M(\underline{r},t) \propto E_0(\underline{r}) \cos [\omega t+\phi_0(\underline{r})]E_R(\underline{r}) \cos [\omega t+\phi_R(\underline{r})] \tag{V.10}$$

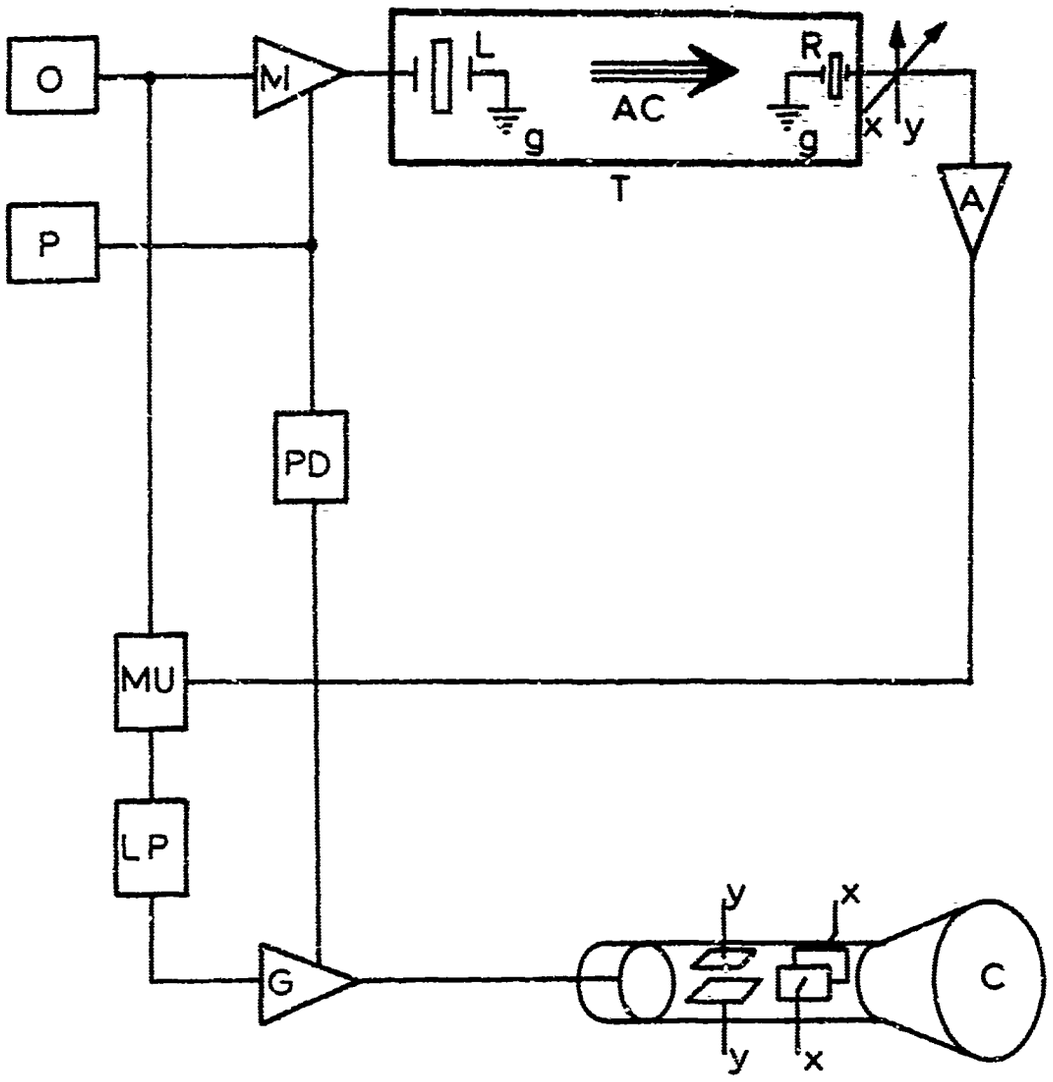

Figure V.9. Schematic of Heterodyne Detection

LP Low pass filter

MU Multiplier

where E_0 and E_R are the amplitudes and ϕ_0 and ϕ_R the phases of the real signals. Using the relation

$$\cos a \cos b = \frac{\cos(a + b) + \cos(a - b)}{2} \tag{V.11}$$

the modulator output becomes

$$E_M(\underline{r},t) \propto E_0(\underline{r})E_R(\underline{r}) \cos\{2\omega t + \phi_0(\underline{r}) + \phi_R(\underline{r})\} + E_0(\underline{r})E_R(\underline{r}) \cos[\phi_0(\underline{r}) + \phi_R(\underline{r})] \quad . \tag{V.12}$$

Clearly, the output of the modulator contains a d.c. term which is identical with the desired standing wave term (V.4)

The second harmonic component is easily eliminated by filtering. The filtered output may then be converted into a transparency according to a linear transformation such that

$$P(\underline{r}) \propto \text{constant} + 2\text{Re}A_0(\underline{r})A_R^*(\underline{r}) \quad . \tag{V.13}$$

Holograms described by Equation (V.13) may have advantage over those described by Equation (V.6). First, the unwanted A_0^2 and A_R^2 terms are automatically eliminated, regardless of the ratio A_R/A_0 or the properties of A_0. Second, greater utilization of the transparency for the storage and retrieval of object information is obtained. Third, by performing the heterodyning in several stages high signal to noise ratios may be obtained.

5. PHOTO-ACOUSTIC CONVERSION PROCESS

Optimization of hologram quality requires that certain characteristics of the hologram forming process be known, particularly the dependence of amplitude transmission P on acoustic field amplitude A and intensity $I = AA^*$. Acoustic hologram formation is conveniently separated into the four stages shown in Figure V.10: (1) detection of the acoustic field and mixing with the reference, (2) the electro-optical conversion, (3) the optical to photographic conversion, and (4) the scale reduction. Determination of the composite response for the acoustic system is given in Appendix E.

6. IMAGE BRIGHTNESS

An acoustic hologram is a mosaic of alternating light and dark fringes, some either opaque or clear; others, varying shades of gray. Ideally $P(\underline{r}) \propto A(\underline{r})A^*(\underline{r})$, but the less restrictive condition that contours $P(\underline{r}) = \text{constant}$ be geometrically similar to contours $A(\underline{r})A^*(\underline{r}) = \text{constant}$ is usually sufficient to ensure good image fidelity in reconstruction. For example, by increasing fringe contrast it is often possible to brighten the image without causing undue distortion, particularly important when the hologram aperture is small as in the acoustic case.

In order to gauge image brightness for interferometric holograms expand $P[A(\underline{r})A^*(\underline{r})]$ in a power series in A^2 about some convenient bias or "quiescent" transmission $P(A_b^2)$ as shown in Figure V.11 obtaining

FIG. E.4

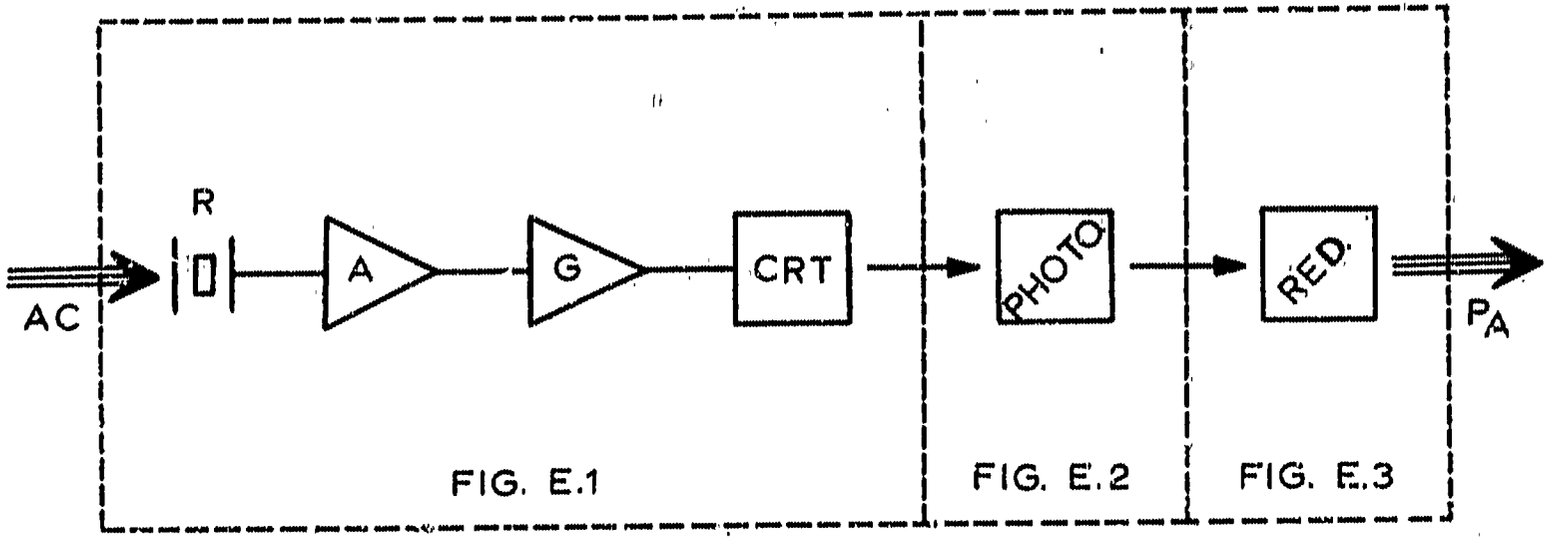

Figure V.10. Schematic of the Photo-Acoustic Conversion Process
AC Acoustic signal input ; P_A Optical transparency replica output

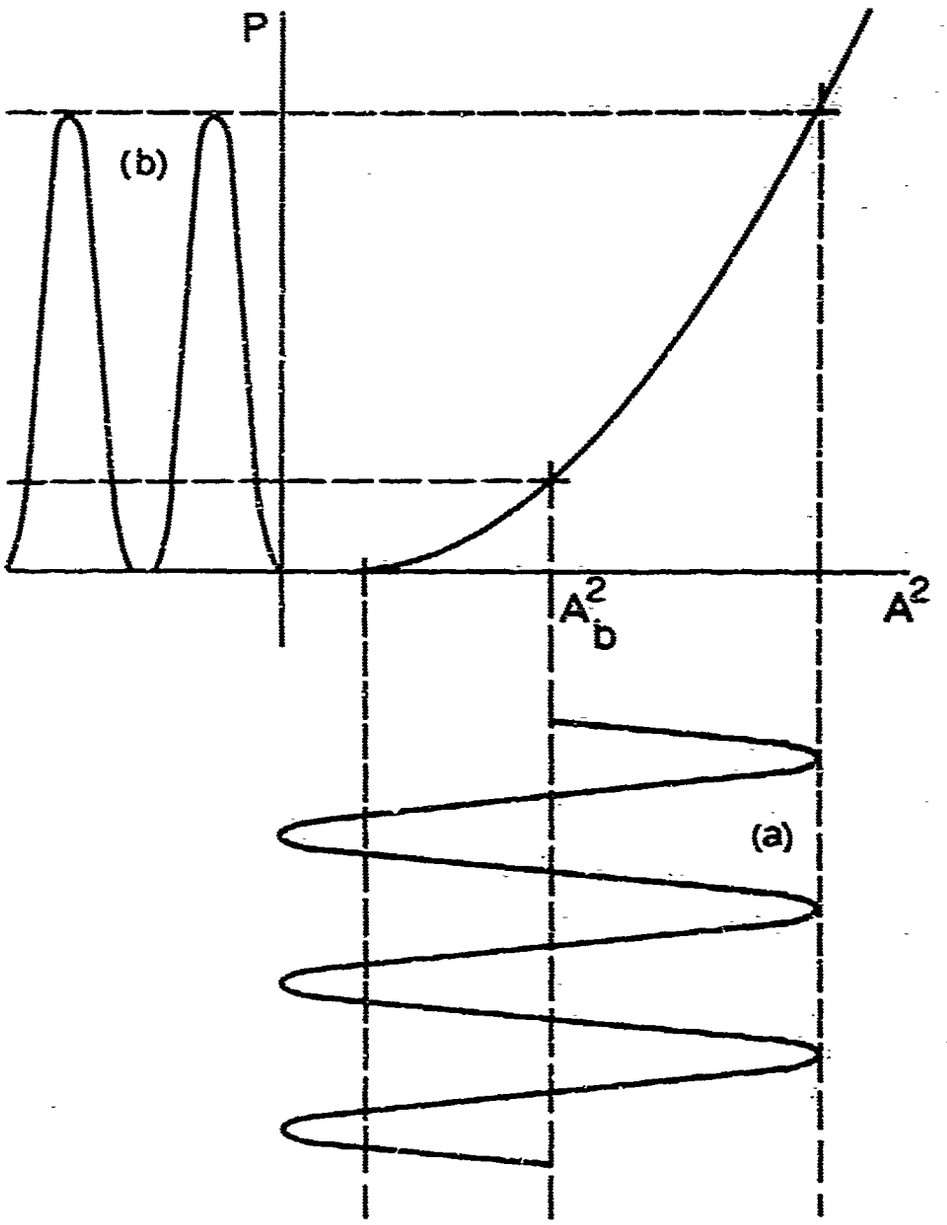

(a) Typical acoustic fringe pattern

(b) Acoustic fringe pattern as recorded photographically

Figure V.11. Typical Relationship During Hologram Recording

$$P(A^2) = P(A_b^2) + \left.\frac{\partial P}{\partial A^2}\right|_{A=A_b} (A^2 - A_b^2) + \ldots \qquad (V.14)$$

If the exposure is restricted to the linear range Equation V.14 becomes using V.6

$$P(A^2) = P(A_b^2) + \left.\frac{\partial P}{\partial A^2}\right|_{A=A_b} (A_R^2 + A_O^2 + 2\mathrm{Re}A_O A_R^* - A_b^2) \quad . \qquad (V.15)$$

It is convenient to choose for the expansion point A_b^2, the exposure A_R^2 due to reference only thereby obtaining

$$P(A^2) = P(A_R^2) + \left.\frac{\partial P}{\partial A^2}\right|_{A=A_R} (A_O^2 + 2\mathrm{Re}A_O A_R^*) \quad . \qquad (V.16)$$

As we have already shown, the source of the reconstructed fields is the term containing $2\mathrm{Re}A_O A_R^*$ which, from V.16, is proportional to the slope of the transmittance-exposure curve for the hologram. Thus, the reconstructed intensity will be proportional to the slope squared.

For heterodyne holograms the corresponding relation is

$$P(A) = P(A_b) + \left(\left.\frac{\partial P}{\partial A}\right|_{A=A_b}\right) 2\mathrm{Re}A_O A_R^* \qquad (V.17)$$

where $P(A_b)$ is the zero-signal transmittance of the transparency and $\frac{\partial P}{\partial A}$ is the slope of $P(A)$. Again, image brightness depends strongly upon slope of the characteristic response for the transparency-forming process.

The slope of the characteristic curve may be related to the visibility or contrast V of the fringes which is defined as

$$V \equiv \frac{P_{max} - P_{min}}{P_{max} + P_{min}} \tag{V.18}$$

where P_{max} is the maximum amplitude transmission of a light fringe and P_{min} is the minimum transmission of the adjacent dark fringe. It is convenient to introduce the concept of fringe contrast because an approximate determination of V is readily obtained simply by visual inspection of the transparency; sharply defined fringes have the greatest contrast. Fringe visibility has useful meaning if the field amplitudes A_O and A_R can be considered constant over the spacing of one fringe pair.

For interferometric holograms the visibility is

$$V = \frac{\left(\frac{\partial P_I}{\partial A^2}\Big|_{A=A_R}\right) 2A_O A_R}{P(A_R^2) + \left(\frac{\partial P_I}{\partial A^2}\Big|_{A=A_R}\right) A_O^2} \quad . \tag{V.19}$$

For heterodyne holograms

$$V = \frac{\left(\frac{\partial P}{\partial A}\Big|_{A=A_D}\right) 2A_D A_R}{P(A_D)} \quad . \tag{V.20}$$

Clearly, image brightness increases monotonically with visibility as well as with slope of the characteristic curve.

The dependence of image brightness upon reference to signal amplitude ratio is contained in Equations (V.19) and (V.20). For heterodyne detection A_R can be as large as desired within the constraint that the emulsion is not operated in a non-linear or saturated condition and that all signals are in the range of first order

multiplication by the modulator. Thus, using heterodyne detection very weak signals can be amplified and holograms with adequate fringe visibility obtained.

In principle, a similar effect can be obtained with the interferometric process. However, Gabor[1] has shown that interferometric magnification is limited by noise in the large reference signal. This noise will mask extremely weak signals. Furthermore, in order to reduce deleterious effects from the extraneous product term A_O^2, the reference amplitude must be made large. In so doing, the camera aperture must be reduced so that $P(A_R^2)$ is maintained at some median transmittance lest the film be hopelessly overexposed by the reference. However, closing the aperture decreases the slope of the characteristic curve, hence visibility and image brightness decrease.

In practice, certain departures from the ideal linear situation described above were found to be desirable. Two considerations influenced choice of the functional dependence of P upon AA^*: (1) minimization of information loss in the reduction stage, and (2) maximization of image brightness. Resolution of fringes in the reduced transparency is limited by the demagnification lens and is maximum for high contrast fringes. However, it should be noted that it was found possible to maintain a gray scale with fair resolution in the reduction.

Maximum image brightness demands high contrast conversion from acoustic standing wave field to photographic transparency. However since high contrast systems have limited dynamic range, non-linear conversion in the form of clipping will usually result. For interferometric holograms the effects of non-linearity are minimized without

sacrificing contrast by reducing the operating point of the characteristic curve to zero transmission, as shown in Figure V.11.

Over most of the holcgram plane the reference to signal amplitude ratio A_R/A_O satisfies $A_R/A_O > 2$, at the signal maxima $A_R/A_O \geq 1$. Thus, in regions of signal maxima the darkest portions of the fringes will be clipped. However, such clipping produces negligible image distortion because $P(AA^*)$ is small in these regions even if linearity is strictly maintained.

7. EXPERIMENTS IN ACOUSTIC IMAGING BY HOLOGRAPHY

The following acoustic imaging experiments were performed using the techniques and apparatus described above and in Appendices D, E, and F.

HOLOGRAM #1 (Figures V.12-V.16)

The simplest possible scene was chosen for hologram number one. The scene (Figure V.12) is a view of the acoustic radiation pattern from the illumination transducer (see Figures D.1, D.2, D.3) without any intervening object and with electronically simulated coplanar reference. Unfortunately, a 3 inch diameter airfilled standpipe protrudes from the bottom of the tank inot the object space in front of the hologram plane. However, since the central lobe of the radiation pattern diverges narrowly (only about 10^o) it was anticipated that the standpipe would not appear in the reconstruction. The hologram is shown in Figure V.13 and the reconstruction in Figure V.14.

The central spot in the reconstruction is clearly the image of the transducer, approximately a point source. Occurrence of a second

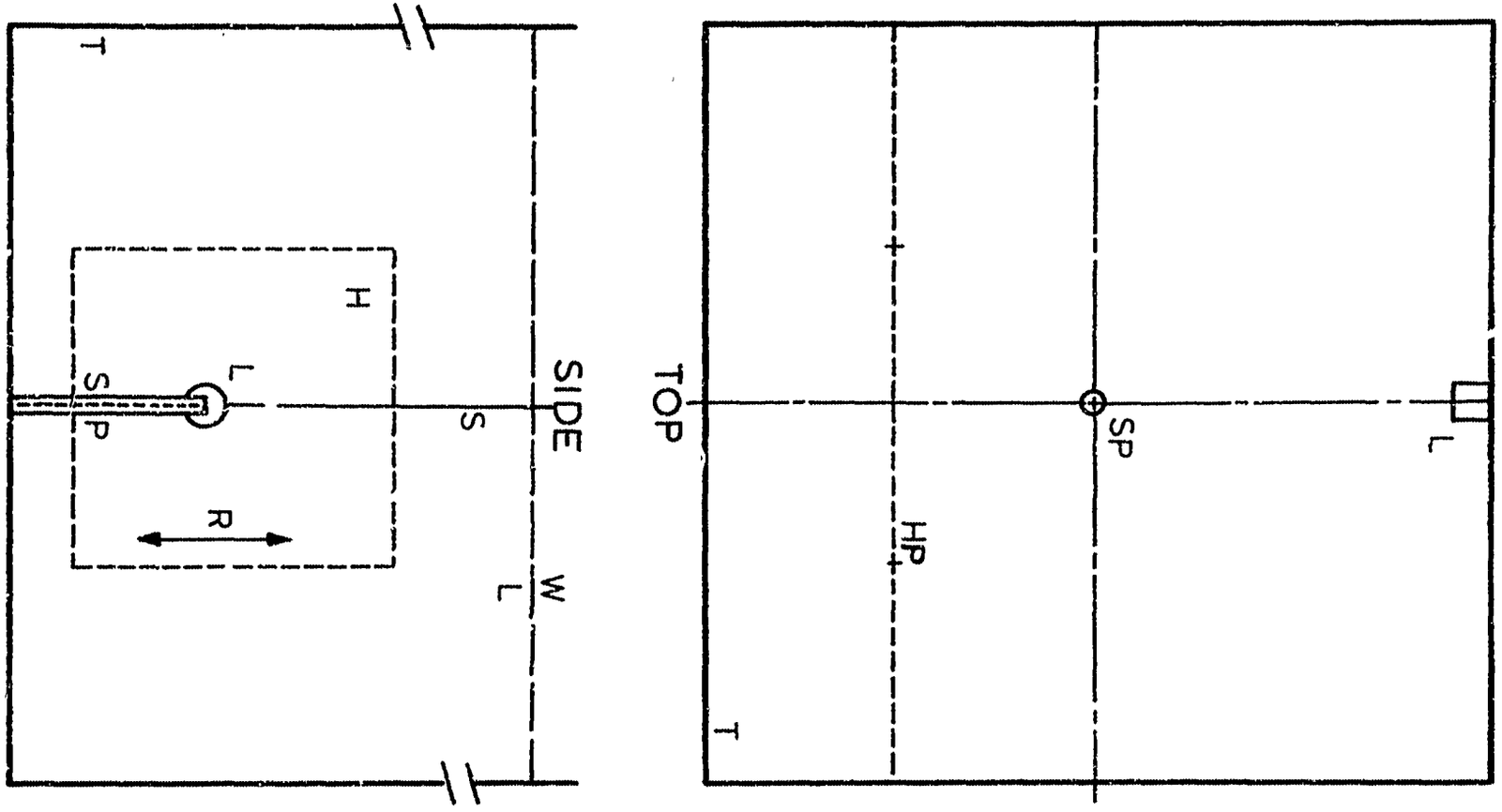

Figure V.12. Layout of Object Scene, Hologram #1

L	Acoustic illumination transducer	WL	Water line
SP	Standpipe (7.5 cm diameter)	S	Support tube
HP	Hologram plane	H	Hologram swept area
T	Anechoic tank	R	Typical raster line

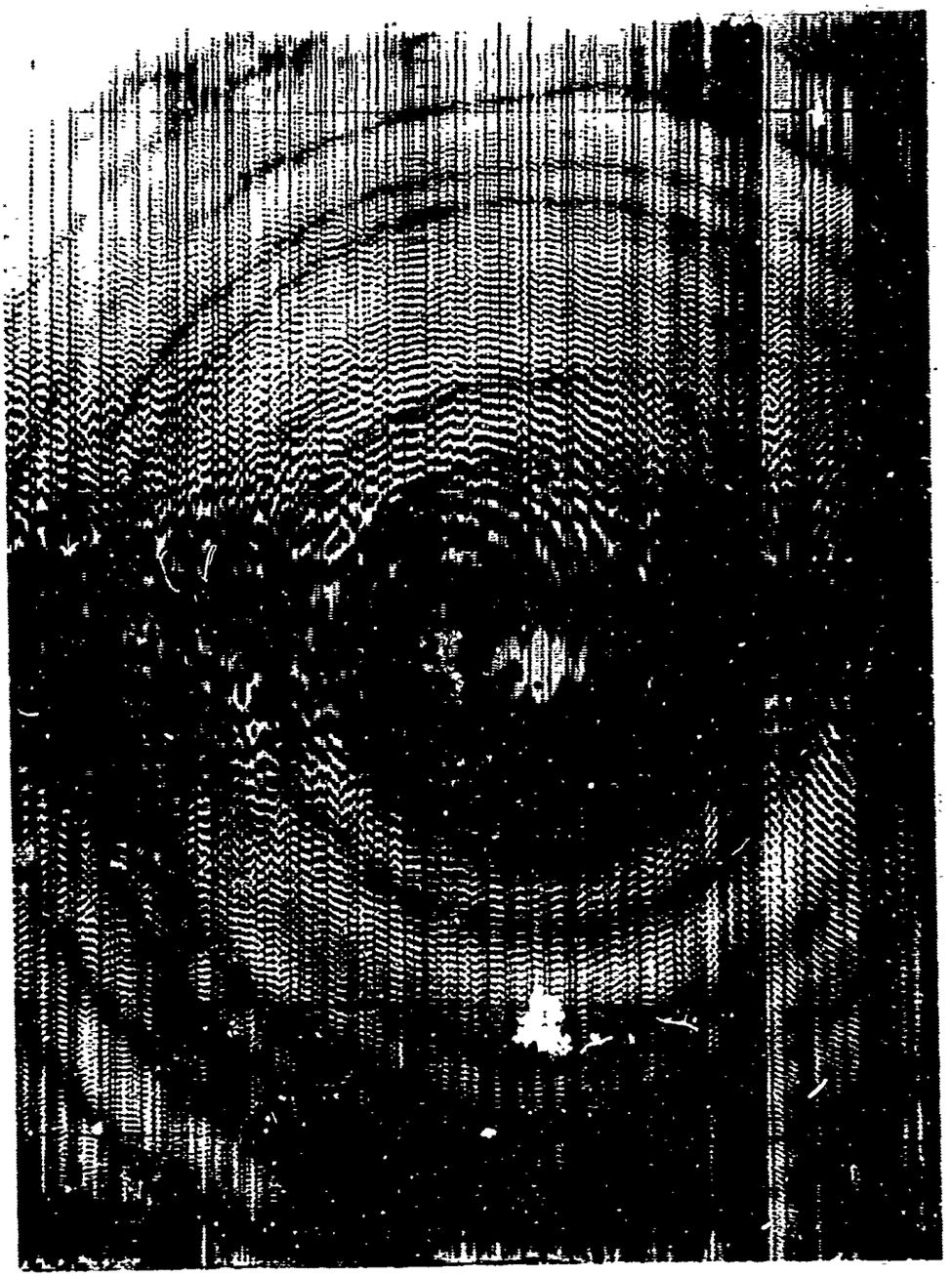

Figure V.13. Hologram #1

Raster lines are vertical.

Regions of high acoustic field are black.

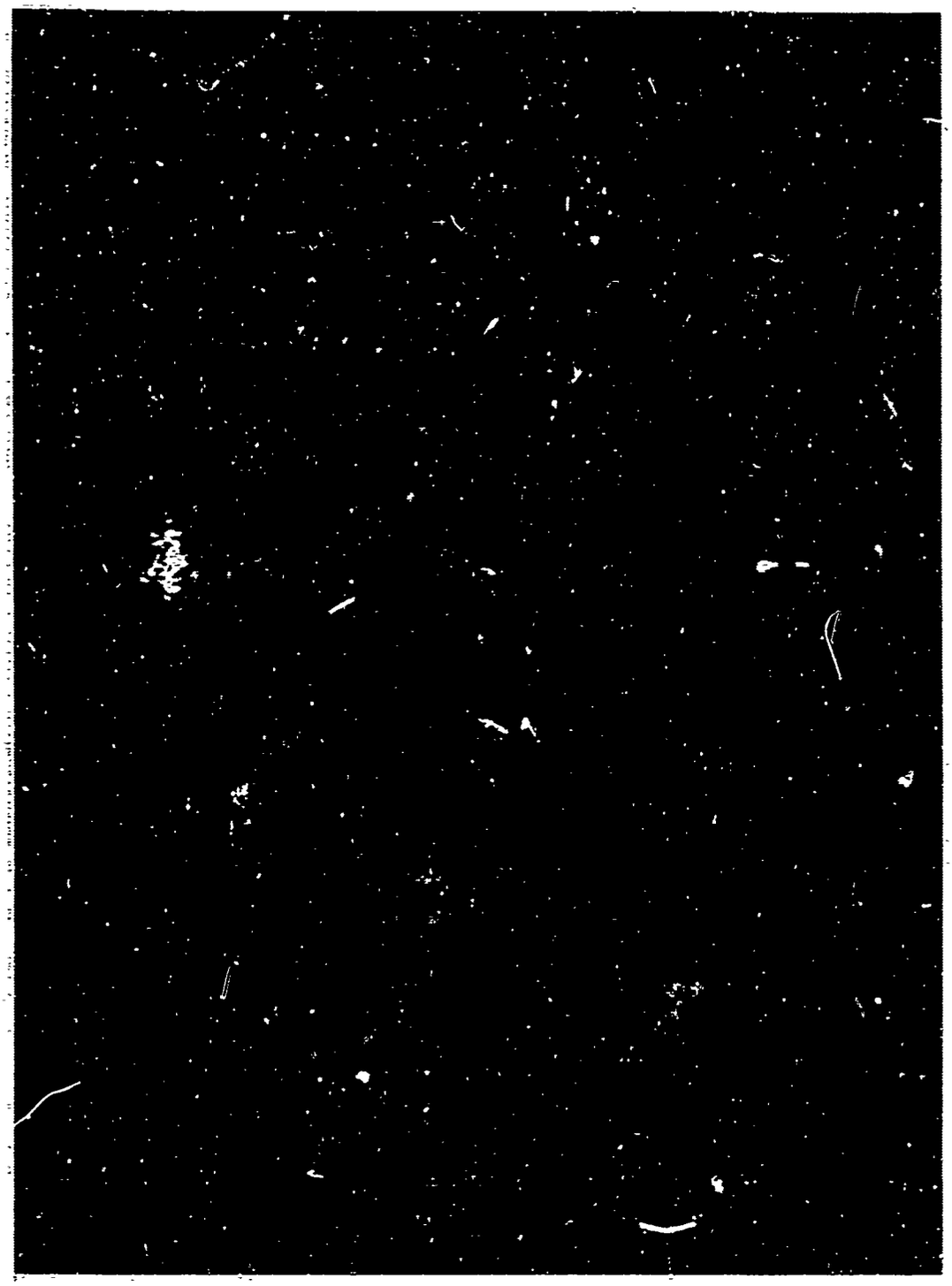

Figure V.14. Reconstruction from Hologram #1
Left half of reconstruction has been cropped. Spot at left corresponds to location of standpipe SP and transducer L.

spot at the right hand side of the reconstruction is somewhat perplexing. (There is also a spot on the left, symmetrical with the one on the right, but somewhat weaker. This spot is not shown in V.14.) By selectively illuminating small areas of the hologram at a time it was determined that the spurious images arise from the fringe structure near the left and right hand edges of the hologram.

Two possible explanations for the occurrence of the edge fringe structure are offered; one is based upon Moire fringe interference, the other upon multiple reflections. Of the two, the Moire theory is more likely. If an equally spaced line grating (Figure V.15a) is superimposed upon a symmetrical Fresnel zone (Figure V.15b) then, according to Moire fringe theory[70], a new fringe system like the one shown in Figure V.15c will be formed. Note the appearance of symmetrical Fresnel zones near the edges of the pattern in addition to the original zone in the center. These spurious zones will form diffraction spots to the right and left of the spot from the original zone. Thus, by identifying the line grating with the scanning raster and the central Fresnel zone with interference between the transducer radiation and the coplanar reference it is clear that the spurious images may be a result of coarse scanning.

One may also explain the existence of spurious fringes at the edge of the hologram by assuming that a portion of the acoustic beam is reflected from the standpipe to both walls of the tank and then from the walls to the hologram plane as shown by the dotted rays in Figure V.12. These doubly reflected rays will form fringepatterns similar to those found in the hologram. Of course, if either the

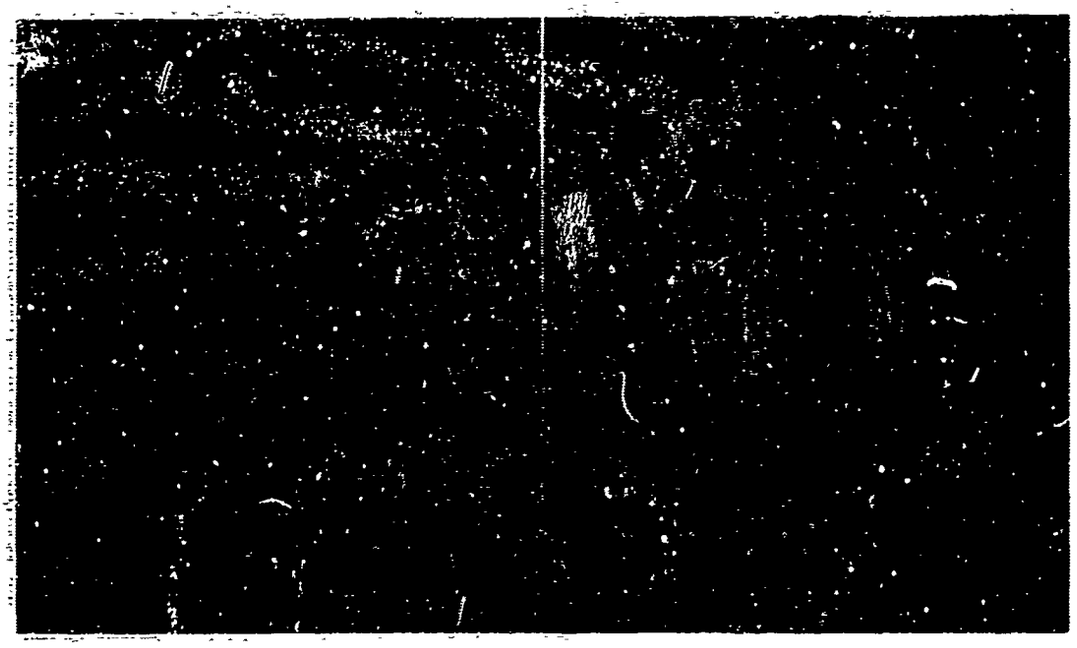

(a) line grating (b) Fresnel zone

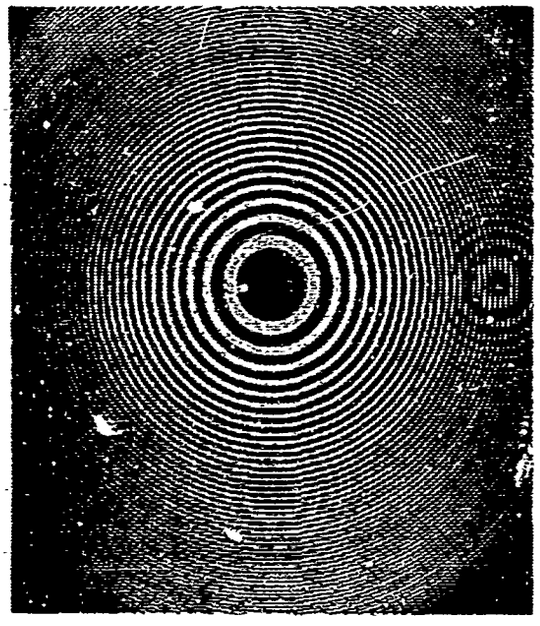

(c) Moire fringe system

Figure V.15. Effect of Scanned Sampling

Superimposing a line grating upon a Fresnel zone yields a spurious Moire fringe pattern.

walls or the standpipe is non-reflecting then this theory does not apply.

Since the standpipe is filled with air it should be a strong reflector for acoustic radiation. The wall is a different matter. The walls of the chamber are composed of a rubber cone structure overlaid upon redwood paneling attached to a reinforced concrete foundation. The cones, approximately 2 cm high by 2 cm base diameter, form a regular close packed square array. The reflected amplitude of normally incident 1 MHz acoustic radiation was found to be 15 db below incident amplitude. However, at sufficiently oblique incidence the reflection may be considerably greater. This was not investigated.

The receiver characteristics introduce additional complications which further obscure the exact origin of the spurious images in reconstruction #1. First, cw illumination was used during the early hologram experiments, hence coincidence techniques (range gating) could not be used to separate reflections from direct radiation. Second, an extremely sensitive non-linear detector was employed in order to maximize the number of fringes recorded. The output of this detector was the same for weak secondary reflections as for strong primary radiation. Thus fringe contrast could not be used to separate the two.

The detector departed from the simple linear amplifier system shown in Figure V.6 because it was felt initially that the number of interference fringes recorded must be maximized in order to insure adequate resolution and signal to noise ratio. This was accomplished by passing the signal through a high gain (10^4) amplifier stage followed by symmetrical clipping before going to the CRT grid. See

Figure V.16a. The large amplification insures that even very weak signals will produce sufficient signal at the CRT grid to turn the beam on, clipping prevents overexposure and the concomitant loss of resolution and fringe contrast with signals of large dynamic range, and the symmetrical design avoids problems with d.c. restoration.

The effect of clipping upon the transmission contour of typical interference fringes in illustrated in Figure V.16a. All fringe amplitudes greater than A_c are clipped so that $A < A_c$. Thus amplitude information is no longer encoded as variations of fringe contrast since fringe contrast is essentially a constant. Amplitude also controls fringe width W, as may be seen in Figure V.16a; however, this is a non-linear dependence (see figure V.16b) so that basically amplitude information is not faithfully recorded in this type of hologram. Non-linear processes of this type are useful for high contrast objects. However, when a gray scale must be maintained - as with imaging of biological tissue - then linearity may be required.

HOLOGRAMS #2 THROUGH #6 (Figures V.17-V.19)

The holograms of this set are almost self-explanatory. The object scene for this group represents the next logical step up in complexity from the object scene for hologram #1. The scene, depicted schematically in Figure V.17, consists of an acoustically opaque screen (3mm thick aluminum sheet bonded on both sides with 6 mm thick sponge rubber) with a circular hole 14.3 mm diameter in the center illuminated from behind. Simple transmission objects of this type are ideal for evaluating various acoustic holographic techniques because the hologram

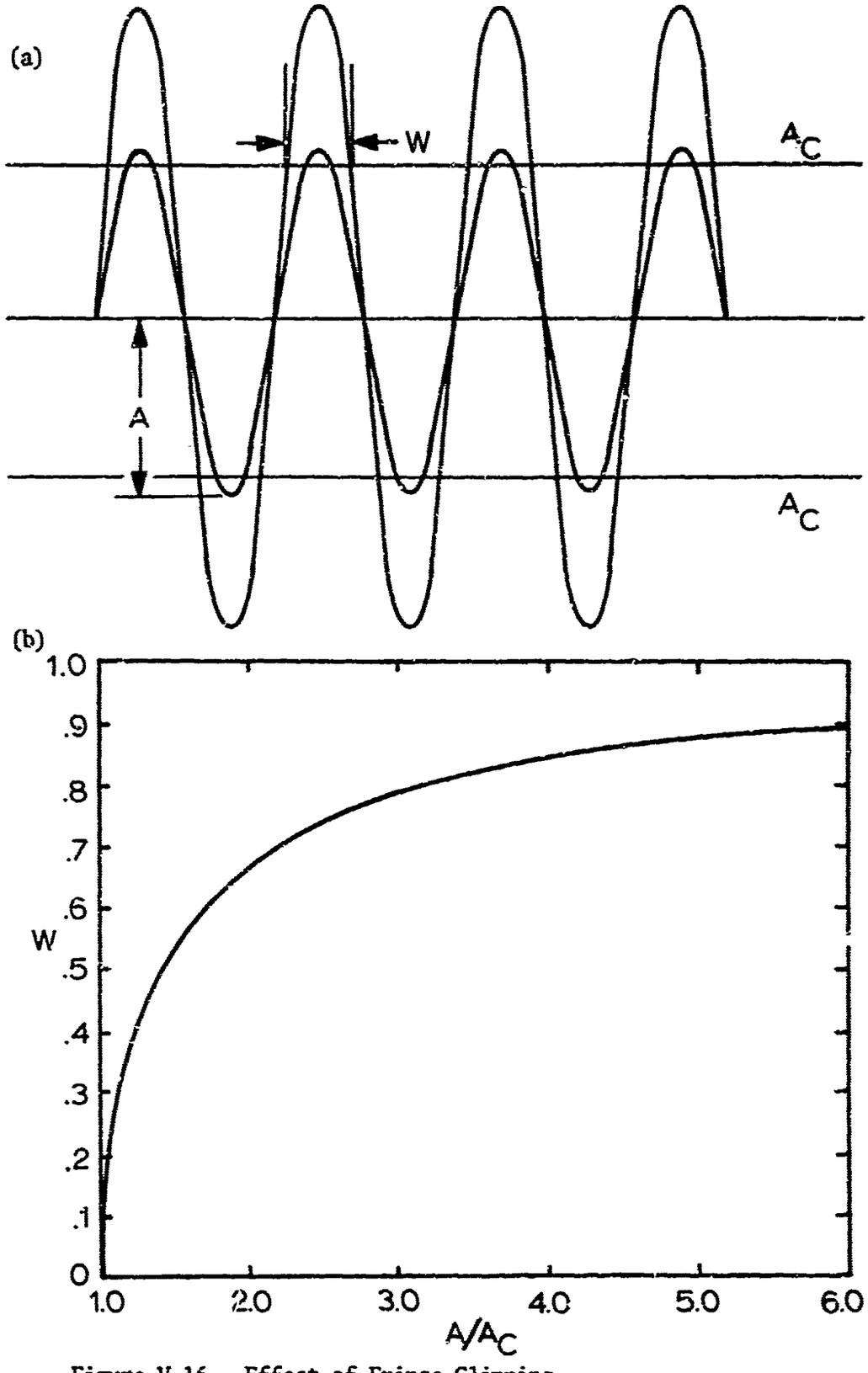

Figure V.16. Effect of Fringe Clipping

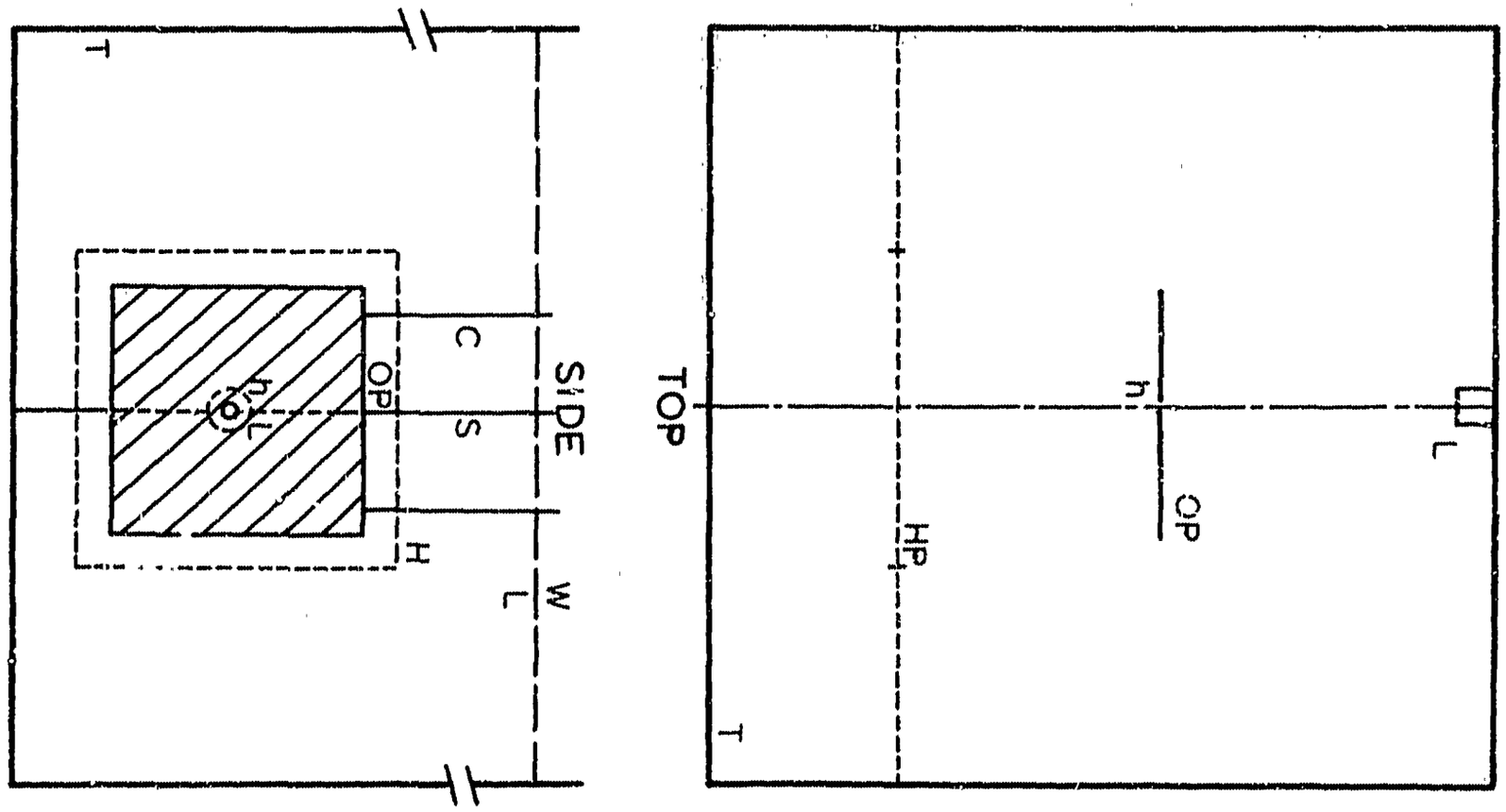

Figure V.17. Layout of Object Scene, Holograms #2 Through #6

OP Acoustically opaque plate
h Hole (14.3 mm diameter)
C Supporting chain

fringe pattern can be easily calculated. Holograms #2 through #6 were produced in order to test the scheme for electronic simulation of off axis reference holograms as described in Section V.3.

The holograms, Figure V.18, were all taken with the same acoustic illumination and opaque screen locations; only the electronic reference signal varied from hologram to hologram. The hologram fringes for this object are readily calculated; for L much larger than x, y, and λ the fringes are given by

$$(x-L \sin \theta)^2 + y^2 = 2n\lambda L + r_0^2 \qquad (V.21)$$

where n = ` 1,2,...; L is the spacing between hole and hologram, x and y are hologram coordinates with origin concentric with the hole, r_0 is the radius of the smallest diameter fringe, λ is the acoustic wavelength, and θ is the angle of inclination of the reference with respect to the normal to the hologram plane .

Figure V.18a shows the hologram with coplanar reference, the raster lines being separated by 5.7 mm. Figure V.18c is identical except that the reference signal is shifted by π for each new line, twice the shift required to uniquely define the reference direction. The ambiguity is visible in the hologram because it appears as two sets of concentric circles whereas V.21 predicts only a single set. This duality is related to the Moire phenomena noted earlier. The ambiguity is eliminated in Figure V.18d by including one additional line between each of the preceding lines and with reference phase shifted by appropriate multiples of π/2. The lines are now spaced half as far apart

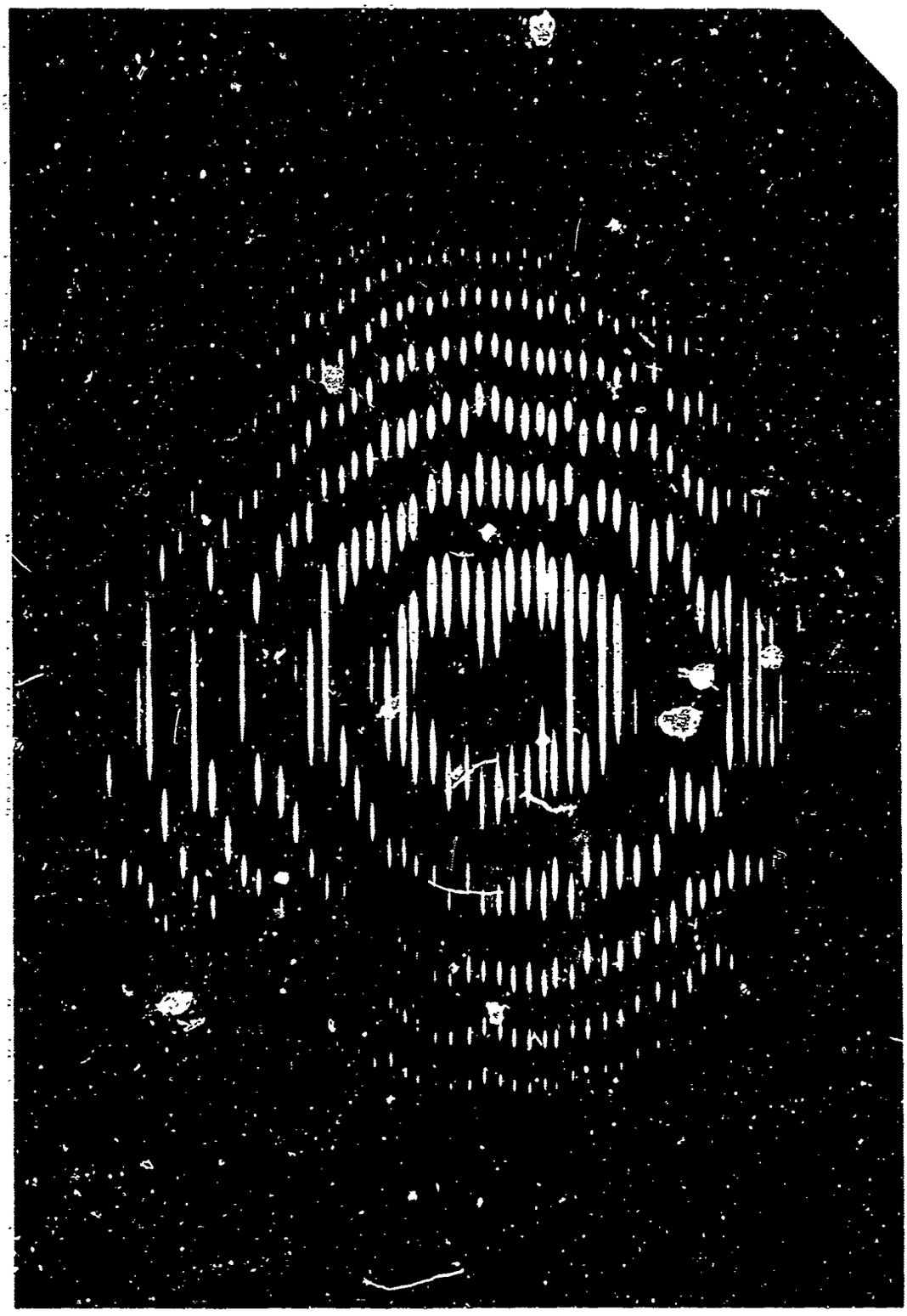

Figure V.18(a). Hologram #2, 0° Simulated Reference Angle
Regions of high acoustic field are white.
Factor of 2 (m = 2) smaller than original acoustic field.

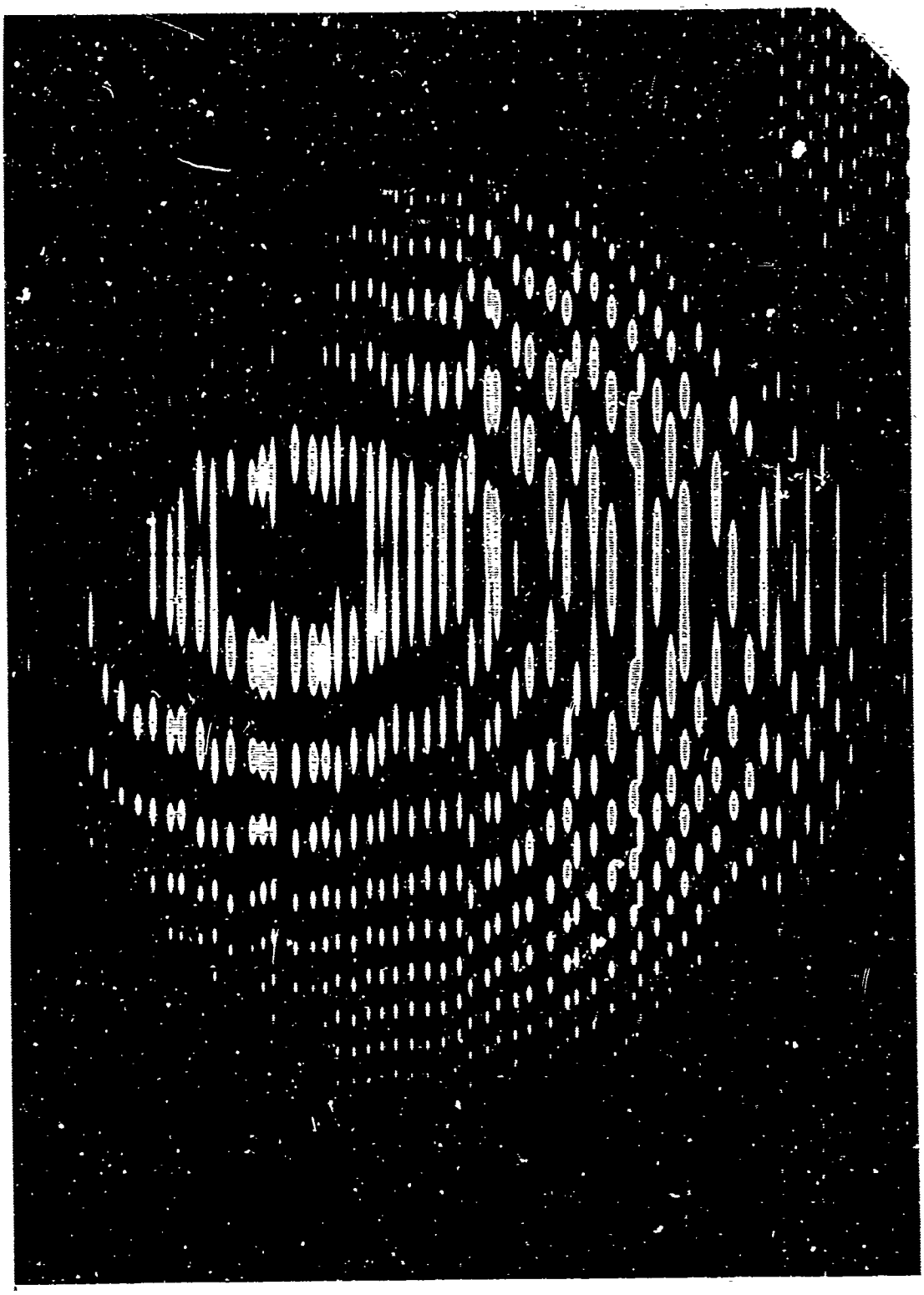

Figure V.18(b). Hologram #3, 3.4° Simulated Reference Angle

Raster line separation = 5.7 mm.
Phase shift per line = $\pi/2$.

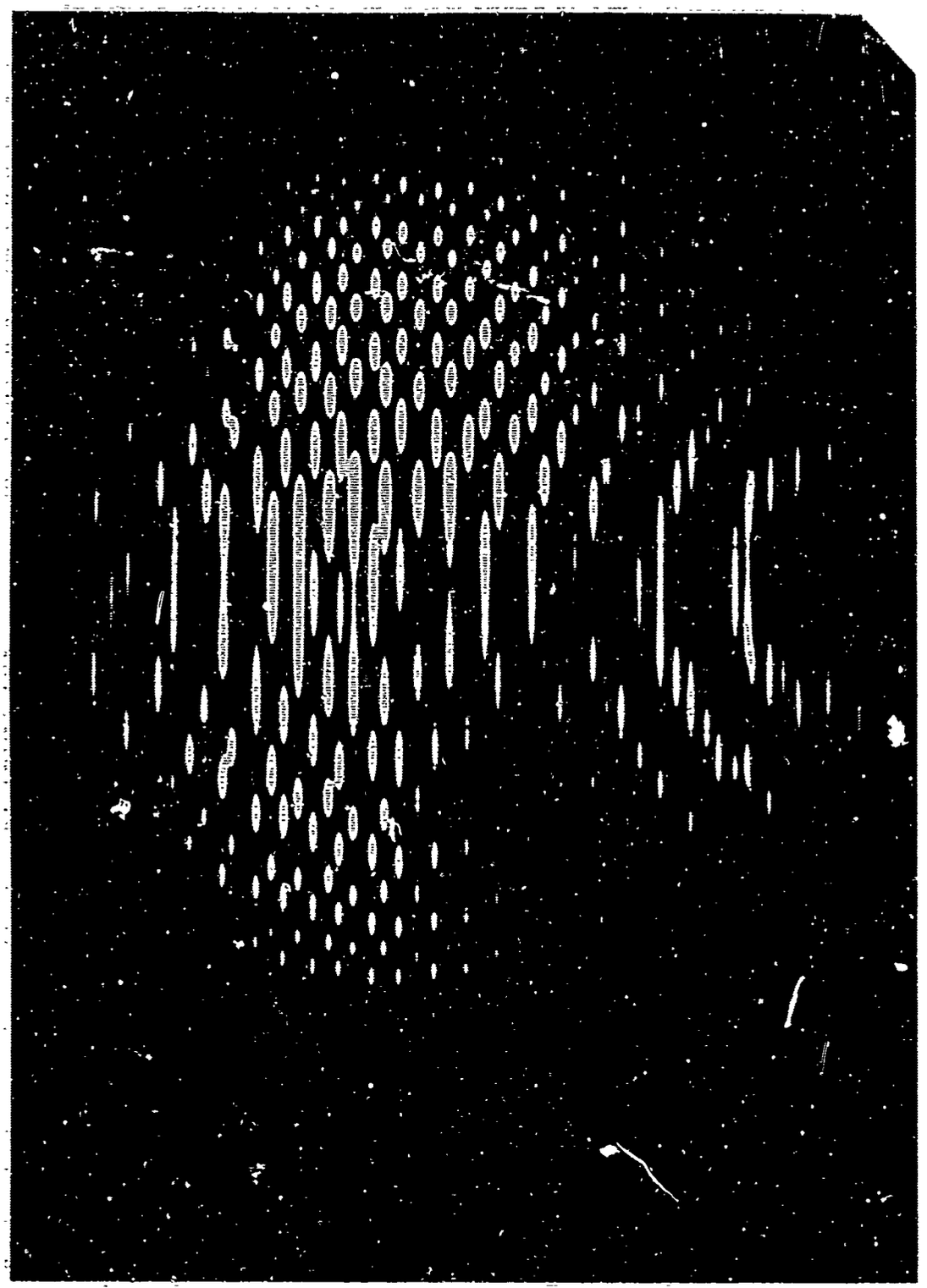

Figure V.18(c). Hologram #4, 7.7° Simulated Reference Angle
Raster line separation = 5.7 mm.
Phase shift per line = π.

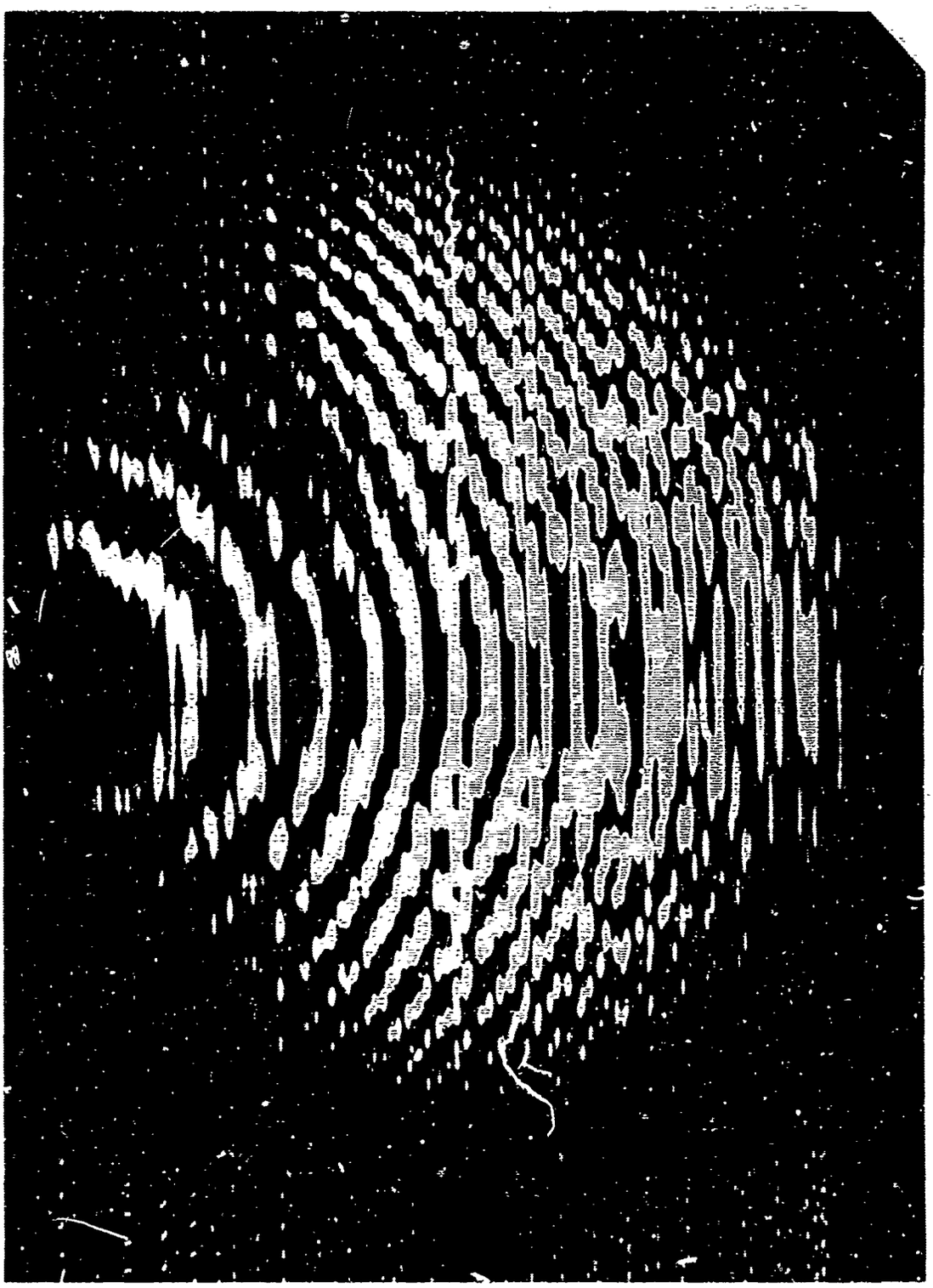

Figure V.18(d). Hologram #5, 7.7° Simulated Reference Angle

Raster line separation = 2.85 mm.
Phase shift per line = $\pi/2$.

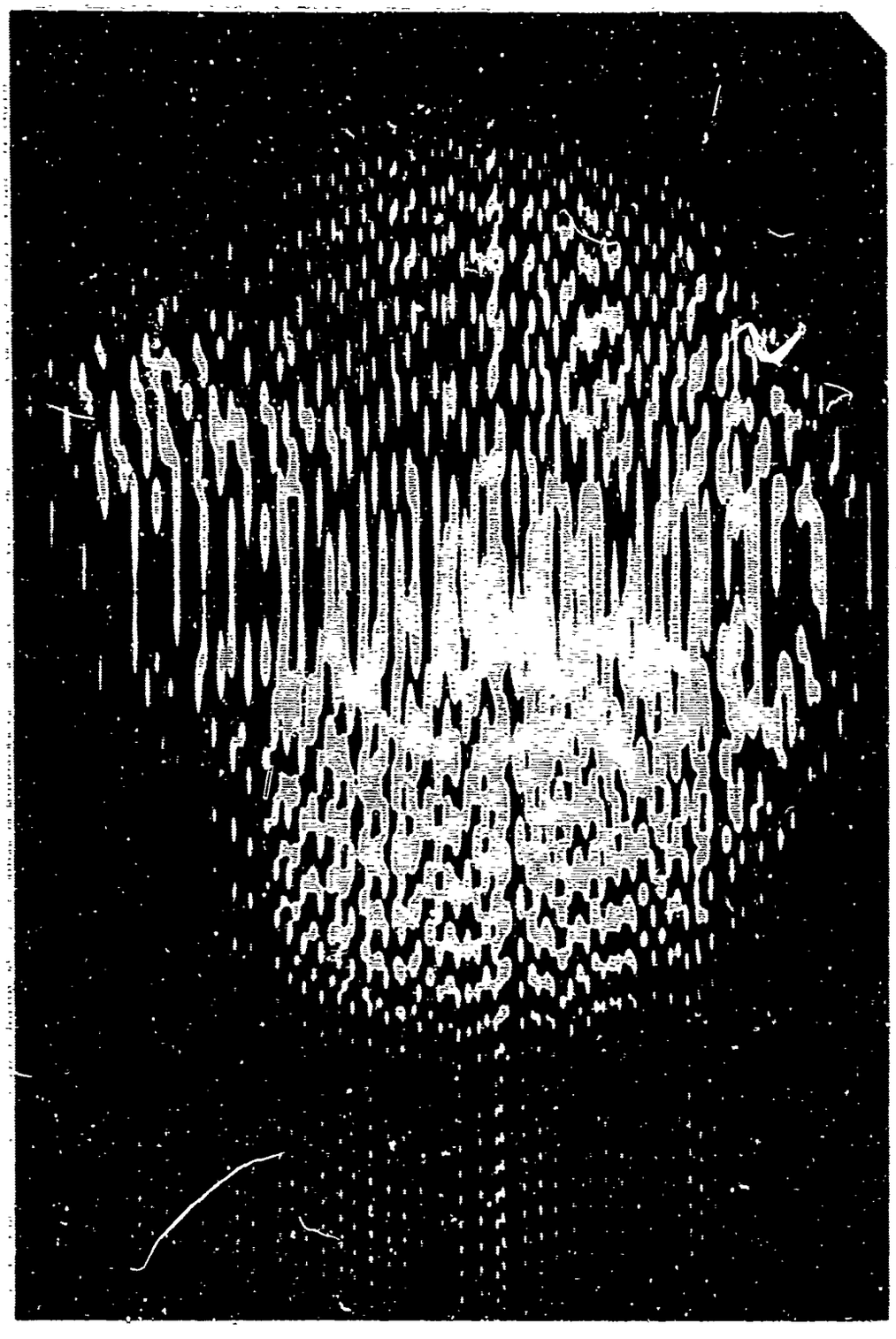

Figure V.18(e). Hologram #6, 15.4° Simulated Reference Angle

Raster line separation = 2.85 mm.
Phase shift per line = π.

(2.8 mm) and the reference is shifted by $\pi/2$ for each new line. Clearly, the ambiguity in Figure V.18c is a result of the finite resolution (.175 lines/mm) of the acoustic sensitive "film." This resolution corresponds to a photographic emulsion able to resolve about 420 lines/mm, which is generally considered too low for planar reference visible holography. Figure V.18e was obtained using the same line spacing as for V.18d except that the phase shift was π between lines rather than $\pi/2$. This is equivalent to doubling the reference angle, however, it is clear that ambiguity is again introduced.

Reconstructions from the various holograms are displayed in Figure V.19. In each case the very bright spot represents an image of the backlighted hole. It will be interesting to compare the size of the spot appearing in the reconstruction with the size of the original hole. The hologram transparency is 1/26.4 the size of the original acoustic field; the reconstruction, Figure V.19b is magnified approximately 12. Thus the reconstructed spot should measure approximately 7 mm diameter. Measurement of the reconstruction indicates that within experimental error this is indeed the case.

In these experiments linear rather than clipped detection was employed thus only the central diffraction zone of the hole contributes to the hologram, the higher zones being below the threshold of the CRT display. However, it is important to note that approximately correct spot size is obtained even so. The higher order diffraction rings were not required in order to obtain proper resolution of this hole. This result is in agreement with visible holography experiments quoted by Develis and Reynolds. If clipped detection had been employed then

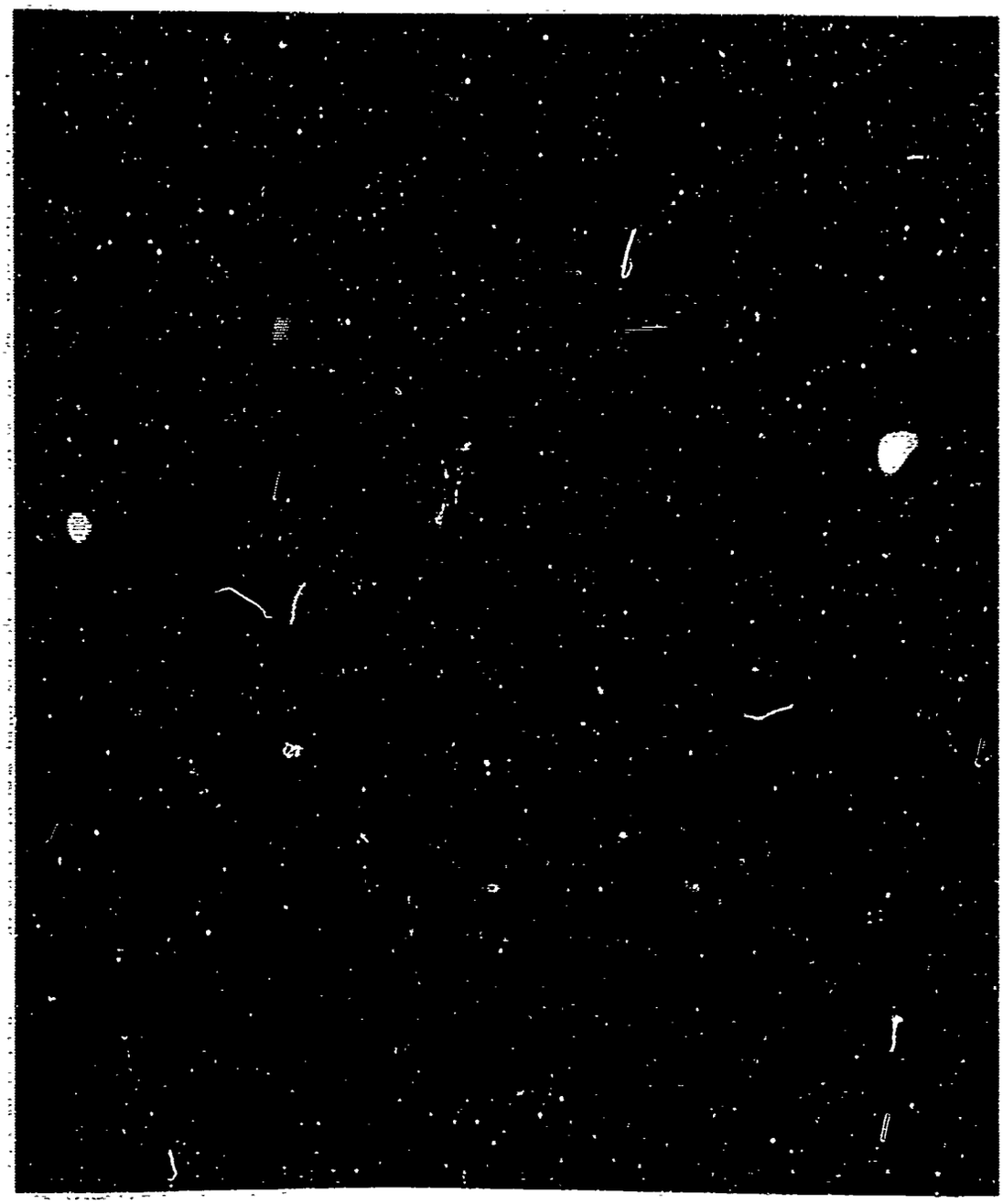

Figure V.19(a). Reconstruction from Hologram #4

Reconstruction photographed on Polaroid 55 P/N film with .6328 micron laser illumination. Positive print made on Eastman Kodak Kodabromide F-5 single weight paper.

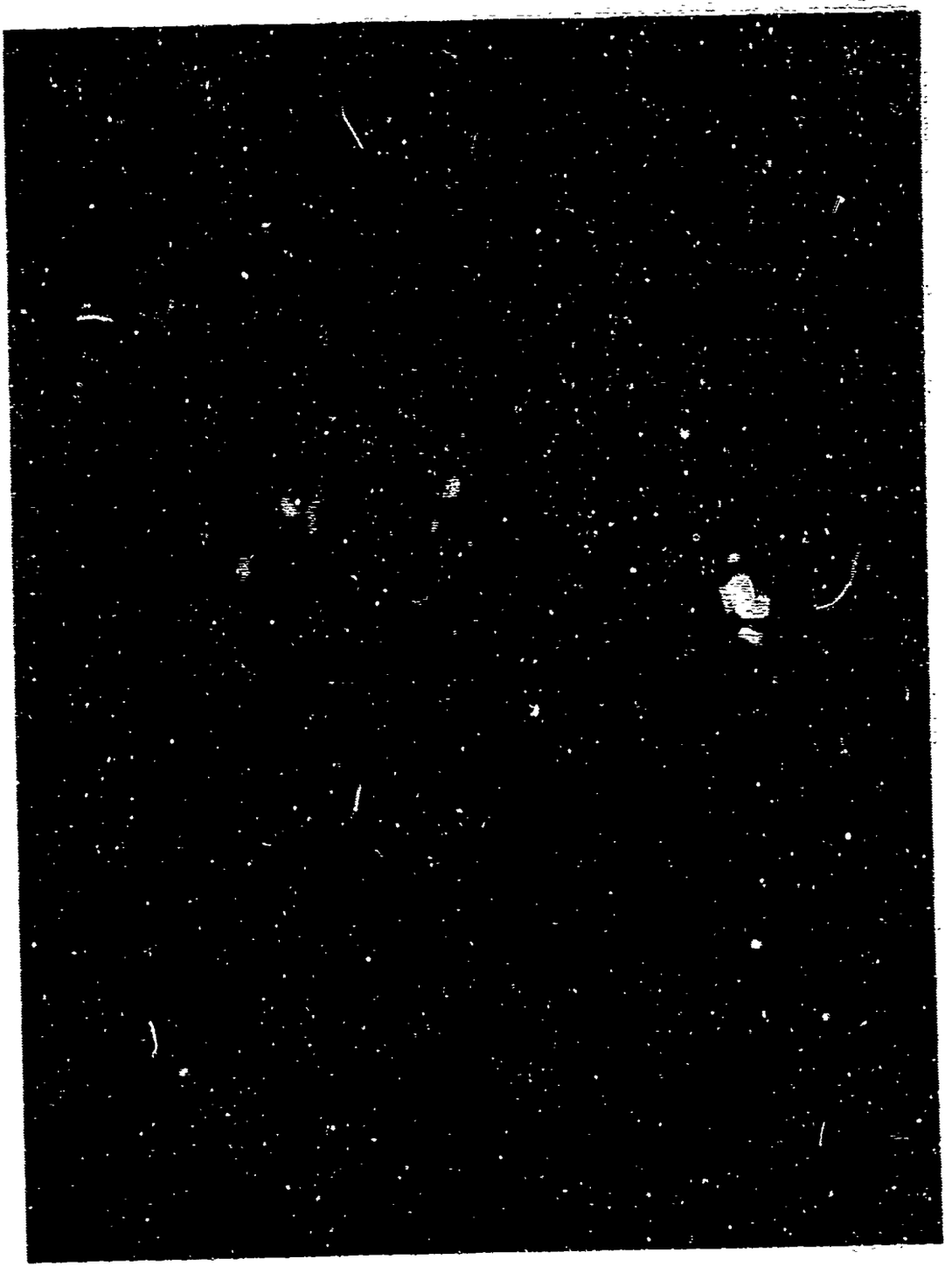

Figure V.19(b). Reconstruction from Hologram #5

Zero order is faint area in center, reconstruction is bright spot near right edge.

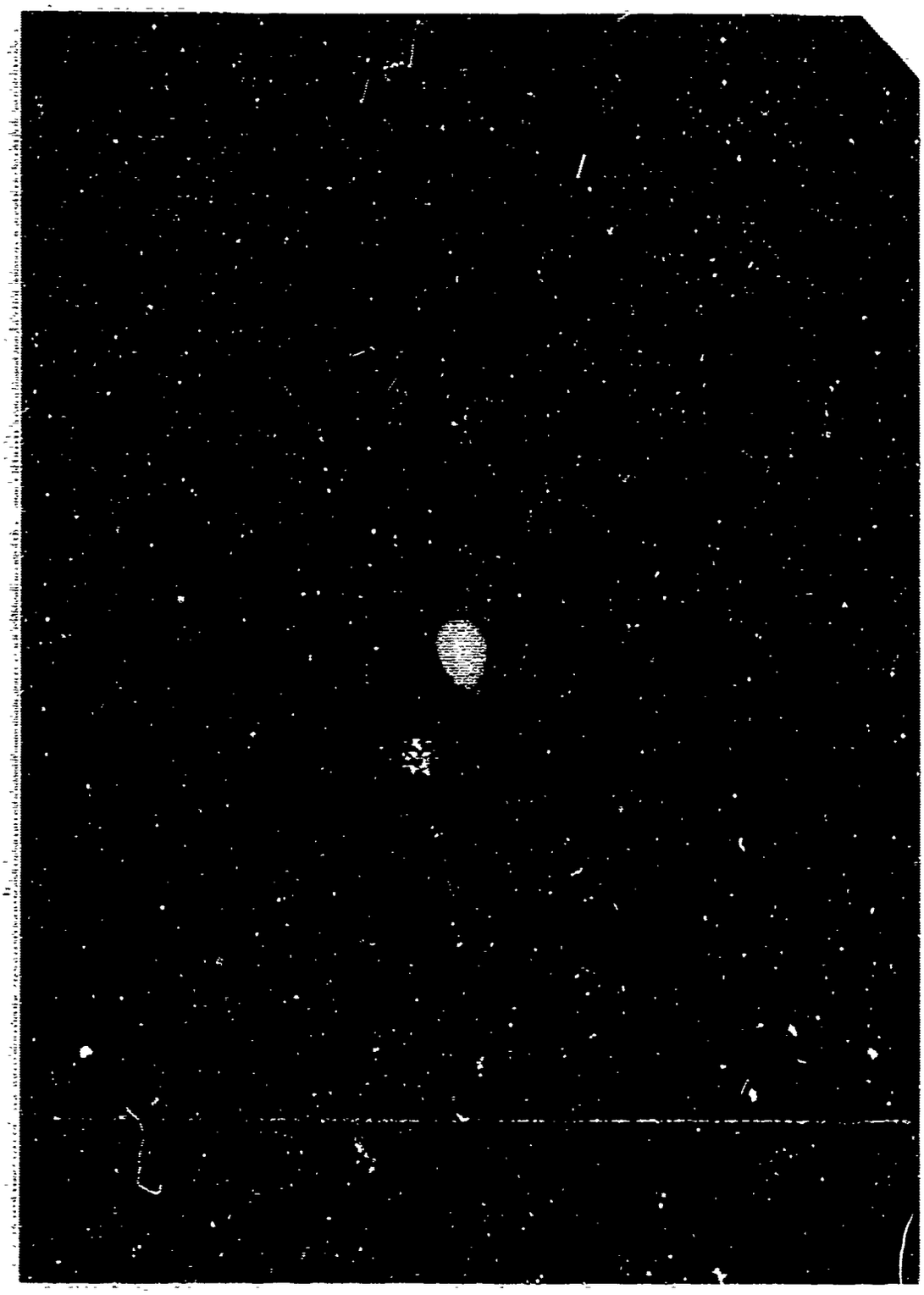

Figure V.19(c). Enlargement of Reconstruction from Hologram #5

Figures V.19 (c), (d), and (e) demonstrate that reconstruction is at least 20 times brighter than background.

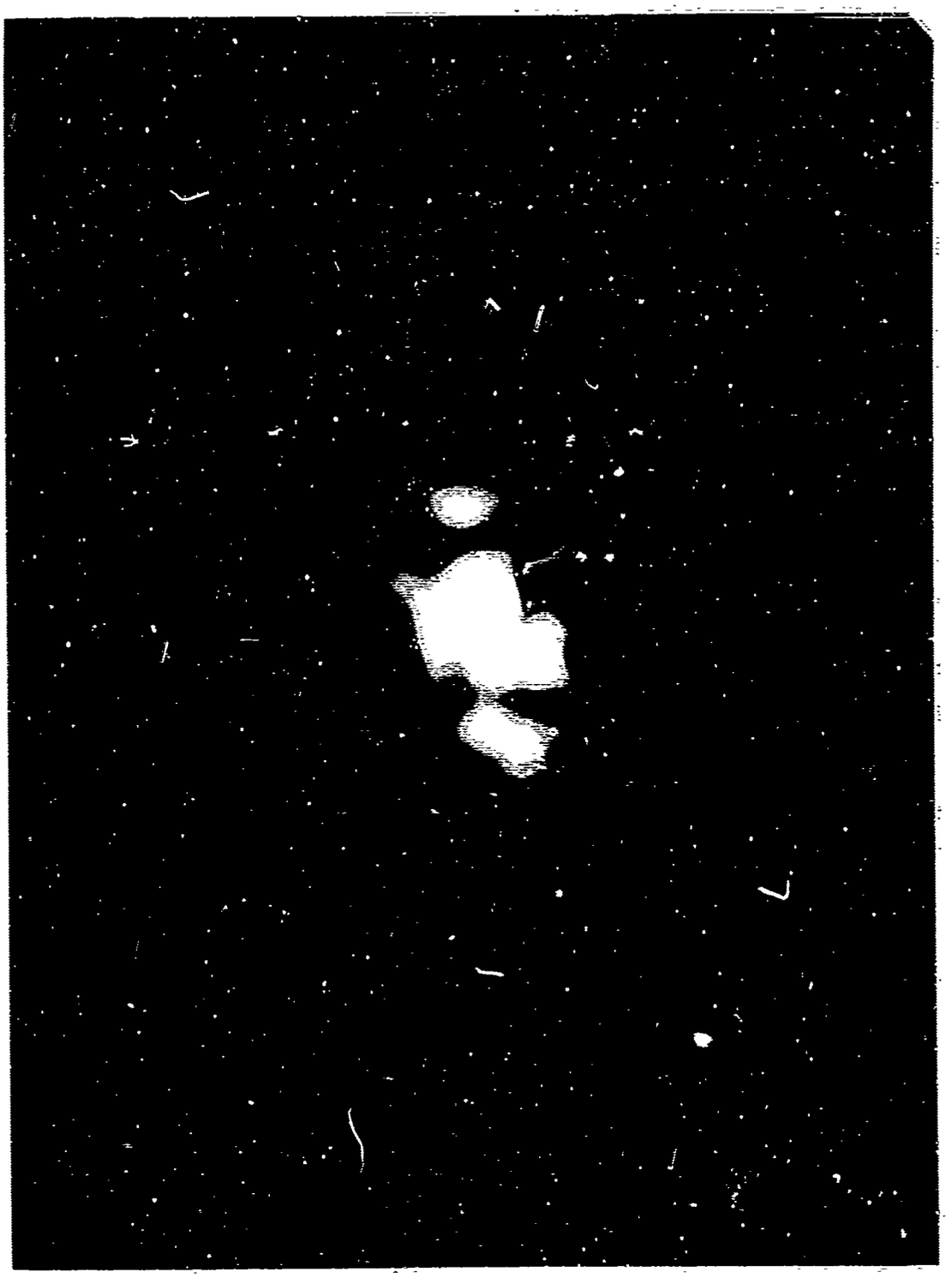

Figure V.19(d). Enlargement of Reconstruction from Hologram #5
Enlargement exposure 5 times less than for Figure V.19(c).

Figure V.19(e). Enlargement of Reconstruction from Hologram #5
Enlargement exposure 20 times less than for Figure V.19(c).

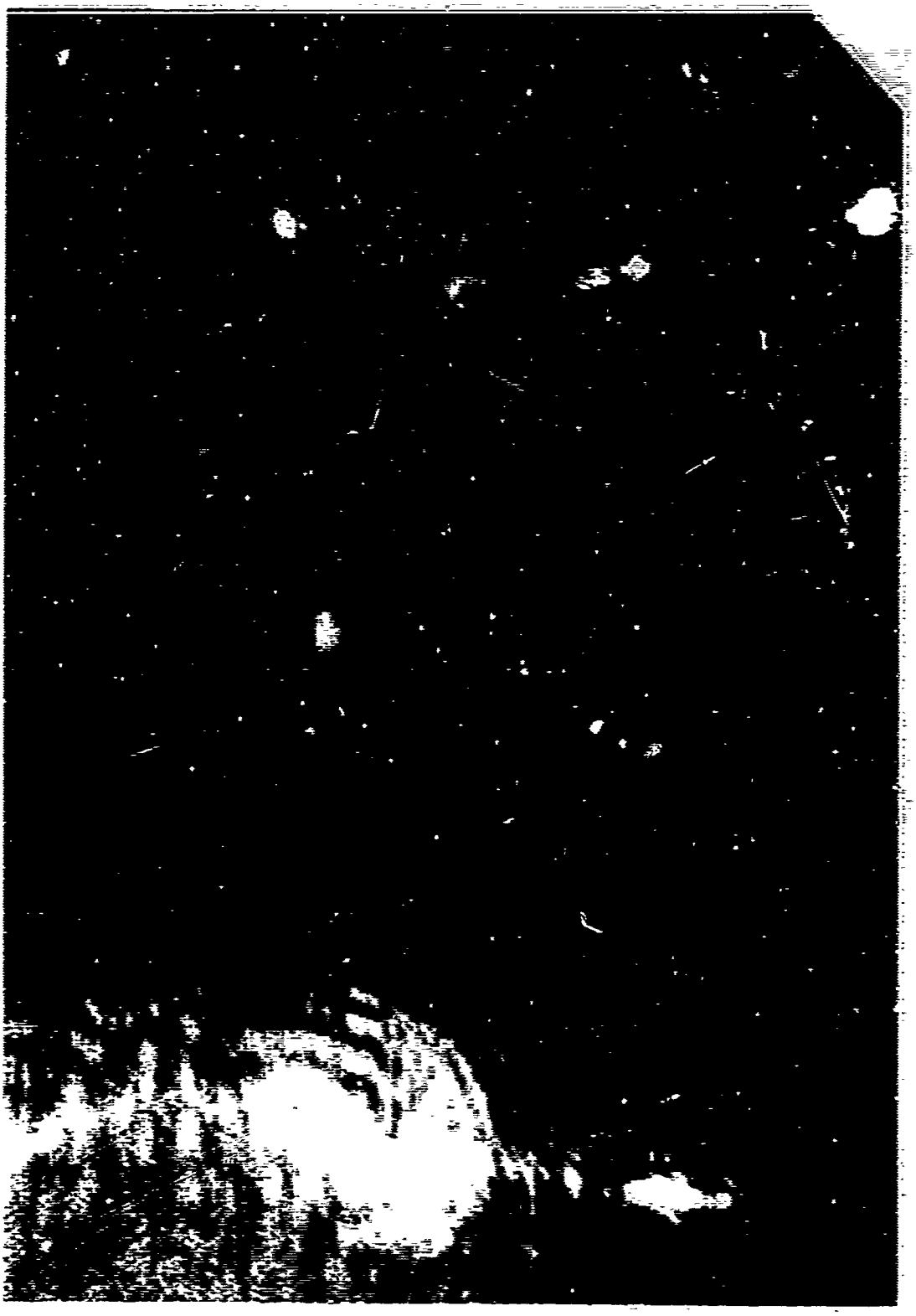

Figure V.19(f). Reconstruction from Holograms #3 and #4

Viewed directly by TV at medium contrast and brightness.
Reconstruction from #4 at top, #3 at bottom.

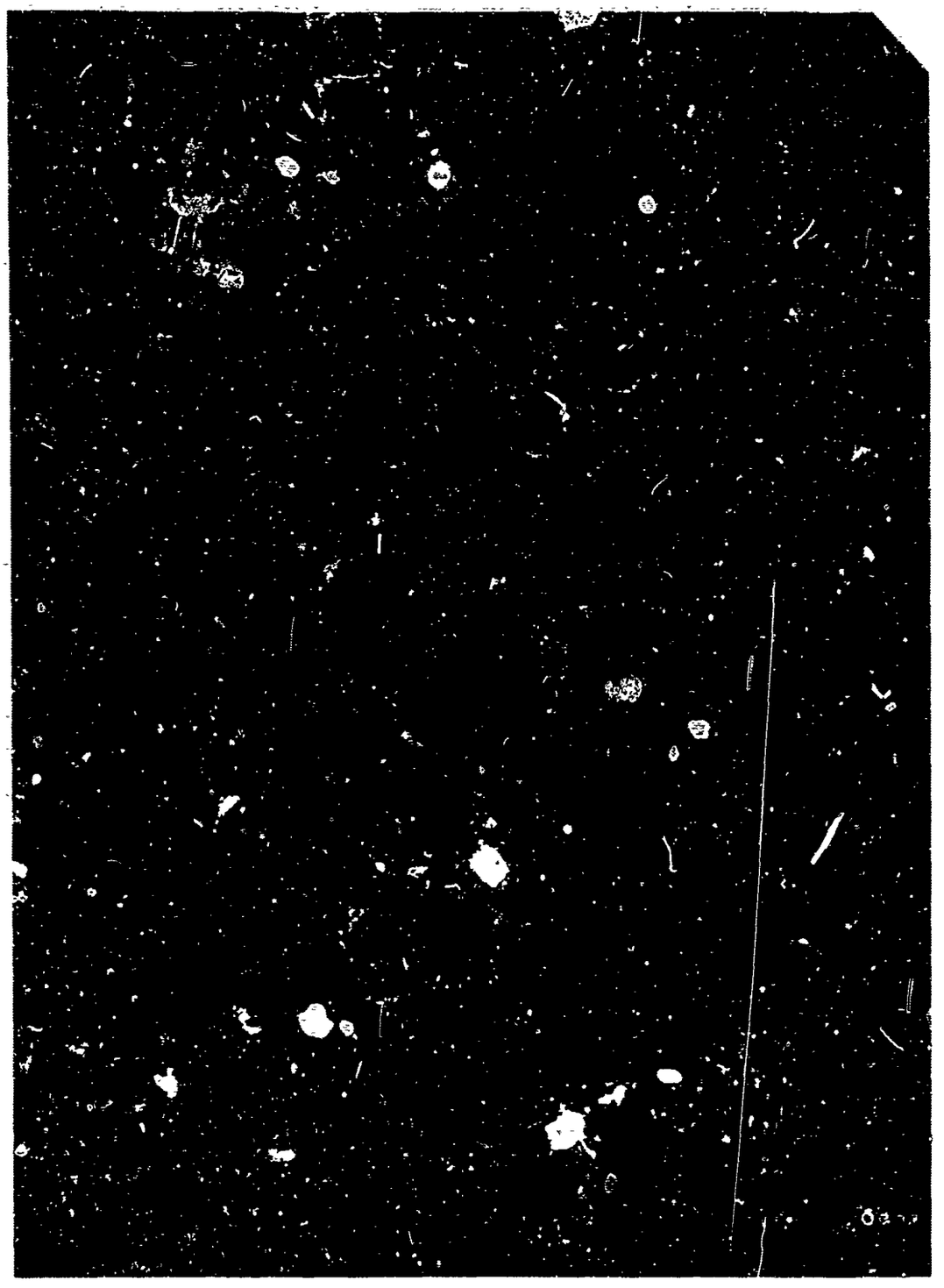

Figure V.19(g). Reconstruction from Holograms #3 and #4

TV at maximum contrast, minimum brightness, illustrating utility of TV displays for viewing acoustic holograms.

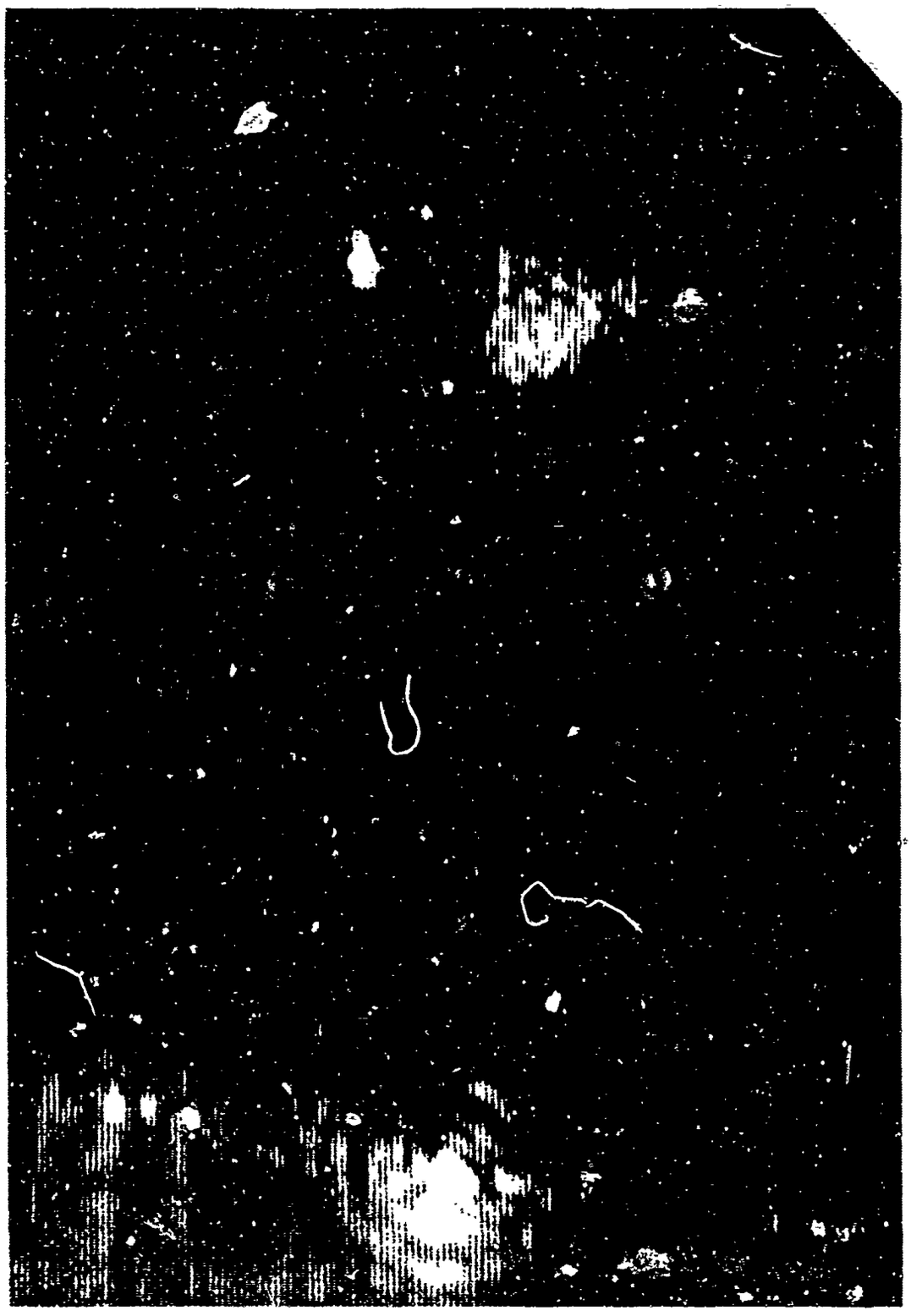

Figure V.19(h). Reconstruction from Holograms #2 and #5

Viewed directly by TV at medium contrast and brightness.
Reconstruction from #5 at top, #2 at bottom.

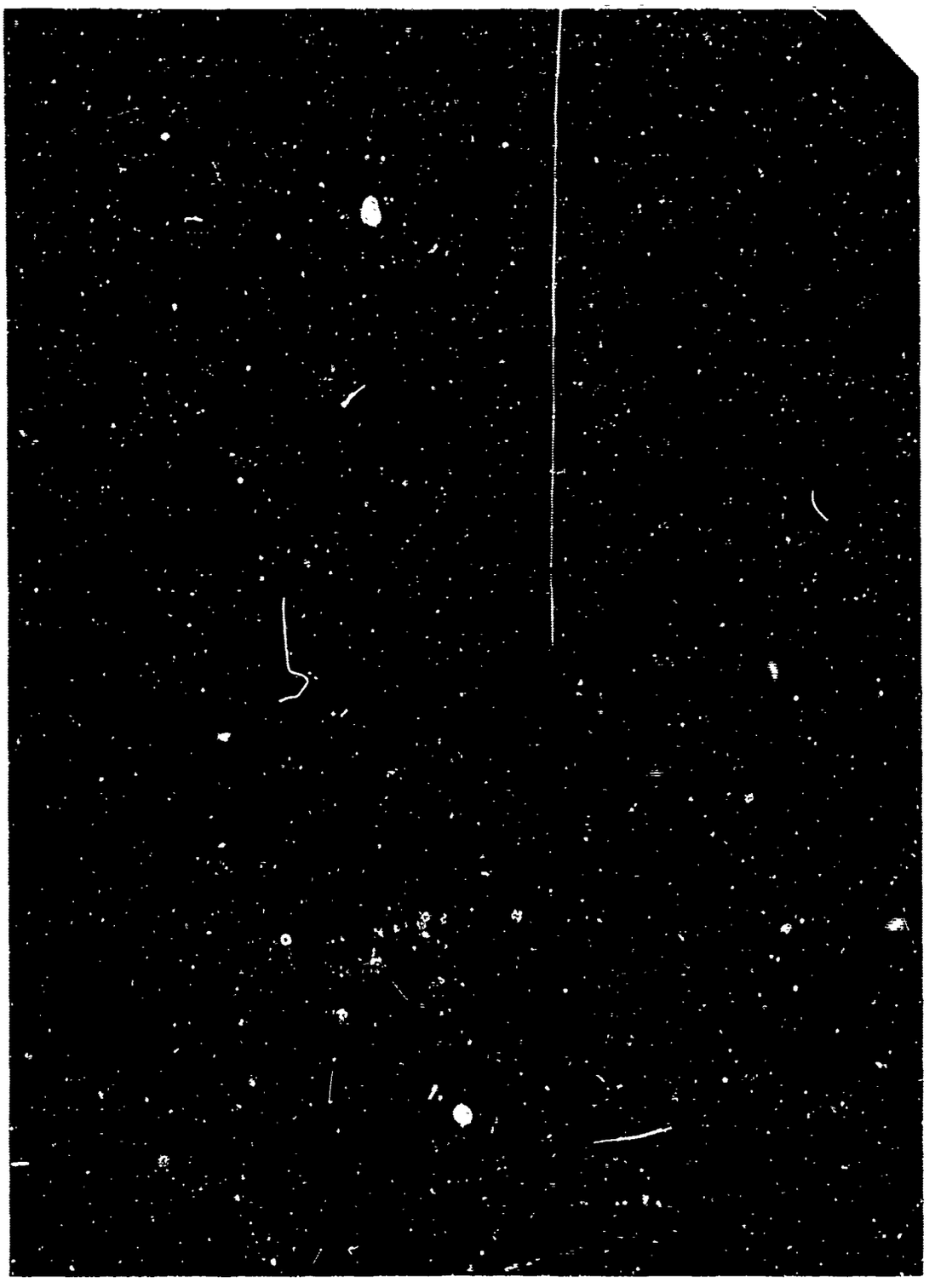

Figure V.19(i). Reconstruction from Holograms #2 and #5 TV at maximum contrast, minimum brightness, illustrating utility of TV displays for viewing acoustic holograms.

the higher order diffraction rings would also have contributed to the hologram and the signal to noise ratio might have been better but an erroneous measure of the hole size might have been obtained. Clipping appears to have some relation to the apodization techniques of conventional optics[71].

HOLOGRAMS #7 THROUGH #10 (Figures V.20-V.28)

Transmission through thin planar objects is useful for evaluating techniques and for visual displays. However, practical applications particularly in acoustic imaging, require that the hologram be made by acoustic radiation reflected from the object scene rather than transmitted through the object scene. Thus, the remainder of the holograms to be presented here are of reflecting object scenes even though such scenes are considerably more difficult to image primarily because of the predominately specular nature of the acoustic reflections from most objects. (See Chapter III.)

Holograms #7 through #10 were the first of the holograms made by reflected acoustic radiation; the objects were simple reflecting laminae fabricated from steel plate (#7 and #8) or aluminum plate (#9 and #10). Holograms #7 and #8 (Figures V.21 and V.22) were made with clipped detection and cw illumination. The reconstruction is shown in Figure V.23.

Holograms #9 and #10 (Figures V.25 and V.26) were made with linear detection and pulsed illumination. The reconstructions are shown in Figure V.27. Pulsed illumination was required in order to prevent spurious signals radiated by the illumination transducer from

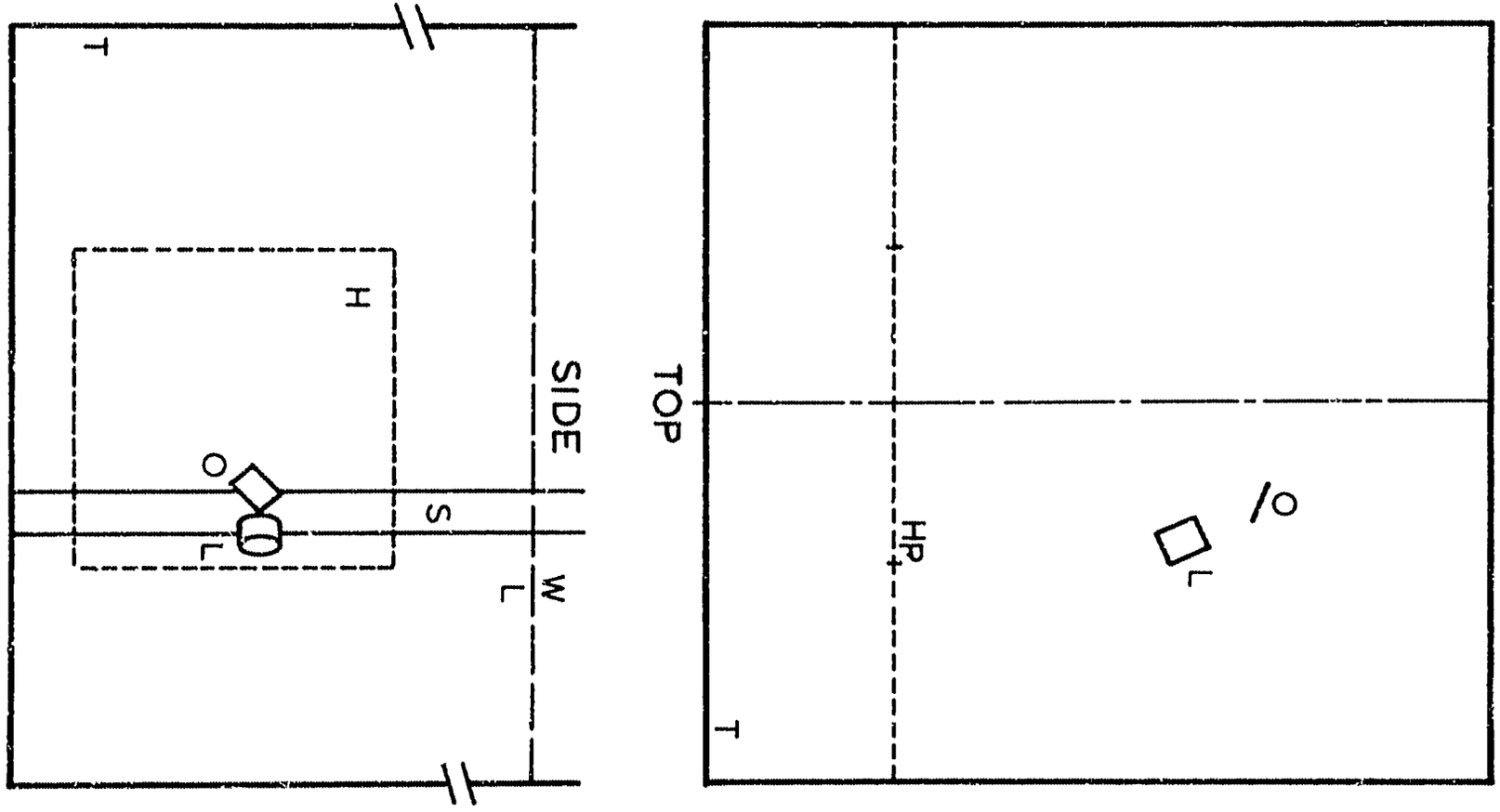

Figure V.20. Layout of Object Scene, Holograms #7 and #8

O Object, 15 cm × 20 cm × .1 cm thick steel plate fixed to support tube S by C-clamp fixed at the upper vertex

Figure V.21. Hologram #7, 0° Simulated Reference Angle

Regions of high acoustic field are white.
Bright spot in center of hologram is the central lobe of transducer L reflected from the object O.
Raster line spacing = 5.7mm, 230 lines total.

Figure V.22. Hologram #8, 7.7° Simulated Reference Angle

Raster line spacing = 5.7 mm.
Phase shift per line = π.

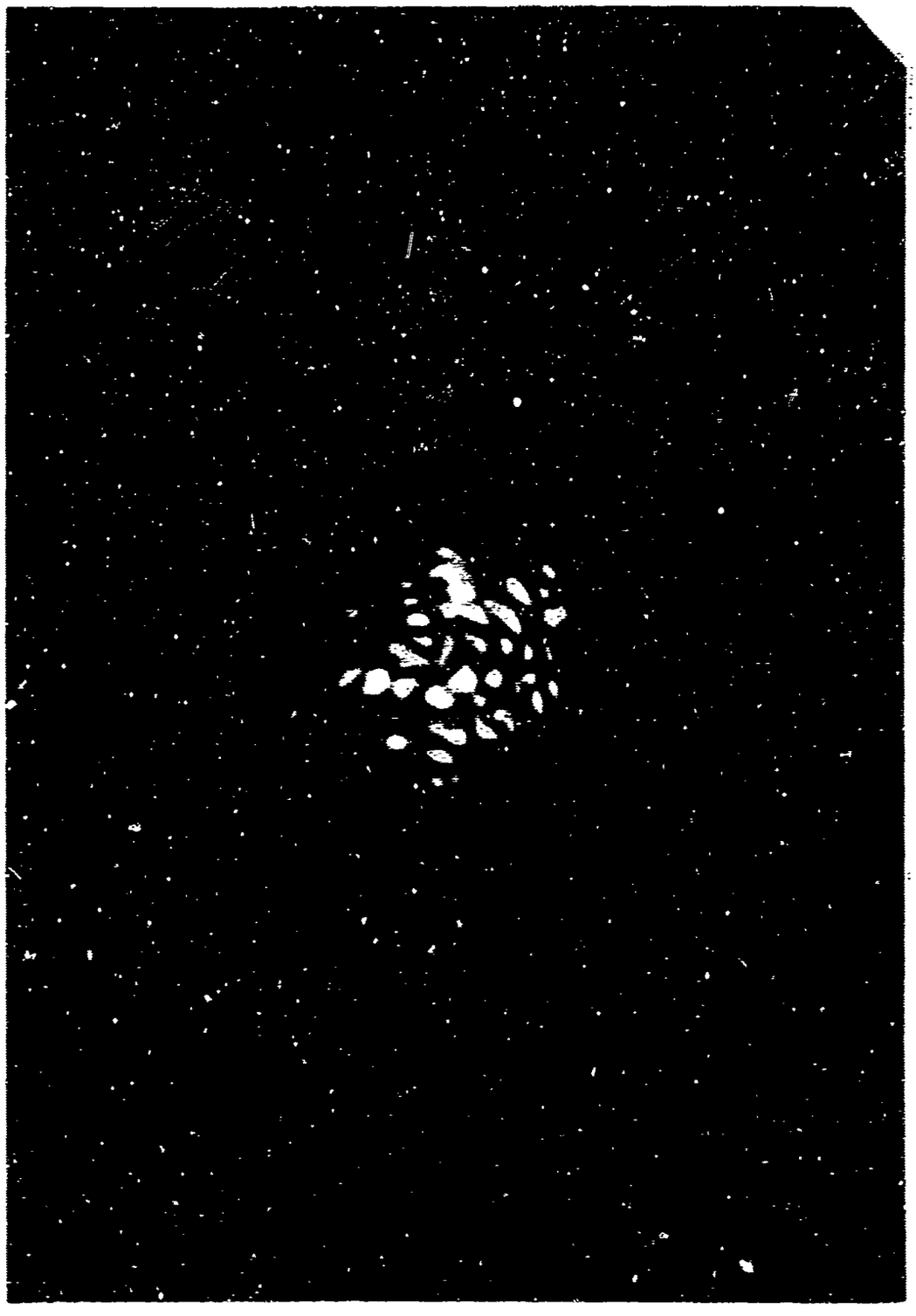

Figure V.23(a). Reconstruction from Hologram #7

Photographed on Polaroid 55 P/N film, positive print on Eastman Kodak Kodabromide F-5 single weight paper.

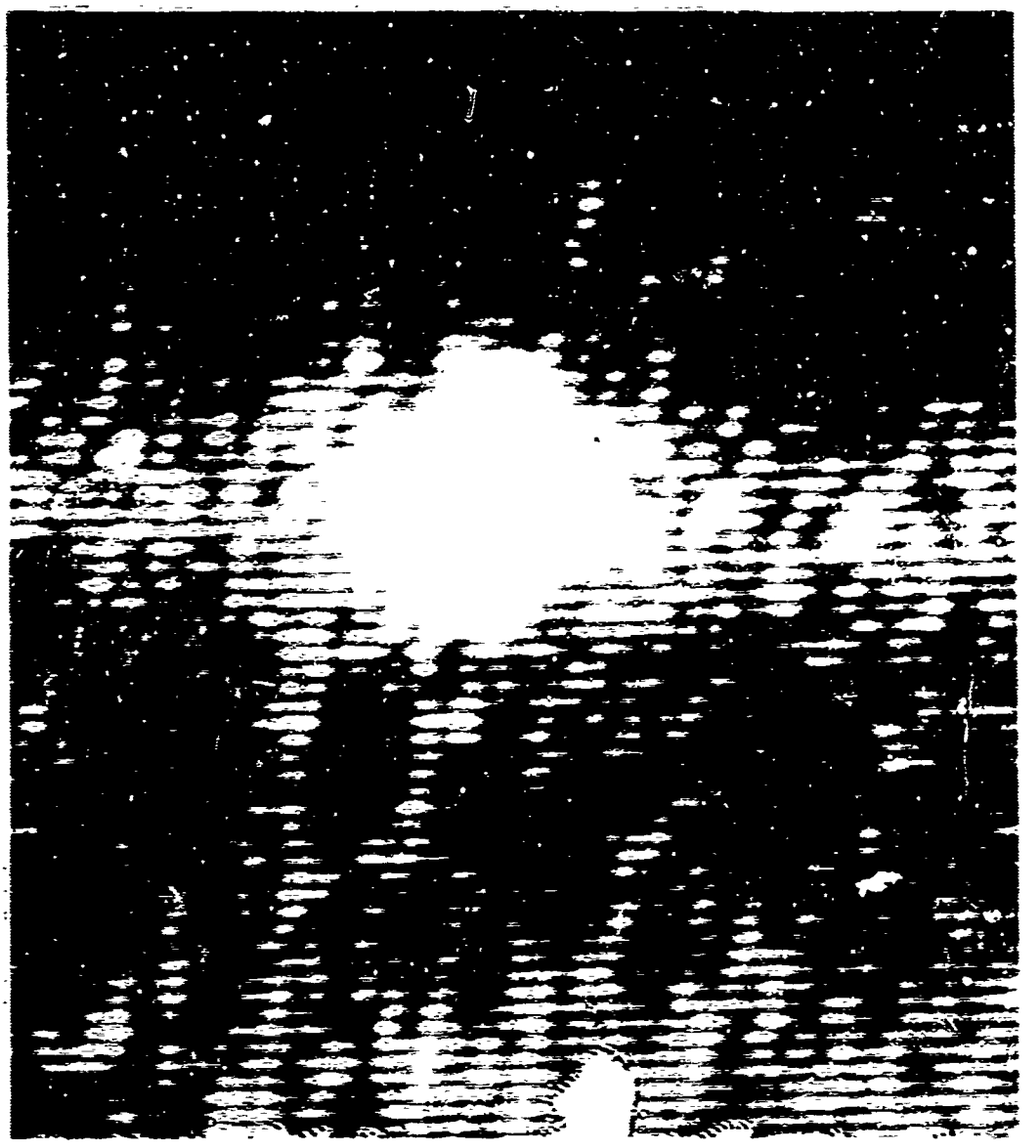

Figure V.23(b). Reconstruction from Hologram #7

Viewed directly by TV at medium contrast and brightness. Photograph of TV monitor on Polaroid 46L film, positive print on Eastman Kodak Kodabromide F-5 single weight paper. Figures V.23(a)-(c) illustrate the utility of viewing acoustic holograms with television systems. The variable contrast, brightness, and threshold of these systems allow instantaneous and continuous adjustment of the display for optimum appearance of the image against the high noise background characteristic of acoustic holograms. The jitter inherent in TV rasters reduces bothersome speckling without serious loss of resolution.

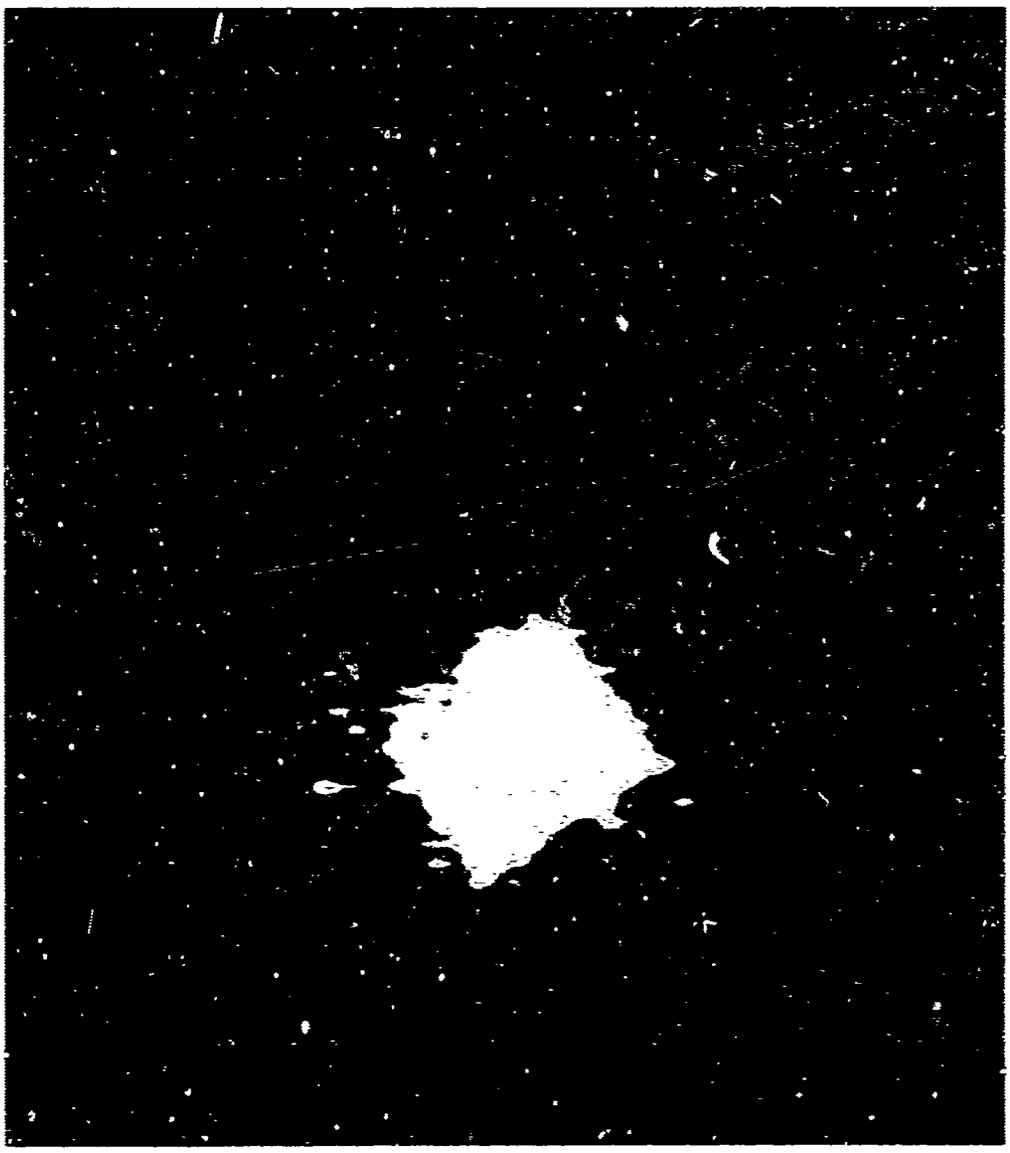

Figure V.23(c). Reconstruction from Hologram #7

Viewed directly by TV at maximum contrast, minimum brightness, clearly demonstrating that the reconstructed image is actually much brighter than background. Viewing directly by eye or continuous tone photography obscures this fact.

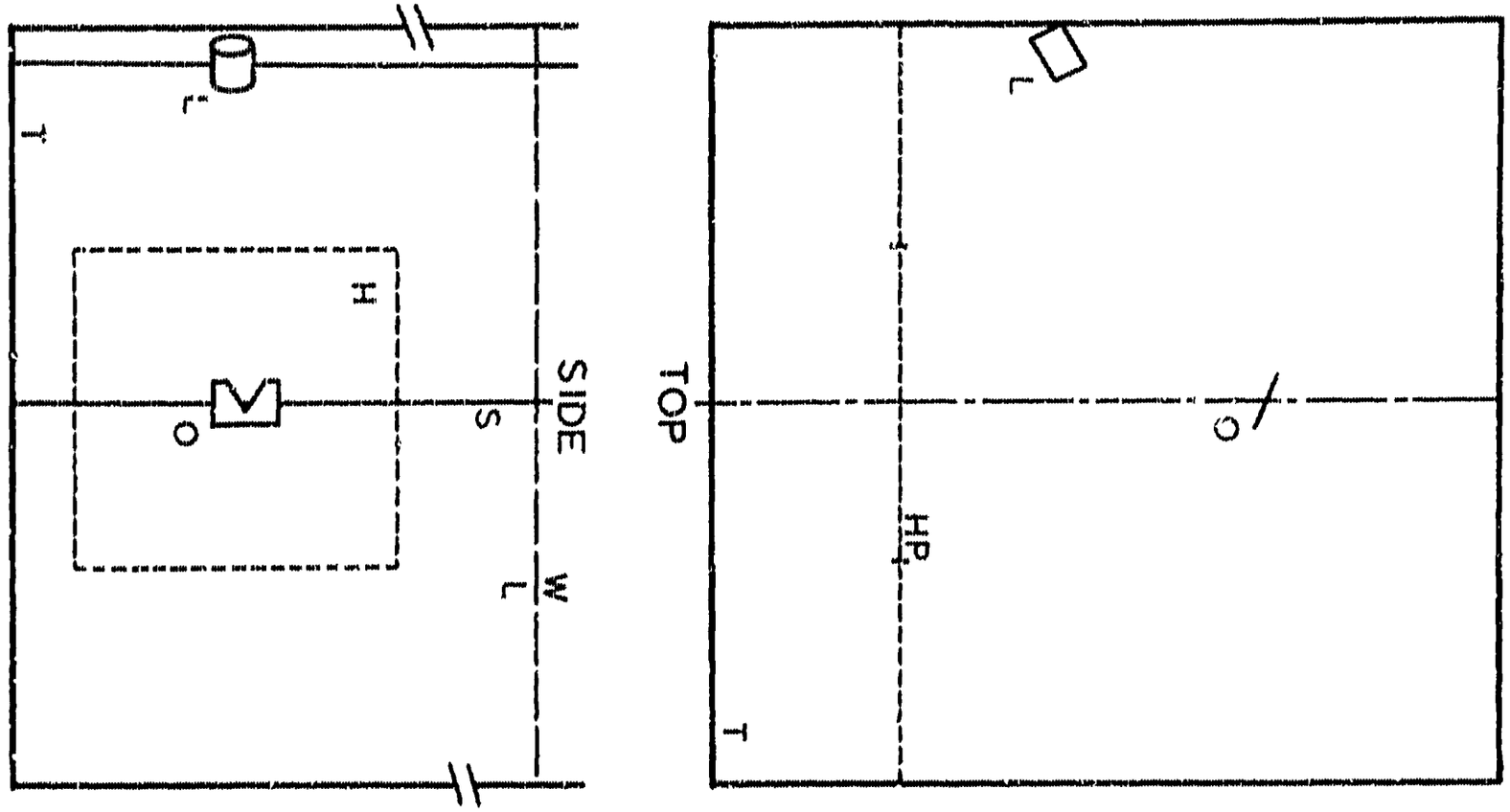

Figure V.24. Layout of Object Scene, Holograms #9 and #10

O Object, 20 cm × 22.5 cm × .2 cm thick bolted to fixed support tube S

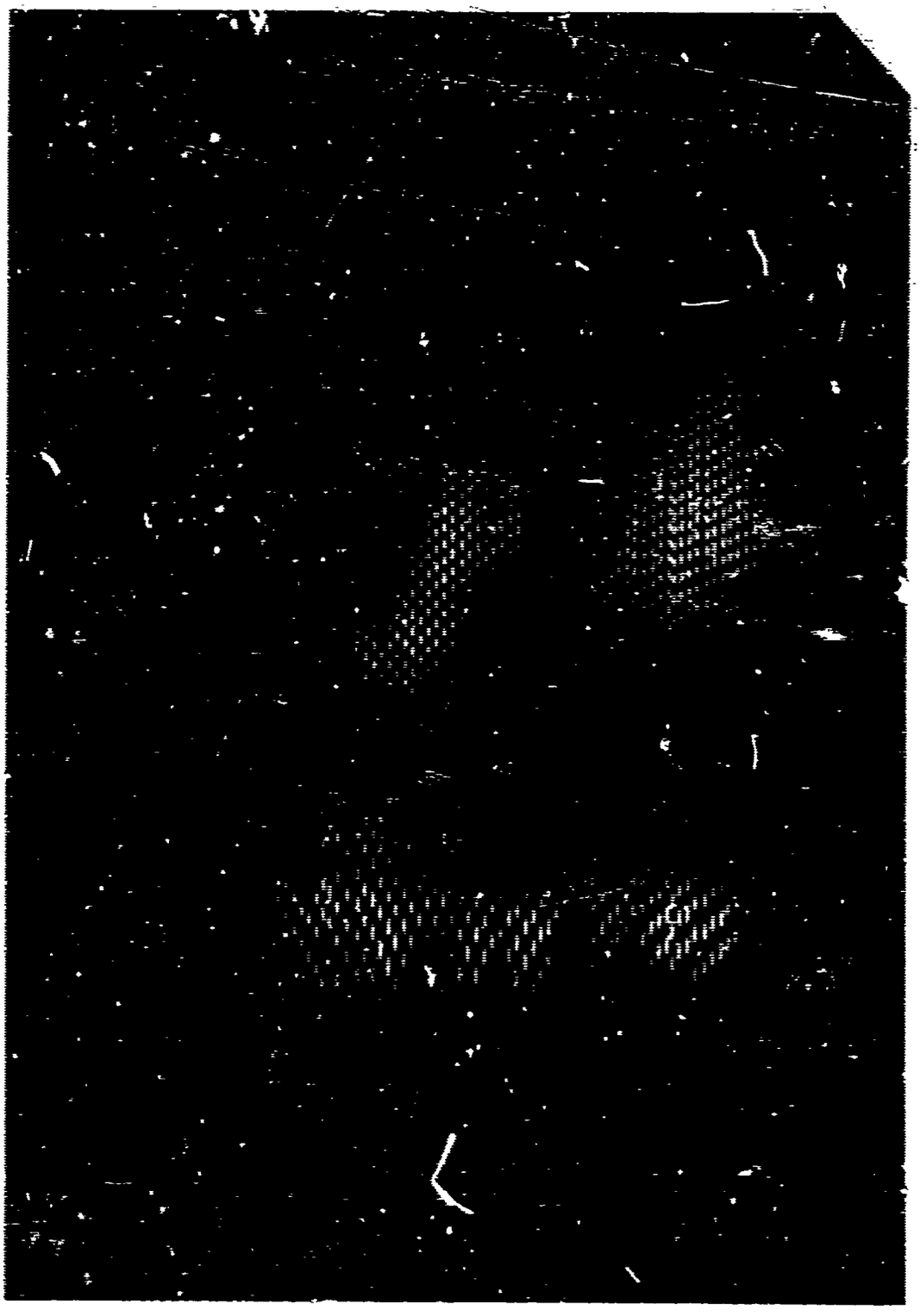

Figure V.25. Hologram #9, 0° Simulated Reference Angle

Regions of high acoustic field are white.
Raster line spacing = 5.7 mm, 110 lines total.

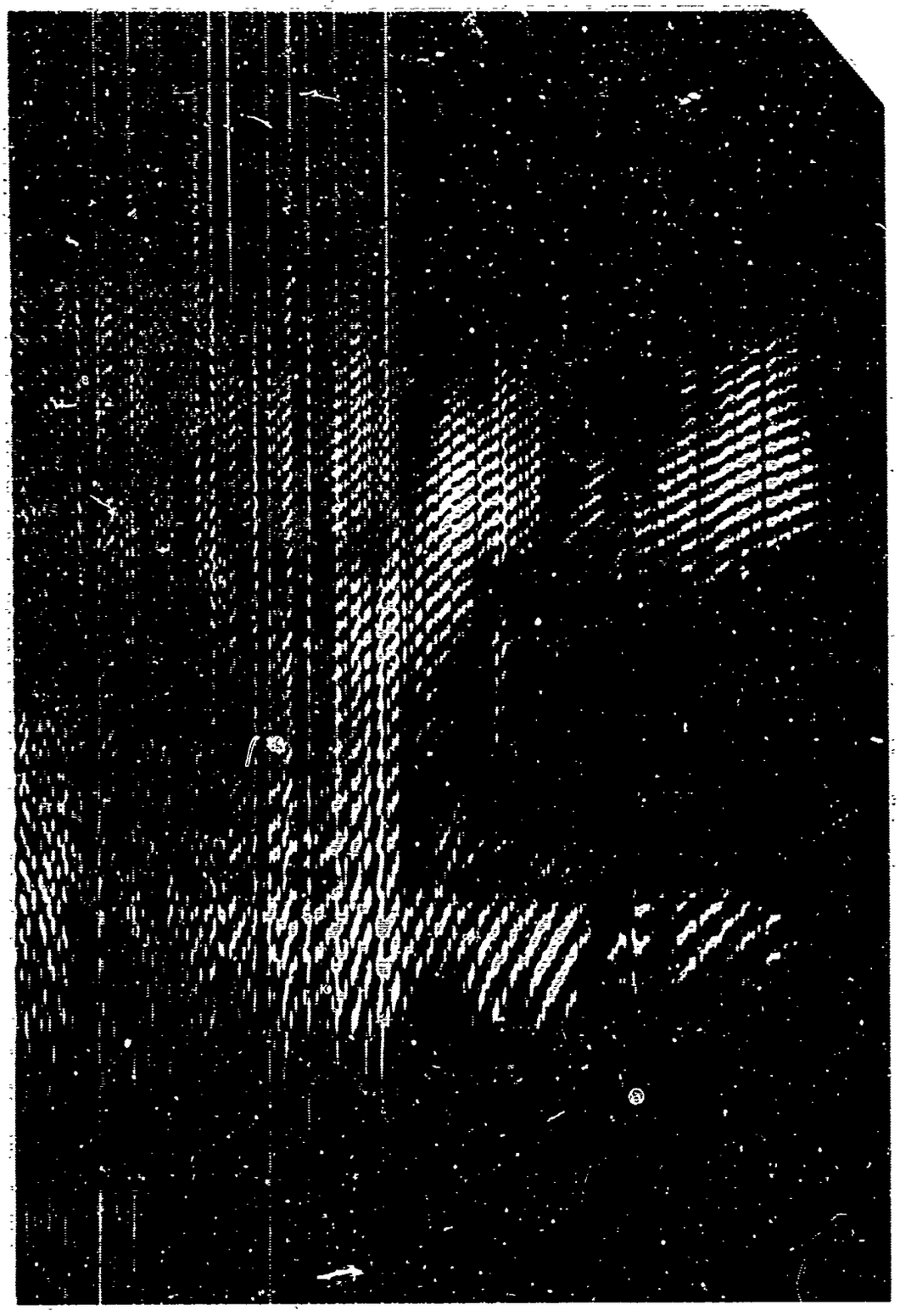

Figure V.26. Hologram #10, 0° Simulated Reference Angle

Identical with hologram #9 except raster line spacing=2.8mm, 195 lines total.

Figure V.27. Reconstruction from Hologram #9

Reconstruction from Holograms #9 and #10 about the same even though raster line spacing is different.

being recorded on the hologram. Spurious radiation was eliminated by range gating the received acoustic pulses; a typical pulse reflected by the target is shown in Figure V.28. The structure at the pulse edges is due to the difference in path length between the front and back of the transducer and between the various positions on the object and hologram plane. Care was taken to adjust the coincidence circuitry so that only a narrow portion from the center of the acoustic pulse was used to form a hologram.

The triangular shaped notch used as the object for holograms #9 and #10 was picked so that some measure of the resolution of the system could be obtained. The object was located approximately 1.7 m from the hologram plane and it appears that object points separated greater than 12 mm could be resolved. This corresponds to 3.6 milliradians angular resolution. Conversely, since the hologram plane measured approximately 79 × 63 cm the Rayleigh criterion predicts that the angular resolution could be no better than 2.3 milliradians. Thus, the resolution seems reasonable for the aperture available.

HOLOGRAMS #11 AND #12 (Figures V.29-V.31)

The next logical step in an elementary study of acoustic holography is to image objects with some measure of three-dimensionality, the simplest of these being multiplanar arrays. In Figure V.29 we show an arrangement of two laminae, one square, the other circular, situated in non-parallel planes with the square approximately 9 cm behind the circle. In Figure V.30 we show a conventional coplanar reference acoustic hologram (#11) of this scene. In Figure V.31 we show a

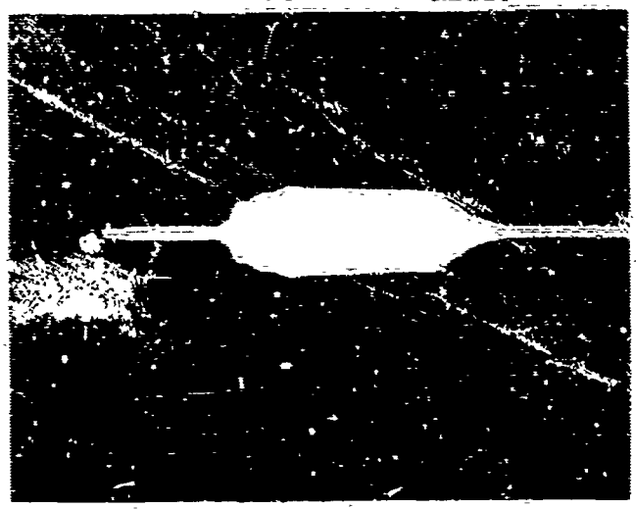

(a) In upper half of hologram.

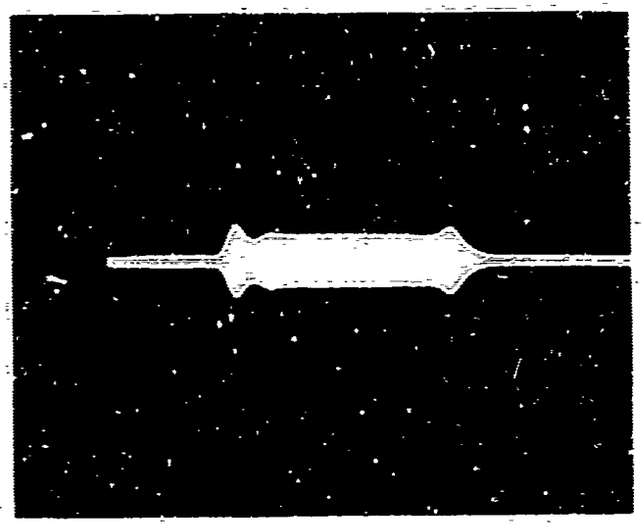

(b) In lower half of hologram.

Figure V.28. Typical Acoustic Pulses Scattered by an Object

Horizontal scale (time) = .2 msec/division.
Vertical scale (voltage input to amplifier G) = .5 volts/div

Note that the acoustic signal requires approximately .2msec for rise and fall due to difference in path length from various portions of the object to the hologram plane. Only center .4 msec of pulse was used for the holograms.

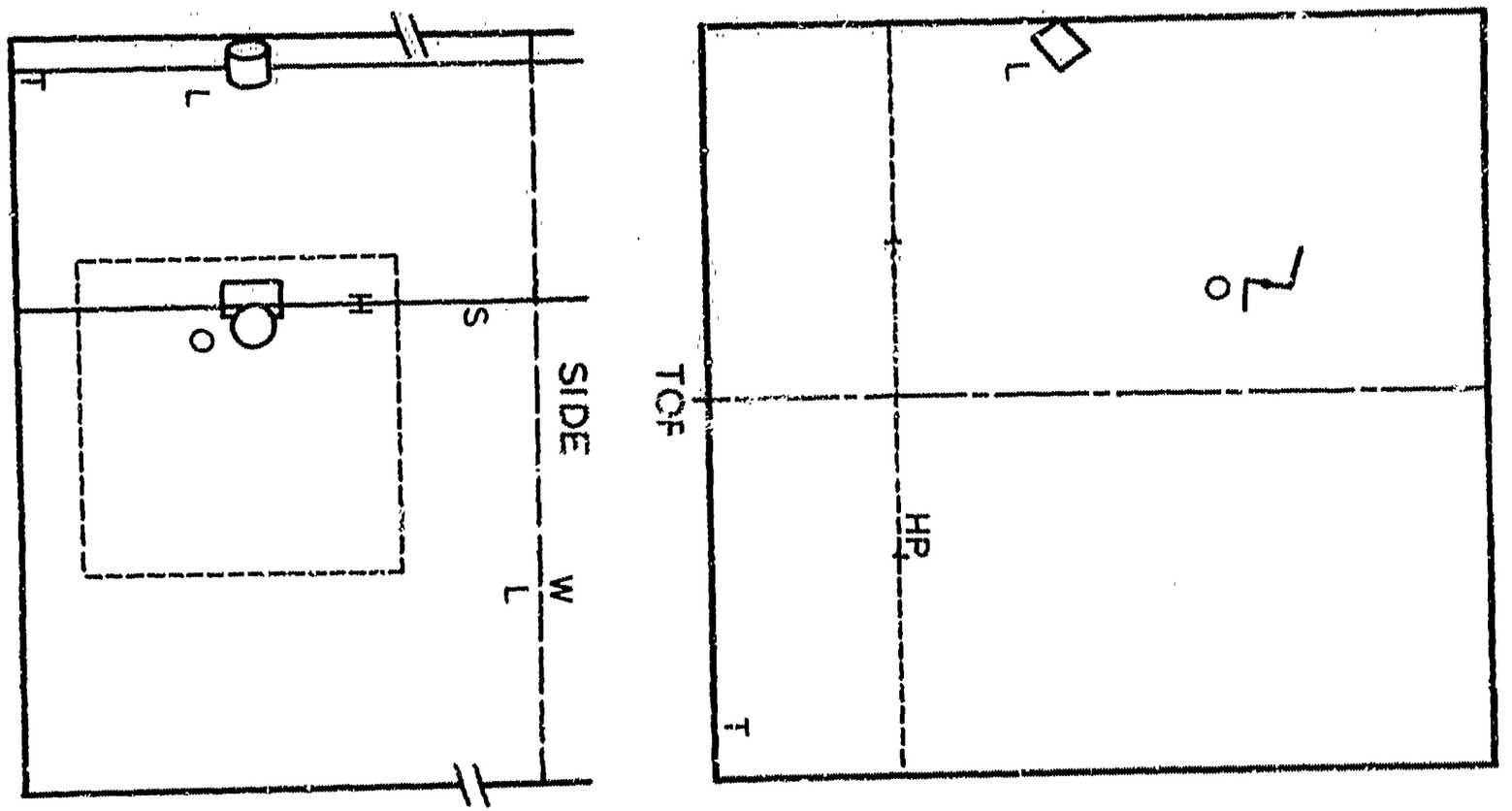

Figure V.29. Layout of Object Scene, Holograms #11 and #12

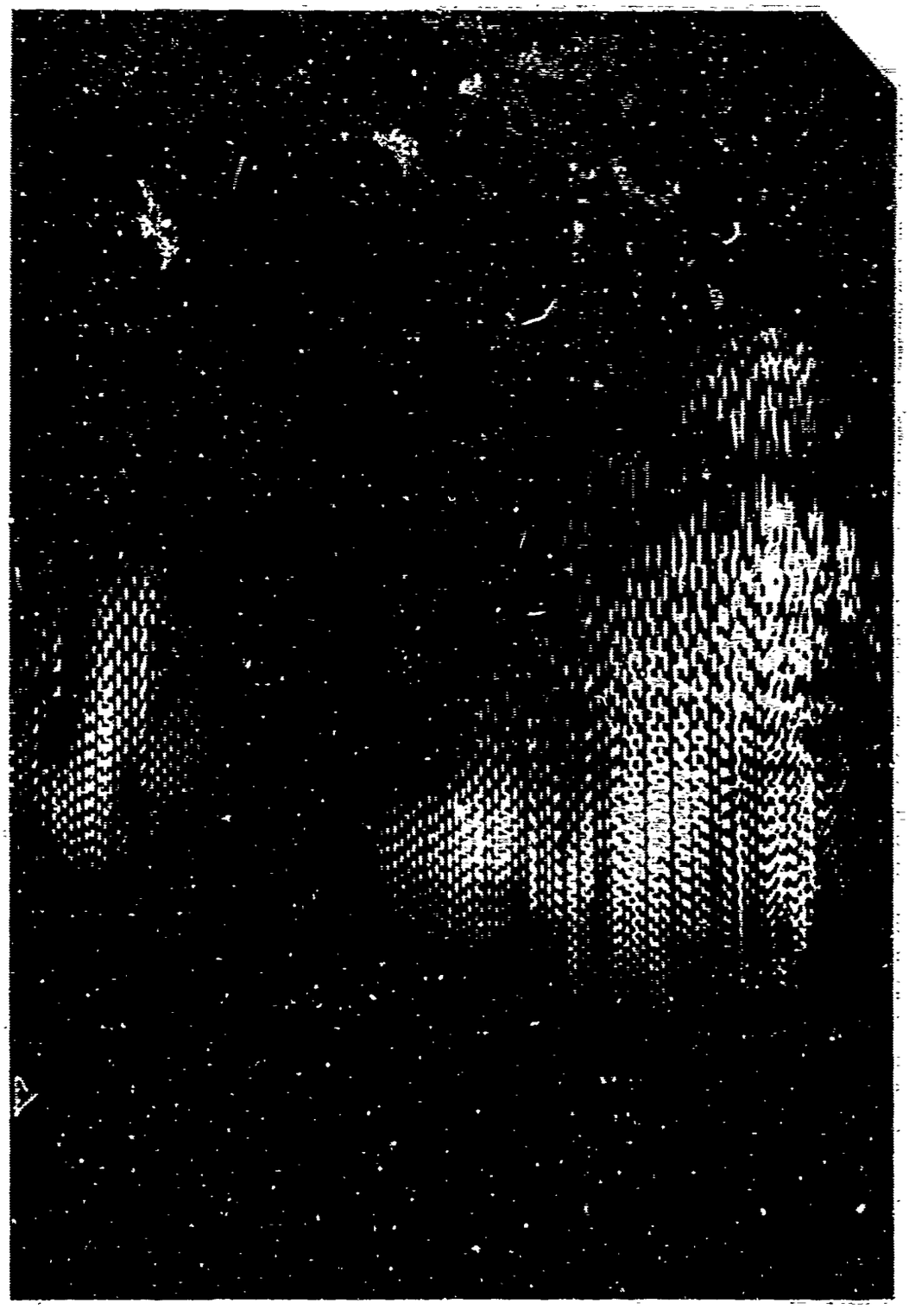

Figure V.30 Hologram #11, 0° Reference Angle Simulated by Interference

Figure V.31. Hologram #12, 0° Reference Angle Simulated by Heterodyning

hologram (#12) identical with hologram #11 except that whereas #11 was generated using conventional interference detection, #12 was generated using the heterodyne detection scheme outlined in Section V.4. By comparing the two holograms it is clear that they are equivalent except that the fringe contrast of #12 is less than #11. However, fringe contrast is easily adjusted by changing system gain and the zero signal intensity of the CRT spot.

The reconstructions from holograms #11 and #12 are rather poor for several reasons. First, because of the narrow beam angle of the acoustic illumination it was not possible to properly illuminate the edges of the laminae, hence the edges were not well defined in the reconstruction. Moreover, because of the narrow beam angle it was not possible to separate the laminae further hence the depth of focus of the hologram overlaps the depth of field of the scene and the two objects appear coplanar in the reconstruction. Finally, it appears that for the small apertures of acoustic holograms one may wish to sacrifice accurate linear display of the hologram fringes for a binary display which improves signal to noise ratio at the expense of a completely true gray scale rendition of the object.

It is interesting to note that the difficulties of specular reflection are already clearly evident even in simple situations like Figure V.29. Note that the acoustic field in the hologram plane is composed of essentially two "bright patches". That on the left is due primarily to reflection from the round object element, that on the right is due primarily to reflection from the square object element. Now the angle of inclination between the two object planes was only

5°. However, if this angle had been increased it would then not have been possible to contain both patches simultaneously within the hologram aperture, hence it would not have been possible to simultaneously image both object elements.

HOLOGRAMS #13 AND #14 (Figures V.32-V.36)

We have presented, in the foregoing, acoustic holograms of various object scenes of progressibely more complicated structure. This procedure was adopted as the most logical way in which to conduct an elementary study of acoustic imaging. By beginning with extremely simple objects, accurate measurements can be compared with theoretical calculations without undue difficulty. Then, the special problems posed by more realistic, but also more complicated, scenes can be readily isolated and studied. We conclude this logical progression with holograms #13 and #14, holograms of a very general object scene representative of those likely to be encountered in practical undersea acoustic imaging situations. These holograms illustrate a serious obstacle to useful acoustic imaging namely the specular nature of acoustic reflection from most objects. (See Chapter III.)

The physical arrangement for holograms #13 and #14 is shown in Figure V.32. The object, which is viewed in reflection, is a cylindrical underwater light globe housing with one end spherical and the other end capped by a flat, bronze fitting. Hologram #13 is shown in Figure V.33, and the reconstruction in Figure V.34. Unlike the preceeding holograms, instead of a complete image of the object only a diffracted highlight is observed. This is a characteristic displayed

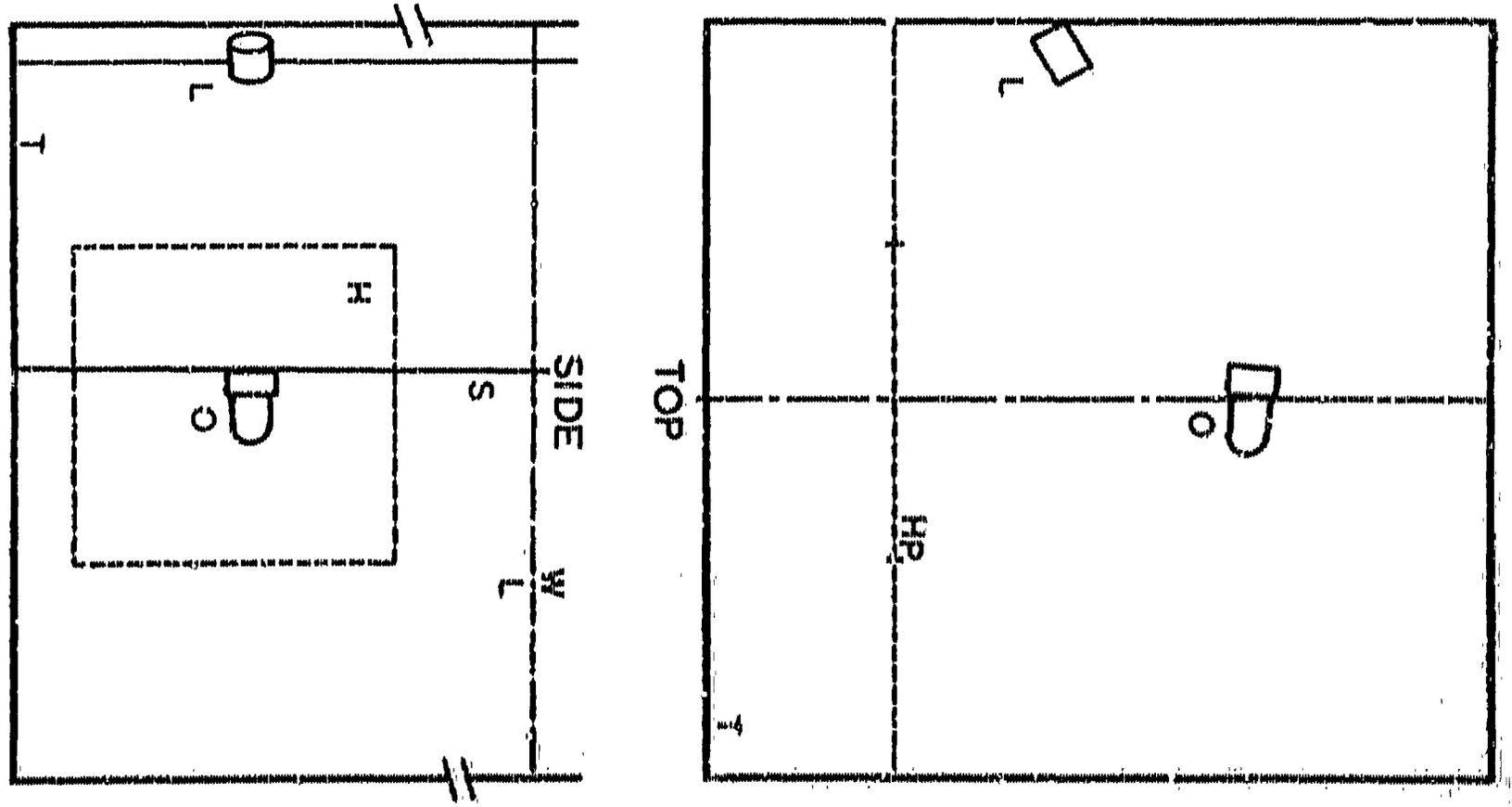

Figure V.32. Layout of Object Scene, Holograms #13 and #14

O Object, waterproof light globe housing approximately 15 cm diameter × 25 cm long

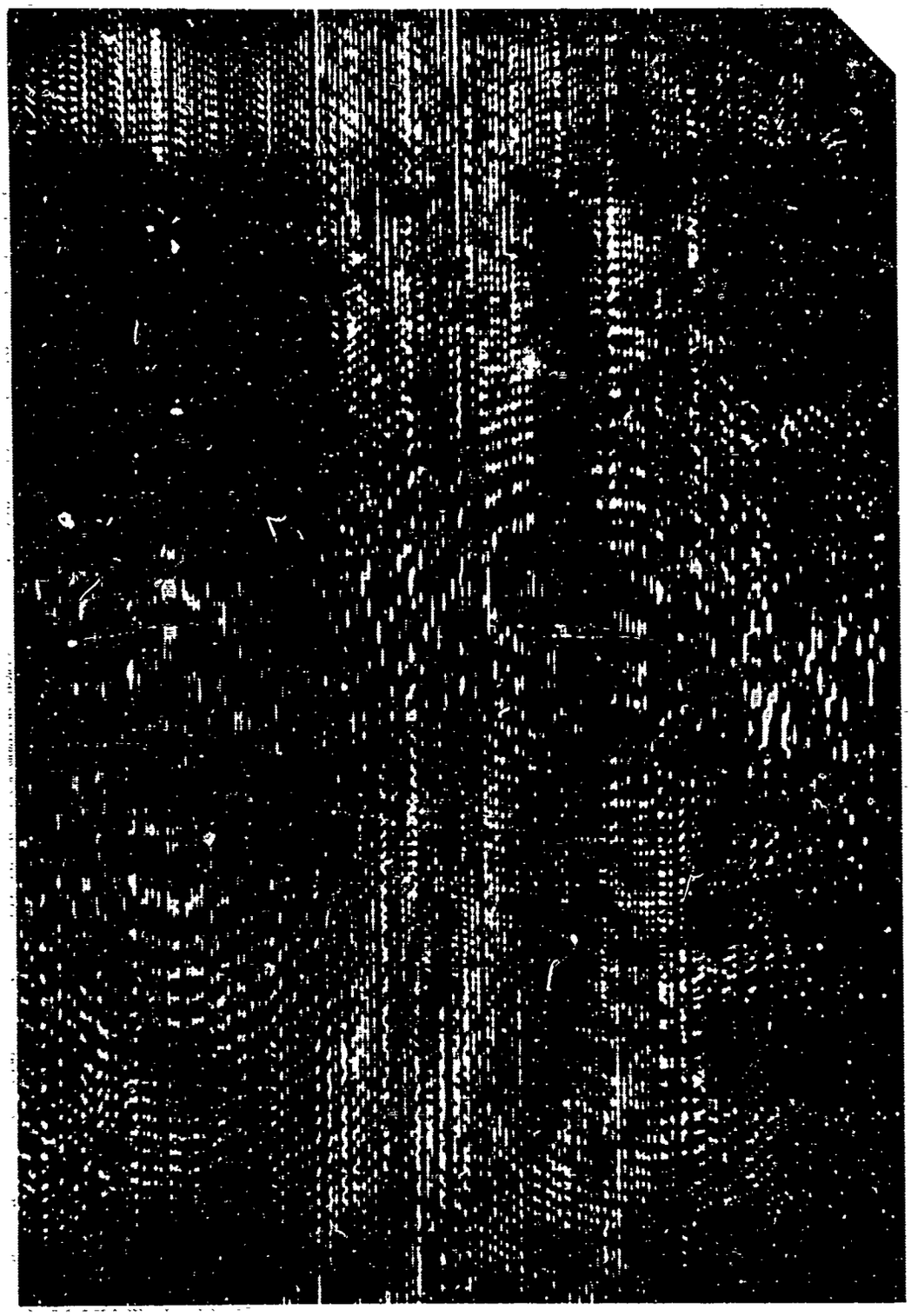

Figure V.33. Hologram #13, 0° Simulated Reference Angle

Fringe system at left due to cylinder, fringe system at right due to spherical end cap.

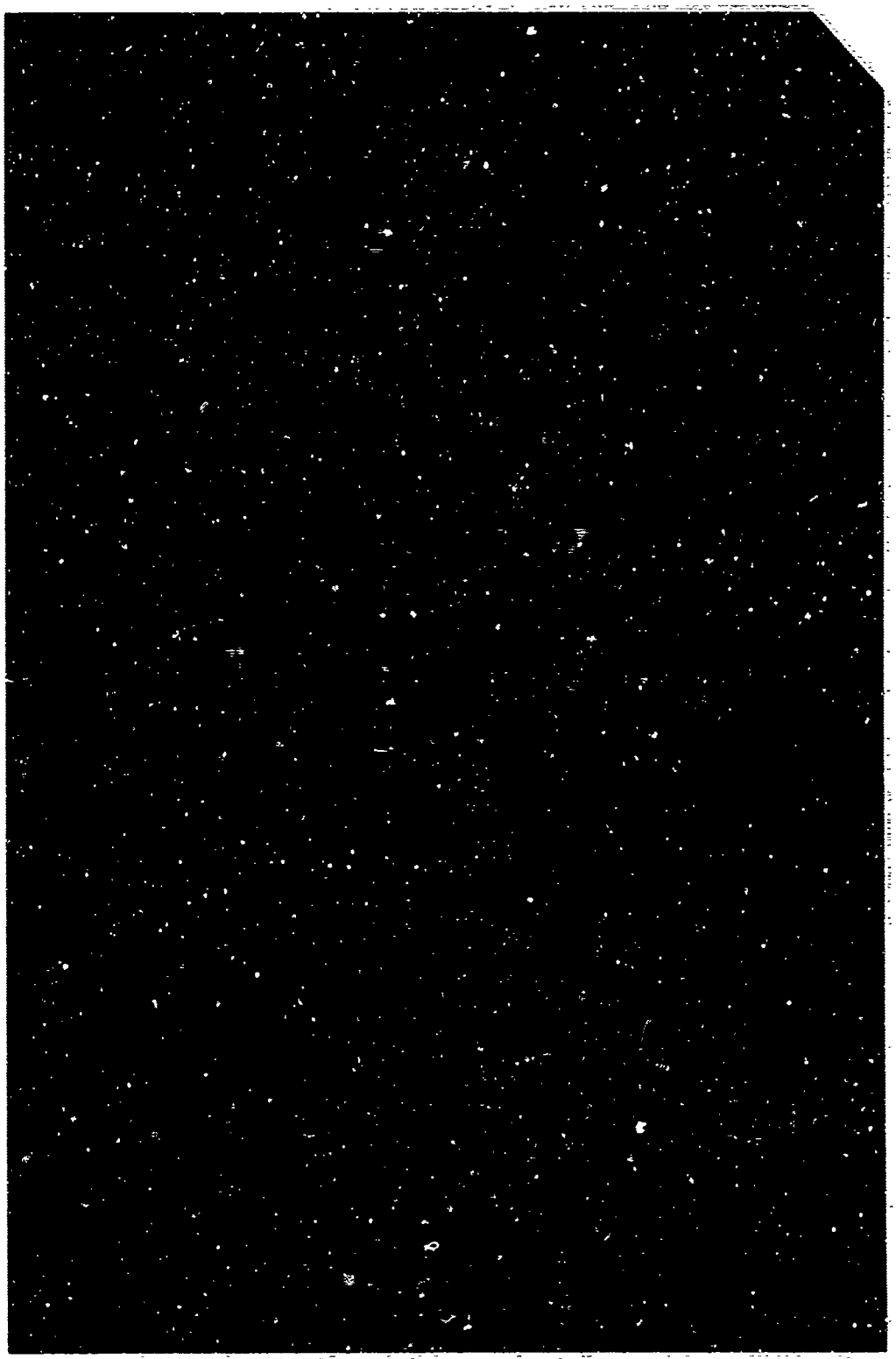

Figure V.34. Reconstruction from Hologram #13

Specular nature of reflection from object is clearly evident. Object diameter is actually 15 times larger.

by most objects illuminated with acoustic radiation. The explanation is quite simple.

In Chapter III the role of surface texture in determining the acoustic scattering properties of material surfaces was discussed. For most surfaces, the characteristic depth of the texture is considerably less than λ (λ = 1.5 mm for 1 MHz acoustic radiation in water), the characteristic correlation length of the texture much greater than λ. Accordingly, most objects observed by acoustic means appear to be smooth; i.e., the acoustic scattering is specular rather than diffuse.

In Chapter III we also discussed the consequences of viewing through small apertures specularly reflecting curved surfaces illuminated with plane or spherical waves; only the central lobe of the diffraction pattern will be observed. Simple geometrical arguements show that this lobe arises mainly from that portion of the reflecting surface directly opposite the center of the viewing aperture, hence the object appears as a diffracted highlight. The glass housing (Figure V.35a) used as the object for hologram #13 is acoustically smooth in the sense outlined above, hence ony would expect that the reconstruction from hologram #13 would show only a diffracted highlight. This is indeed the case.

To circumvent the highlight problem one usually resorts to diffuse illumination. However, generation of diffuse but coherent acoustic radiation is not a simple task. Instead we choose to make the object quasi-diffusely reflecting by attaching to it airfilled glass spheres approximately 2.5 cm diameter as shown in Figure V.35(b). This artifice simulates a surface texture with a characteristic depth

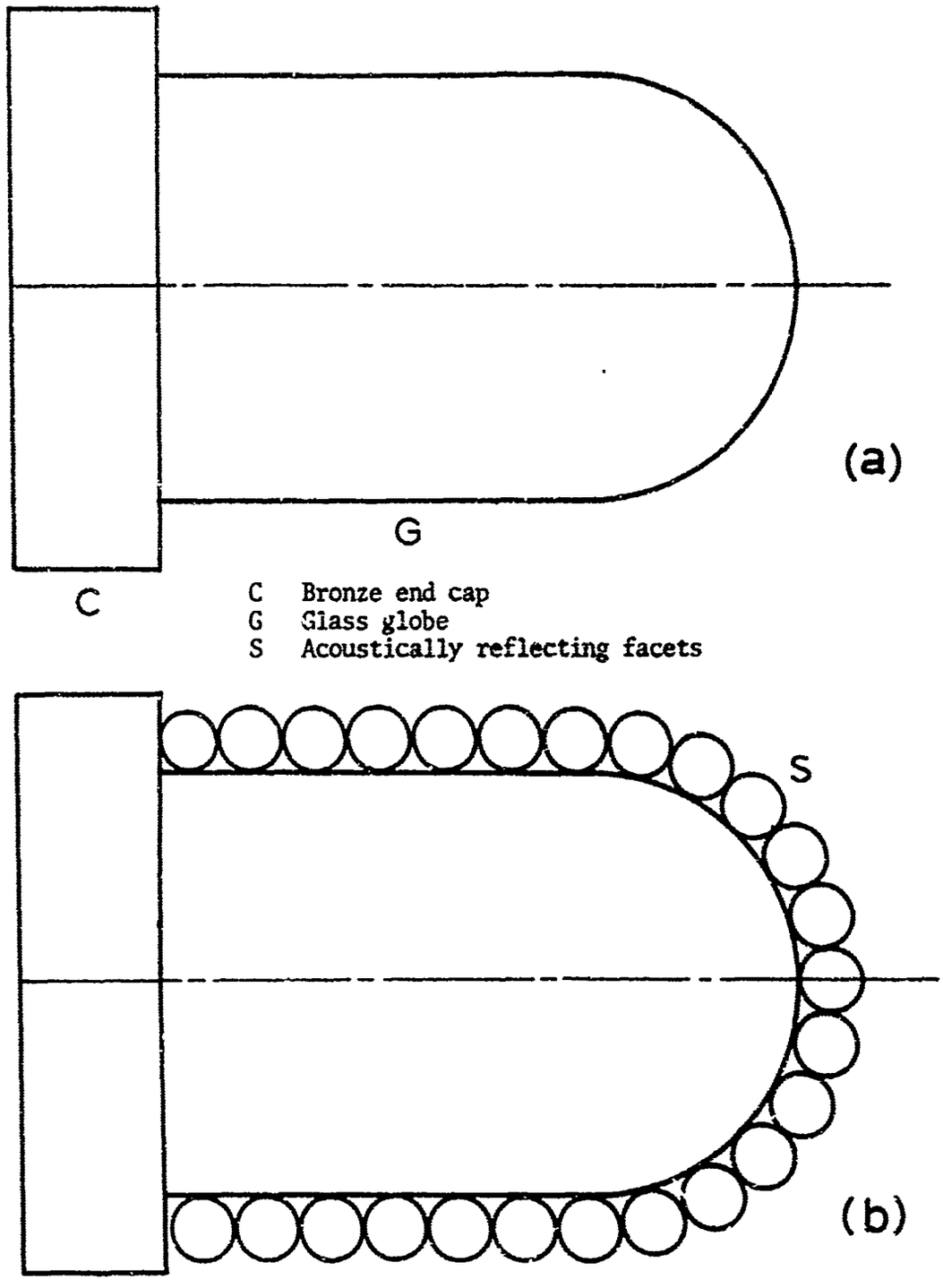

Figure V.35. A Quasi-diffusely Reflecting Object

of several wavelengths.

The modified glass housing was replaced in exactly the same position as for hologram #13 and a hologram was then made of the new object scene using the same hologram parameters as before. The new hologram (#14) is shown in Figure V.36. Note that it bears a certain resemblance to #13 although many of the fringes are now considerably mottled or even washed out completely. Of course, this is precisely what one would expect as a specular object is gradually "roughened" into a diffuse object. Many areas of the hologram exhibit very fine fringe structures again indicitive of diffuse reflection.

Because the resolution of the CRT display was limited, the fringe detail in the physical hologram plane was inadequately preserved in the recorded hologram. By watching the spot during a typical scan it was apparent that there was definite, high contrast fringe detail in the hologram at spacings as small as one fifth the resolvable spacing of the CRT. To obtain the required display resolution would require the use of a magnetically focused CRT. Thus, a useful reconstruction from hologram #14 was not possible. However, simply by comparing holograms #13 and #14 it is apparent that diffuse acoustic illumination of rough surfaces will indeed allow imaging of the entire object, not just the highlights.

8. SUMMARY

A simple scanning technique for generating acoustic holograms of underwater objects in the laboratory has been described. Using this system acoustic holograms have been recorded which show angular

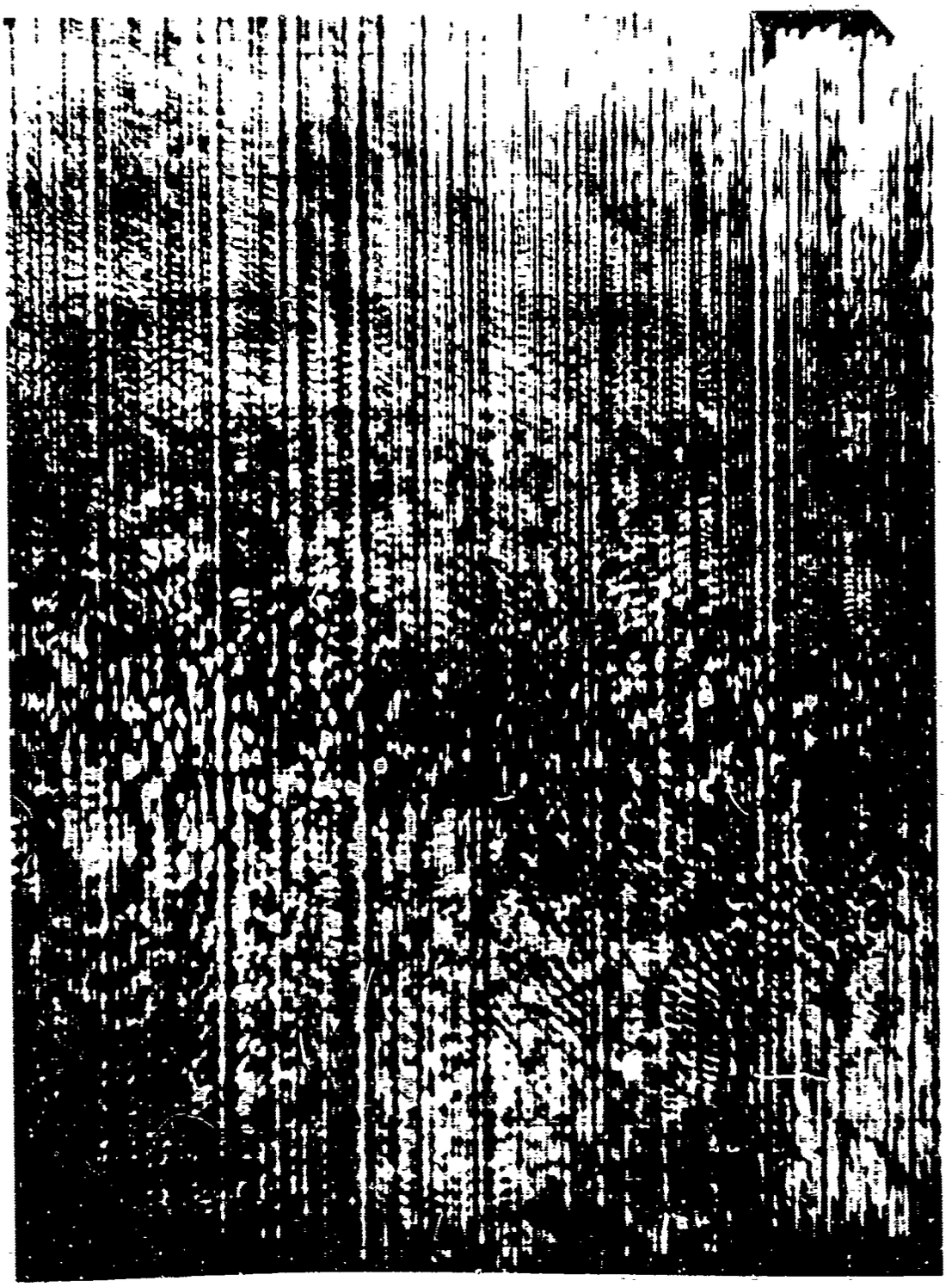

Figure V.36. Hologram #14, 0° Simulated Reference Angle

Hologram #14 appears to be a "perturbation" of hologram #13. Regions of high acoustic field are dark.

resolution of 3.6 milliradians, approximately 1.5 times the Rayleigh limit. These experiments were performed at 1 MHz, a frequency suitable for long range underwater imaging and detection.

Because instantaneous amplitude is an acoustic observable, the reference field can be simulated electronically. Moreover, by resorting to heterodyne or phase detection the cross product term between object and reference signals may be generated without the undesired extraneous terms which occur in conventional holography. Holograms of the Leith-Upatnieks type, with the inclined planar reference simulated electronically, and heterodyne detection holograms are presented.

By using a CRT for the acousto-optic conversion it is possible to synthesize electronically a wide variety of conversion characteristics from linear to hard limiting. Because of the rather small apertures involved it appears that hard limiting (high fringe contrast) or clipping is often desirable in order to maximize reconstructed image brightness.

Various other aspects of acoustic imaging are presented. In particular, the severity of specular acoustic reflection is clearly evident in these experiments.

Finally, the utility of variable contrast television displays for viewing acoustic holograms is demonstrated.

APPENDIX A

FOURIER TRANSFORM CONVENTIONS

In optics we shall have occasion to calculate Spatial Fourier Transforms. Consider the general function of position $A(\underline{r})$ where

$$\underline{r} = x\hat{x} + y\hat{y} + z\hat{z} \tag{A.1a}$$

and $\hat{x}$, $\hat{y}$, $\hat{z}$ are cartesian coordinate unit vectors with $\hat{z}$ lying along the general direction of propagation. Position in a specific transverse plane $z = z_C$ = const. is denoted $\underline{r}_C$ where

$$\underline{r}_C = x\hat{x} + y\hat{y} + z_C\hat{z} \quad . \tag{A.1b}$$

The Spatial Fourier Transform $\widetilde{A(\underline{r}_C)}$ of $A(\underline{r}_C)$ is taken as the two-dimensional Fourier Transform in the transverse plane $z = z_C$. Thus

$$\widetilde{A(\underline{r}_C)} \equiv \tilde{A}(\underline{x}, z_C) = \iint_{-\infty}^{\infty} A(\underline{r}_C) e^{-2\pi i(s_x x_C + s_y y_C)} dx_C dy_C$$

$$= \int_I A(\underline{r}_C) e^{-2\pi i \underline{r}_C \cdot \underline{s}} d^2 r_C \tag{A.2}$$

with the inverse

$$\widetilde{A(\underline{s},z_C)} = \int\int_{-\infty}^{\infty} \tilde{A}(\underline{s},z_C) e^{2\pi i(s_x x_C + s_y y_C)} ds_x ds_y$$

$$= \int_{s} \tilde{A}(\underline{s},z_C) e^{2\pi i\, \underline{s}\cdot\underline{r}_C} d^2s = A(\underline{r}_C) \qquad (A.3)$$

Here $\int_C$ denotes integration over the entire transverse plane $z = z_C$, $\int_s$ denotes integration over the entire $\underline{s}$ plane and

$$\underline{s} = s_x\hat{x} + s_y\hat{y} \qquad (A.4)$$

is the spatial frequency in cycles/length. In general, the Spatial Fourier Transform depends upon which plane z = const. is chosen for the transformation; this z dependence is explicitly stated. For example, in the plane z = 0 the Spatial Fourier Transform of $A(\underline{r})$ is denoted $\tilde{A}(\underline{s},0)$.

Temporal Fourier Transforms are also required. The Temporal Fourier Transform $A(\underline{r},t)$ of a function of time and position $A(\underline{r},t)$ is taken as

$$\widetilde{A(\underline{r},t)} = \tilde{A}(\underline{r},\nu) = \int_{-\infty}^{\infty} A(\underline{r},t) e^{-2\pi i\nu t} dt \qquad (A.5)$$

with the inverse

$$\widetilde{\tilde{A}(\underline{r},\nu)} = \int_{-\infty}^{\infty} \tilde{A}(\underline{r},\nu) e^{2\pi i\nu t} d\nu = A(\underline{r},t) \qquad (A.6)$$

and ν is the temporal frequency in cycles/sec. In general, the Temporal Fourier Transform depends upon position; this $\underline{r}$ dependence is explicitly stated. Positional dependence will always be denoted prior to temporal dependence.

APPENDIX B

CONVOLUTION AND CORRELATION THEOREMS

The convolution A*B of two functions A(x) and B(x) is taken as

$$A(x) * B(x) = \int_{-\infty}^{\infty} A(u)B(x-u)du \quad . \tag{B.1}$$

The correlation A★B of two functions A(x) and B(x) is taken as

$$A(x) \bigstar B(x) = \int_{-\infty}^{\infty} A(u)B(x+u)du \quad . \tag{B.2}$$

In optics two-dimensional convolutions and correlations are also needed. They are taken as

$$A(x,y) * B(x,y) = \iint_{-\infty}^{\infty} A(u,v)B(x-u,y-v)du\,dv \tag{B.3}$$

and

$$A(x,y) \bigstar B(x,y) = \iint_{-\infty}^{\infty} A(u,v)B(x+u,y+v)du\,dv \quad . \tag{B.4}$$

For functions of position in transverse planes $z = z_C$, $z = z_D$, convolution and correlation become

$$A(\underline{r}_C) * B(\underline{r}_C) = \int_{-\infty}^{\infty} A(\underline{r}_D)B(\underline{r}_C-\underline{r}_D)d^2r_D \tag{B.5}$$

and

$$A(\underline{r}_C) \bigstar B(\underline{r}_C) = \int_{-\infty}^{\infty} A(\underline{r}_D)B(\underline{r}_C+\underline{r}_D)d^2r_D \quad . \tag{B.6}$$

Convolution and correlation in both space and time are encountered. If the meaning is not clear then $*_r$ and $\bigstar_r$ will denote spatial operations, $*_t$ and $\bigstar_t$ will denote temporal operations, $*_s$ and $\bigstar_s$ will denote spatial frequency operations, $*_\nu$ and $\bigstar_\nu$ will denote temporal frequency operations.

The following properties of convolutions will prove useful.

$$\widetilde{A(x) * B(x)} = \tilde{A}(s)\tilde{B}(s) \tag{B.7}$$

$$\widetilde{A(x) * B^*(x)} = \tilde{A}(s)\tilde{B}^*(-s) \tag{B.8}$$

$$\widetilde{A(x) * B^*(-x)} = \tilde{A}(s)\tilde{B}^*(s) \tag{B.9}$$

$$\widetilde{\tilde{A}(s) * \tilde{B}(s)} = A(x)B(x) \quad . \tag{B.10}$$

The following properties of correlations will prove useful.

$$\widetilde{A(x) \bigstar B(x)} = \tilde{A}(-s)\tilde{B}(s) \tag{B.11}$$

$$\widetilde{A(x) \bigstar B^*(x)} = \tilde{A}(-s)\tilde{B}^*(-s) \tag{B.12}$$

$$\widetilde{A(-x) \bigstar B(x)} = \tilde{A}(s)\tilde{B}(s) \tag{B.13}$$

$$\widetilde{\tilde{A}(s) \bigstar \tilde{B}(s)} = A(-x)B(x) \quad . \tag{B.14}$$

In addition, convolutions and correlations are distributive, associative, and commutative. From the preceding relations we obtain

$$\widetilde{|A(x)|^2} = \tilde{A}(s) * \tilde{A}^*(-s) = \tilde{A}(-s) \bigstar \tilde{B}^*(-s) \quad . \tag{B.15}$$

If the spectrum of A is real and even

$$\widetilde{|A(x)|^2} = \tilde{A}(s) * \tilde{A}(s) = \tilde{A}(s) \bigstar \tilde{A}(s) \quad . \tag{B.16}$$

APPENDIX C

DECOMPOSITION INTO PLANE WAVE SPECTRUM

Any field $\xi(\underline{r}_C)$ satisfying the Helmholtz equation can be decomposed, into a spectrum of plane waves thus [72]

$$\xi(\underline{r}_C) = \xi(\rho, z_C) = \int_{-\infty}^{\infty} W(\underline{\kappa}) e^{i[\underline{\kappa}\cdot\underline{r}_C + k_z(\underline{\kappa})z_C]} d^2\kappa \qquad (C.1)$$

where $W(\underline{\kappa})$ is a weighting function giving the amplitude of the $\underline{k}$th directed plane wave component of $\xi(\underline{r}_C)$ and $\underline{\kappa}$ is the transverse wave number

$$\underline{k} = \underline{\kappa} + k_z\hat{z}$$
$$k^2 = \kappa^2 + k_z^2 \quad . \qquad (C.2)$$

Alternatively, the field can be decomposed into a spectrum of spatial frequency components by taking a Spatial Fourier Transform thus

$$\xi(r_C) = \int_{-\infty}^{\infty} \tilde{\xi}(\underline{s}, z_C) e^{2\pi i \underline{s}\cdot\underline{r}_C} d^2s \qquad (C.3)$$

where

$$\underline{s} = s_x\hat{x} + s_y\hat{y} \qquad (C.4)$$

represents a spatial frequency (number of periodic variations of any physical feature per unit length), the direction of $\underline{s}$ indicating the orientation of the spatial variations in the transverse plane.

Equating (C.1) with (C.3) demands

$$\underline{\kappa} = 2\pi\underline{s} \tag{C.5}$$

and

$$\tilde{\xi}(\underline{s},z_C) = (2\pi)^2 e^{ik_z(2\pi\underline{s})z_C} W(2\pi\underline{s}) \quad . \tag{C.6}$$

Evidently

$$\begin{aligned} \tilde{\xi}(\underline{s},0) &= (2\pi)^2 W(2\pi\underline{s}) \\ \tilde{\xi}(\underline{s},z_C) &= \tilde{\xi}(\underline{s},0) e^{ik_z(2\pi\underline{s})z_C} \quad . \end{aligned} \tag{C.7}$$

Thus, the plane wave spectrum $W(\underline{\kappa})$ is preserved in propagating between transverse planes but the spatial frequency spectrum is not. Even so, it is usually more convenient to obtain the plane wave spectrum from the spatial frequency spectrum rather than the converse. The reason is that the fields of interest usually arise from sources located on boundaries of known geometry. These boundary fields are easily decomposed into known spatial spectra to which the resulting plane wave spectrum is simply related. Thus, writing

$$W(\underline{\kappa}) = \frac{\tilde{\xi}\left(\frac{\underline{\kappa}}{2\pi}, z_C'\right)}{(2\pi)^2} e^{-ik_z(\underline{\kappa})z_C'} \tag{C.8}$$

the plane wave spectral decomposition becomes

$$\xi(\underline{r}_C) = \int_{-\infty}^{\infty} \frac{\tilde{\xi}\left(\frac{\underline{\kappa}}{2\pi}, z_C'\right)}{(2\pi)^2} e^{i\underline{\kappa}\cdot\underline{r}_C} e^{ik_z(\underline{\kappa})(z_C - z_C')} d^2\kappa \quad . \tag{C.9}$$

Substituting

$$\tilde{\xi}(\underline{s},z_C') = \int_{-\infty}^{\infty} \xi(\underline{r}_C') e^{-2\pi i \underline{s}\cdot\underline{r}_C'} d^2\underline{r}_C' \qquad (C.10)$$

into Equation (C.9) we obtain

$$\xi(\underline{r}_C) = \int_{-\infty}^{\infty}\int_{-\infty}^{\infty} \frac{\xi(\underline{r}_C')}{(2\pi)^2} e^{i\underline{\kappa}\cdot(\underline{r}_C-\underline{r}_C')} e^{ik_z(\underline{\kappa})(z_C-z_C')} d^2\underline{\kappa} d^2\underline{r}_C' \qquad .(C.11)$$

Finally

$$\xi(\underline{r}_C) = \xi(\underline{r}_C') * \underbrace{e^{ik_z(2\pi\underline{s})(z-z')}} \qquad . \qquad (C.12)$$

It is inviting to consider the equivalence of the plane wave expansion (C.12) with the Rayleigh-Sommerfeld-Green expression for diffraction by a planar apperture located in the transverse plane $z = z_C'$ [73]

$$\xi(\underline{r}_C) = \int_{-\infty}^{\infty} \xi(\underline{r}_C') \frac{\partial}{\partial z} \left(\frac{e^{ik|\underline{r}_C-\underline{r}_C'|}}{|\underline{r}_C-\underline{r}_C'|} \right) d^2\underline{r}_C' \qquad (C.13)$$

thereby emphasizing the non-paraxial nature of the latter. The integral (C.13) can be written in more compact form as a convolution

$$\xi(\underline{r}_C) = \xi(\underline{r}_C') * G(\underline{r}_C') \qquad (C.14)$$

where

$$G = \frac{\partial}{\partial z} \left(\frac{e^{ik|\underline{r}_C-\underline{r}_C'|}}{|\underline{r}_C-\underline{r}_C'|} \right) = \frac{(z_C-z_C')}{|\underline{r}_C-\underline{r}_C'|} \left(ik - \frac{1}{|\underline{r}_C-\underline{r}_C'|} \right) \frac{e^{ik|\underline{r}_C-\underline{r}_C'|}}{|\underline{r}_C-\underline{r}_C'|} \qquad . \qquad (C.15)$$

Equivalence of the Rayleigh theory with the plane wave expansion demands

$$\underbrace{e^{ik_z(2\pi\underline{s})(z_C-z'_C)}}_{\sim} = \frac{(z_C-z'_C)}{|\underline{r}_C-\underline{r}'_C|}\left(ik-\frac{1}{|\underline{r}_C-\underline{r}'_C|}\right)\frac{e^{ik|\underline{r}_C-\underline{r}'_C|}}{|\underline{r}_C-\underline{r}'_C|} \quad . \quad (C.16)$$

If this assertion is valid then the two theories are equivalent, and we may use the plane wave expansion instead of the non-paraxial Rayleigh theory whenever it proves convenient.

To prove (C.16) we must show

$$\frac{\partial}{\partial z}\left(\frac{e^{ik|\underline{r}_C-\underline{r}'_C|}}{|\underline{r}_C-\underline{r}'_C|}\right) = \int_{-\infty}^{\infty} e^{i\sqrt{k^2-(2\pi)^2(s_x^2+s_y^2)}(z_C-z'_C)} e^{i2\pi(s_x x+s_y y)} \cdot \quad (C.17)$$

$$\cdot\, ds_x ds_y$$

which is equivalent to showing

$$\frac{e^{ik|\underline{r}_C-\underline{r}'_C|}}{|\underline{r}_C-\underline{r}'_C|} = \int_{-\infty}^{\infty} \frac{e^{i\sqrt{k^2-(2\pi)^2(s_x^2+s_y^2)}(z_C-z'_C)} e^{i2\pi(s_x x+s_y y)}}{i\sqrt{k^2-(2\pi)^2(s_x^2+s_y^2)}} \quad . \quad (C.18)$$

The relation (C.18) has been demonstrated by several authors [74,75].

APPENDIX D

APPARATUS DETAILS

1. ACOUSTIC ILLUMINATION SOURCE

The source of acoustic illumination was a barium titanate disk (6.3 cm dia × 1.3 cm thick) driven in a higher order thickness mode at 1 MHz, by a crystal controlled oscillator and power amplifier delivering 40 watts of r.f. power. In order to maximize conversion of r.f. power to acoustic power the disk was air-backed, however, it is doubtful that conversion efficiency exceeded 30%. The disk was mounted in an aluminum housing with O-rings to seal against approximately 1/2 atmosphere pressure. The transducer assembly is shown in Figures D.1 and D.2.

Standard calculations[76] indicate that the angular beam width (first lobe) for a simple piston 42λ diameter should be approximately 1^{o}. In order to increase this beam width a horn was placed in front of the disk. The resulting beam width was about 10^{o}. The beam pattern is shown in Figures D.3 and D.4. The lack of circular symmetry is thought to be due to the clamping bolts which were located in a regular hexagonal pattern.

2. ACOUSTIC RECEIVER

The device used to detect the scattered acoustic radiation was a barium titanate disk (.304 cm dia × .203 cm thick) operating in the fundamental thickness mode. Because of mechanical problems associated with the ambient water pressure it was not possible to air-back the disk although this would have been desirable. The disk was mounted in

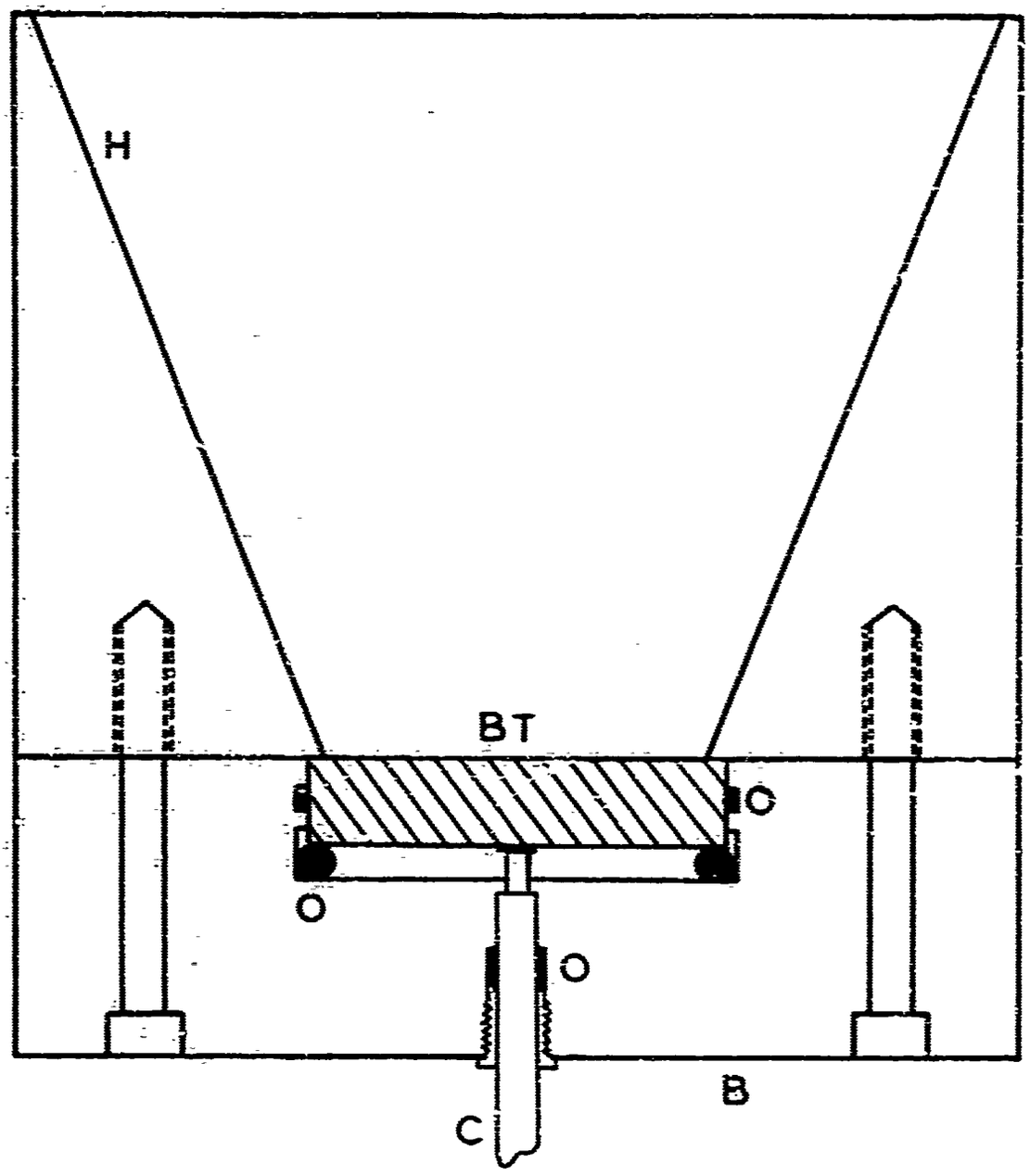

B 6061 T6 aluminum housing

BT barium titanate disk

C RG 62/U cable

H 6061 T6 aluminum horn

O neoprene "O" ring

Figure D.1 Illumination Transducer Assembly

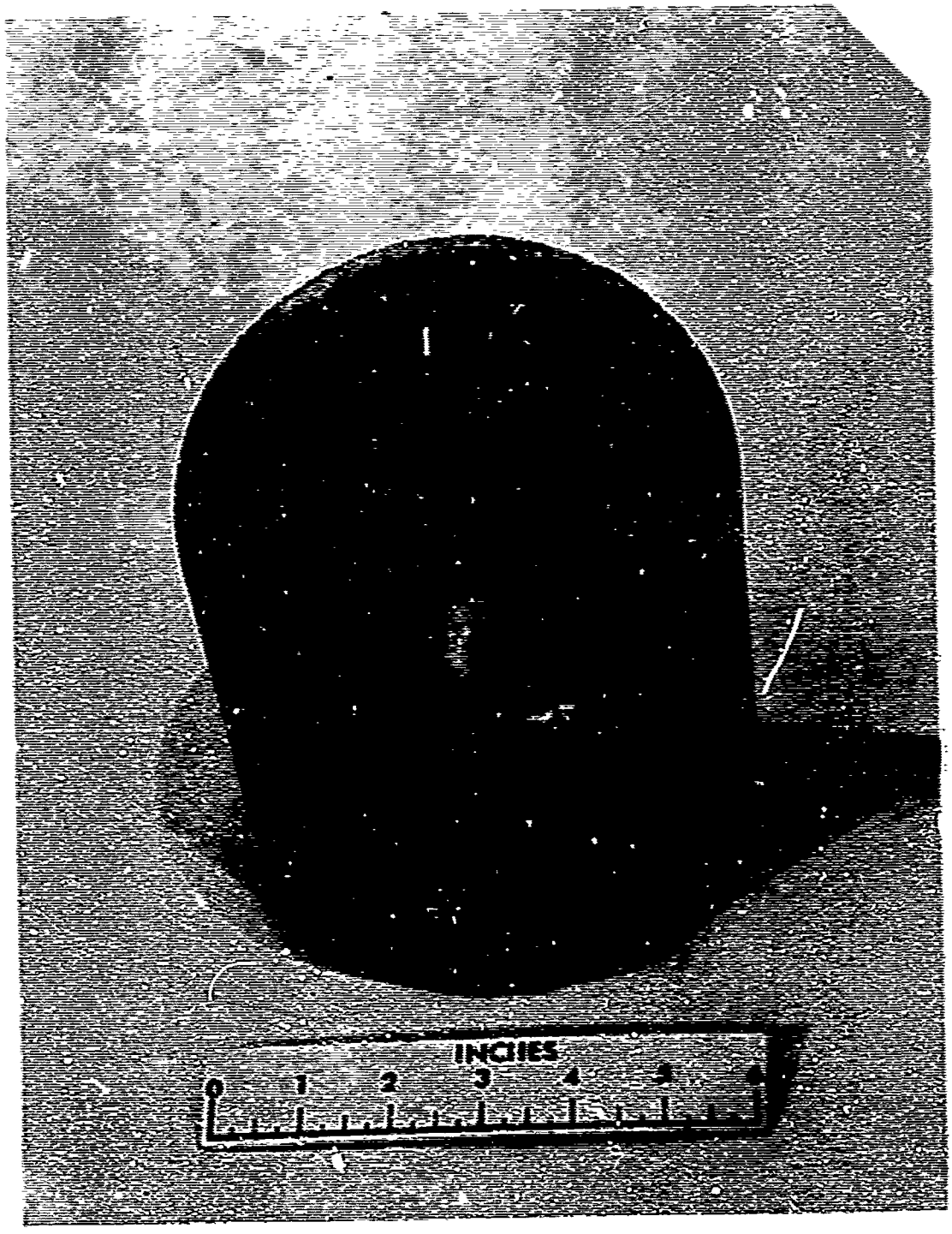

Figure D.2. Illumination Transducer

The pronounced corrosion of the aluminum housing was due to some chemical agent of unknown origin in the water.

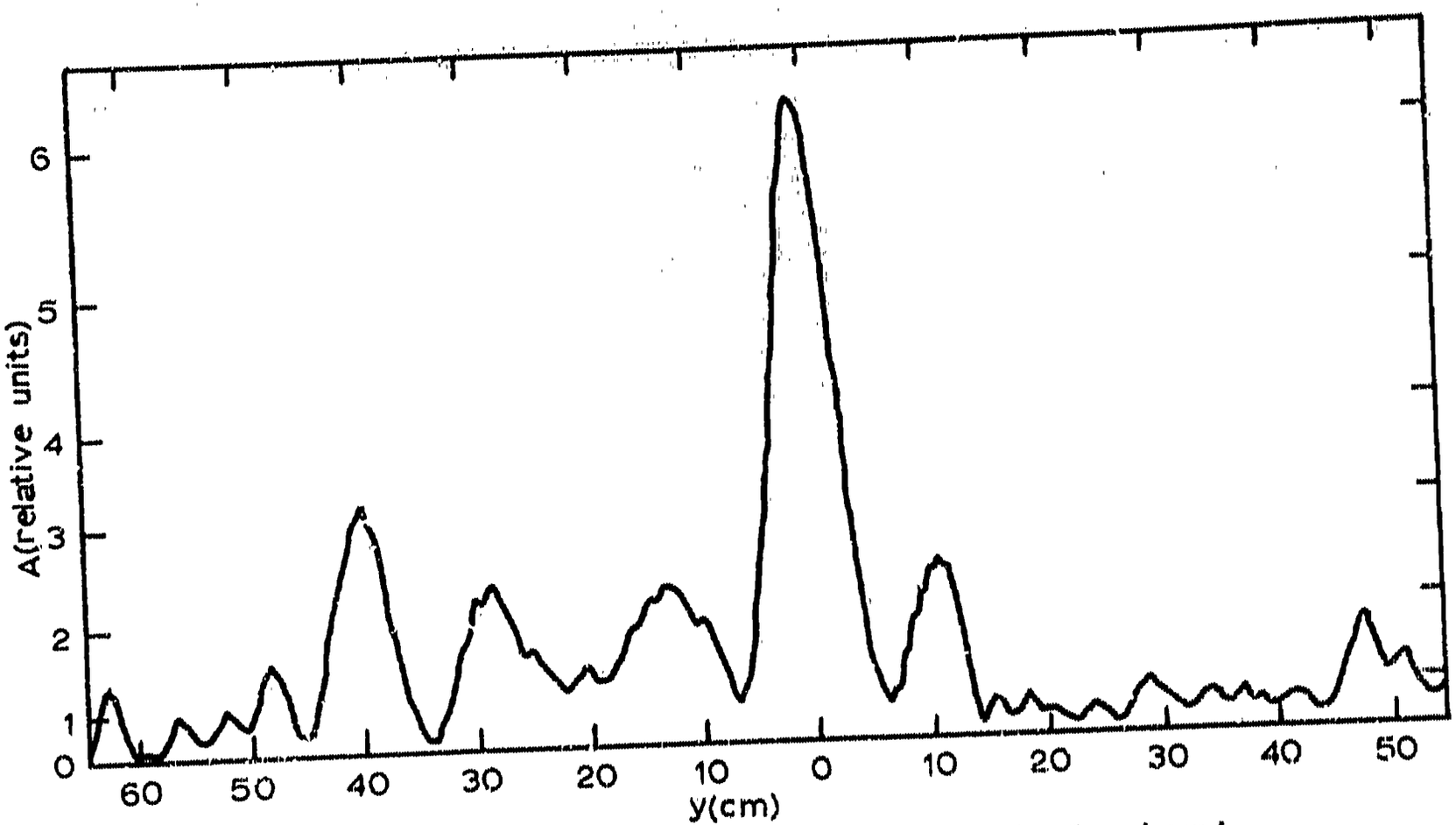

Figure D.3. Relative Acoustic Pressure Amplitude From Illumination Transducer L.
Distance from transducer = 2 meters.
Corresponds approximately to single line, left hand edge of Figure D.4.

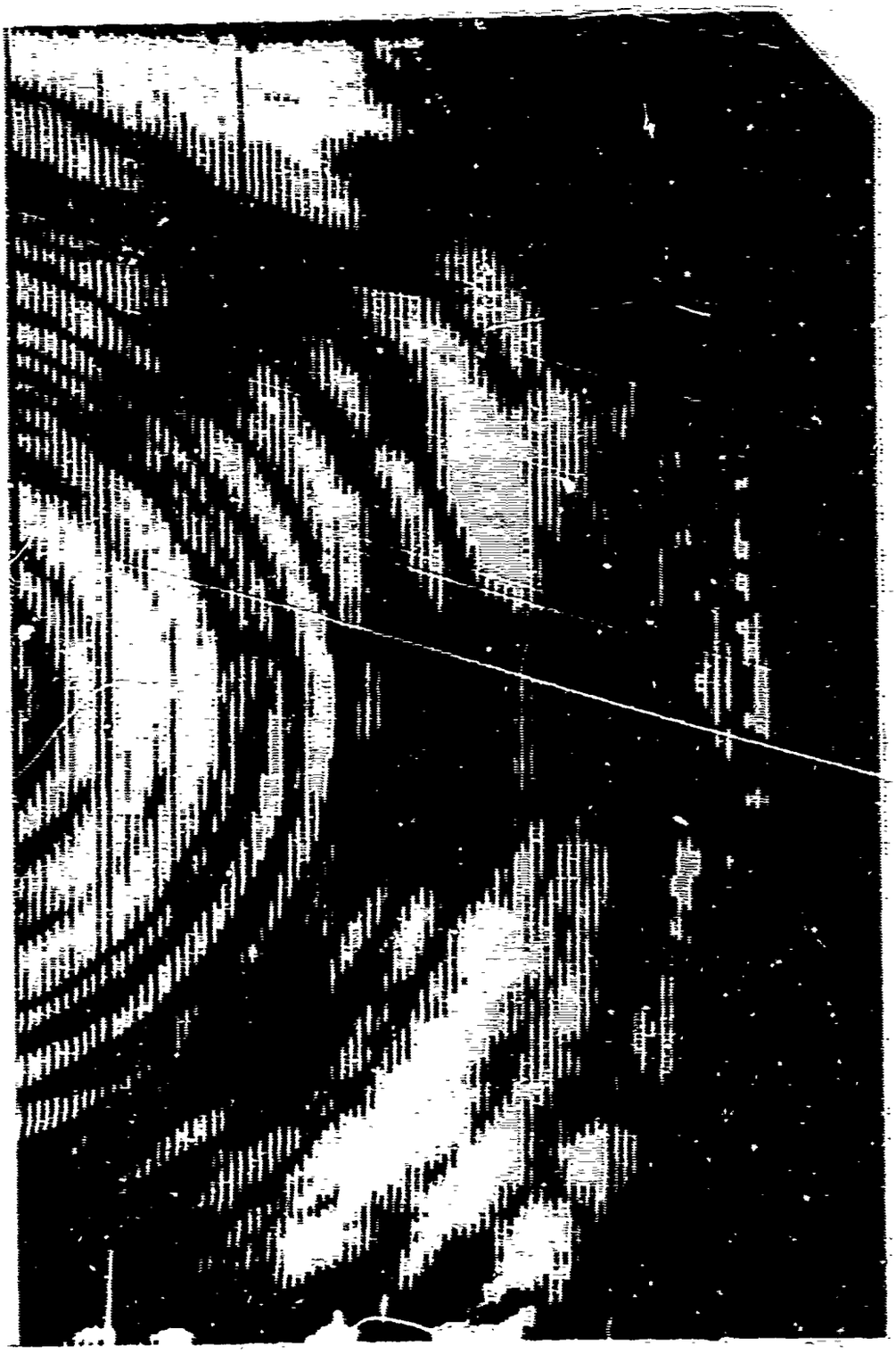

Figure D.4. Radiation Pattern of Illumination Transducer

Regions of high acoustic field are white. Corresponds to a contour level A = 1, Figure D.3.

a slender, tapered aluminum housing attached to the end of a long steel probe (2.5 cm dia × 460 cm long). The acoustic sensing element was coupled to an amplifier chain providing a voltage gain of approximately 10^6. Because of the high gain and because of the proximity of receiver and transmitter special precautions were required in order to eliminate stray r.f. pickup in the receiver chain. Elimination of stray r.f. pickup is especially important in acoustic holography because such spurious signals will be manifested as a coplanar reference signal. Accordingly, the first two stages of amplification were housed inside the probe immediately adjacent to the sensing element and were powered by self-contained batteries. Thus the low level stages were isolated by at least 250 cm of water. The receiver assembly is shown in Figures D.5 through D.8.

Standard calculations[76] indicate that the angular beam pattern width (first lobe) for a simple piston 2λ diameter should be approximately 35^o. This basic pattern will be modulated by the response characteristic of the crystal lattice and by internal reflections. The pattern for the receiver used is shown in Figure D.9.

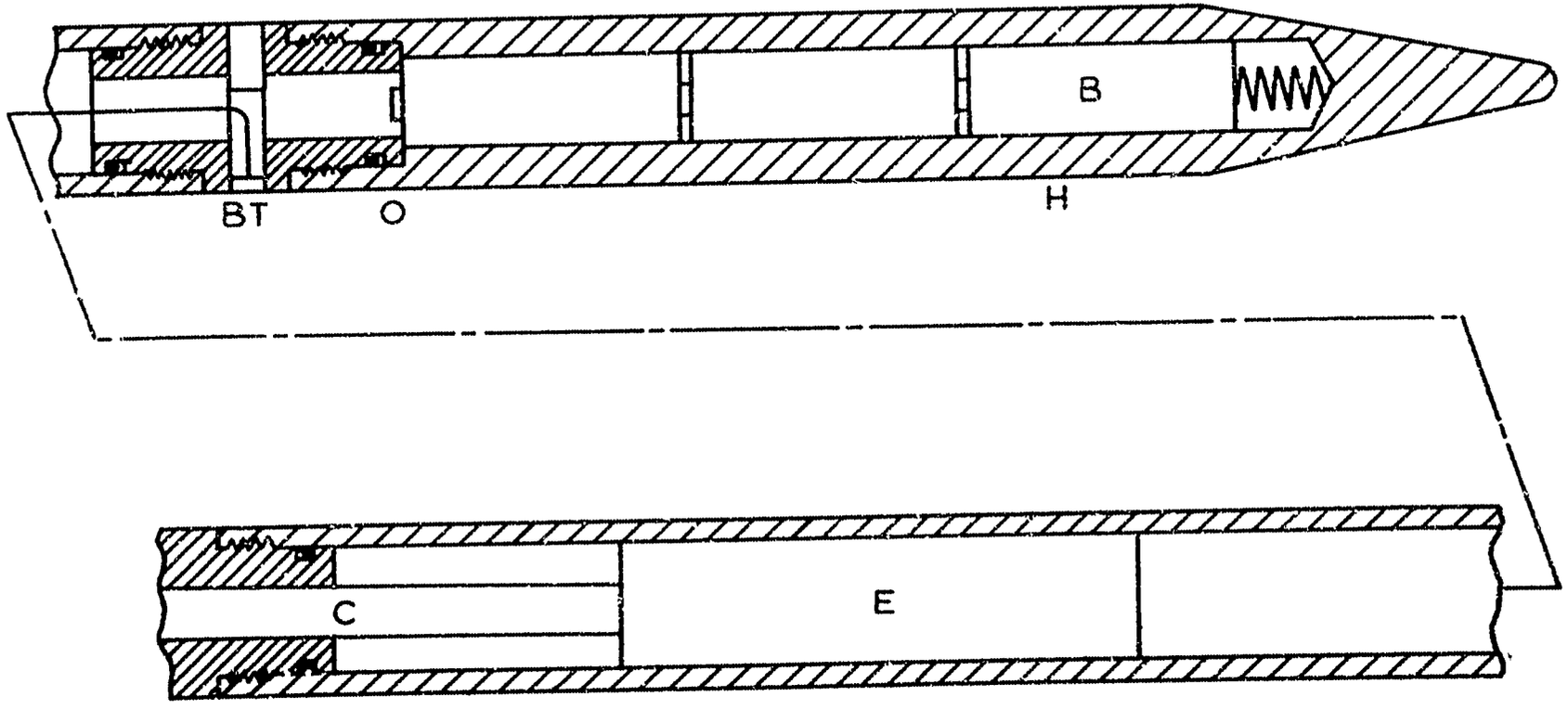

B batteries

BT barium titanate disk

C RG 62/U cable

E electronics

H 6061 T6 aluminum housing

O neoprene "O" ring

Figure D.5. Receiving Transducer Assembly

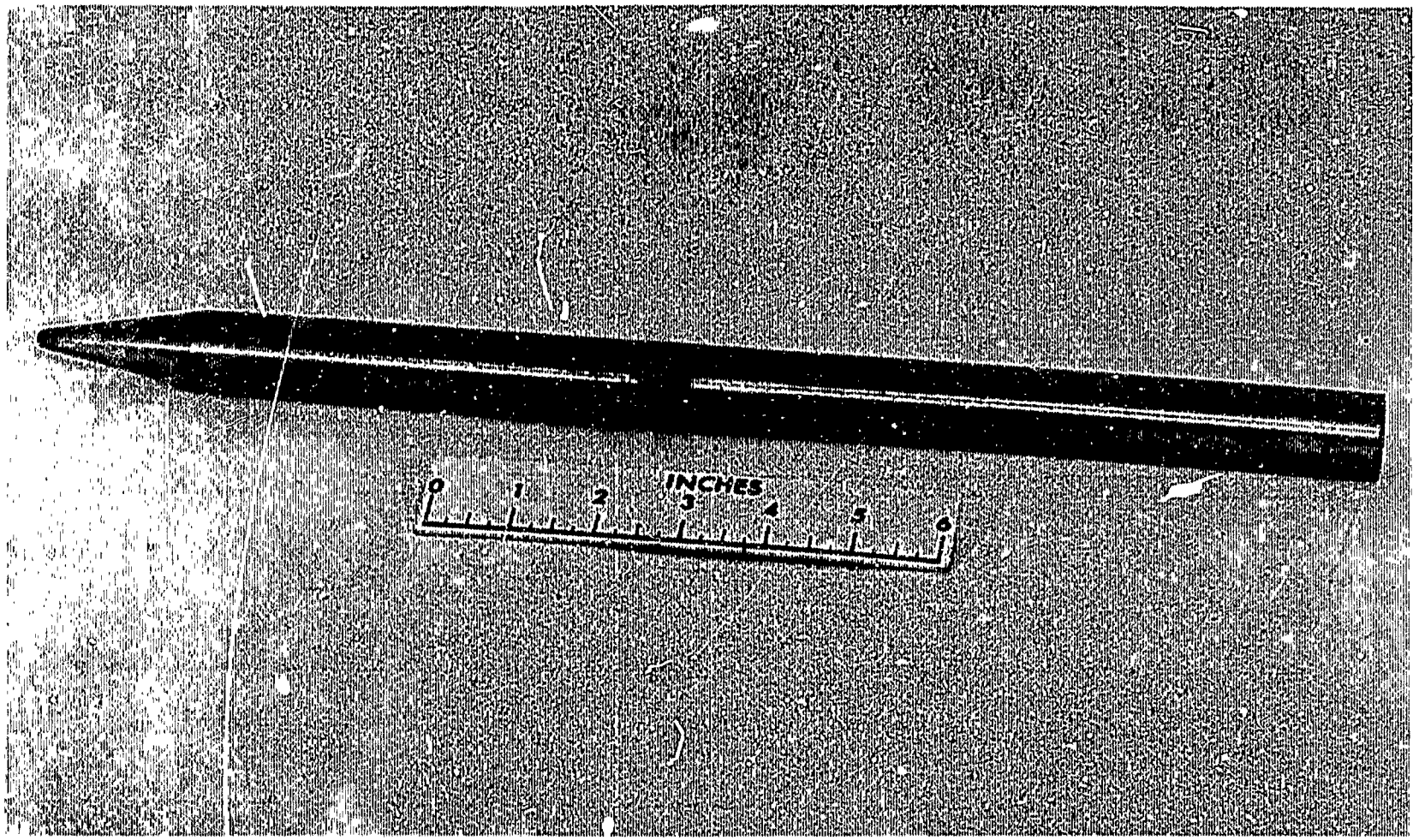

Figure D.6. Receiving Transducer Body, Assembled

Detector element,3 mm diameter, located in the relief between the 2 and 3 inch marks.

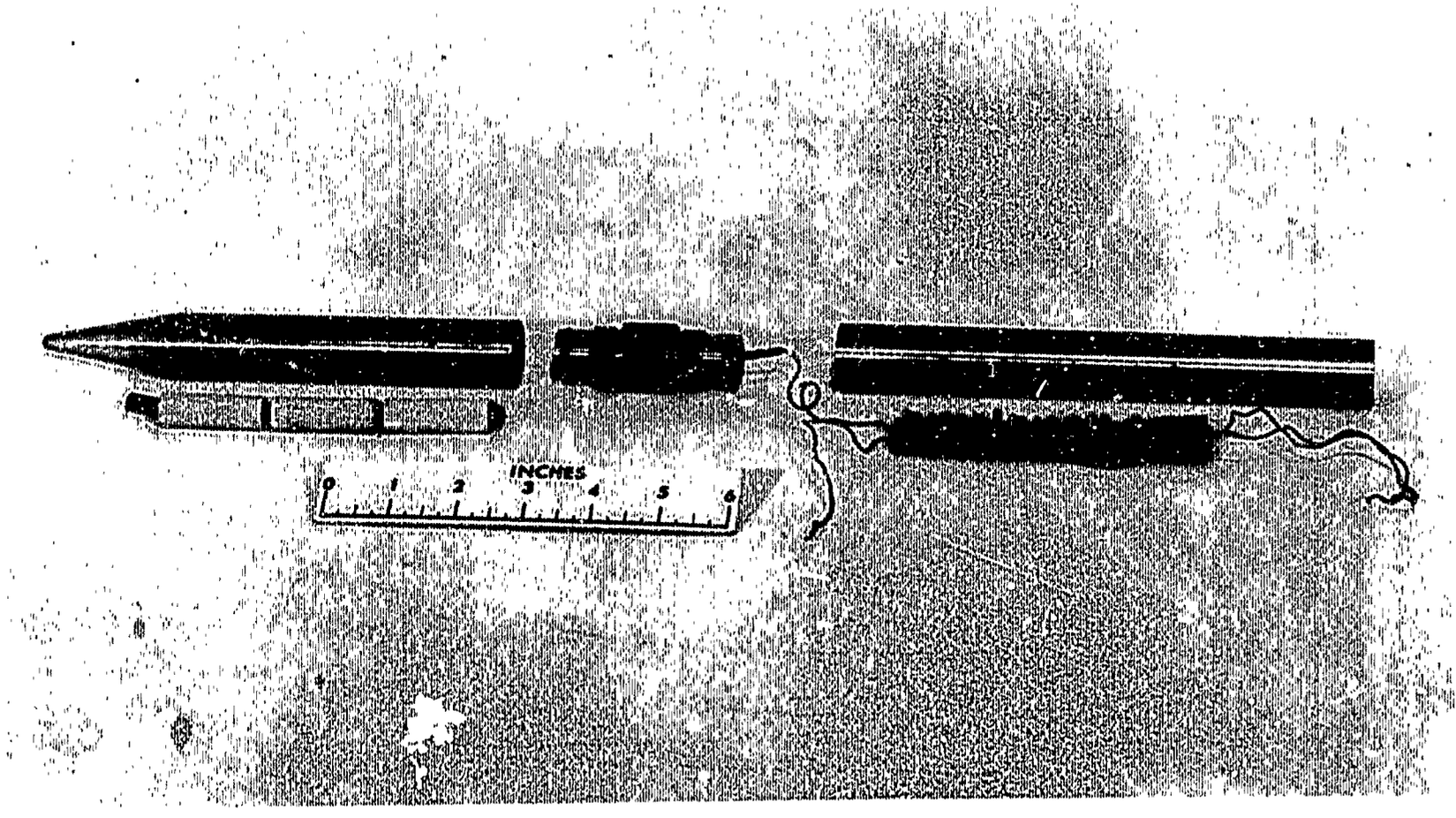

Figure D.7. Receiving Transducer Body, Disassembled

From left to right: 27.5V battery pack, detector element assembly, amplifier (gain =100).

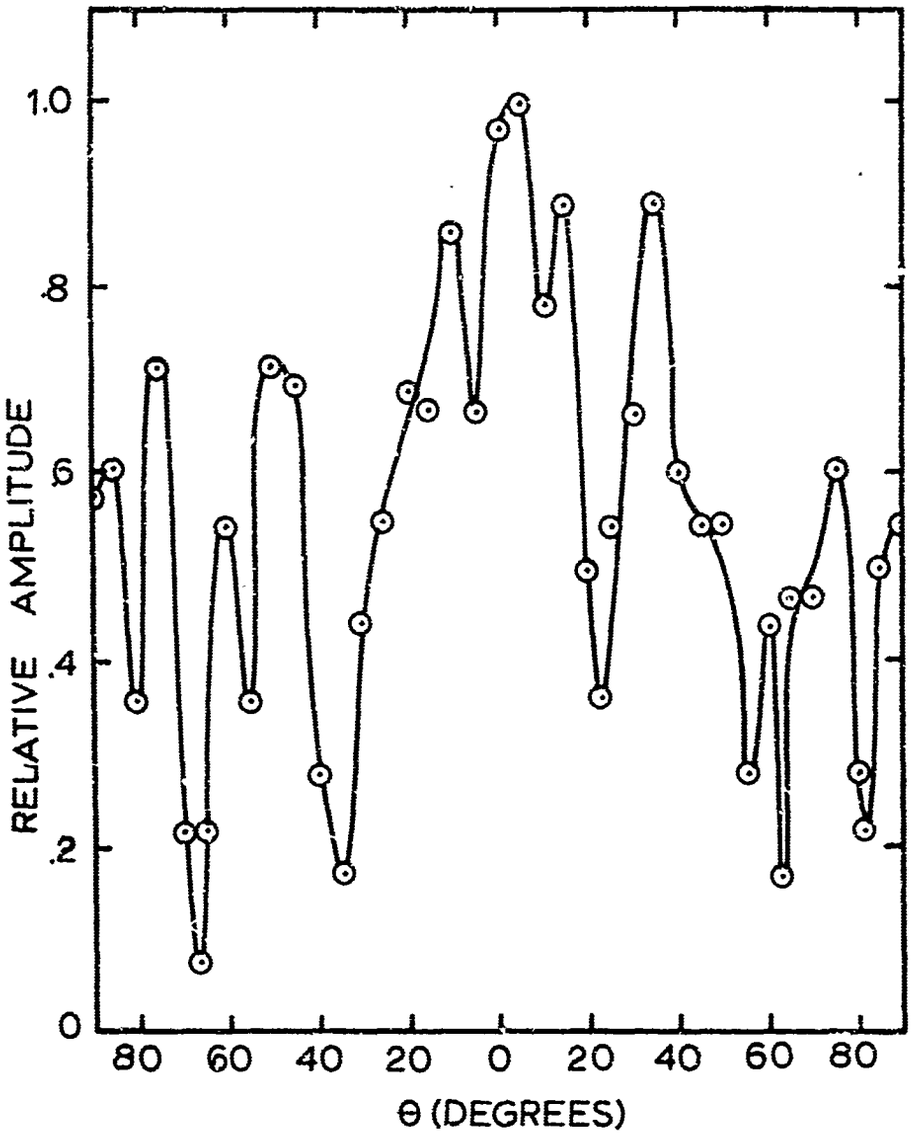

Figure D.9. Sensitivity of Receiver as Function of Angle θ About Normal to Hologram Plane

APPENDIX E

CHARACTERISTICS OF THE PHOTO-ACOUSTIC CONVERSION

The process by which a photographic transparency $P(\underline{r})$ is formed from an acoustic field $A(\underline{r})$ is conveniently separated into three stages: 1) the electro-optical conversion, 2) the optical to photographic conversion, and 3) the scale reduction. See Figure V.10. Dependence of P upon A is most easily controlled electronically in the electro-optical conversion stage rather than photographically in the following stages.

The barium titanate receiving transducer generates an electric potential E proportional to the incident acoustic field. Since E is a low level signal it is amplified 100 by preamplifier A located inside the probe, deep underwater where stray RF fields are small. The amplified signal is combined with the reference and then passed to the cathode of the CRT display through gated amplifier G. By appropriate choice of G and electronic processing U a wide range of characteristics P(A) may be obtained.

A Tektronix type 561 oscilloscope with P-31 phosphor was used for the CRT display because the electrostatically focused CRT of this unit has a small spot size (.25 mm diameter) which is relatively uniform in size and intensity over an 8 × 10 cm display area (320 × 400 resolution cells). The P-31 phosphor produces a bright green spot (spectral peak at .52 micron, spectral range from .4150 to .6000 micron) which decays in 32 msec. to 0.1% of peak intensity, long enough to adequately time average 1 MHz signals but fast enough to follow fringe variations

during scanning. In retrospect, a magnetically focused CRT with P-15 phosphor (.05 msec. decay time) would have been of great value since these devices may have resolutions almost 10 t-mes greater than the best electrostatically focused CRT, particularly important when diffuse scattering is involved (holograms #13 and #14).

Typical characteristics of the electro-optical conversion are shown in Figure E.1 plotted as normalized CRT spot intensity $I/\alpha I_0$ as a function of signal amplitude input E to amplifier G; two linear gains are shown. By introducing non-linear amplification it is possible to alter the shape of I(E). For example, the Child'sLaw response of the CRT electron gun may be compensated to give an overall square law response for I(E).

The CRT spot intensity was obtained by measuring the open circuit voltage of an International Rectifier type ASM selenium photocell placed in the camera film plane with aperture set at f/1.9. The open circuit voltage V_{OC} of this cell is given by [77]

$$V_{OC} = \frac{KT}{e} (1 + I/\alpha I_0) \qquad (E.1)$$

where I_0 is the dark current of the cell, α is a conversion constant relating junction current to incident light intensity I, T is cell temperature, K is Boltzmann's Constant, and e is the electronic charge. Normalized intensity $I/\alpha I_0$ is sufficient information since proper film exposure is most easily determined by trial-and-error.

The scanned CRT display is time photographed with a Tektronix type C-12 camera equipped with f/1.9 lens. Choice of film was based

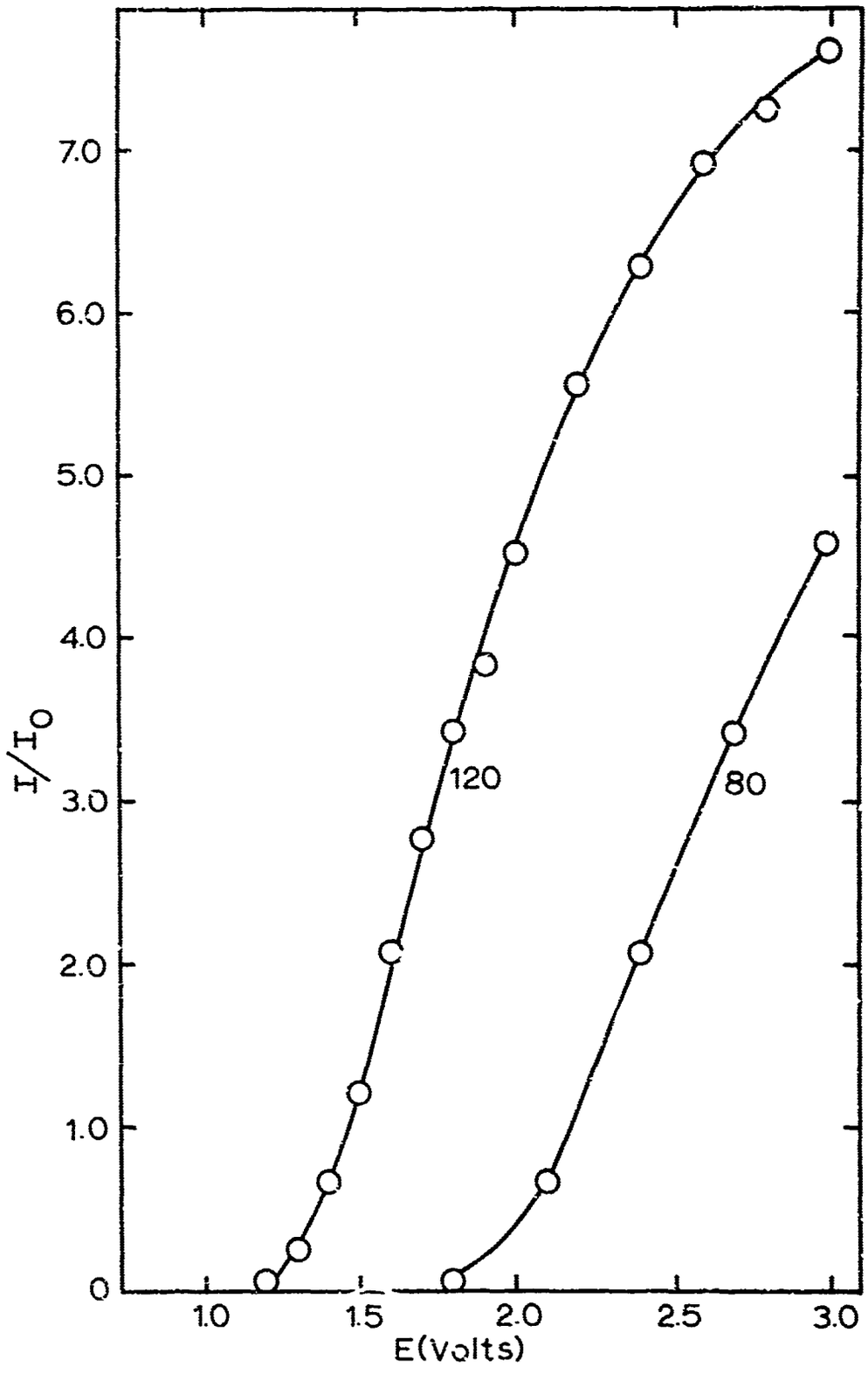

Figure E.1. Electro-optical Conversion Characteristic for Two Different Gains for Amplifier G

upon obtaining high resolution and contrast of the scanned fringes. This demanded a fine grain emulsion (100-150 lines/mm resolution) with anti-halation backing and a photographic speed approximately ASA 50. It was anticipated that an orthochromatic spectral response would be required in order to prevent any cathode glow penetrating the CRT phosphor layer from exposing the film during the long exposure period (4 - 9 hours). This precaution proved unnecessary.

Two film types were tried: Kodak Contrast Process Ortho, a high contrast emulsion, and Kodak Panatomic-X, a continuous tone emulsion. Both provide gray scale rendition but the relative dynamic range of the high contrast emulsion is much smaller. Polaroid type 55 P/N is also suitable and is convenient to use, but its self-developing feature allows little lattitude in developing.

Photographic exposure-development characteristics are usually plotted as photographic density ($\log_{10} 1/P_I$ where P_I represents intensity transmittance of the developed emulsion) against $\log_{10} E$ where E is the exposure (total energy). Such plots are known as Hurter-Driffield curves. In this work it is more convenient to plot P_I versus E for incoherently illuminated transparencies but P_A (amplitude transmittance of the developed emulsion) versus E for coherently illuminated transparencies[78]. Typical H-D curves for Contrast Process Ortho film processed in a high contrast developed, Kodak type D-11, and Panatomic-X film processed in a continuous tone developer, Kodak type D-76, are shown in Figure E.2[79].

After processing, the transparency (on one of the above emulsions) obtained from the CRT display is reduced in size approximately 5 to 1

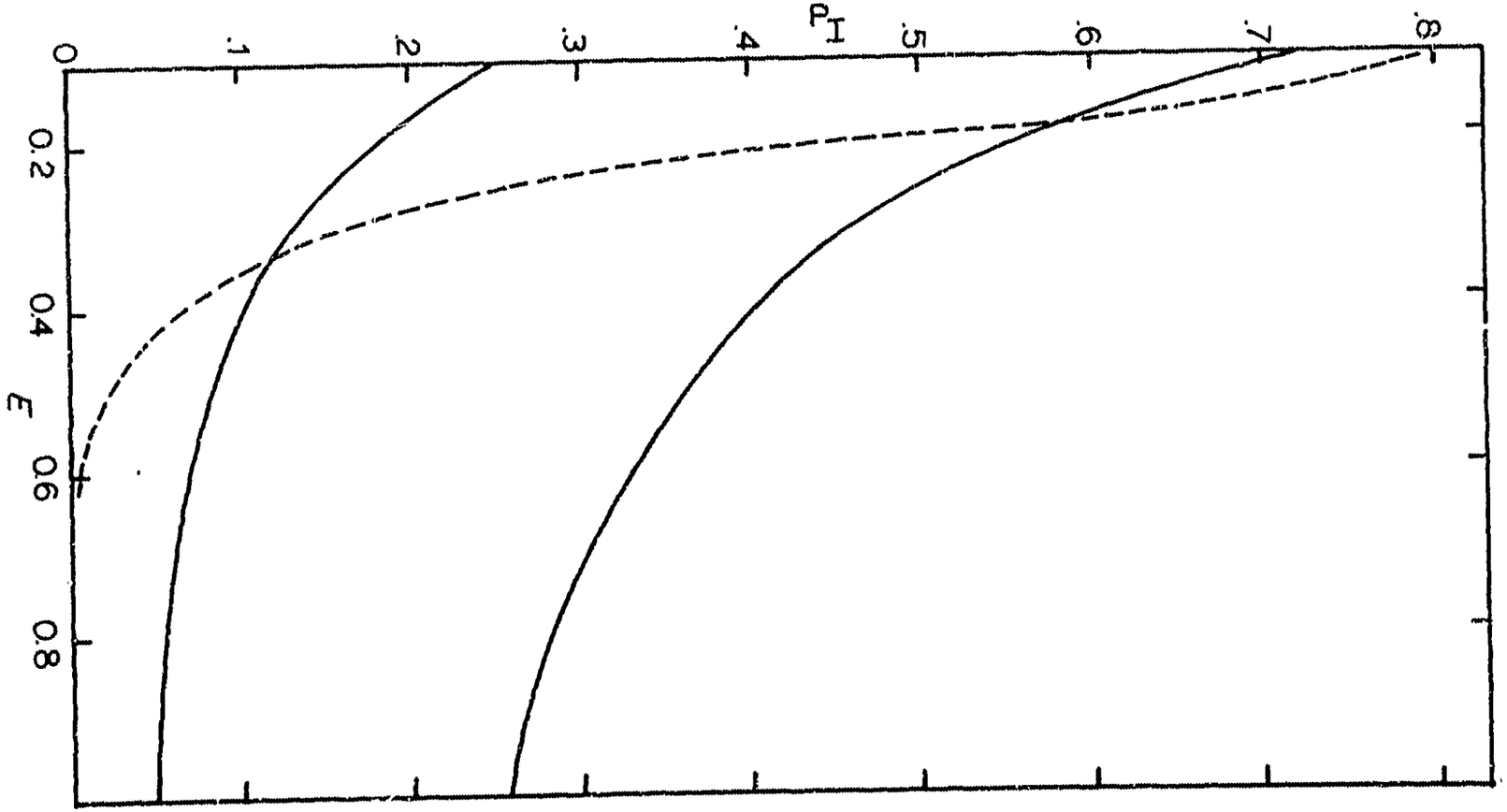

Figure E.2. Intensity Transmittance as a Function of Exposure
Dotted line - Contrast Process Ortho in D-11 for 5 min at 68°F (Exposure scale × 1.0)
Lower solid line - Panatomic-X in DK-50(1:1) for 7 min at 68°F (Exposure scale × 1.0)
Upper solid line - Panatomic-X in DK-50(1:1) for 7 min at 68°F (Exposure scale × 0.1)

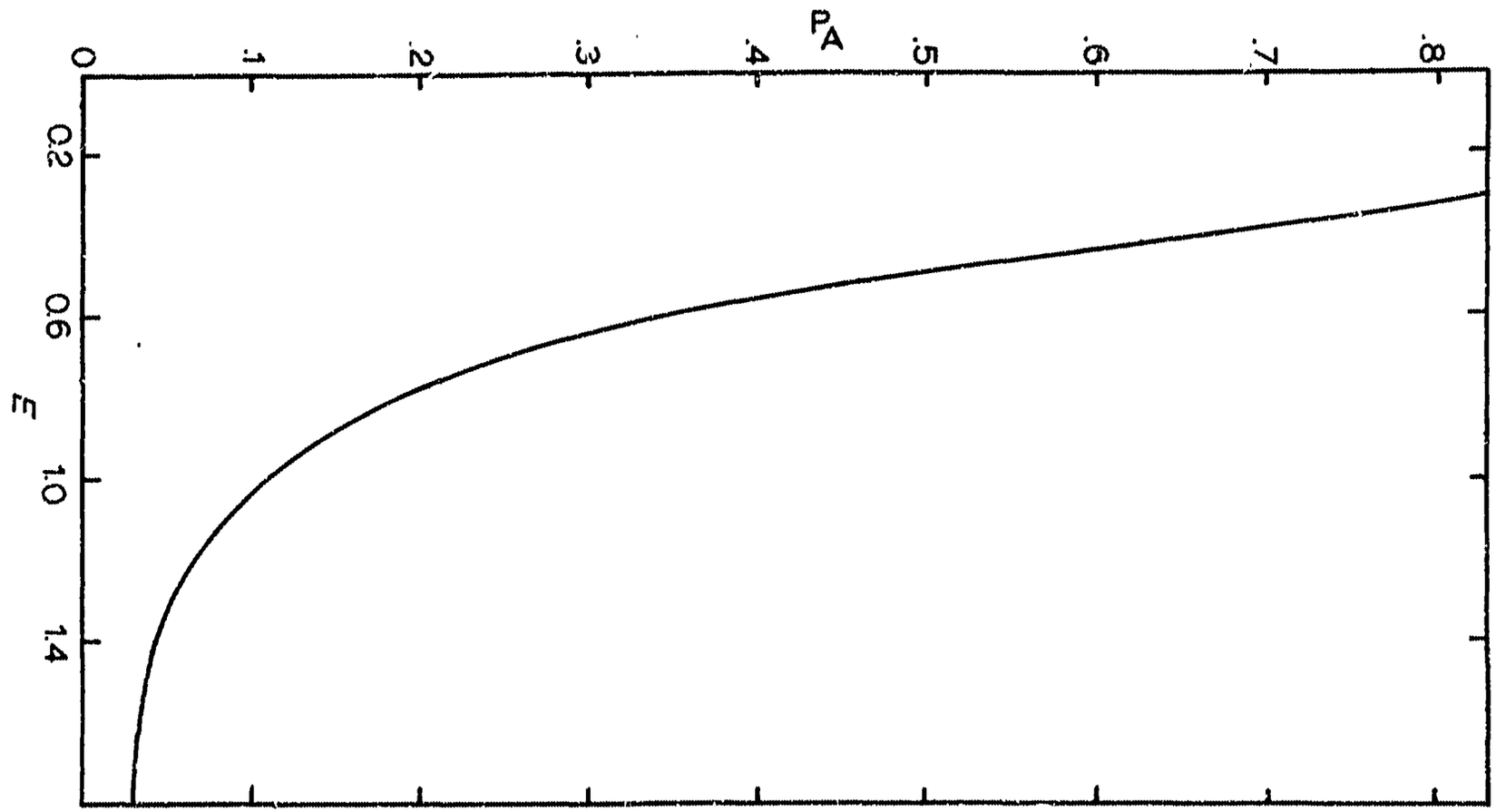

Figure E.3. Amplitude Transmittance as a Function of Exposure for Kodak High Resolution Glass Plates
D-19 developer for 5 minutes at 68° F. (Exposure scale × 100)

onto Kodak High Resolution Glass Plates processed with Kodak Type D-19 developer. Typical P_A versus E characteristics for this emulsion are given in Figure E.3[80]. The final reduced transparency, the acoustic hologram, is a "positive" of the acoustic field, that is, fringes of large acoustic amplitude are recorded as fringes of high light amplitude transmittance in the hologram. The overall response characteristic for the acoustic hologram transparency is obtained by combining the three component responses preceeding. Typical characteristics are shown in Figure E.4.

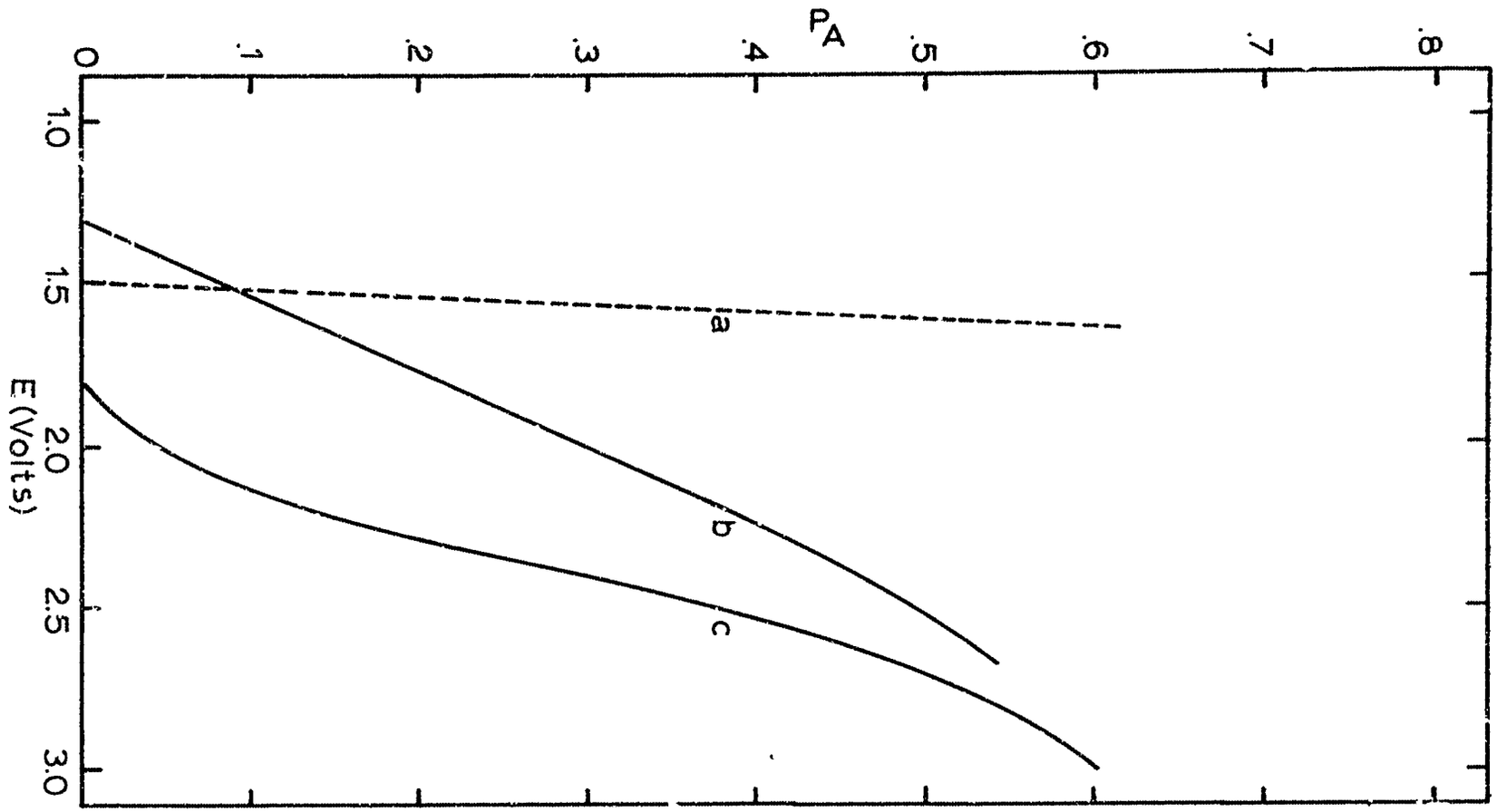

Figure E.4. Composite Conversion Characteristic for Acoustic Hologram

a Using Contrast Process Ortho and gain of 120. Approximately a hard limiter.

b Using Panatomic-X and gain of 12[illegible]. Approximately linear.

c Using Panatomic-X and gain of 80. [illegible]proximately square law.

APPENDIX F

RECONSTRUCTION FROM COPLANAR REFERENCE HOLOGRAMS

We present here the special techniques required in order to obtain quality reconstruction from coplanar reference holograms (often encountered in acoustic holography). The basic problem with coplanar reference holograms is that the zero order diffracted wave (geometrical shadow of the hologram) is superimposed upon and interferes with the reconstructed images. In order to obtain useful reconstructions this interference must be eliminated. (There is also interference between the two images but this is of relatively less importance.)

The process for eliminating zero order interference can be understood by examining relations (IV.56) and (IV.62) for the distance z_I between reconstructed image planes and the hologram plane. These equations are summarized as

$$z_{I\pm} = \frac{\mu z_O}{\pm m^2(1 - z_O/z_R) + \mu z_O/z_C} \qquad (F.1)$$

where m is the ratio of original acoustic field dimension to corresponding hologram transparency dimension, μ is the ratio of acoustic recording wavelength to visible reconstruction wavelength, z_O is the distance between object point and hologram plane, z_R is the distance between reference focus and hologram plane, and z_C is the distance between reconstruction illumination focus and hologram plane.

For the important case $z_R \to \infty$ (valid for all holograms described in Chapter V) Equation F.1 reduces to

$$z_{I\pm} = \frac{z_C}{1 \pm (m^2/\mu)(z_C/z_0)} \quad . \tag{F.2}$$

If the demagnification, the wavelength scale, and the distances z_C and z_0 are such that

$$\frac{m^2 z_C}{\mu z_0} > 1 \tag{F.3}$$

then z_{I+} corresponds to a real image located between z_C and the hologram plane, and z_{I-} corresponds to a virtual image located behind the hologram plane. If condition (F.3) is not satisfied then both images are real, z_{I+} lying beyond z_C, z_{I-} lying between z_C and the hologram plane. The later condition is illustrated in Figure F.1.

It is now clear how to eliminate the zero order field; simply use convergent illumination during reconstruction. Then the zero order will come to focus at z_C which, as we have already seen, lies between the two images. By placing a minute opaque stop S at z_C as shown in Figure F.1, the zero order can then be removed without appreciably effecting the image fields. Zero order removal can also be accomplished by placing the converging lens directly in front of rather than behind the hologram.

From Equations (IV.61) and (IV.62) the lateral magnification M, the fraction by which the image is smaller than the object in planes parallel to the hologram plane, is

$$M_{\pm} = \frac{\pm 1}{m(1 - z_0/z_R) \pm (\mu/m)(z_0/z_C)} \quad . \tag{F.4}$$

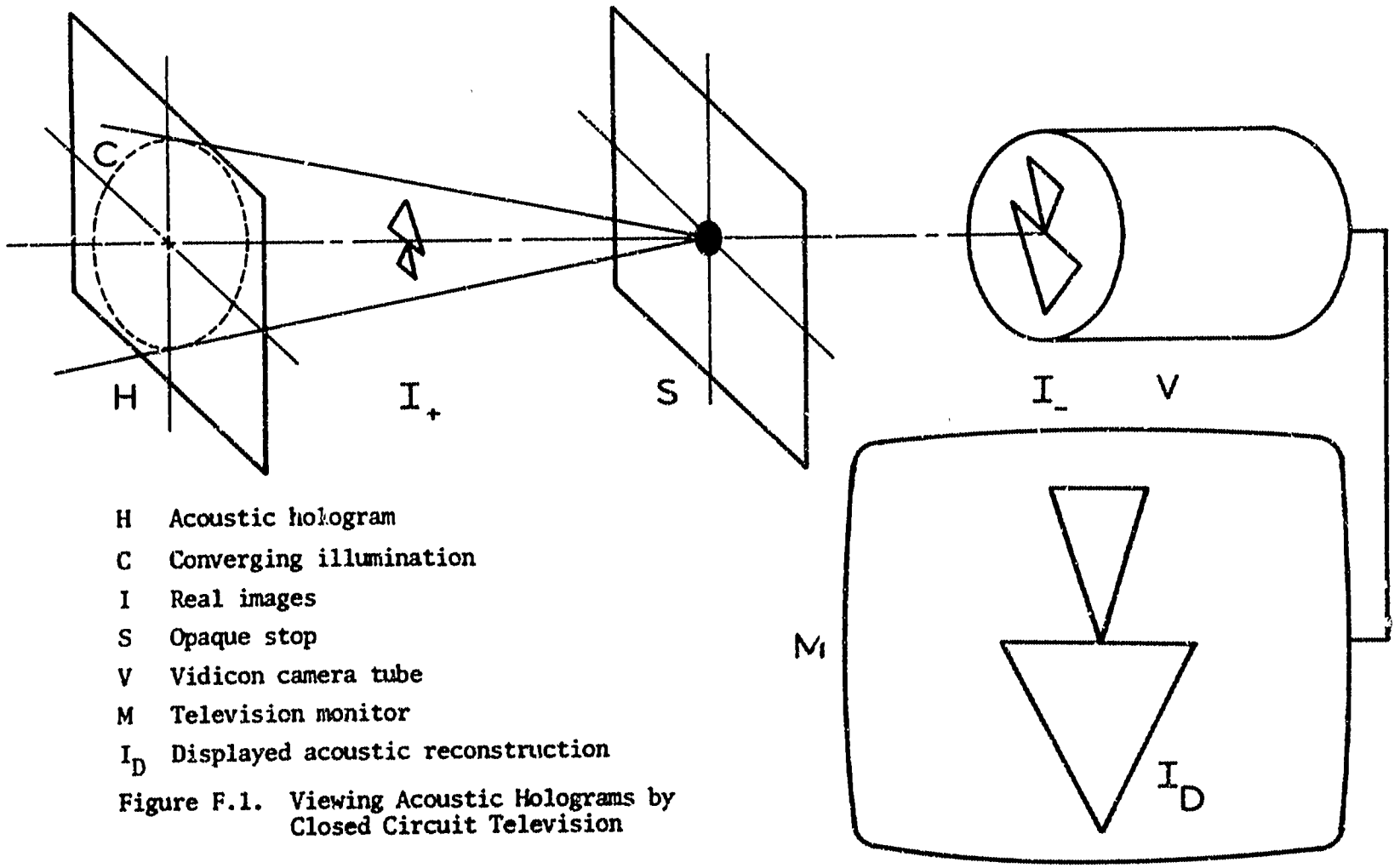

H Acoustic hologram

C Converging illumination

I Real images

S Opaque stop

V Vidicon camera tube

M Television monitor

I_D Displayed acoustic reconstruction

Figure F.1. Viewing Acoustic Holograms by Closed Circuit Television

Under the condition $z_R \to \infty$

$$M_{\pm} = \frac{\pm 1}{m \pm (\mu/m)(z_O/z_C)} \quad . \tag{F.5}$$

Thus, when both images are real, the one lying closest to the hologram will be smaller and reversed from the other. Equation (F.5) shows that by suitable adjustment of the parameters large magnifications can be obtained. However, as the magnification increases so does z_I and, as a matter of practicality, the images will be restricted to rather small sizes as a result of the large demagnification m. Thus, in order to view the images magnification will be required, for example by placing a lens behind the zero order stop.

We now briefly discuss a unique method for display of the images reconstructed from acoustic holograms. As we have shown these images will usually be real rather than virtual and will be of small size. Hence, the display of acoustic hologram reconstructions is a problem in real image visualization. Conventionally, acoustic holograms are viewed by magnifying and then projecting the reconstructed real images onto a diffusely reflecting or transmitting screen. However, there is another technique which is often more useful.

We show in Figure F.1 a scheme for viewing acoustic holograms in which the real image is projected directly onto the photosensitive surface of a vidicon television camera tube and the reconstruction is then viewed on a TV monitor. There are several advantages to this system of viewing:

1) the image is magnified electronically (typically between 12

and 25 to one depending upon the relative size of vidicon and monitor),

2) the slight jitter inherent in the TV raster tends to average out the speckling due to coherence effects,

3) saturation effects tend to eliminate the mottling characteristic of acoustic images,

4) the contrast, brightness, and threshold sensitivity of the display may be varied instantaneously and continuously over a wide lattitude.

The last is most important because acoustic reconstructions appear as bright images against a uniform background and it is often difficult to distinguish one from the other using conventional methods. With the variable display it is quite easy to separate the bright image from the dim background. Numerous examples of the utility of this viewing technique are presented in Chapter V; for example, compare Figures V.23(a) and V.23(c).

REFERENCES

1. D. Gabor, "Light and Information", Progress in Optics, Vol. I, Edited by E. Wolf, North-Holland (1961), 118.

2. Kodak Plates and Films for Science and Industry, Kodak Publication P-9 (1962), 5-d.

3. J. A. Rajchman, "Integrated Computer Memories", Scientific American 217, 18-31 (1967).

4. S. Q. Duntley, "Visibility in the Oceans", Optical Spectra, 4th Quarter (1967), 64-69.

5. Private communication with Dr. William D. Squire of the Naval Undersea Research and Development Center, Pasadena, California.

6. R. E. Danielson, "Large Telescopes in Orbit", Science and Technology 67, 54-64 (1967).

7. D. Gabor, "A New Microscopic Principle", Nature 161, 777-778 (1948).

8. D. Gabor, "Microscopy by Reconstructed Wave-Fronts", Proc. Roy. Soc. (London) A197, 454-487 (1949).

9. D. Gabor, "Microscopy by Reconstructed Wave-Fronts, II", Proc. Phys. Soc. B64, 449-469 (1951).

10. E. N. Leith and J. Upatnieks, "Reconstructed Wavefronts and Communication Theory", J. Opt. Soc. Am. 52, 1123, 1130 (1962).

11. E. N. Leith and J. Upatnieks, "Wavefront Reconstruction with Continuous-Tone Objects", J. Opt. Soc. Am. 53, 1377-1381 (1963).

12. E. N. Leith and J. Upatnieks, "Wavefront Reconstruction with Diffused Illumination and Three-Dimensional Objects", J. Opt. Soc. Am. 54, 1295-1301 (1964).

13. J. T. McCrickerd and N. George, "Holographic Stereogram from Sequential Component Photographs", Appl. Phys. Letters 12, 10-12 (1968).

14. H. Berger, "A survey of Ultrasonic Image Detection Methods", presented at the First International Symposium on Acoustical Holography, held at the Douglas Advanced Research Laboratories, Hunington Beach, California,(1967).

15. P. M. Morse and H. Feshback, Methods of Theoretical Physics, Vol.I, McGraw-Hill (1953), 676-706.

16. M. Born and E. Wolf, Principles of Optics, Second Edition, Pergamon Press (1964).

17. T. J. Skinner, "Energy Considerations, Propagation in a Random Medium and Imaging in Scalar Coherence Theory", Ph.D. Thesis, Boston University, (1964).

18. R. Bracewell, The Fourier Transform and Its Applications, McGraw-Hill (1965), 269-271.

19. M. Born and E. Wolf, op. cit., Chapter X.

20. M. J. Beran and G. B. Parrent, Theory of Partial Coherence, Prentice-Hall, Inc. (1964).

21. W. R. Beam, Electronics of Solids, McGraw-Hill (1965), 370-385.

22. W. B. Davenport and W. L. Root, An Introduction to the Theory of Random Signals and Noise, McGraw-Hill (1958), 244-247.

23. M. J. Lighthill, An Introduction to Fourier Analysis and Generalized Functions, Cambridge (1964).

24. J. R. Klauder and E. C. G. Sudarshan, Fundamentals of Quantum Optics, W. A. Benjamin, Inc. (1968), Chapter I.

25. M. J. Beran and G. B. Parrent, op. cit., Section 4.3.

26. S. F. Edwards and G. B. Parrent, "The Form of the General Unimodular Analytic Signal", Optica Acta 6, 367-371 (1959).

27. P. B. Fellgett and E. H. Linfoot, "On the Assessment of Optical Images", Trans. Roy. Soc. (London) A 247, 369-407 (1955).

28. E. N. Leith and J. Upatnieks, "Recent Advances in Holography", Progress in Optics, Vol.VI, Edited by E/ Wolf, North-Holland (1967).

29. A. W. Lohmann, "Wavefront Reconstruction for Incoherent Objects", J. Opt. Soc. Am. 55, 1555-1556 (1965).

30. C. Sparrow, "On Spectroscopic Resolving Power", Astrophysics Journal 44, 76 (1916).

31. Unpublished data furnished by the Naval Undersea Research and Development Center, Pasadena, California.

32. G. M. Wenz, "Acoustic Ambient Noise in the Ocean: Spectra and

Sources", J. Acous. Soc. Am. 34, 1936-1956 (1962).

33. I. Tolstoy and C. S. Clay, Ocean Acoustics, McGraw-Hill (1966), 4.

34. J. B. DeVelis and G. O. Reynolds, Theory and Applications of Holography, Addison-Wesley (1967).

35. G. Tricoles and E. L. Rope, "Reconstructions of Visible Images from Reduced-Scale Replicas of Microwave Holograms", J. Opt. Soc. Am. 57, 97-99 (1967).

36. P. A. M. Dirac, The Principles of Quantum Mechanics, Oxford (1958).

37. R. Courant and D. Hilbert, Methods of Mathematical Physics, Vol.II, Interscience Publishers (1962), 320-322.

38. J. D. Jackson, Classical Electrodynamics, John Wiley and Sons, Inc. (1962), 17.

39. R. Mittra and P. L. Ransom, "Imaging with Coherent Fields", Antenna Laboratory Report 67-3, Antenna Laboratory, Dept. of Elec. Eng., University of Illinois, 1967.

40. R. J. Collier, "Holography and Integral Photography", Physics Today, July (1968), 54-63.

41. G. W. Stroke and A. E. Labeyrie, "White-Light Reconstruction of Holographic Images Using the Lippmann-Bragg Diffraction Effect", Phys. Letters 20, 368-370 (1966).

42. E. N. Leith and J. Upatnieks, "Recent Advances in Holography", op. cit., 31-35.

43. N. George and J. W. Matthews, "Holographic Diffraction Gratings", Appl. Phys. Letters 9, 212, 215 (1966).

44. J. W. Matthews, "Theory of Holography", Ph.D. Thesis, California Institute of Technology, Pasadena, California, (1967).

45. A. Sommerfeld, Optics, Academic Press (1964), Chapter V.

46. W. V. Lovitt, Linear Integral Equations, Dover Publications, Inc. (1950).

47. R. J. Collier and K. S. Pennington, "Ghost Imaging by Holograms Formed in the Near Field", Appl. Phys. Letters 8, 44-46 (1966).

48. J. A. Armstrong, "Fresnel Holograms: Their Imaging Properties and Aberrations", IBM J. Res. Dev. 9, 171-178 (1965).

49. E. B. Champagne, "Nonparaxial Imaging, Magnification, and Aberration Properties in Holography", J. Opt. Soc. Am. 57, 51-55 (1967).

50. E. N. Leith, J. Upatnieks, and K. A. Hains, "Microscopy by Wavefront Reconstruction", J. Opt. Soc. Am. 55, 981-986 (1965).

51. G. W. Stroke, An Introduction to Coherent Optics and Holography, Academic Press (1966).

52. J. Mathews and R. L. Walker, Mathematical Physics, W. A. Benjamin, Inc. (1964), Chapter X.

53. A. E. Covington and N. W. Broten, "An Interferometer for Radio Astronomy with a Single Lober Radiation Pattern", IRE Trans. Ant. Prop. AP-5, 247-255 (1957).

54. R. W. Meier, "Magnification and Third-Order Aberrations in Holography", J. Opt. Soc. Am. 55, 987-992 (1965).

55. R. W. Meier, "Depth of Focus and Depth of Field in Holography", J. Opt. Soc. Am. 55, 1693-1694 (1965).

56. R. W. Meier, "Cardinal Points and the Novel Imaging Properties of a Holographic System", J. Opt. Soc. Am. 56, 219-223 (1966).

57. S. Sokolov, U. S. Patent No. 216185 (1937).

58. G. S. Bennett, "A New Method for the Visualization and Measurement of Ultrasonic Fields", J. Acous. Soc. Am. 24, 470-474 (1952).

59. J. A. Kennedy and R. Muenow, "Practical Improvements and Applications for the Ultrasonic Image Converter", IEEE Trans. Son. Ult. SU-14, 47-52 (1967).

60. H. Berger and R. E. Dickens, "A Review of Ultrasonic Imaging Methods, With a Selected, Annotated Bibliography", Argonne National Laboratory Report ANL-6680, (1963).

61. H. Berger and J. Kraska, "Photographic Film Detection Method for Ultrasonic Field Visualization", J. Acous. Soc. Am. 34, 518-519 (1962).

62. J. Upatnieks, A. Vander Lugt, and E. Leith, "Correction of Lens Aberrations by Means of Holograms", Appl. Opt. 5, 589-593 (1966).

63. H. R. Worthington, "Production of Holograms with Incoherent Illumination", J. Opt. Soc. Am. 56, 1397-1398 (1966).

64. J. E. Jacobs, W. J. Collis, and H. Berger, "An Evaluation of an Ultrasonic Inspection System Employing Television Techniques", Materials Evaluation 22, 209-212 (1964).

65. R. K. Mueller and N. K. Sheridon, "Sound Holograms and Optical Reconstruction", Appl. Phys. Letters 9, 328-329 (1966).

66. K. Preston and J. L. Kreuzer, "Ultrasonic Imaging Using a Synthetic Holographic Technique", Appl. Phys. Letters 10, 150-152 (1967).

67. F. L. Thurstone, "Ultrasound Holography and Visual Reconstruction", Proc. Symp. Biomed. Eng. 1, 12-15 (1966).

68. A. F. Metherell, H. M. A. El-Sum, J. J. Dreher, and L. Larmore, "Image Reconstruction from Sampled Acoustical Holograms", Appl. Phys. Letters 10, 277-279 (1967).

69. R. B. MacAnally, "Inclined Reference Acoustic Holography", Appl. Phys. Letters 11, 266-268 (1967).

70. G. Oster, "The Science of Moire Patterns", Edmund Scientific Co. (1951).

71. P. Jacquinot and B. Roizen-Dossier, "Apodisation", Progress in Optics, Vol. III, North-Holland (1964), 29-186.

72. E. T. Whittaker and G. N. Watson, A Course of Modern Analysis, Fourth Edition, Cambridge (1962), Chapter XVIII.

73. G. C. Sherman, "Application of the Convolution Theorem to Rayleigh's Integral Formulas", J. Opt. Soc. Am. 57, 546-547 (1967).

74. H. Weyl, "Ausbreitung elektromagnetischer Wellen über einem ebenen Leiter", Ann. d. Physik 60, 481-500 (1919).

75. P. C. Clemmow, The Plane Wave Spectrum Representation of Electromagnetic Fields, Pergamon Press (1966), 35-36.

76. P. M. Morse, Vibration and Sound, McGraw-Hill (1948), Section 28.

77. A. Van der Ziel, Solid State Physical Electronics, Prentice-Hall, Inc. (1957), 381-382.

78. A. Kozma, "Photographic Recording of Spatially Modulated Coherent Light", J. Opt. Soc. Am. 56, 428-432 (1966).

79. Negative Making with Kodak Black-and-White Sheet Films, Kodak Publication F-5, (1966).

80. Kodak High Resolution Plates, Kodak Pamphlet P-47 (1967).

Unclassified

Security Classification

DOCUMENT CONTROL DATA - R & D

(Security classification of title, body of abstract and indexing annotation must be entered when the overall report is classified)

1. ORIGINATING ACTIVITY (Corporate author)	2a. REPORT SECURITY CLASSIFICATION
School of Engineering and Applied Science University of California Los Angeles, California	Unclassified 2b. GROUP

3. REPORT TITLE

Acoustic Imaging by Holography

4. DESCRIPTIVE NOTES (Type of report and inclusive dates)

Technical Report - August 1969

5. AUTHOR(S) (First name, middle initial, last name)

MacAnally, Richard B.
Yeh, C.

6. REPORT DATE	7a. TOTAL NO. OF PAGES	7b. NO. OF REFS
August 1969	249	80

8a. CONTRACT OR GRANT NO	9a. ORIGINATOR'S REPORT NUMBER(S)
N00014-67-A-0111-0014 b. PROJECT NO.	69-48
c. d.	9b. OTHER REPORT NO(S) (Any other numbers that may be assigned this report)

10. DISTRIBUTION STATEMENT

Reproduction in whole or in part is permitted for any purpose of the United States Government

11. SUPPLEMENTARY NOTES	12. SPONSORING MILITARY ACTIVITY
	Department of Navy Office of Naval Research

13. ABSTRACT

A method for visualizing objects immersed in water is formulated analytically and demonstrated experimentally. The technique, called "acoustic holography," is an adaptation of Gabor's two-step imaging process known as wavefront reconstruction or holography. The hologram is first formed from coherent acoustic radiation and then the image is reconstructed optically using coherent light source. Acoustic holography has advantage over other schemes for imaging in optically opaque media in that lenses or other focusing devices are not required, and a complete amplitude and phase reconstruction of the scattered field may be obtained. Since instantaneous amplitude is an acoustic observable, the reference field may be simulated electronically. Moreover, by resorting to heterodyne or phase detection the cross product term between object and reference signals may be generated without the undesired extraneous terms which occur in conventional holography. A scanning technique for generating acoustic holograms of underwater objects in the laboratory is described in detail. Using this system acoustic holograms have been recorded which show angular resolution of 3.6 milliradians, approximately 1.5 times the Rayleigh limit. A variable contrast television display was used to view the acoustic holograms. To limit the attenuation of acoustic wave in sea water to a tolerable value, only acoustic signal with frequencies below 1 MHz should be used. We used 1 MHz signal for our experiment. Consequently, the quality of any acoustic image is degraded by poor resolution and specular reflection. It is suggested that diffuse or incoherent illumination be used to overcome the defect that acoustic images often appear as diffracted highlights rather than as extended forms. Thus, it appears that acoustic holography is not necessarily optimum for all acoustic imaging situations.

DD FORM 1 NOV 65 1473 (PAGE 1)

S/N 0101-807-6801

Security Classification

14. KEY WORDS	LINK A		LINK B		LINK C	
	ROLE	WT	ROLE	WT	ROLE	WT
Acoustic Imaging						
Acoustic Holography						
Underwater Acoustics						